Vehicle Path Optimisation and Controllability on the Limit using Optimal Control Techniques

by

Ayao Komatsu

A Doctoral Thesis

Submitted in partial fulfilment of the requirements
for the award of
Doctor of Philosophy of Loughborough University
On the 26th July 2010

Abstract

Vehicle behaviour near the limit of adhesion is studied using linear optimal control techniques and relatively simple vehicle models. Both time-invariant and time-varying approaches are used. Controllability is applied as a post-processing tool to analyse the resultant vehicle behaviour.

First, a 4WS controller is developed using a linear time-invariant method, with a reference model control structure. Two handling objectives are defined, which are thought to provide predictable dynamics. Advantages of using a reference model control are clearly shown. With a developed control structure, it is shown that the prescribed target dynamics is achieved, provided tyre forces are available. It is also found that the controller is robust to small changes in the various vehicle parameter values.

As a next step, time-varying modelling approach was used in order to better represent the vehicle operating conditions through the various dynamic range, including the limit of adhesion. An iterative vehicle path optimisation problem is formulated using a linear time-varying control approach. The validity of the optimisation method is studied against the steady-state simulation result at the limit of adhesion. It is shown that the method is capable of finding a trajectory in the vicinity of the friction limit, where the front tyres are used fully whilst retaining some margin at the rears. However, a couple of Issues are discovered. First, due to the quadratic nature of the road geometry cost function, the trajectory could get locked if the vehicle runs very close to the edge of the road. Hence, the optimisation needs to be formulated such that the level of "optimality" on the trajectory remains consistent throughout the manoeuvre at each iteration. Secondly, it is found that inappropriate control demands are produced if the system matrix becomes poorly conditioned near the limit. This results in optimisation failure.

In order to understand the mechanism of this failure, controllability of linear time-varying system was analysed and its properties were discussed in detail. First, the calculation methods of the controllability gramian matrix are investigated and some practical limitations are found. The gramian matrix is then used to define an open loop control sequence. It is found that the damping of the system has a significant influence on the control strategy. Subsequently, "the moving controllability window of a fixed time period" is found to provide the most relevant information of changing dynamics through the time. The study showed that the failure of the optimisation in the vicinity of the friction limit was indeed due to lack of controllability and the optimisation method itself was functioning correctly.

The vehicle path optimisation problem is then extended to include longitudinal dynamics, enabling simulation of more general manoeuvres. The single corner simulation showed that the optimisation converges to an "out-in-out" path, with

iterative solution improving continuously in a first order manner. Simulations with various controller settings showed that the strategy is reasonably robust provided that the changes in parameter settings are kept within a reasonable magnitude. It is also confirmed that the optimisation is able to drive a vehicle close to the limit under different types of operations required, i.e. braking, cornering and acceleration. The study was then performed with slightly more complex road geometry in order to investigate if the optimisation is capable of prioritising certain part of the manoeuvre in order to achieve better overall result. Unfortunately, this problem could not be solved successfully. The optimisation concentrated on the latter part of the manoeuvre as it had higher sensitivity to the final cost. This resulted in clearly sub-optimal overall performance.

Finally, relatively simple study is conducted to investigate the correlation between various vehicle settings and optimisation results. Using the path optimisation problem formulation, it is found that the more oversteer vehicles are able to achieve better result with more margin left in rear tyre force capacity. The handling objective functions used for the 4WS controller is also calculated for the resultant trajectories. It is found that the neutral steer cost had a strong correlation, whereas the linearity cost showed no noticeable correlation.

The controllability analysis was applied on the various vehicle settings using step steer simulation. It showed that more understeering vehicle retains higher controllability throughout the dynamics range. It is also found that higher inertia gives better controllability near the limit, however, it gives less controllability at more moderate operating conditions.

Keywords :

Vehicle Dynamics, Limit Handling, Controllability, Optimisation, Optimal Control

Abstract

Vehicle behaviour near the limit of adhesion is studied using linear optimal control techniques and relatively simple vehicle models. Both time-invariant and time-varying approaches are used. Controllability is applied as a post-processing tool to analyse the resultant vehicle behaviour.

First, a 4WS controller is developed using a linear time-invariant method, with a reference model control structure. Two handling objectives are defined, which are thought to provide predictable dynamics. Advantages of using a reference model control are clearly shown. With a developed control structure, it is shown that the prescribed target dynamics are achieved, provided tyre forces are available. It is also found that the controller is robust to small changes in the various vehicle parameter values.

As a next step, time-varying modelling approach was used in order to better represent the vehicle operating conditions through the various dynamic range, including the limit of adhesion. An iterative vehicle path optimisation problem is formulated using a linear time-varying control approach. The validity of the optimisation method is studied against the steady-state simulation result at the limit of adhesion. It is shown that the method is capable of finding a trajectory in the vicinity of the friction limit, where the front tyres are used fully whilst retaining some margin at the rears. However, a couple of issues are discovered. First, due to the quadratic nature of the road geometry cost function, the trajectory could get locked if the vehicle runs very close to the edge of the road. Hence, the optimisation needs to be formulated such that the level of "optimality" on the trajectory remains consistent throughout the manoeuvre at each iteration. Secondly, it is found that inappropriate control demands are produced if the system matrix becomes poorly conditioned near the limit. This results in optimisation failure.

In order to understand the mechanism of this failure, controllability of linear time-varying system was analysed and its properties were discussed in detail. First, the calculation methods of the controllability gramian matrix are investigated and some practical limitations are found. The gramian matrix is then used to define an open loop control sequence. It is found that the damping of the system has a significant influence on the control strategy. Subsequently, "the moving controllability window of a fixed time period" is found to provide the most relevant information of changing dynamics through the time. The study showed that the failure of the optimisation in the vicinity of the friction limit was indeed due to lack of controllability and the optimisation method itself was functioning correctly.

The vehicle path optimisation problem is then extended to include longitudinal dynamics, enabling simulation of more general manoeuvres. The single corner simulation showed that the optimisation converges to an "out-in-out" path, with iterative solution improving continuously in a first order manner. Simulations with various controller settings showed that the strategy is reasonably robust provided that the changes in parameter settings are kept within a reasonable magnitude. It is also confirmed that the optimisation is able to drive a vehicle close to the limit under different types of operations required, i.e. braking, cornering and acceleration. The study was then performed with slightly more complex road geometry in order to investigate if the optimisation is capable of prioritising certain part of the manoeuvre in order to achieve better overall result. Unfortunately, this problem could not be solved successfully. The optimisation concentrated on the latter part of the manoeuvre as it had higher sensitivity to the final cost. This resulted in clearly sub-optimal overall performance.

Finally, a relatively simple study is conducted to investigate the correlation between various vehicle settings and optimisation results. Using the path optimisation problem formulation, it is found that the more oversteer vehicles are able to achieve better result with more margin left in rear tyre force capacity. The handling objective functions used for the 4WS controller is also calculated for the

resultant trajectories. It is found that the neutral steer cost had a strong correlation, whereas the linearity cost showed no noticeable correlation.

The controllability analysis was applied on the various vehicle settings using step steer simulation. It showed that more understeering vehicle retains higher controllability throughout the dynamics range. It is also found that higher inertia gives better controllability near the limit, however, it gives less controllability at more moderate operating conditions

Acknowledgements

This work was conducted in and funded by the School of Aeronautical and Automotive Engineering at Loughborough University.

Without the support and encouragement from so many people, this thesis would never have been completed. I would like to take this opportunity to give my sincere thanks to some of them.

The research was conducted under the supervision of Professor T.J.Gordon and Dr. M.C.Best. I would like thank their exceptional supervision and encouragement. They did not only guide the research tremendously, but also have been very open-minded in the research direction throughout the four long years. Owing to this, I was always able to carry out the work in the area which I had keen interest in. It also allowed me to explore more practical side of engineering, which in turn had a positive impact on more theoretical work covered in this thesis. I also like to thank Dr. M.N.Howell for his inputs.

I would like to thank my parents Keiko and Yuichiro Komatsu for their continuous encouragement and support, believing that I can actually finish this thesis. They made it possible for me to study in England as an undergraduate. Without such a support and understanding, I certainly won't be writing this sentence now. I would like to thank Sachie, my wife, who has been very supportive throughout my slow write-up process.

I have made some great friends at Loughborough. Rob encouraged me throughout, even had a bet on me finishing PhD for an extra incentive. I had numerous inspiring discussions with Phil, who also proof read my thesis together with his wife, Gia. Andrew and Ashley made my research life more colourful in the office.

Finally, I would like to thank every staff in the department for being so helpful and friendly, which made my time there very enjoyable.

Contents

List of Figures

List of Tables

List of Notations

Notation	Description	Units
a_x, a_y	Longitudinal / Lateral acceleration	m/s^2
b	Distance of C.G. to front axle	m
B	Stiffness factor for Pacejka tyre model	-
b_s, b_t	Suspension / Tyre Damping for Quarter Car model	kNs/m
$b_{\phi f}$, $b_{\phi r}$	Front / Rear Damping	kNs/m
c	Distance of C.G. to rear axle	m
C	Shape factor for Pacejka tyre model	-
$C_{\alpha f}$, $C_{\alpha r}$	Front / Rear Cornering stiffness	N / rad
D	Peak factor for Pacejka tyre model	-
D_{index}	Dynamic index	-
E	Curvature factor for Pacejka tyre model	-
F_f, F_r	Front / Rear Tyre force	N
F_x, F_y	Longitudinal / Lateral force	N
g	Gravity acceleration	m/s^2
G_d	Weighting factor for road geometry cost	-
Gr	Yaw rate gain	-
h	Proportional human control action / gain	-
H	Hamiltonian matrix	-
h_f, h_r	Front / Rear Roll centre height	m
h_g	Centre of Gravity height	m
h_0	Roll axis height at CoG	m
I_{xx}	Roll moment of inertia	kgm^2
I_{zz}	Yaw moment of inertia	kgm^2
I_{xz}	Roll & Yaw Product of inertia	kgm^2
$J(x,u)$	LQR cost function	-
J_d	Road geometry cost function	-
k	Yaw radius of gyration	m
K	Understeer gradient	deg / g

K	LQR control gain	
k_s, k_t	Suspension / Tyre Stiffness for Quarter Car model	N/m
$k_{\phi f}$, $k_{\phi r}$	Front / Rear Spring stiffness	N/m
K_{space}	Lateral spacing between suspension springs	m
l	Wheelbase	m
m	Total vehicle mass	kg
m_1, m_2	Unit direction vectors for road geometry cost	-
M	Solution of an algebraic Riccati equation at final time	-
Mc	Weighting factor for final state deviation cost	-
m_b, m_w	Sprung / Unsprung mass	kg
M_x, M_y, M_z	Roll, Pitch and Yaw moment	Nm
n	Number of states	-
p	Roll velocity	rad/s
P	Solution of an algebraic Riccati equation	
q	Pitch velocity	rad/s
Q	State cost for LQR	-
Q_u	Pseudo forward velocity deviation cost	-
r	Yaw velocity	rad/s
R	Control input cost for LQR	-
R	Road curvature radius	m
S	Scaling matrix	-
S_h, S_v	Horizontal and vertical shifts for Pacejka tyre model	
$Stab$	Front Anti-Roll-Bar Stiffness	Nm/deg
t_{rf}, t_{rr}	Front / Rear Track width	m
T_{sa}	Braking torque generated by DYC	Nm
u	Vehicle longitudinal velocity	m/s
U_{crit}	Critical velocity	m/s
U_d	Characteristic damping velocity	m/s
U_p	Pseudo forward velocity state	m/s
v	Vehicle lateral velocity	m/s
V_b, V_w	Body / Wheel Vertical velocity	m/s
V_x , V_r	Tyre Model: Longitudinal & Rolling velocities	m/s

V_{sx}, V_{sy}	Tyre Model: Longitudinal & Lateral slip velocities	m/s
V_r	Road vertical velocity	m/s
W	Controllability Gramian matrix	-
Y_p	Pseudo displacement state	m
z	Scaled states	-
Z_b, Z_w	Body / Wheel Vertical displacement	m
α_f, α_r	Front / Rear Slip angles	rad
β	Side slip angle	rad
ϕ	Roll angle	rad
γ	Camber angle	rad
δ	Steering Angle	deg
δ_d, δ_f, δ_r	Driver / Front / Rear Steer input	rad
δ_{ns}	Neutral Steering Angle	deg
δ_U	Steering Angle for lateral acceleration compensation	deg
ε	Roll axis inclination angle	rad
ε	Floating-point relative accuracy	-
λ	Weighting parameter for LQR cost function	-
σ, σ_x, σ_y	Tyre Model: Resultant / Longitudinal / Lateral slip	-
τ	Control time window	s
τ_D, τ_I	Derivative and Integral terms for a driver model	-
τ_L	Human reaction time	s
ϖ_n	Undamped yaw natural frequency	Hz
$\xi(\tau)$	State transition matrix	-
ζ, ζ_0	Yaw damping ratio / yaw damping ratio at zero speed	-
Φ	State transition matrix	-

Chapter 1

Introduction and Literature Review

The topic of vehicle dynamics and its control has been explored for many years, including the limit-performance enhancement at the edge of a friction envelope. Mechanical linkages / parts of a vehicle are often replaced by solenoid valves and actuators, equipped with real-time controllers. Probably one of the most well known systems using such technology in the early days is an active suspension control developed by Lotus in early 80s. The continuous advances in such technologies have enabled engineers to tailor a vehicle to have "desired characteristics" more freely. For instance, various steering geometries can be tested on one test vehicle with active systems, rather than developing multiple test linkages. Such advantages have been accelerating the development and understanding of vehicle dynamics.

Moreover, safety has increasingly become a more important issue for manufactures due to a rapid increase in the amount of traffic as well as the travelling speed of vehicle itself. Active control systems are now taking a significant role in the active safety as well as the passive safety [Holzmann, 2006; Nagai, 2007]. Some controllers are designed to improve the emergency / accident avoidance manoeuvres, some are designed to provide more predictable dynamics through the various range of dynamics (assumption here is that more predictable dynamics are easier to control).

In such a wide and well-researched field, the work summarised in this thesis concentrates on using a linear control law on relatively simple vehicle handling models. The purpose is to produce analytical results based on the theoretical assumptions constructed, therefore it encourages the understanding of the problem formulated.

This thesis considers the application of Linear Optimal Control theories, both in time-invariant and time-variant cases, to enhance the driver-vehicle dynamic characteristics. The major emphasis is on the design and development of an optimisation methodology within a highly nonlinear environment using a linear control law. Since the large part of this thesis deals with the vehicle operating at near the limit of adhesion, the significance of controllability in the optimisation process is highlighted and is investigated.

1.1 Background and Motivation

There exist various control laws / systems to enhance vehicle handling dynamics to date. A couple of well-known control strategies, Direct Yaw Moment Control and Four-Wheel Steer, are reviewed as well as Integrated control strategies. Driver model development is then reviewed which forms a key part in understanding driver-vehicle interface. Finally, application of various control theories is discussed.

1.1.1 Direct Yaw Moment Control

Direct Yaw Moment Control aims to control braking or traction forces at individual tyres in order to generate the desired yaw moment.

Shibahata pointed out that minimising the variation in vehicle dynamics at different operating conditions makes a vehicle easier to control as it is more predictable [Shibahata, 1992]. Shibahata then discussed that the decreasing in the stabilising/restoring yaw moment, Equation 1.1, has a major influence in causing this variation, and proposed a β-method Direct Yaw Moment Control (DYC) where it controls the yaw moment proportional to the longitudinal and lateral accelerations of the vehicle. The stabilising yaw moment is defined as shown in Equation 1.1 below.

$$M = -b * F_{yf} + c * F_{yr} + \sum_{k=1}^{4} Tsa_k \qquad (1.1)$$

Although the vehicle sideslip angle has a significant influence on the decreasing yaw moment, it is not directly used within the control law due to its measurement difficulty. Instead, yaw rate feedback is used to compensate for the error. It must be noted that with a current technology, it is possible to measure the vehicle sideslip angle fairly accurately provided that the road surface remains reasonably consistent. However, this is probably still not suitable for production vehicle applications. It is also possible to estimate the sideslip angle in real time using a linear observer with yaw rate as the only measured signal [Aoki et al, 2006].

As it is well-documented in many papers [Matsumoto and Yamaguchi, 1992], DYC benefits from a direct generation of yaw moment through left/right difference in traction or braking forces. By contrast, front/rear force distribution control generates yaw moment indirectly by utilising friction circle property [Motoyama et al, 1992]. In other words, the amount of lateral force generation is controlled by the longitudinal usage of tyre performance envelope. This indirect method is not as effective, since the control depends on highly nonlinear tyre characteristics to produce desired tyre forces laterally. Moreover, the longitudinal weight transfer has a dominant effect on its dynamics. In order to maintain stability, particularly on low friction surface, it is essential to distribute appropriate amount of longitudinal forces with regard to tyre's combined force capacity [Sakai et al, 2002].

Raksincharoensak et al [Raksincharoensak, 2006; Raksincharoensak, 2008] used DYC with two different cost functions; lateral deviation regulation (lane keeping) and side-slip angle regulation (stability control). The controller switches between the two cost functions depending on driver's intention, which is identified from the driver's steering activity by applying Hidden Markov Model (statistical model applied to a Markov process system (random evolution of state is only dependent on its present state) with the states not directly visible to observer). Meng et al [Meng, 2006] used Hidden Markov Model to identify and capture driver behaviour for an intelligent vehicle security application.

Although not used within this thesis, such recognition technique can also be applied to assess the severity of vehicle operating condition and hence modify the cost function / target vehicle behaviour accordingly. For instance, zero side-slip target might be appropriate only up to a certain level of lateral acceleration. Beyond such point, cost function may be altered to accept certain level of increase in side-slip and actually use this dynamic information as a feedback to the driver to make him/her aware that the limit is approaching.

Hancock et al [Hancock, 2005] compared the performance of active brake control and overdriven differential control (torque can be transferred in both directions). Both systems used exactly the same yaw moment controller. Note that this active brake control is different from conventional DYC as braking is applied to only a single tyre to generate yaw moment. The two systems produced a similar vehicle dynamic performance, although the active differential offered some advantages. This is mainly due to the fact that active differential generated yaw moment from two tyres instead of one. However, it was noted that the strategy for active brake controller can be improved to compensate this disadvantage. More significantly, the differential controller was found to be considerably more efficient. This is because it attempts to re-proportion the torque rather than dissipating it as heat through one wheel. This makes the active differential control more attractive throughout the operating range, whereas it makes the braking control undesirable except for limit manoeuvres (where one needs to slow the car down).

1.1.2 Four-Wheel-Steer (4WS)

In parallel with the development of DYC strategy, Four-Wheel-Steer (4WS) has also been researched to enhance vehicle performance at the limit of adhesion. Some [Higuchi et al, 1992; Lugner et al, 1992] controlling both front and rear steering angles (4WS) and the other controlling the rear steering angle only (Rear Wheel Steer), keeping the conventional driver authority at the front axle. The simplest controller of the early days just steers the rear wheels in proportion to the fronts.

Many researchers [Ackerman, 1994; Harada et al, 1996; Lee, 1995; Kleine et al, 1998] proposed controllers to achieve zero side-slip angle/velocity whose implications on vehicle dynamics are as discussed earlier. Well-known problem for this type of controller is that the vehicle exhibits heavy understeer characteristics at high lateral acceleration range [Lin, 1992]. As the vehicle behaves much more towards oversteer in the low lateral acceleration range, this significant change in dynamics is thought undesirable. In order to keep the vehicle characteristics more consistent throughout the operating speed range, Lin used extra feedback to maintain constant yaw response time. Yaw rate following control was also used in many 4WS strategy to maintain certain steer to yaw rate relationship [Nagai and Ohki, 1989; Hirano and Ono, 1994; Tran, 1992; Hirano and Fukatani, 1996; Song and Yoon, 1998]. However, as the tyre starts to saturate near the limit of adhesion, there is only so much lateral force that can be generated. In the worst case, the controller will keep demanding more slip angle that actually reduces the lateral force generated. Canale et al [Canale, 2008] proposed a control system structure using Internal Model Control (IMC), which was able to guarantee robust stability in the presence of saturation function.

In addition, the control strategy often differs depending on the vehicle speed. At low speed (approx less than 35 kph), the rear wheels are steered in the opposite direction to the front wheels. Whereas the front and rear wheels are steered in the same direction at high speed. This is because the manoeuvrability is the priority in low speed, whereas the stability concern is great at high speed. Such change of dynamics between low and high speed may or may not be desirable.

Wang [Wang et al, 2002] investigated the influence of active rear wheel steering vehicle for the aged driver. Aged drivers often have worse feedback information due to decline in vision and perception abilities, as well as his/her control ability & adjustability and reaction time. It was found that a 4WS vehicle is easier to drive for aged drivers than a conventional 2WS vehicle. A 4WS vehicle performance was consistent when the driver reaction time was increased and was

more roust with respect to gain magnitude change due to variation in road surface friction.

1.1.3 Integrated Vehicle Dynamics Control

Abe et al compared the benefits of 4WS and DYC [Abe et al, 1994], highlighting the limitation of 4WS strategy as the tyre lateral force capability saturates. By comparison, tyres are expected to have capability to produce more longitudinal force even when the lateral force reached its limit. Moreover, 4WS has a greater time delay in vehicle response. His research found that the 4WS is suitable to the zero sideslip control strategy, and DYC is more suitable for the yaw rate model following control. This is because DYC does not use lateral force, hence cannot control sideslip motion directly. He also found that 4WS strategy strongly depends on the tyre vertical load and hence sensitive to the variation of running conditions [Abe, 1996]. Therefore 4WS control coupled with Roll moment distribution control (RDC), which regulates the front/rear lateral load transfer ratio and hence controlling the resultant yaw moment, is a more robust solution [Kageyama and Jo, 1996; Li et al, 2008].

Moreover, as it is covered in many papers, DYC can be used in conjunction with 4WS to suppress the deterioration of steering control effects in nonlinear operating range [Kageyama and Jo, 1996; Nagai et al, 1996]. Mokhiamar [Mokhiamar et al, 2002] compared the stability and responsiveness of three different combinations of chassis control (DYC + RWS, DYC + FWS, DYC + FWS + RWS). DYC + RWS control had detrimental effect on vehicle stability limit as the work loads on rear tyres are high. By contrast, DYC + FWS solution had good stability, but had worse response due to front tyre saturation. DYC + FWS + RWS was found to utilise the tyre capacities best, maximising the stability. Mokhiamar [Mokhiamar et al, 2005] then performed a comparison of "optimum tyre force distribution control" and "DYC + Active 4WS". Both controllers showed their effectiveness near the limit handling condition. However, under the very severe manoeuvre, it was found that "DYC + Active 4WS" failed

since DYC part of the controller used up the tyre capacity as it tried to generate large yaw moment to stabilise the vehicle. This resulted in loss of controllability. By contrast, "optimum tyre force distribution control" was able to achieve the objective by prioritising steering control. It was also found that the driver could adapt his driving more easily with the optimum tyre force distribution control.

In Chapter 3 of this thesis, the author suggested a model reference 4WS controller that targets zero sideslip and neutral steer yaw rate gain in both linear and nonlinear operating conditions. It must be noted that the main emphasis was on the development of the control system structure rather than the definition of the "desired" dynamics itself.

1.1.4 Application of Tyre Model and Friction Estimation

As a vehicle relies on the performance of tyres, it is obvious that having a well-represented tyre model and friction estimator are incredibly important. Clearly, the degree of tyre model's complexity depends on the accuracy of the measurements / estimations available and the purpose of the model. For instance, it is important to include thermal effect if the model is to be used for race car tyres, whereas this is not essential for passenger car tyres. In addition, structural tyre models require detailed measurements / data to simulate the tyre contact patch behaviour to high frequency [Lugner et al, 2005].

Wakamatsu et al [Wakamatsu et al, 1996] estimated the friction coefficient from the ratio of actual yaw rate to the linear model yaw rate at high friction roads using least-squares identification. By contrast, Furukawa et al [Furukawa, 1996] used a relatively simple on-board tyre model to estimate tyre forces and found that the fairly low level of accuracy in the friction coefficient estimation was acceptable. On-board-tyre model was then used to estimate vehicle sideslip angle that allowed DYC to regulate sideslip angle directly rather than controlling the resultant yaw moment [Furukawa, 1998; Abe et al, 1998]. Abe et al reported that the adaptation of tyre-track friction coefficient due to the variation in the track

condition was not necessary [Abe, 1999]. In other words, only an approximate measure of the track condition was good enough for their control application. Gordon et al [Gordon, 1999] proposed a Lyapunov Friction Adaptive controller where the rough estimation of friction is made from vehicle response in order to adapt demand signals.

In this thesis, the nonlinear tyre model proposed by Pacejka et al [Pacejka, 1989] is used. This type of tyre model does not necessarily give insight into tyre dynamics itself and hence not suitable for a tyre development. However, it is well-suited for fundamental vehicle dynamics studies as it only requires a map with certain physical significance. This empirical model approach is considered appropriate for this thesis, since the main aim is not to improve the tyre performance itself or to understand the mechanism of tyre construction, but to improve the way in which the available tyre forces are used in order to enhance the vehicle dynamics. The effects of friction variation are not investigated and it is assumed that tyre force information is readily available to the controller. In addition, the constant time delay is used for the tyre force generation although this varies in real life [Higuchi, 1996]. Other parameters such as wear, temperature and compound degradation are not considered.

1.1.5 Driver Model / Path Optimisation

Driver modelling is the final piece in the study of Vehicle Dynamics and Control. As the driver characteristics gets superimposed on the vehicle characteristics (vice-versa), it is very important to understand its influences. However, it poses a major challenge as a human is an incredibly complex system and there is no guarantee to understand its control mechanism mathematically at present time. Therefore the simplification has to be made in order to capture some human control dynamics. It is well–known that a human control action can be divided into feedforward and feedback actions. Assuming that the driver produces linear feedback action, one of the simplest forms of driver model can be expressed as a transfer function in a following form [Abe, 1992]. This equation includes a time

delay for human reaction, which is represented by $e^{-\tau_L s}$, where τ_L is the reaction time. Simplest form of human control action is proportional control, which is represented by h. It also includes derivative and integral actions, represented by coefficients τ_D and τ_I, respectively.

$$H(s) = h\left(\tau_D s + 1 + \frac{1}{\tau_I s}\right)e^{-\tau_L s}$$

The above transfer function basically represents PID control with time delay. Human learning means that the parameters in the above transfer function are variable (adaptive). Ishio et al [Ishio, 2008] performed an experiment to investigate how simple driver model parameters (proportional, derivative and time constant) can be determined. It was found that while these parameters are defined based on his / her inherent characteristics, they also respond to the derivative term change in active front wheel steer controller. This demonstrated human ability to adapt to a change in vehicle dynamic characteristics. It is also interesting that drivers responded differently to the same change in dynamics. Hence, it can be said that the way in which a driver adapts to such changes is coupled with his / her inherent characteristics.

Lugner and Plöchl [Lugner, 1994; Lugner, 1999] presented 3-level driver model. On top of a standard anticipatory (feedforward) and compensatory (feedback) controls, 3rd level controller is added to compensate for large deviations, which will then bring the vehicle back to the desired trajectory with smooth transition. It is reported that the 3rd level of the driver model enabled a good adaptation to different driver behaviour or driving tasks.

Sharp [Sharp et al, 2000] proposed a steering controller via path preview using a set preview time (i.e. distance becomes a function of vehicle velocity). As well as the preview path errors, two state feedbacks are used (lateral offset and attitude angle relative to the tangent angle of the intended path). Optimal linear discrete time preview control structure is used with the limitation on control magnitude placed via saturation functions in order to avoid tyres operating at heavily non-linear range. In his work, longitudinal and lateral controls are decoupled, hence

infeasible condition may occur. This was monitored by using an inverse of vehicle forward velocity as a scaling factor. Sharp [Sharp, 2005] conducted a further study of a relationship between preview distance and vehicle characteristics. He found that a large saloon car required the driver to use much extended preview distance compared to a small sports car. Sensitivity study showed that for good tracking performance with short preview distance, yaw inertia and mass should be small, whereas wheelbase and tyre cornering stiffness should be large. Thus, it was suggested to use required preview distance as a car handling criterion.

Cole et al [Cole, 2006] compared predictive and LQR control theories for the path-following problem. Influence of various combination of preview and control horizons on controller gain are examined. Identical control gains were obtained for both approaches when the preview and control horizons are long. Different gains were obtained when the preview horizon is longer than the control horizon. This difference comes from the cost function where the path-following errors were evaluated up to preview horizon for the preview controller, whereas LQR control evaluates errors up to control horizon.

Gordon et al [Gordon, 2002] produced an automated driver based on the convergent vector field approach. For the path planning part of the control (feedforward), road geometry is represented using a vector field. At the current vehicle position, the automated driver has its desired velocity vector. It was shown that feedback control is then applied to guarantee stable asymptotic tracking of a reference path, with the physical constraints (friction, acceleration, etc).

Yamakado et al [Yamakado, 2008] compared the driving strategy of "normal driver" and "expert driver". They found that "expert driver" rarely uses pure braking. In stead, "expert driver" performs combined steering and braking operation from the beginning. Of course, this depends on a type of the corner driver is negotiating. However, this indicates that "expert driver" is able to co-ordinate and distributes longitudinal and lateral controls better. They also stated that drivers' bodies are sensitive to jerk (first derivative of acceleration), which

reflects the changing forces applied to the vehicle. Hence, they developed a jerk sensor and a driver model utilising such information. The model used a preview-follower model (lateral) as a steering input and lateral jerk information (as a result of steering input) to determine longitudinal acceleration. In other words, longitudinal movement is decided by lateral movement. This model structure was able to emulate the driving strategy used by "expert driver".

Neural Network is often used in an attempt to mimic human-like behaviour, including learning aspect. MacAdam et al [MacAdam, 1998] used Neural Network to categorise the driver behaviours. It was then used to model the longitudinal control behaviour with the presence of other traffic.

Pick and Cole [Pick, 2007; Pick 2008] investigated the dynamic properties of driver steering control from the neuromuscular system point of view. It studied the changes in stiffness and damping of driver's arm when the torque offset was applied. Similar change in stiffness was observed when the pair of muscles co-contracted in order to stabilise the joint. Through mathematical model study, it was reported that increase in stiffness and reflex gain improved driver's path following ability, although increasing reflex gain has a destabilising effect. In addition, muscle co-contraction reduced as the driver learnt to predict the steering feedback torque. Inclusion and understanding of such human factors is crucial in advancing driver-vehicle interface, however, is outside of the scope for this thesis.

Casanova et al [Casanova 2000; Casanova 2002] developed the minimum time manoeuvring method based on non-linear programming. The optimum racing line was computed for a lap of racing circuit, which was discretised into short, totally de-coupled segments. The length of segment was set short enough so that the vehicle does not have enough time to get seriously out of shape within each segment. Automatic differentiation was used to improve the efficiency of the computation.

In this thesis, time-varying linear optimal feedback controller is used as a driver, for a vehicle path optimisation, rather than trying to mimic the human-like control. The controller does not include human's physical characteristics such as; their reaction / information processing time, the way in which human treats visual information and the information obtained from the vestibular (inner ear) and kinaesthetic (body distributed) channels. All of these are key factors in human driving operation [MacAdam, 2003]. Therefore, the approach taken in thesis does not necessarily give insight into how a human actually operates. However, together with the other work described in this thesis, it is hoped to gain insight into kind of vehicles that are relatively easy to control and are able to achieve the set target. Moreover, use of linear optimal control technique provides analytical results rather than numerical results. Nonlinearity of the vehicle dynamics is addressed by using time-varying approach. Initial study focused on developing a steering controller with constant longitudinal vehicle velocity. The model was then extended to optimise the lateral and longitudinal dynamics simultaneously in order to achieve the maximum distance for a given time period.

1.1.6 Driver-Vehicle System

So far, researchers have discussed the objective of controllers to give consistent, hence predictable dynamics throughout the operating range. This consistency has to cover not only steady-state, but also transient and frequency responses. As discussed earlier, one of the most popular objectives is to achieve zero sideslip in order to maintain stabilising yaw moment. Hogg et al [Hogg, 1992] reported that as well as keeping a consistent yaw gain, shifting a yaw damped natural frequency towards the frequency limit of driver bandwidth contributes to driver control and enhanced stability. Findings of Hoffman and Joubert [Hoffman, 1966] also state that the yaw damping of a car has a major influence on its path following ability. Higuchi et al [Higuchi, 1996] reported that yaw natural frequency, lateral acceleration gain & phase and yaw velocity phase have major influences on the driver subjective evaluations. Waterhouse [Waterhouse, 2002] also mentioned that minimising phase difference between yaw velocity and lateral acceleration had a

positive correlation with drivers' subject feedback, however, only up to a certain point. Chen and Crolla [Chen, 1996; Chen, 1997; Chen, 1998] have carried out an extensive work in subjective-objective correlation of vehicle handling dynamics, however reported that there is still some way to go before constructing a correlation matrix that covers wide handling range.

"Driver-in-loop simulation" is becoming increasing common [Cipelli, 2008] as a tool to evaluate driver-vehicle interaction. This is a logical step as the actual vehicle response is determined by both system dynamics and driver operation. Using a simulator, Miura et al [Miura, 2007] investigated a correlation between driver model parameters and subjective handling quality rating. It was reported that frequency response of steering angle to yaw rate had a strong correlation to driver's subjective evaluation.

In this thesis, work in this area has been approached from a theoretical point of view. Through the application of controllability theory at different operating conditions, the relationship between dynamics, including the objective function and the driver controllability is investigated.

1.1.7 Control Strategy

Various control strategies, both linear and nonlinear, are applied in the area of vehicle dynamics control. As mentioned earlier, some of the early production control scheme only employed an open-loop proportional control. However, the yaw rate feedback control is most commonly used scheme for such systems as it is relatively easy to measure the required signals and provides fundamental vehicle information both in transient and steady-state.

Inoue and Sugasawa [Inoue, 1992] compared the feedforward and feedback control for a yaw rate follower type 4WS controller. It was found that the feedback controller improved vehicle stability against disturbance.

Sliding mode control was used by Furukawa et al [Furukawa, 1996] for the Direct Yaw moment Control where the vehicle was also equipped with a linear feedforward zero-slip 4WS controller. Sliding mode control was also used for the stand-alone DYC by Abe et al [Abe, 1999], as a sideslip model following controller. It succeeded in stabilising the vehicle motion in the nonlinear region. Lugner and Plöchl [Lugner, 1999] used sliding control for a driver model, mentions that it has an advantage in disturbance rejection and robustness to vehicle parameter variations. Yoshioka et al [Yoshioka, 1999] used sliding model control for DYC. It was also reported that the controller was able to deal with significant error in model parameter, hence showed good robustness.

Lugner et al [Lugner, 1992] used a reduced observer with a linear optimal control based on yaw rate feedback. The observer was utilised for the split – mu condition recognition strategy, and was found to improve the states control in such a critical situation.

Hirano and Ono [Hirano, 1994] combined H∞ and mu synthesis to achieve robust control for the 4WS & 4WD integrated system. It reported that the need of an adaptive logic with respect to the different road surface condition was eliminated as the robust control performance was improved by an addition of mu synthesis (H∞ only guarantees robust stability, not robust performance).

Nagai et al [Nagai, 1994] used Neural Network in conjunction with a linear yaw rate feedback control law for a 4WS control system. Based on the bicycle model, Neural Network was used to identify the vehicle characteristics variation through the operating condition as well as serving as a nonlinear controller. It was found that addition of Neuro control enlarged the range of lateral acceleration at which the objective function was met successfully.

Gordon and Best [Gordon, 1999] applied Lyapunov-based controller for a handling control on a variable friction surface. When compared to the dynamics controlled by Linear Quadratic Regulator (LQR), it has shown very similar result.

However, it was mentioned that Lyapunov control is simpler to implement in real time. This Lyapunov-based controller was then extended to adopt the control demand signal based on the estimated friction available (Lyapunov Friction Adaptive controller). In other words, when the initial control demand is not reasonable with regard to the estimated friction, the controller signal would be modified so that the undesirable transient dynamics can be avoided.

Alfi el al [Alfi, 2009] proposed a fuzzy logic 4WS controller that combines the state-feedback controller and sliding model controller. A fuzzy system is used to decide when to use each of these controllers or a combination of both. This enabled the resultant system to benefit from the advantages of both controllers. The controller performance showed faster yaw rate response, reduced side slip and better disturbance rejection.

Throughout this thesis, a relatively simple linear controller is used. The aim of this thesis is not to compare and determine the best control method available, but to produce results that can be analysed qualitatively. It is thought that using a linear controller enables more analytical approach to the problem, hence enhancing one's understanding.

1.2 Approach & Objective of the Thesis

The objective of this thesis is not to identify THE controller for the optimisation task, but to formulate a methodology with a controller which can be investigated analytically. From this point of view the optimisation carried out is based on the linear control theory. This also means that human factor in driver model is not included even though it was identified as important factor in improving our understanding of driver-vehicle interaction. In order to focus on obtaining analytical results, topic of driver-vehicle interaction is approached from controllability point of view.

The main objectives of the thesis are:

- To investigate the application of linear optimal control within a certain structure such that it can be successfully applied to a highly nonlinear environment with the information from the simplest possible vehicle model.
- To establish a methodology and measurement parameter for the vehicle dynamics performance under various operating conditions.
- To establish a system that is capable of finding a limit of adhesion and hence provides more insight into dynamics around this peak.
- To investigate a relationship between mathematical and practical understanding in the vehicle handling dynamics. (i.e. does mathematical results reflect the actual physical phenomena?)

1.3 Outline of Thesis

Chapter 2 introduces the "tools" used in this thesis. This includes the modelling of vehicle handling dynamics at various Degree-of-freedom; together with the tyre and Quarter-Car vehicle ride models. The fundamental characteristics of handling dynamics are then investigated. It also covers the theories of time-invariant and time-variant linear optimal control theories.

Chapter 3 investigates the application of Linear Quadratic Regulator as a reference model tracking controller. It is implemented as the controller for an active Four-Wheel-Steer vehicle, where the objective of the controller is defined solely from a vehicle handling dynamics point of view. Reference model control structure uses both 2DOF and 3DOF vehicle handling models.

Chapter 4 describes the design, application and analysis of vehicle path optimisation based on time-variant linear optimal reference control. The method is developed using a 3DOF vehicle handling model, where the forward vehicle velocity is set constant. The algorithm is validated against the steady-state simulation at the limit of adhesion. A limitation of the optimisation method within the vicinity of friction limit is discussed.

Chapter 5 presents in-depth discussion of controllability, mainly with time-variant linear models, in order to understand the optimisation limitation experienced in the previous chapter. A couple of calculation methods are presented and their relative merits and demerits are discussed. The open loop regulation control based on the controllability analysis is then performed to investigate the meaning of controllability within a context of vehicle dynamics. Various measurement parameters are investigated and discussed. The controllability information was then applied to the path optimisation result obtained in the previous chapter. It was concluded that the optimisation failed as a result of poorly conditioned matrix due to lack of controllability, and that the optimisation method itself was functioning correctly.

Chapter 6 extends the vehicle path optimisation problem formulation with the longitudinal degree of freedom to simulate more realistic manoeuvre. Path optimisation was performed successfully using simple corner geometry, and various robustness evaluations were carried out. As a next step, the optimisation was applied to slightly more complex road geometry. This is to investigate whether the controller was capable of prioritising a certain part of manoeuvre in order to obtain better overall performance.

Chapter 7 discusses the effect of various vehicle parameters on the vehicle path optimisation result. The handling objective employed for the 4WS project in chapter 3 is re-visited in order to assess its significance with respect to the optimised manoeuvres / path.

Chapter 2

Vehicle Dynamics Modelling, Fundamental Analysis and Control Theories

In order to carry out research in the topic of vehicle dynamics and control, certain types of tools are required. The types of research could broadly be divided into the following three groups: theoretical, experimental and the combination of both. The research in this thesis does not involve any experimental works, but is fully based on theoretical simulations. In order to perform the research in an analytical manner, various suitable mathematical theories and models need to be developed and applied. Working within such an "idealised" theoretical field allows one to isolate certain dynamics to the others, hence aids the understanding of certain system mechanism. Clearly, the assumptions and limitations need to be addressed so that their relationship to much more complicated real life problems can be understood.

This chapter summarises such "tools" used to conduct the research projects covered in this thesis. First of all, the brief introduction on the subject of vehicle dynamics is given, where the background to the requirements for simulation work is discussed. The derivation of various models used in the thesis is covered in Section 2, where the differences in the aim of each model are highlighted. Simulations are then performed in order to investigate the fundamental vehicle dynamic characteristics as well as comparing the effect of different degrees of freedom involved in the various models developed. Finally, the control theories used in the thesis are reviewed in Section 4.

2.1 Background

Optimisation of vehicle dynamics is a hugely popular topic due to the obvious requirements such as enhanced safety, handling and ride. There has been significant progress made in the field, coupled with the control engineering, as mentioned in Section 2 of Chapter 1. Due to the nature of vehicle dynamics being highly nonlinear, it is not straightforward to determine the global optimum. Moreover, the optimum vehicle dynamics varies depending on the objective of a specific vehicle. Therefore, even if it was possible to determine the global optimum, it is likely that such optimum remains "local" to a particular requirement. Often the final characteristics of a vehicle are decided by the preference of experienced and skilled test drivers. Establishing a link between this subjective and objective assessments has been performed in the past [Chen, 1996; Chen, 1997; Chen 1998], however there certainly are areas of investigation remaining.

In order to attempt the tasks mentioned, quantitative and analytical investigation of the dynamics is required. Thus the mathematical models of the system have to be established and applied appropriately. Moreover, as a vehicle has to be controlled dynamically by a driver, the application of control theories is also an essential subject.

2.2 Vehicle Dynamics Modelling

This section covers the derivation of the various models considered in this thesis. Most of the work has been designed and developed using the relatively simple models, bicycle and 3 Degrees-of-Freedom (3 DOF) vehicle handling models. It is important to keep the model degree of freedom as low as possible in order to avoid unnecessary complications and computational time. This is especially the case, where a relatively new theory / structure / system are being developed. However, at the same time, one has to make sure that the models represent the dynamic characteristics of the system well enough to meet the requirement of the project. For example, a fast dynamics mode, which decays very quickly, may be omitted from the model at the early stage of the project. It makes the computation

less demanding and yet the dynamics can remain effectively unchanged. More complex 10 Degrees-of-Freedom (10 DOF) model is used only when the algorithm is validated with lower Degree-of-Freedom models. This enables to apply the developed method in more challenging environment and hence closer to real life problems.

The axis system used in this thesis is right handed. The positive rotation is clockwise around the axis when viewed from the origin along the positive direction (as indicated by the direction of arrows). The origin of the co-ordinates is at the vehicle centre of gravity (C.G.) and is a vehicle fixed moving co-ordinate system. The picture of this axis system is shown in Figure 2.1 below.

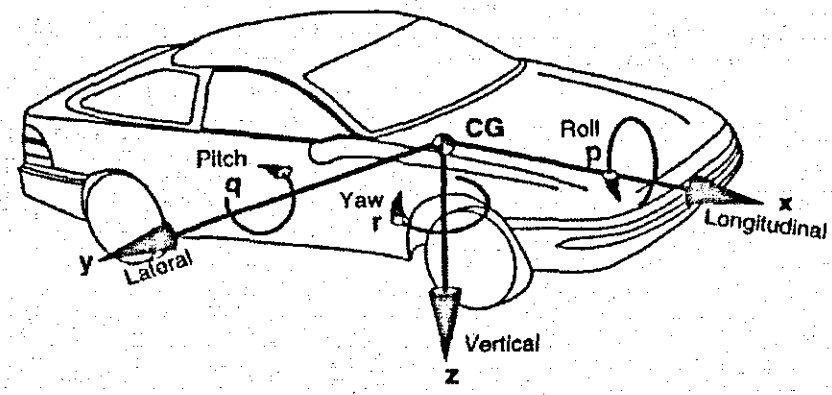

Figure 2.1 Vehicle Axis System [Gillespie, 1992]

2.2.1 Bicycle Handling Model

This well-known "Bicycle Model" is the simplest and the most fundamental form of vehicle handling models. It has yaw and lateral degrees of freedom, which provides the fundamental information required in the early stages of a development. The tyre slip angles purely arise from these two effects, together with the steering input as shown in Equations 2.3 and 2.4. The properties of the pair of wheels at each axle are represented by single wheels on the vehicle centre line. No weight transfer effects have been considered. The most significant use of

this model in the thesis is for Four-Wheel-Steer project described in Chapter 3. The concept of the model is shown in Figure 2.2.

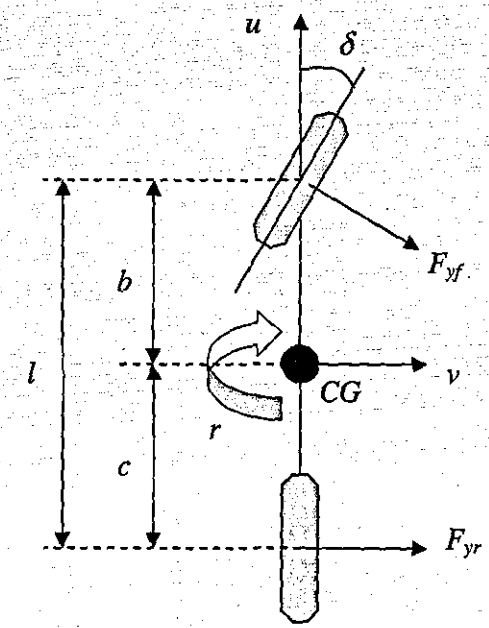

Figure 2.2 Bicycle Handling Model

Dynamic equations of motion are summarised in the following equations.

$$m(\dot{v}+ur) = F_{yf} + F_{yr} \tag{2.1}$$

$$I_{zz}\dot{r} = bF_{yf} - cF_{yr} \tag{2.2}$$

where the front and rear lateral forces are expressed as

$$F_{yf} = C_{\alpha f}\alpha_f = C_{\alpha f}\left(\delta_f - \left(v+br/u\right)\right) \tag{2.3}$$

$$F_{yr} = C_{\alpha r}\alpha_r = C_{\alpha r}\left(-\left(v-cr/u\right)\right) \tag{2.4}$$

System states are: $x = [r \quad v]'$

In the most basic form, the tyre cornering stiffness can be regarded as constant. However, nonlinear tyre model can also be applied depending on the objective of a work.

2.2.2 Three Degree of Freedom Model

This can be considered as the simplest model with lateral load transfer effect. On top of the bicycle model described in the previous section, an additional roll degree of freedom is introduced. It also incorporates nonlinearities due to lateral force saturation and the vertical load dependency through the use of a Pacejka 'magic formula' tyre model [Pacejka, 1989]. The roll freedom and lateral weight transfer dynamics of the vehicle results in the more realistic dynamic tyre loading information than that of the Bicycle model.

Since this model gives a suitable representation of lateral vehicle dynamics with the least complexity, this model is used for majority of work described in this thesis. Figure 2.3 shows the diagrammatic representation of 3DOF handling model.

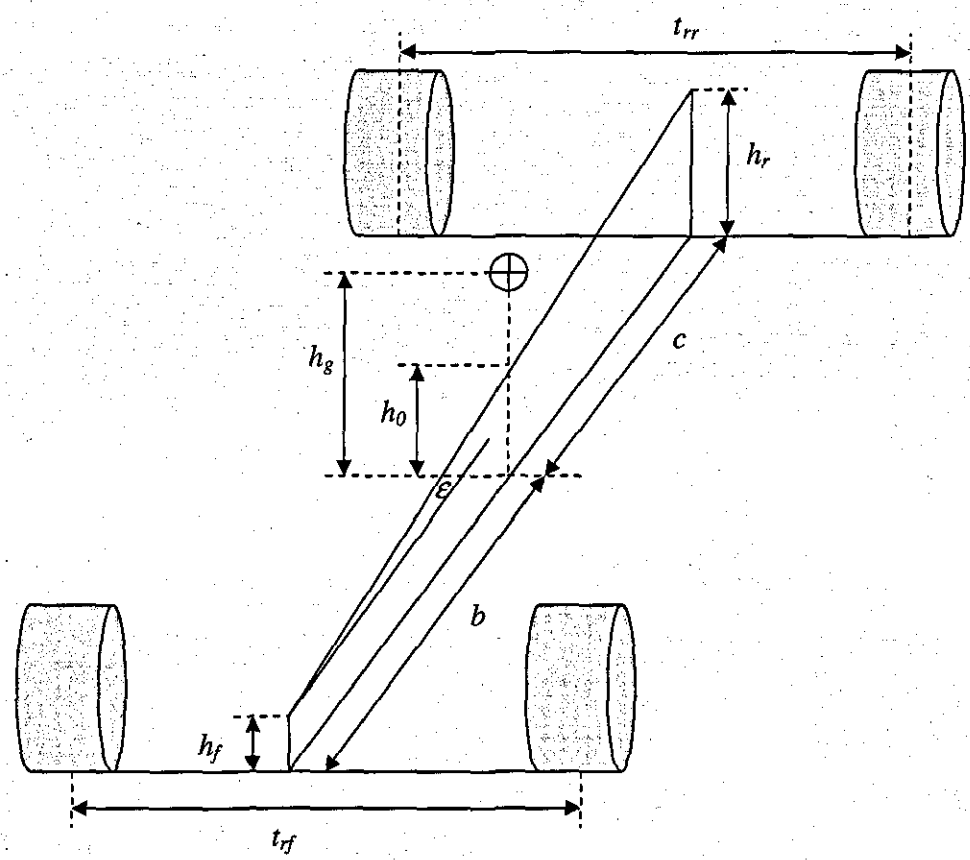

Figure 2.3 Three-degree of freedom Handling Model

The dynamic equations of motion for this system are derived as shown in equations 2.5 to 2.7.

$$m\left(\dot{v}+ur+h_g\dot{p}\right)=\overset{*}{F}_{yf}+\overset{*}{F}_{yr} \tag{2.5}$$

$$\begin{aligned} &mh_g(\dot{v}+ur)+\dot{p}(I_{xx}-\varepsilon I_{xz})-I_{xz}\dot{r}=(h_f-h_0)\overset{*}{F}_{yf} \\ &-(h_r-h_0)\overset{*}{F}_{yr}+\left(mgh_g-k_{\phi f}-k_{\phi r}\right)\phi-\left(b_{\phi f}+b_{\phi r}\right)p \end{aligned} \tag{2.6}$$

$$I_{zz}r+(\varepsilon I_{xz}-I_{xx})\dot{p}=b\overset{*}{F}_{yf}-c\overset{*}{F}_{yr} \tag{2.7}$$

System states are: $x=\begin{bmatrix} r & v & \phi & p \end{bmatrix}^t$

$\overset{*}{F}_f$ *and* $\overset{*}{F}_r$ denote the lateral forces computed using the Pacejka tyre model.

$k_{\phi f}$ and $k_{\phi r}$ represent the front and rear roll stiffness respectively, and are determined depending on the suspension types. Similarly, $b_{\phi f}$ and $b_{\phi r}$ are the roll damping at front and rear axles. Non-independent suspension is used for the model, hence the roll stiffness is determined as follows.

$$k_\phi=0.5*k*\left(k_{space}\right)^2$$

Front roll stiffness also includes the anti-roll-bar contribution. Roll damping can be determined in a similar manner. In (2.7), the effect of roll and yaw product of inertia is included with the roll axis inclination information.

2.2.3 Ten Degree of Freedom Model

In order to examine some of the method developed in this research, a manoeuvre including braking and acceleration is required. This is a natural progression when the method is validated with lateral dynamics model, such as 3DOF model described earlier.

The 10DOF model includes an additional freedom in longitudinal velocity state, together with the four corresponding unsprung mass rotation states. Moreover, the separate steer degrees of freedom are included for both left and right front tyres.

Pitch dynamics are not modelled in order to avoid computationally expensive calculation. Subsequently, the longitudinal weight transfer is determined only using the longitudinal force, not including the pitch velocity and displacement.

Newton-Euler Equation for this model is as shown below.

$$m\dot{u} = mrv + mrph_1 + F_x \tag{2.8}$$

$$m(\dot{v} + ur + h_1\dot{p}) = F_y \tag{2.9}$$

$$I_{zz}\dot{r} + (\varepsilon I_{zz} - I_{xz})\dot{p} = M_z \tag{2.10}$$

$$mh_1(\dot{v} + ur) + \dot{p}(I_{xx} - \varepsilon I_{xz}) - I_{xz}\dot{r} = M_x \tag{2.11}$$

System states for vehicle body are: $x = [u \quad r \quad v \quad \phi \quad p]$

For this model, slip angle calculations include the effect of yaw rate and roll rate as shown below.

$$\alpha_1 = \delta - \left(\frac{v + br - p(h_g - h_f)}{u + r\left(t_{rf}/2\right)} \right)$$

$$\alpha_2 = \delta - \left(\frac{v + br - p(h_g - h_f)}{u - r\left(t_{rf}/2\right)} \right)$$

$$\alpha_3 = \left(\frac{v - cr + p(h_g - h_r)}{u + r\left(t_{rr}/2\right)} \right)$$

$$\alpha_4 = \left(\frac{v - cr + p(h_g - h_r)}{u - r\left(t_{rr}/2\right)} \right)$$

2.2.4 Quarter Car Vehicle Ride Model

As well as all the handling models described previously, Quarter Car Vehicle Ride Model is also used in the project. This model is widely used as it contains the fundamental vertical dynamics of a vehicle. Dynamic load variation at the tyre contact patch and the isolation of sprung mass motion from road input can be analysed in detail. Thus it is often used in a design of the systems such as active suspension. In this thesis, the main objective of employing this model is to test and validate the control algorithms during the development stage. It is found to be a very effective tool to analyse the fundamental characteristics of the developed system, due to its relatively simple dynamics. Figure 2.4 shows the model structure of a single corner of a vehicle, hence Quarter Car, with respect to the vertical motion induced due to a road surface profile.

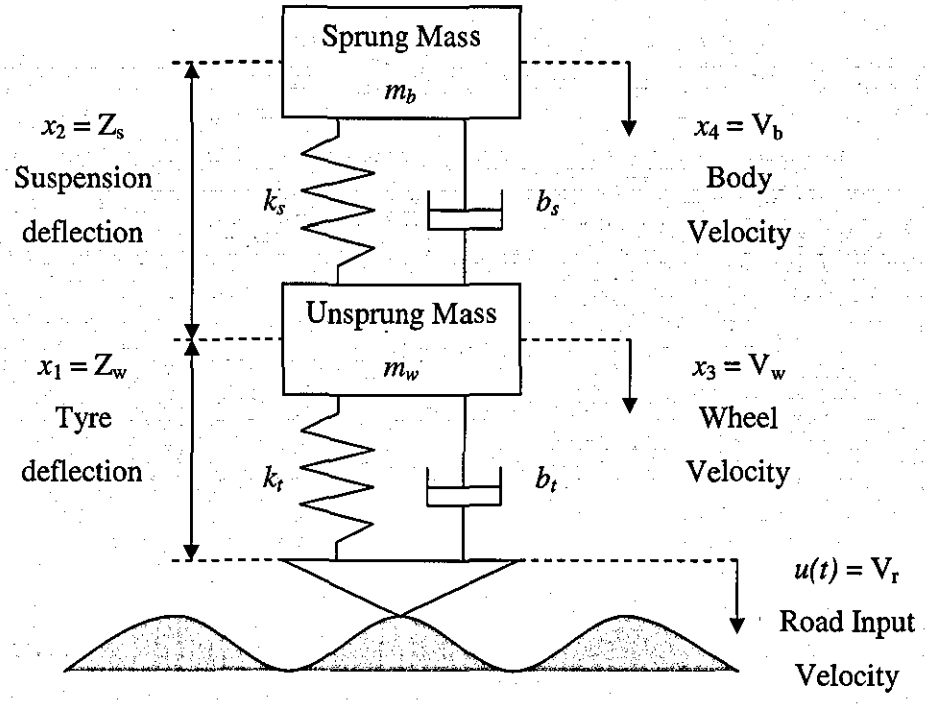

Figure 2.4 Quarter Car Vehicle Ride Model

As it is shown in the above figure, the system consists of sprung and unsprung masses. Passive suspension and tyre characteristics are expressed in terms of the stiffness and damping. Point contact is assumed between the tyre and the road.
The governing equations for the above system are as shown below.

Sprung mass: $m_b\ddot{z}_b = k_s z_s + b_s\dot{z}_s = k_s z_s + b_s(v_w - v_b)$

Unsprung mass: $m_w = -k_s z_s - b_s(v_w - v_b) + k_t z_w + b_t(v_r - v_w)$

System states are: $x = [z_w \quad z_s \quad v_w \quad v_b]'$

Following parameter values were used for this thesis.

Parameters	Notation	Values	Units
Sprung mass	M	290	kg
Unsprung mass	m	32	kg
Suspension stiffness	k_s	20000	N/m
Tyre vertical stiffness	k_t	140000	N/m
Suspension damping	b_s	1200	Ns/m
Tyre vertical damping	b_t	100	Ns/m

Table 2.1 Quarter Car Model Parameters

2.2.5 Tyre Model

All the handling models require a tyre performance model at least in terms of the tyre slip angles and cornering stiffness. The simplest model of all is a constant cornering stiffness gain, which is used for Bicycle model as mentioned in 2.2.1. In a 3 DOF model, lateral force saturation and vertical load dependency is included. For 10 DOF model, the longitudinal force calculation as well as the lateral force is required. Thus the tyre slip ratio is required as an input parameter. In this thesis, the tyre parameters are assumed to remain constant. In other words, the effect of tyre wear and degradation is not taken into account. Moreover, an empirical model is used rather than more physical based models. This is because the aim of this thesis is not to understand tyre dynamics itself, but to understand how to best use the given tyre characteristics in order to enhance the vehicle performance.

The SAE axis system [Dixon, 1997] shown in Figure 2.5 is employed in order to describe the operating condition in terms of forces and moments.

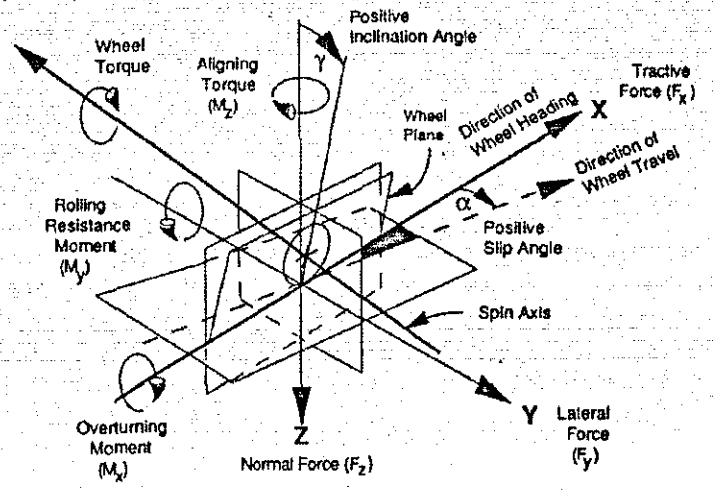

Figure 2.5 Tyre Axis System

Tyre model used in this thesis is based on the Pacejka "magic formula" as mentioned in Section 2.2.2; the governing equation is shown in (2.12).

$$y(x) = D\sin\left\{Ca\tan\left[Bx - E\left(Bx - a\tan(Bx)\right)\right]\right\} \tag{2.12}$$

$$y(x) = y(x) + S_v$$

$$x = x + S_h$$

[Pacejka et al, 1989]

The product of B, C and D values determines the initial slope of the curve, hence determines the linear cornering stiffness in the case of lateral force calculation. The coefficient E, curvature factor, controls the shape of the curve around the peak in a way that the stiffness and the peak value remain unaffected. It also controls the value of slip angle or ratio at which the maximum force or moment occurs. The shape factor C defines the limits of the argument of the sine function. This value is varied in order to fit the curve depending on whether it is for lateral force, longitudinal force or self-aligning moment. For a passenger car, the typical C values are known to be 1.30, 1.65 and 2.40 respectively, which are practically

independent of vertical loads [Pacejka et al, 1987; Pacejka et al, 1989]. Curvature factor, E, was set at -1.29. Horizontal and vertical shift of the curve occurs in the presence of ply steer and conicity effects. In addition, rolling resistance also gives the offset to longitudinal force characteristics. Raw data is often supplied in terms of more detailed coefficients, which can then used to calculate the above four parameters. An example of these calculations for lateral force is shown below. It is clear from (2.13) and (2.14) that the effect of vertical load on the peak force is included. Moreover the camber angle influence on the cornering can also be seen in (2.14), although it was set to zero within this study. Parameter values used for the lateral force calculation is shown in Table 2.2.

$$D = (a_1 F_z + a_2) F_z \tag{2.13}$$

$$BCD = a_3 \sin\left\{2a \tan\left(F_z / a_4\right)\right\}\left(1 - a_5 |\gamma|\right) \tag{2.14}$$

Notation	Description	Values
a_1	Load dependency of friction level	-0.042
a_2	Friction level	1.028
a_3	Maximum cornering stiffness	1050
a_4	Fz at maximum cornering stiffness	6000
a_5	Camber dependency of cornering stiffness	0

Table 2.2 Pacejka Tyre Model Parameters

In a case of combined slip model, the input value is expressed as a combination of the slip angle, α, and the longitudinal slip, k. Figure 2.6 shows a plan view of a tyre when it is subjected to a combined braking and cornering [Pacejka, 1989]. The calculations of the input values are as shown in Equations (2.15) to (2.19).

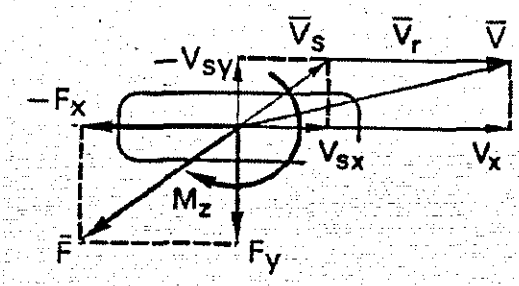

Figure 2.6 Tyre Force and Moment Vector Diagram

Longitudinal Slip Velocity: $V_{sx} = kV_x$ (2.15)

Rolling Velocity: $V_r = V_x - V_{sx}$ (2.16)

Lateral Slip Velocity: $V_{sy} = V_x\{\tan(\alpha)\}$ (2.17)

Longitudinal, Lateral Theoretical Slip: $\sigma_{(x,y)} = {V_{(sx,sy)}}/{V_r}$ (2.18)

Resultant Slip: $\sigma = \sqrt{\left(\sigma_{(x)}{}^2 + \sigma_{(y)}{}^2\right)}$ (2.19)

The resultant Forces are then calculated as shown in Equation 2.21, where $F(\sigma)$ denotes the solution of (2.12) with σ as an input variable.

$$F_{(x,y)} = -\left({\sigma_{(x,y)}}/{\sigma}\right)F(\sigma) \quad (2.20)$$

[Pacejka et al, 1989]

Finally, the force generation takes an exponential manner when a step change is made to an input value, and is a function of inflation pressure and rolling speed of the tyre. This effect is modelled simply as a constant time delay of 0.01 seconds, the velocity dependency is not included for simplicity.

Figure 2.7 shows the effect of vertical load on the tyre forces. It is clear that the cornering stiffness is affected as well as the peak magnitude. Hence, the slip ratio at which the peak force is produced also varies depending on the vertical load. Moreover, it can be seen that the increase in cornering stiffness with regard to the

increase in vertical load is nonlinear. Understanding of these characteristics is essential in developing control systems. For instance, the traction control strategy need to take this peak slip ratio variation with respect to the vehicle speed (vertical load).

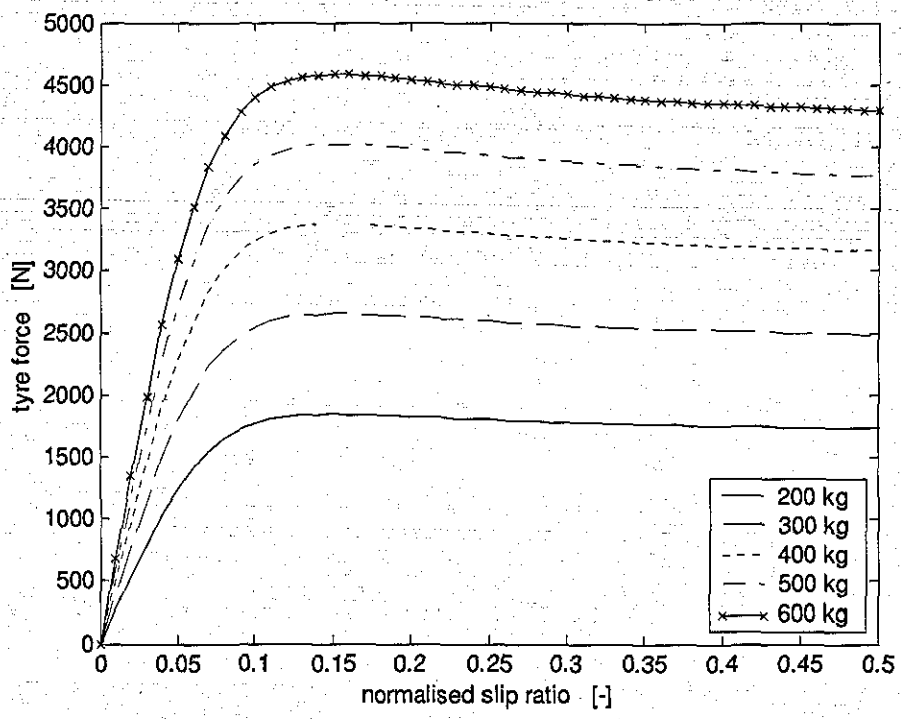

Figure 2.7 Vertical Load Effect on Tyre Forces

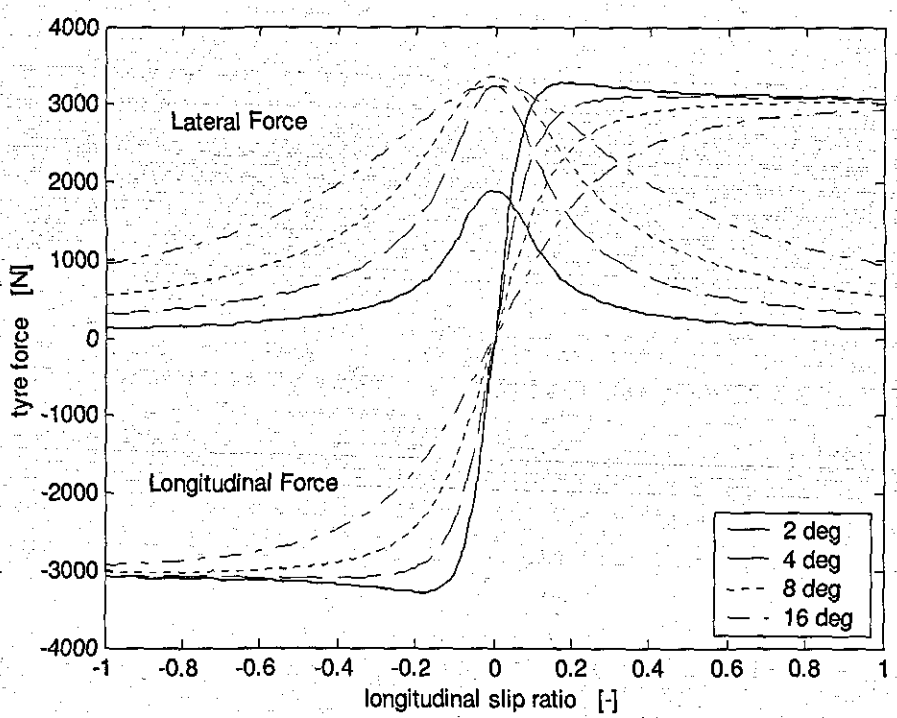

Figure 2.8 Combined Slip Effect on Tyre Forces

Figure 2.8 shows the effect of slip angle and slip ratio on tyre forces. Longitudinal force decreases, and its point of peak magnitude is shifted as the slip angle increases. Nonlinear relationship between slip angle and lateral force can also be noticed. For the very large slip angle, magenta line, it is shown that the peak lateral force is reduced at zero longitudinal slip. The part of Figure 2.8 which shows the combined slip effect on lateral force is re-plotted using 3D surface map as shown in Figure 2.9.

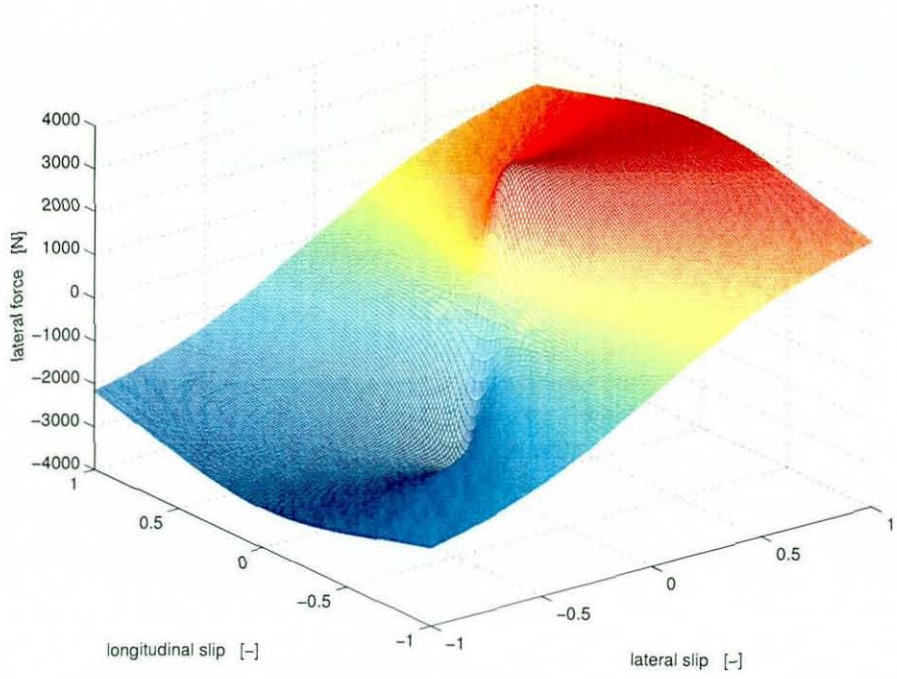

Figure 2.9 Three-Dimensional Lateral Force Map

2.3 Fundamental Analysis of Vehicle Dynamics

In order to investigate the vehicle dynamics characteristics analytically, the system equations are manipulated in a way so that the effect of parameters on the vehicle behaviour is more apparent. Simple bicycle model analysis is summarised in Section 2.3.1 and is used for all the vehicle set-ups. Simulations in both steady-state and transient conditions are also performed, and the results are discussed with reference to the analytical results. From these simulations, effects of vehicle set-up change in the subsequent performance can be analysed both in trend (directions) and quantity (sensitivity). Moreover, the validity and limitations of the simplified models are investigated by performing comparable simulations. This information is then used when assessing a vehicle-controller performance, and is described in the later part of this thesis.

2.3.1 Bicycle Model Linear Analysis

The most fundamental form of handling characteristics can be represented by the curve of steering angle against lateral acceleration. Steering angle to negotiate a given radius of curvature is defined as follows [Dixon, 1997].

$$\delta = \frac{L}{R} + \delta_U a_y \tag{2.21}$$

The first term in (2.21) is often refereed as the kinematic steering angle where there is no lateral acceleration present. The second term represents the amount of correction required to keep a vehicle on a given radius at various lateral accelerations. *Understeer gradient* is defined as the amount of steering correction required with respect to the neutral steer angle for given lateral acceleration. Using (2.3) and (2.4) shown earlier, *Understeer Gradient*, K, is defined as shown in (2.22) [Dixon, 1997].

$$K = \frac{d\delta_U}{da_y} = \frac{m}{l}\left(\frac{c}{C_{\alpha f}} - \frac{b}{C_{\alpha r}}\right) \tag{2.22}$$

Derivation of (2.22) is included in Appendix 1 at the end Chapter 2.
This concept of *Understeer Gradient* is used in the analysis of steady-state handling characteristics in Section 2.3.2.

Recall Equations (2.1) and (2.2) for bicycle model. By substituting the front and rear lateral force definitions in terms of cornering stiffness, the following equations can be defined for translational and rotational dynamics.

$$m\dot{v} + \left(\frac{C_{\alpha f} + C_{\alpha r}}{u}\right)v + \left(\frac{bC_{\alpha f} - cC_{\alpha r}}{u} + mu\right)r = 0 \tag{2.23}$$

$$I_{zz}\dot{r} + \left(\frac{bC_{\alpha f} - cC_{\alpha r}}{u}\right)v + \left(\frac{b^2C_{\alpha f} + c^2C_{\alpha r}}{u}\right)r = 0 \tag{2.24}$$

The characteristic equation (C.E.) for this system is written as shown in (2.25), [Abe, 1992], with D representing a state derivative with respect to time.

$$mI_{zz}D^2+\left(\frac{mC_2+I_{zz}C_0}{u}\right)D+\left(\frac{C_0C_2-C_1^2}{u^2}-mC_1\right)=0 \qquad (2.25)$$

C terms denote the zeroth, first and second moments of the tyre cornering stiffness about the centre of gravity, as shown below.

$$C_0 = 2*(C_{\alpha f}+C_{\alpha r})$$

$$C_1 = 2*(b*C_{\alpha f}-c*C_{\alpha r})$$

$$C_2 = 2*(b^2*C_{\alpha f}+c^2*C_{\alpha r})$$

Dynamic stability is governed by the sign of the first derivative term, damping coefficient, being positive. From (2.25) and the definition of C_0 and C_2, it is clear that the dynamic stability is guaranteed for all positive vehicle forward velocity, u. By contrast, static stability is only conditional, dictated by the following inequality.

$$C_0C_2 > C_1^2 + C_1mu^2 \qquad (2.26)$$

From the definition of understeer gradient, (2.22), it can be seen that C_1 is negative for an understeer vehicle. Hence, (2.26) holds for all vehicle forward velocity. However, for an oversteer vehicle, with positive C_1, following condition has to be met in order to satisfy (2.26).

$$u^2 < \frac{C_0C_2-C_1^2}{C_1m} \quad \text{or} \quad u^2 < \frac{l^2C_{\alpha f}C_{\alpha r}}{C_1m}$$

Therefore the critical velocity, U_{crit}, at which the vehicle becomes unstable, is defined as shown in (2.27) below [Dixon, 1997].

$$U_{crit} = \sqrt{\frac{C_0C_2-C_1^2}{C_1m}} = \sqrt{\frac{l^2C_{\alpha f}C_{\alpha r}}{C_1m}} = \sqrt{\frac{l}{-K}} \qquad (2.27)$$

From (2.25) and the definition of standard second order system C.E., undamped yaw natural frequency, ω_n, for the bicycle model is defined as

$$\omega_n = \sqrt{\frac{\left(\frac{C_0 C_2 - C_1^2}{u^2} - mC_1\right)}{mI_{zz}}} \tag{2.28}$$

From (2.27), it is clear that ω_n goes to zero at the critical velocity. For a neutral steer vehicle, (2.28) can be simplified as C_1 is zero. Equation (2.28) also shows that the natural frequency decreases as the forward velocity increases, regardless to the handling characteristics of the vehicle. In terms of steady-state balance change, the frequency decreases as the vehicle is set to oversteer more.

Yaw damping is discovered to have a significant influence on vehicle's path following ability [Hogg, 1992]. It is represented in the second term in (2.25) and with the definition of 2nd order system C.E., the yaw damping ratio is defined as follows.

$$\zeta = \frac{mC_2 + I_{zz}C_0}{2umI_{zz}\omega_n} \tag{2.29}$$

Substituting the definition of undamped natural frequency from (2.28) and the critical velocity from (2.27) into (2.29) yields

$$\zeta = \frac{mC_2 + I_{zz}C_0}{2mI_{zz}\sqrt{\left(\frac{C_1}{I_{zz}}\right)}\sqrt{U_{crit}^2 - u^2}} = \frac{U_d}{\sqrt{U_{crit}^2 - u^2}} \tag{2.30}$$

where the characteristic damping velocity, U_d, is defined as

$$U_d = \frac{mC_2 + I_{zz}C_0}{\sqrt{4m^2 I_{zz}C_1}} = \frac{C_2 + k^2 C_0}{\sqrt{4I_{zz}C_1}} \tag{2.31}$$

where k is a yaw radius of gyration.

Hence, by rearranging (2.30), the damping ratio is

$$\zeta = \frac{U_d / U_{crit}}{\sqrt{1 - u/U_{crit}^2}} = \frac{\zeta_0}{\sqrt{1 - u/U_{crit}^2}} \tag{2.32}$$

where ζ_0 indicates the damping ratio at zero velocity.

$$\zeta_0 = \frac{U_d}{U_{crit}} = \frac{C_2 + k^2 C_0}{\sqrt{4k^2\left(C_0 C_2 - C_1^2\right)}}$$

In addition to the above calculations, *Prodrive* found that the *Dynamic Index* has a good correction with the subjective rating of vehicles [Waterhouse, 2002].

$$D_{index} = \frac{k^2}{bc} \tag{2.33}$$

Rearranging (2.33) with the definition for radius of gyration, the relationship between the yaw moment of inertia, vehicle mass and its weight distribution is formed.

$$I_{zz} = (bcm) D_{index} \tag{2.34}$$

The product of b and c is maximum when they are equal, in other words when 50:50 weight distribution is achieved. Thus according to (2.34), assuming the mass is constant, more unequal the weight distribution and smaller the *Dynamic Index* are, smaller the resultant yaw moment of inertia is. *Prodrive* found that the dynamic index of 0.92 corresponds to most of "good handling" production vehicles and has good correlation with subjective assessments. This represents a compromise between minimising phase delay between yaw rate and lateral acceleration, while preventing a significant increase in yaw acceleration magnitude [Waterhouse, 2002].

It is obvious from (2.34) that the identical value of *Dynamic Index* can be obtained at different weight distribution with the yaw inertia remaining unchanged. As shown in Figure 2.10, it implies that the equal subjective handling quality is achieved with significantly different handling balance (i.e. the values are identical for both 40% and 60% weight distribution).

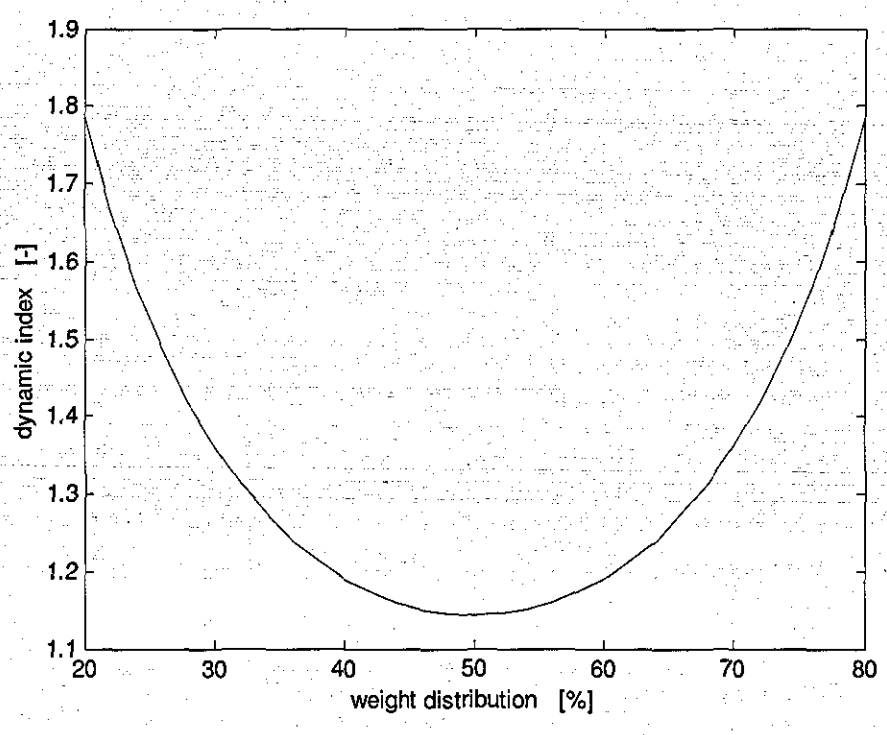

Figure 2.10 Dynamic Index

2.3.2 Summary of Vehicle Settings

This section lists and summarises the original and altered vehicle settings used in this thesis. Table 2.3 below shows the reference vehicle, Vehicle "A", setting. Values are chosen to represent typical saloon type vehicle.

Parameters	Notation	Values	Units
Total vehicle mass	m	1400	kg
Wheelbase length	l	2.5	m
Roll moment of inertia	I_{xx}	200	kgm^2
Yaw moment of inertia	I_{zz}	2500	kgm^2
Product of inertia	I_{xz}	0	kgm^2
Centre of Gravity height	h_g	0.6	m
Distance of C.G. to front axle	b	1.07	m
Front Track width	t_f	1.5	m
Rear Track width	t_r	1.5	m
Front Spring stiffness	k_f	20000	N/m
Rear Spring Stiffness	k_r	22000	N/m
Front Anti-Roll-Bar Stiffness	$stab$	400	Nm/deg
Front Damper	b_f	1100	kNs/m
Rear Damper	b_r	1200	kNs/m
F/R roll centre	h_f, h_r	0.2, 0.5	m

Table 2.3 Reference Vehicle (Vehicle "A") Setting

Table 2.4 summarises the altered parameters on the seven comparison vehicle set-ups. The vehicles B, C, D and E are set-up so that their steady-state characteristics are different with varying front to rear weight distribution. The vehicles F, G, and H are set-up to investigate the effect of transient dynamics change through the yaw inertia variation. For each vehicle, only one parameter is varied in order to investigate its effect clearly. The results of these changes on the fundamental

vehicle characteristics described in previous section are shown in the following sections.

	Altered Paramter	Notation	Value	Unit
Vehicle B	Distance of C.G. to front axle	b	0.9375	m
Vehicle C	Distance of C.G. to front axle	b	0.8750	m
Vehicle D	Distance of C.G. to front axle	b	1.2500	m
Vehicle E	Distance of C.G. to front axle	b	1.5000	m
Vehicle F	Yaw moment of inertia	I_{zz}	2862.9	kgm^2
Vehicle G	Yaw moment of inertia	I_{zz}	2142.1	kgm^2
Vehicle H	Yaw moment of inertia	I_{zz}	1820.8	kgm^2

Table 2.4 List of Vehicle Parameter Changes

Following is the list of the performance parameters. These parameters are chosen as they could provide further insight into the dynamics of a vehicle. The corresponding values for the each test vehicles are shown in Table 2.4 for the steady-state change and Table 2.5 for the transient parameter change.

1) Front Mass Distribution
2) Yaw Radius of Gyration
3) Yaw Natural Frequency at 25 m/s
4) Yaw Damping at 25 m/s
5) Dynamic Index
6) Characteristic / Critical Velocity

From Table 2.5, it can be seen that the yaw natural frequency decreases as the vehicle balance is moved towards oversteer. The vehicle E has its critical velocity at 25 m/sec, at this speed the yaw natural frequency goes to zero, indicates the yaw response from this point onwards is non-oscillatory. All understeering vehicles are under-damped in yaw degree of freedom. As Vehicles A, B and C have fundamentally understeer balance, their characteristic speeds are noted. This

speed reduces as the understeer becomes stronger. As explained in the previous section, Dynamic index is at its minimum with 50:50 weight distribution.

Index	Unit	C	B	A	D	E
Balance (us / os)	--	us	us	**us**	os	os
Mass Distribution	%	65.0	62.5	**57.0**	50.0	40.0
Yaw Natural Frequency	Hz	1.07	1.02	**0.89**	0.68	0.02
Yaw Damping	---	0.74	0.77	**0.87**	1.14	53.02
Dynamic Index	---	1.256	1.219	**1.167**	1.143	1.190
Characteristic/Critical Velocity	m/s	25.90	29.10	**43.5**	52.50	25.00

Table 2.5 Vehicle Performance Parameters: Steady-State Change

The vehicle "F" is set up so that the yaw radius of gyration equals to the distance between CoG to rear axle. According to Chen and Crolla's findings [Chen, 1996], it is found that the vehicles with such a set-up are deemed to "handle well" subjectively. Undamped yaw oscillation frequency increases with the decreasing yaw inertia. Vehicle "G", which has approximately 14% reduction in yaw inertia, has the lowest yaw damping. Dynamic index decreases as the yaw inertia decreases, note that Vehicle "H" is the only vehicle that has a smaller value than Prodrive's magic number of 0.92.

	Units	F	A	G	H
Yaw Radius of Gyration	m	1.430	**1.336**	1.237	1.140
Yaw Natural Frequency	Hz	0.83	**0.89**	0.96	1.04
Yaw Damping		0.878	**0.872**	0.870	0.874
Dynamic Index	---	1.336	**1.167**	1.000	0.850

Table 2.6 Vehicle Performance Parameters: Transient Change

2.3.3 Steady-State Analysis

Steady-state analysis is carried out using a constant forward velocity of 20m/s with gradually increasing steering angle at the rate of 1/3 degrees per second. In order to ensure the absence of transient dynamics, this steering rate has to be kept low. The result is analysed in terms of understeer and oversteer terminology. Understeer is defined as the vehicle whose steer angle has to be increased as the lateral acceleration increases, in order to negotiate a given cornering radius. Similarly, an oversteering vehicle requires the steering angle to be reduced to track a given radius as lateral acceleration increases. The neutral steer angle is determined with respect to the normalised lateral acceleration, $\overline{a}_y$, and is shown in (2.35) [Dixon, 1997].

$$\delta_{ns} = \left(gl/u^2\right)\overline{a}_y \tag{2.35}$$

where the normalised lateral acceleration, $\overline{a}_y$, is defined as

$$\overline{a}_y = \left(u^2/(gR)\right) = (ur)/g$$

The relationship between the steering angle and the actual lateral acceleration experienced during the test is defined in terms of a polynomial of an appropriate order. The first derivative of the polynomial is then used to determine the *Understeer Gradient* of a vehicle as shown in (2.22).

The blue line in Figure 2.11 shows the understeer gradient of vehicle "A". It is clear that the vehicle has slight understeer characteristics for the majority of lateral acceleration range. The understeer becomes more significant beyond the moderate lateral acceleration range and finally reaches the terminal understeer at around 0.8g. Terminal understeer is exhibited when no increase in lateral acceleration can be achieved with the further increase of steering angle [Dixon, 1997].

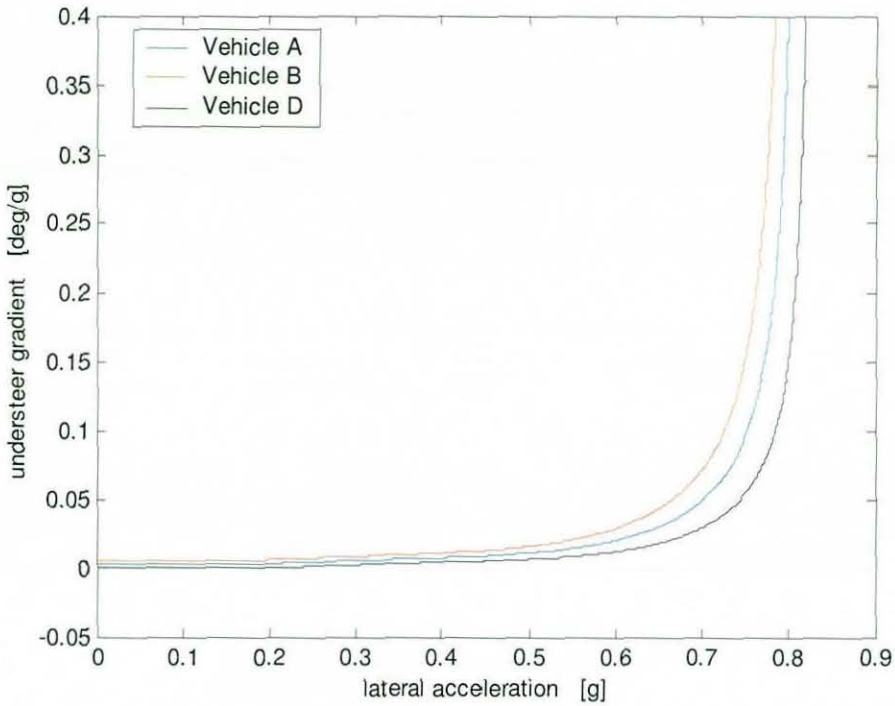

Figure 2.11 Influence of Weight Distribution Change on Understeer

Figure 2.11 also shows the variation in understeer gradient due to the fore/aft weight distribution change. A vehicle exhibits more understeer when the front axle weight is increased, shown by Vehicles B trajectory. This is due to the decrease in the total lateral force generated for a given steering angle. Hence the steering has to be increased further to achieve a lateral acceleration of neutral steer vehicle. This undesirable effect comes from the reduced slip angles at both front and rear tyres when the front axle weight is increased. Although the lateral weight transfer is reduced at both axles, the reduced slip angle at the rear results in significant decrease in lateral force generated from rear axle. It has to be noted that the lateral force at front axle increases despite the reduced slip angle, this is due to the static vertical load available. However, this is not enough to compensate the lack of lateral force at rear axle. Hence the reduction in total lateral force.

A great deal of care needs to be taken on the interpretation of terminology. Above case follows the understeer/oversteer definition defined earlier in terms of steering angle and lateral acceleration. However, the terminology is sometimes referred to the balance of lateral forces between the front and rear axles. If such cases, increasing front axle weight is actually referred as an oversteering effect. Although the total lateral force and hence lateral acceleration per steering angle is decreased, the ratio of lateral force generated from the front axle is far greater due to the tyre vertical load dependency.

2.3.4 Transient Analysis

Transient characteristics of a vehicle is analysed using a 2 degrees step of steer input at the constant forward velocity of 20 m/s. As the true step change cannot be applied in testing, the simulated input can be filtered through first order time delay in order to obtain more realistic data. However, it is not applied in this study for the clarity of analysis.

Figure 2.12 shows the effect of weight distribution variation on yaw rate response. Little overshoot is observed for the vehicles A, B and C, which indicate understeer characteristics [Dixon, 1997]. Understeer/Oversteer characteristics can also be determined from this test using a steady-state yaw rate value. As the vehicle dynamics is changed towards steady-state oversteer, the overshoot disappears and also steady-state values are reached at later time. Clearly, this increases 90% rise-time which is undesirable. Therefore vehicles A, B and C are said to have more desired dynamics since the overshoot is kept minimum for all the vehicles.

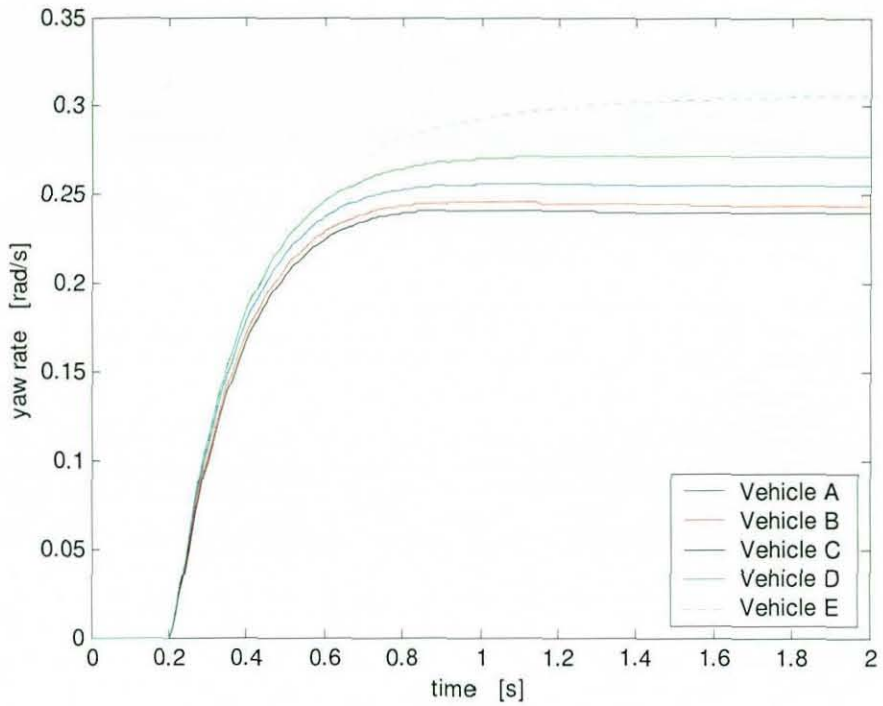

Figure 2.12 Influence of Weight Distribution Change on Yaw Response

Theoretical yaw rate gain is defined as the ratio between yaw rate and steering angle, and is formulated as shown in (2.36).

$$Gr(u) = \frac{r}{\delta} = \frac{u}{l + \left(Ku^2 / g \right)} \tag{2.36}$$

In the case of a neutral steer vehicle, the understeer gradient, K, would be zero. Thus it simply becomes the ratio between vehicle forward velocity and wheelbase. The neutral steer yaw rate is calculated to be 0.279 rad/s for the simulated vehicle forward velocity. Based on this calculation, vehicle D has the handling characteristics closest to the neutral steer. As the largest steady-state yaw rate achieved from vehicles A, B and C is 0.265 rad/s, it can be said that these vehicles exhibit understeer. Overshoot response can be seen with these understeer vehicles. The speed at which the overshoot occurs depends on static margin and yaw radius of gyration. As the static margin (and hence more understeer) increases, the response starts becoming oscillatory at lower speed. In a case of an oversteering

vehicle such as vehicle E, no overshoot exists as the vehicle is over damped in yaw. However, it takes longer to reach steady-state.

One of the most important parameters in the transient dynamics is a yaw moment of inertia and associated yaw radius of gyration. Clearly high yaw moment of inertia slows down a vehicle in yaw degree of freedom. Hence, it is not a desirable as it makes it more difficult to transfer the vehicle from one state to the other. It can also be described dull subjectively. On the other hand, if it is too low, then a driver would not be able to control a vehicle as it requires the control input with much more accuracy in both magnitude and phase.

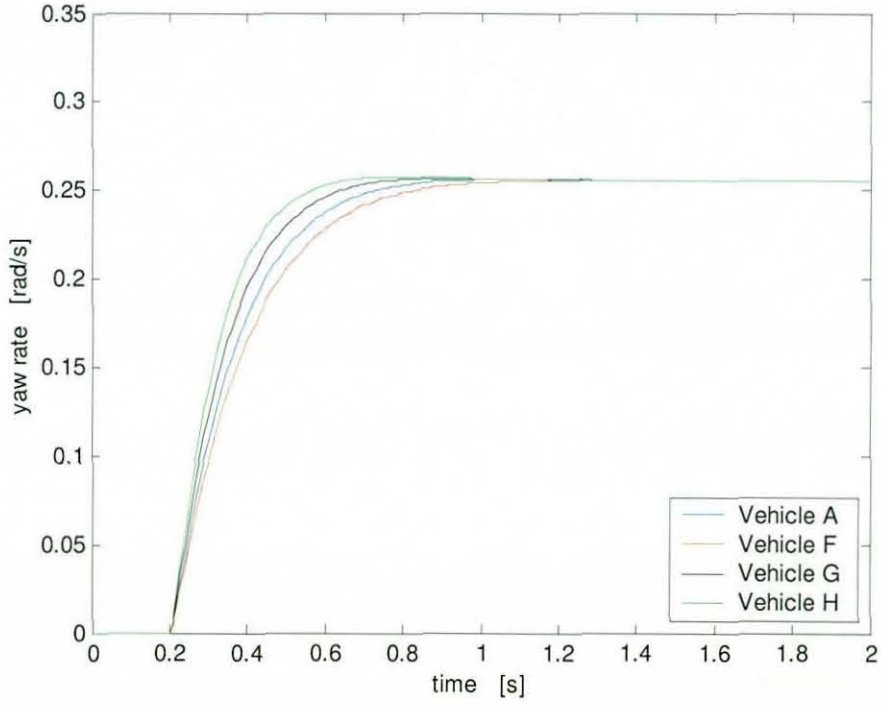

Figure 2.13 Influence of Yaw Moment of Inertia change on Yaw Response

Figure 2.13 shows the effect of varying yaw moment of inertia values. It does not change the steady-state value as it only has an effect on the transient dynamics. The red line shows the response of vehicle F, where the yaw radius of gyration is equal to the distance between C.G. and the rear axle. This set-up provides minimum yaw damping [Dixon, 2004] which in turn has a significant influence on

vehicle's path following ability [Hogg, 1992]. Vehicle G has *Dynamic Index* equal to one, meaning that the yaw oscillation centre lies on the rear axle. Finally, vehicle G has the smallest yaw moment of inertia, hence the quick yaw rate response shown. This fast response is achieved with the expense of increased overshoot magnitude.

2.4 Control Theories

There are various control theories applied successfully in the area of vehicle dynamics as mentioned in Chapter 1. In this thesis, focus is on linear control theories since it can be investigated more analytically. In addition, its ability to guarantee the optimality for a given environment is another advantageous factor. It has to be noted that it is not an objective of this thesis to iterate and then conclude the best controller (control theory) for a given application. However, the objective is to apply a linear control theory with modifications if required, and to establish a methodology so that linear optimal control can be used successfully in highly nonlinear environment.

2.4.1 Linear Quadratic Regulator (LQR)

Consider the linear time-invariant system

$$\dot{x} = Ax + Bu \tag{2.37}$$

Seek a control law $u(t) = -Kx(t)$, which minimises the following cost function.

$$J = \int_0^\infty \left(x^T Q x + u^T R u\right) dt \tag{2.38}$$

Solution is obtained by solving an *algebraic Riccati Equation* [Barnett, 1985]

$$0 = -PA + PBR^{-1}B^T P - Q - A^T P \tag{2.39}$$

P is the unique r.s.p.d. matrix which satisfies (2.39). The existence of solution and its condition is only ensured when the system (2.37) is *completely controllable* and $\begin{bmatrix} A & Q_1 \end{bmatrix}$ is *completely observable*.

Control input is then given as shown in (2.40), [Barnett, 1985], on the assumption that the control weighting matrix R is non-singular, hence invertible.

$$u = -R^{-1}B^T Px = -Kx \tag{2.40}$$

Substituting (2.40) into (2.37) gives the closed system equation as

$$\dot{x} = \left(A - BR^{-1}B^T P\right)x = \overline{A}x \tag{2.41}$$

For the cases where a cross term between input and state variables is also present, the cost function is expressed as

$$J = \int_0^\infty \left(x^T Qx + u^T Ru + 2x^T Nu\right)dt \tag{2.42}$$

N term controls the coupling effect of input and state variables [Barnett, 1985]. Algebraic Riccati equation in (2.39) can be written using $\overline{A}$ in Equation (2.41)

$$0 = -\hat{P}\overline{A} + \hat{P}BR^{-1}B^T\hat{P} - \overline{Q} - \overline{A}^T\hat{P} \tag{2.43}$$

Re-writing Equation (2.43) with the original state matrix, A, yields

$$0 = -PA + \left(PB + N\right)R^{-1}\left(B^T P + N^T\right) - Q - A^T P$$

Control input is given as

$$u = -\left(R^{-1}B^T P + R^{-1}P\right)x = -Kx$$

[Barnett, 1985]

Linear time-invariant (LTI) optimal control is used to design a Four-Wheel-Steer (4WS) reference model controller, and is presented in Chapter 3.

2.4.2 Time-Variant Linear Optimal Control

In order to deal with the nonlinearity, piece-wise linear models can be used to describe the vehicles at various operating conditions. This is thought to be a good compromise as it still retains the analytical capability of linear approach, while better representing the actual dynamics. Accordingly, a time-varying controller is required that is based on the piece-wise linear models. In this section, the linear time-varying (LTV) optimal control theory is introduced.

Consider the time varying system

$$\dot{x}(t) = A(t)x(t) + B(t)u(t) \tag{2.44}$$

with a performance criterion

$$J(u) = \frac{1}{2}x^T(t_f)Mx(t_f) + \frac{1}{2}\int_0^{t_f}\left[x^TQx + u^TR(t)u\right]dt \tag{2.45}$$

R is a real symmetric positive definite matrix, and M and Q are real symmetric positive semidefinite matrices. M is a cost on the state at the final time, t_f, to either regulate or track the desired state value. The matrix is only positive semidefinite when some of the desired state values are not specified, in other words, when the corresponding elements of M will be zero. [Barnett, 1985]

Using the Lagrange multiplier to establish the relationship between the system and the constraints, the Hamiltonian, $H(x,u,t) = F(x,u,t) + p^T f$, is defined as

$$H = \frac{1}{2}x^TQx + \frac{1}{2}u^TRu + p^T(Ax + Bu)$$

The significance of using Lagrange multiplier is that it allows to replace the problem of determining the minima of f subject to the constraints $g_i = 0$, j=1,2, …, m, with the problem of determining the minima of the function

$$G(x, p_1, p_2, \ldots, p_m) = f(x) + p_1g_1(x) + p_2g_2(x) + \ldots + p_mg_m(x)$$

The necessary condition, $\left(\frac{\partial H}{\partial u_i}\right)_{u=u^*} = 0$ [Barnett, 1985], for optimality gives

$$\frac{\partial}{\partial u}\left[\frac{1}{2}(u^*)^TRu^* + (p^*)^TBu^*\right] = Ru^* + B^Tp^* = 0$$

so that

$$u^* = -R^{-1}B^Tp^* \tag{2.46}$$

$R(t)$ being non-singular since it is positive definite.

The adjoint equations, $\dot{p}_i = -\frac{\partial H}{\partial x_i}, i = 1,2,\ldots,n$, are

$$\dot{p}^* = -Qx^* - A^T p^* \tag{2.47}$$

p is some as yet unspecified piecewise continuous *n-vector-valued* function, and is called as the *costate*, or *adjoint*, vector.

Substituting (2.46) into (2.44) gives

$$\dot{x}^* = Ax^* - BR^{-1}B^T p^*$$

and combining this equation with the adjoint equations in (2.47) produces the system of $2n$ linear equations *Hamilton's equation*

$$\frac{d}{dt}\begin{bmatrix} x^*(t) \\ p^*(t) \end{bmatrix} = \begin{bmatrix} A(t) & -B(t)R^{-1}(t)B^T(t) \\ -Q(t) & -A^T(t) \end{bmatrix}\begin{bmatrix} x^*(t) \\ p^*(t) \end{bmatrix} = H\begin{bmatrix} x^*(t) \\ p^*(t) \end{bmatrix} \tag{2.48}$$

H = Hamiltonian Matrix

Since $x(t_f)$ is not specified, the boundary condition is $p_i(t_f) = \left(\frac{\partial \phi}{\partial x_i}\right)_{t=t_f}$, with $\phi = \frac{1}{2}x^T Mx$, i.e.

$$p^*(t_f) = Mx^*(t_f) \tag{2.49}$$

[Barnett, 1985]

It is convenient to express the solution of (2.48) using the state transition matrix, $x(t) = \Phi(t, t_0)x(t_0)$, but in terms of the conditions at time t_f, i.e.

$$\begin{bmatrix} x^*(t) \\ p^*(t) \end{bmatrix} = \Phi(t, t_f)\begin{bmatrix} x^*(t_f) \\ p^*(t_f) \end{bmatrix} = \begin{bmatrix} \phi_1 & \phi_2 \\ \phi_3 & \phi_4 \end{bmatrix}\begin{bmatrix} x^*(t_f) \\ p^*(t_f) \end{bmatrix} \tag{2.50}$$

where Φ is the transition matrix for (2.48). Hence, using the relationship between the costate and final state cost in (2.49), the following definition can be derived.

$$x^*(t) = \phi_1 x^*(t_f) + \phi_2 p^*(t_f) = \phi_1 x^*(t_f) + \phi_2 Mx^*(t_f) = (\phi_1 + \phi_2 M)x^*(t_f) \tag{2.51}$$

Using (2.51), with (2.49) and (2.50) also gives

$$p^*(t) = (\phi_3 + \phi_4 M)x^*(t_f) = (\phi_3 + \phi_4 M)(\phi_1 + \phi_2 M)^{-1}x^*(t) = P(t)x^*(t) \tag{2.52}$$

$P(t)$ is used for simplification purpose.

It now follows from (2.46) and (2.52) that the optimal control is of linear feedback form

$$\begin{aligned} u^* &= -R^{-1}B^T p^* \\ u^*(t) &= -R^{-1}(t)B^T(t)P(t)x^*(t) \end{aligned} \tag{2.53}$$

In order to determine the matrix $P(t)$, (2.52) can be differentiated to give the following.

$$\begin{aligned} \dot{p}^* &= \dot{P}x^* + P\dot{x}^* \\ \dot{P}x^* + P\dot{x}^* - \dot{p}^* &= 0 \end{aligned}$$

Substituting appropriate expressions from (2.48) produces the following [Barnett, 1985]

$$\dot{P}x^* + P\left(Ax^* - BR^{-1}B^T p^*\right) - \left(-Qx^* - A^T p^*\right) = 0$$

From (2.52), $p^* = Px^*$, thus

$$\left(\dot{P} + PA - PBR^{-1}B^T P + Q + A^T P\right)x^*(t) = 0$$

Since this must hold throughout $0 \le t \le t_f$, it follows that $P(t)$ satisfies the following *matrix Riccati differential equation.*

$$\dot{P} = -PA + PBR^{-1}B^T P - Q - A^T P \tag{2.54}$$

with boundary condition given by (2.49) and (2.52) as

$$P(t_f) = M \tag{2.55}$$

Since M is symmetric, $P(t)$ is symmetric for all t, hence (2.54) represents $\frac{1}{2}n(n+1)$ first order quadratic differential equations, which can be integrated numerically [Barnett, 1985]. As the numerical integration would be performed reverse in time with Equation (2.55) as an initial condition, R.H.S. of matrix Riccati differential equation, (2.54), has to be multiplied by –1.

This time-varying control theory is applied in a vehicle path optimisation problem, and is presented in Chapters 5, 6 and 7.

2.5 Summary

In this chapter, all the models used within this thesis are introduced and their significances are discussed. In addition, the characteristics of various vehicles used for sensitivity and robustness analysis are also analysed using simple steady-state and transient manoeuvre. Some of the vehicle parameters which are thought to provide an insight into vehicle dynamics are also noted. Finally, the control theories used throughout this thesis is introduced.

Appendix 1: Derivation of *Understeer Gradient*, Equation 2.22

$$\delta = \frac{L}{R} + Ka_y = \frac{L}{R} + \alpha_f - \alpha_r$$

hence, $K = \dfrac{\alpha_f - \alpha_r}{a_y}$

From vehicle fore/aft weight distribution

$$m_f = \frac{c}{l}m \qquad m_r = \frac{b}{l}m$$

Front and rear lateral forces are defined as

$$Fy_f = m_f a_y = \alpha_f C\alpha_f \qquad Fy_r = m_r a_y = \alpha_r C\alpha_r$$

Thus the slip angles are derived as follows.

$$\alpha_f = \frac{m_f a_y}{C\alpha_f} \qquad \alpha_r = \frac{m_r a_y}{C\alpha_r}$$

Therefore understeer gradient, K, is:

$$K = \frac{m_f}{C\alpha_f} - \frac{m_r}{C\alpha_r} = \frac{m}{l}\left(\frac{c}{C\alpha_f} - \frac{b}{C\alpha_r}\right)$$

Chapter 3

4WS Control of Handling Dynamics using a Linear Optimal Reference Model

This chapter discusses the application of linear optimal control theory to the Four Wheel Steer (4WS) vehicle using a reference model controller.

With 4WS, the rear tyres are controlled actively to improve low speed manoeuvrability and high speed cornering performance of the vehicle. The project concentrates on the latter of the two. Both front and rear steering angles are controlled actively with respect to the driver steering input as a reference signal (4WS – by – wire). This study was originally presented at the 5th International Symposium on Advanced Vehicle Control (AVEC), 2000.

3.1 Introduction

Design and implementation of an active control system to enhance vehicle dynamics is important in order to achieve high quality vehicle handling, especially in the limit handling condition. Moreover, improving a vehicle's dynamic response close to this limit handling condition leads to improved driving safety. However, as the vehicle goes into the limit handling region and nonlinearity becomes significant, the altered dynamic response can be considered as useful feedback information for skilled drivers, and control objectives are restricted to achieving a progressively linear response. The assumption here is that LQR control can be used to extend the linear range without corrupting this feedback.

The study is carried out through simulation using a 2 Degree-of-Freedom (2DOF) linear reference model and a 3 Degree-of-Freedom (3DOF) nonlinear vehicle model as described in Section 2 of the previous chapter. The controller is designed and applied at two different levels. The primary controller, which controls the

reference model, is designed based on a cost function that describes the desired vehicle performance. Secondary control is then applied in order to minimise errors between the vehicle and the reference model.

The overall view of the suggested control system is shown in Figure 3.1. There are two layers of control: A primary feedback coupled to a linear reference model provides a controlled reference system based on the yaw and sideslip degrees of freedom. A second feedback is then applied to reduce vehicle/reference error via state feedback. Both of the layers generate both front and rear steering modification, and for simplicity, it is assumed that all relevant vehicle states are directly available.

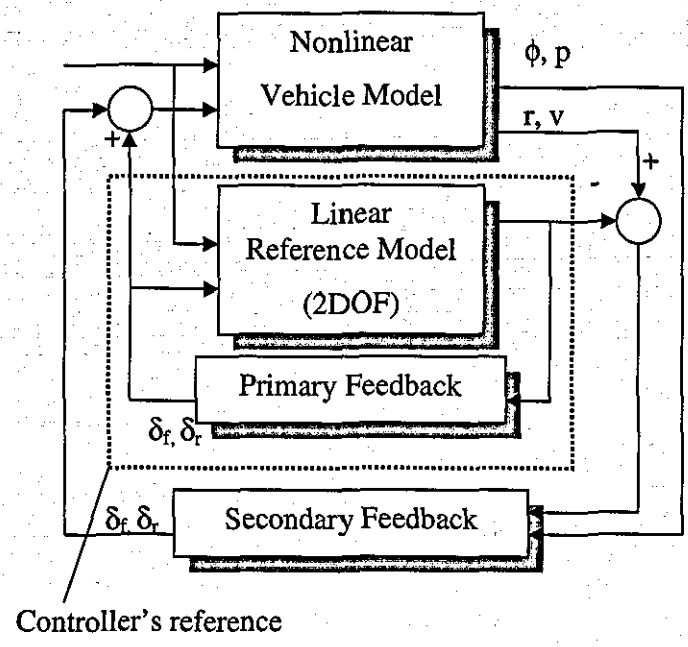

Figure 3.1 Reference Model Control Structure

The aim of this work is to investigate the feasibility of using a simple linear reference model and applying linear optimal control theory for both primary and secondary controllers.

First, the design of the primary controller is discussed and the results using this primary controller in isolation are then presented. The secondary controller is designed and the performance of the overall controller is assessed in terms of a

number of design parameters. Finally, an informal examination of the algorithm's robustness to plant parameter variations is carried out.

Since this is a nonlinear problem and only a linear controller is applied, there is a limitation to the capability of this specific controller set-up. However, it is important to understand and assess the feasibility of using a linear controller with the reference model approach within the nonlinear environment.

3.2 Reference Model Controller

The Linear Quadratic Regulator (LQR) is used for this study since it is a simple linear optimal control theory and hence is applicable for a linear reference model. Its cost function is defined as;

$$J = \int \left(x^T Q x + u^T R u + 2 x^T N u \right) dt \qquad (3.1)$$

The optimal gain matrix K is determined by solving the algebraic Riccati equation [Barnett, 1985], as described in the previous chapter.

By definition, a regulator tends to drive all the states to zero. However, this is clearly not applicable for this study since it will force the vehicle along a straight line with zero yaw! The standard application of LQR must therefore be changed to allow state tracking.

This is most conveniently achieved by modifying the reference model to include an additional state for the command steer input, δ_d. This allows costs, J, to be prescribed in terms of the desired steady state for any given δ_d. Choosing a very slow first order dynamic for δ_d, the LQR promotes regulation only over a long time period. This slow filter is then removed in practice by substituting the known steering input during operation.

3.2.1 Choice of Cost Function

There are many ways to interpret the effectiveness of 4WS control, however it is not immediately obvious what should be used as *the* measurement of handling performance [Harada, 1996]. Moreover, according to the type of the vehicle to be developed, the design criteria may change.

The main aim of the cost function for this study is to obtain a vehicle with good controllability for the driver. This can be interpreted as linearity in the handling dynamics, and therefore a linear relationship between yaw rate and lateral acceleration with respect to forward velocity is chosen as the *linearity cost*. From the dynamic equations of motion for the bicycle model, show in Equation 2.1 in Chapter 2, it is clear that this cost function requires vehicle sideslip acceleration to be minimised.

$$J_1 = \int \left(a_y - ur\right)^2 dt \tag{3.2}$$

However, using this cost function on its own would not be suitable, since the controller would tend to cancel out the driver input. This is because minimised sideslip is readily achievable by applying zero net steer this will minimise both yaw rate and lateral acceleration! Clearly an additional constraint is required to force the vehicle to yaw.

It is generally considered that vehicles with neutral steer characteristic have the best handling dynamics when assessed purely objectively. Using the definition of steady-state yaw rate gain, Equation 3.3, it is possible to derive the neutral steer yaw rate as a function of driver steering input,

$$\frac{r}{\delta_d} = \frac{u}{l + \frac{Ku^2}{g}} \tag{3.3}$$

where K represents the understeer gradient. For the neutral steer vehicle (K equal to zero), the yaw rate gain is simply the ratio of vehicle forward velocity to the wheelbase length. Thus an additional cost function, the *neutral steer cost*, is stated as follows.

$$J_2 = \int \left(r - \frac{u}{l}\delta_d \right)^2 dt \tag{3.4}$$

An aggregate cost function is then defined simply as a combination of these two functions and is shown in Equation 3.5.

$$\begin{aligned} J = (1-\lambda)\int \left(a_y - ur\right)^2 dt + \lambda \int \left(r - \frac{u}{l}\delta_d \right)^2 dt \\ + \begin{bmatrix} \delta_f & \delta_r \end{bmatrix} \begin{bmatrix} k_1 & 0 \\ 0 & k_2 \end{bmatrix} \begin{bmatrix} \delta_f \\ \delta_r \end{bmatrix} \end{aligned} \tag{3.5}$$

The weighting parameter λ was determined by minimising an auxiliary cost function,

$$\tilde{J} = \max\left\{ \frac{J_1(\lambda)}{\bar{J}_1}, \frac{J_2(\lambda)}{\bar{J}_2} \right\}$$

where $J_1(\lambda)$ is the cost associated with Equation 3.2 for the particular design, and $\bar{J}_1$ is the corresponding cost for the conventional 2WS, similarly for $J_2(\lambda)$ and $\bar{J}_2$. Sharp [Sharp, 2005] studied the influence of the rear to front steering ratio on the required preview distance. At low speed, this had negligible influence. However, at higher speeds (64 m/s), required preview distance increased up to the ratio of 0.6. The distance then decreased when the proportion of rear wheel steer is increased further. In this thesis, this ratio is not regulated. The controller is simply asked to minimise the cost function shown in Equation 3.5. The control parameters k_1 and k_2 in Equation 3.5 are then chosen to impose an overall constraint on the steering magnitude. Sharp stated that further work needs to be carried out to investigate the correlation between the required preview distance and handling qualities.

3.2.2 Performance

To examine the effectiveness of the basic reference model control structure, the LQR feedback gain is applied both within the reference model (Figure 3.1 with the secondary controller set to zero) and as a direct feedback to the nonlinear plant. This plant includes nonlinearity due to lateral force saturation and the

vertical load dependency (and hence weight transfer). A sinusoidal steer command (δ_d) is used for this simulation in order to emulate a single lane change manoeuvre and a conventional uncontrolled 2ws response is also shown for comparison. Figure 3.2 shows the characteristics of the neutral steer cost, Equation 3.4, where zero cost is obtained via a unit slope straight line, and it is clear that the controller performs distinctively better when applied through reference model control.

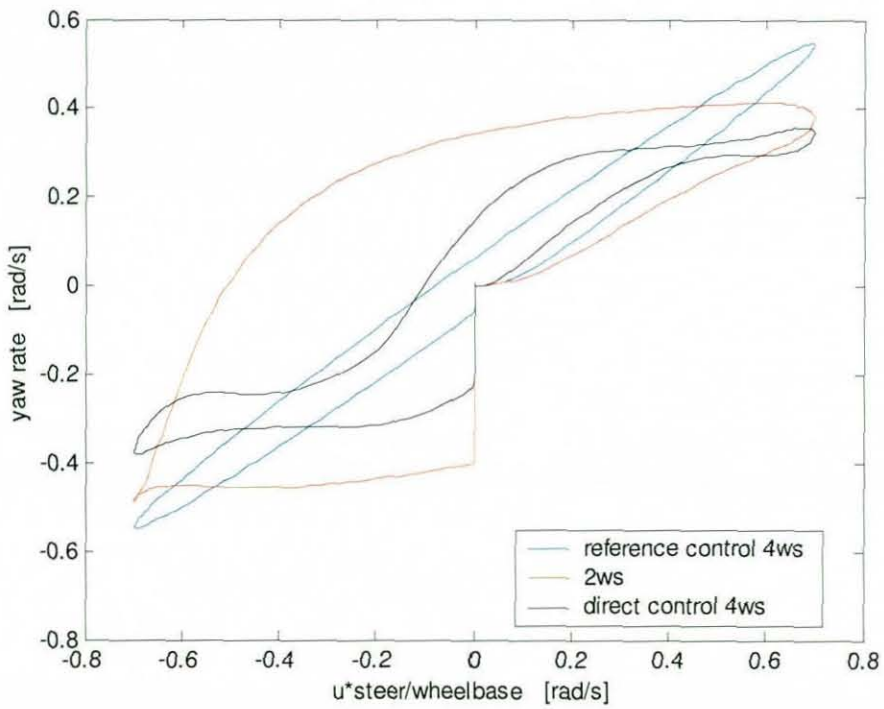

Figure 3.2 Neutral Steer Cost

Figure 3.3 compares the corresponding vehicle paths. The reference model controller enables the vehicle to turn in sharper, hence achieving steady state lateral displacement quicker than the conventional vehicle. In comparison, the direct controller cannot perform a single lane change manoeuvre in the desired manner for the same running condition.

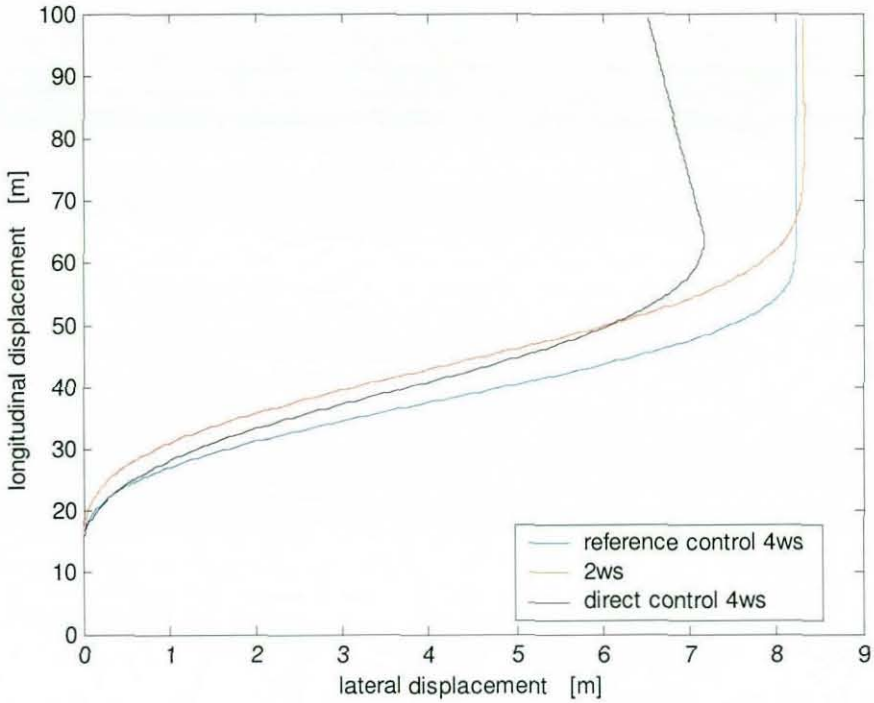

Figure 3.3 Vehicle Path

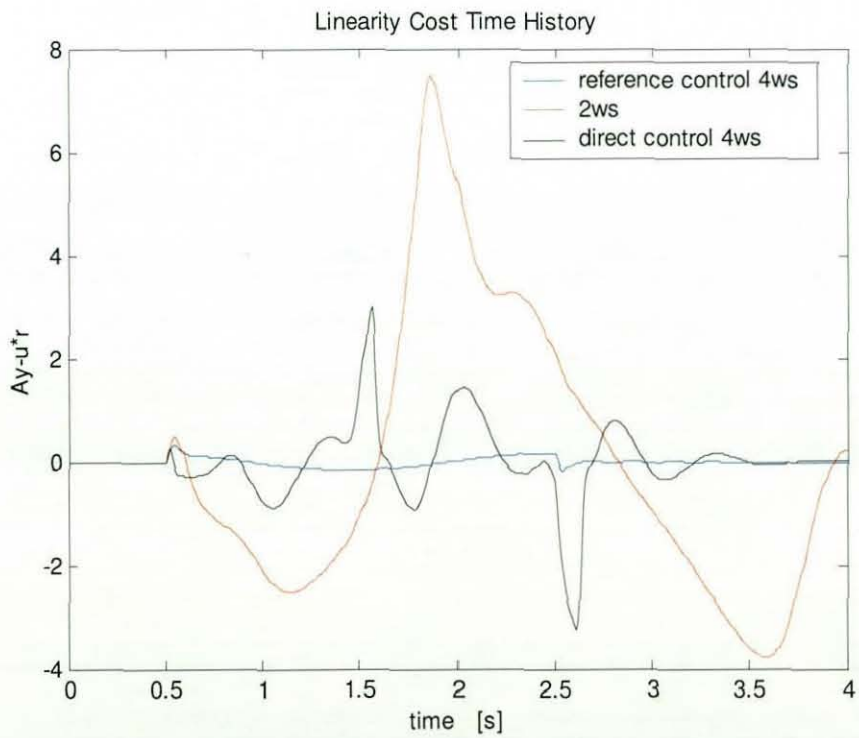

Figure 3.4 Linearity Cost Time History

Figure 3.4 shows the time history for the linearity cost term (a_y - ur) for the three cases. It is clear that the conventional 2ws vehicle has the worst cost. By contrast, the cost is controlled very well when the primary controller is applied via the linear 2DOF plant. When this controller is applied directly to the 3DOF nonlinear plant, the performance degrades.

From the above results, it can be concluded that the primary controller should only be used as a reference model controller. In order to improve the management of nonlinearity still further, the secondary feedback is now considered.

3.3 Secondary Feedback Controller Design

The secondary controller is designed to minimise differences between the reference model and the vehicle. Since the reference model is linear, this secondary controller is required to compensate for the nonlinearity of the system and also the additional vehicle roll mode. The secondary feedback is again designed using LQR, but here the system model is taken to be the linearised combined reference and vehicle model as shown in Figure 3.5 below. In other words, reference model controlled vehicle becomes the "new system plant", which is then linearised in order to obtain Secondary LQR control gain. Flow-chart for the controller design is shown in Figure 3.6.

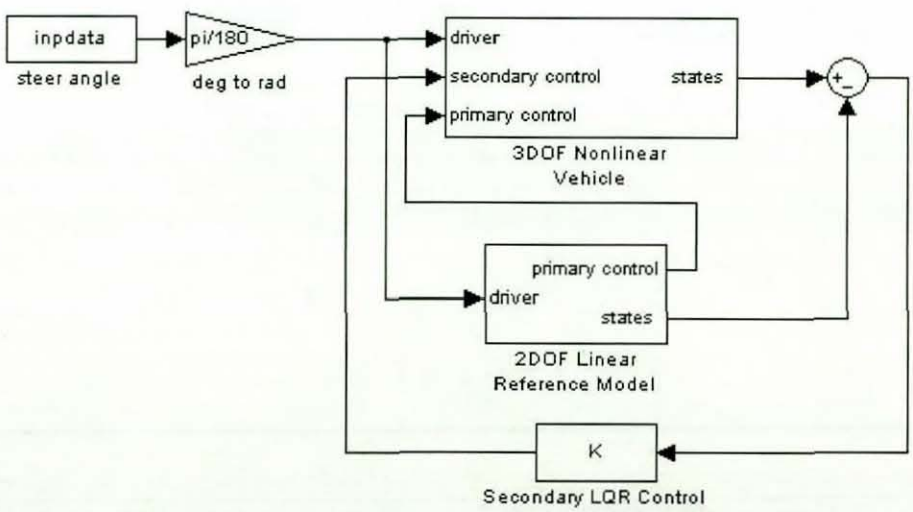

Figure 3.5 Simulink Reference Model Control Structure

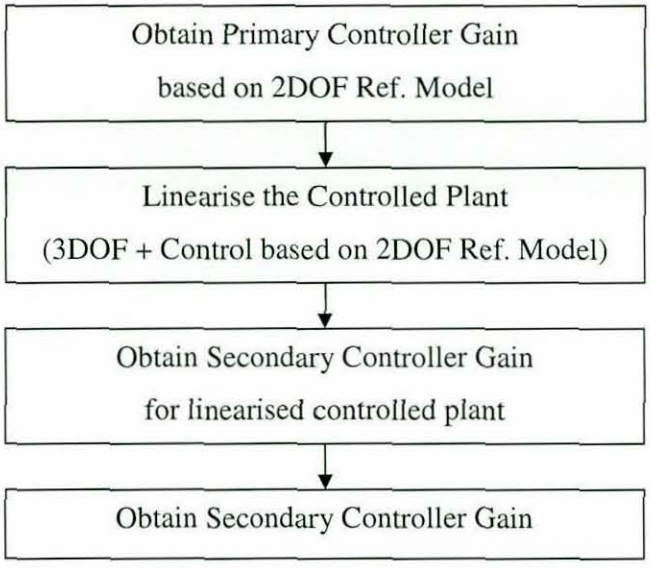

Figure 3.6 Secondary Feedback Controller Design Flow Chart

The cost function for the secondary controller is taken as;

$$\lambda_1\left(r_e^{\,2}\right)+\left(1-\lambda_1\right)\left(v_e^{\,2}\right)+\lambda_2\phi^2+\lambda_3 p^2 \qquad (3.6)$$

where the subscript e represents error values. λ values are then set such that the *original* cost function, Equation 3.5, is minimised. Three different controller types are obtained by applying various restrictions to λ_1, λ_2 and λ_3.

3.3.1 Parameter Optimisation

Type1 - $\lambda_2 = \lambda_3 = 0$

Yaw velocity and sideslip velocity information is available from both the linear reference model and the nonlinear vehicle. Thus the controller could be designed simply to minimise the difference between these states from the two models. This is the most basic form of the secondary controller since the roll degree of freedom is not directly controlled. The weighting λ_1 between the sideslip and yaw velocity errors is determined by minimising the dynamic cost function in Equation 3.5 for the total system simulation, including the non-linear vehicle model.

Type2

Using the λ_1 value obtained from the Type 1 controller, weighting factors for roll velocity and roll angle are now also determined using the standard Nelder-Mead downhill simplex minimisation. Results are shown in Tables 2 and 3, and it is clear that a large improvement in the linearity cost, J_1 is achieved with additional roll damping. Figure 3.7 shows the time history of yaw rate and sideslip velocity along with the driver steering input (scaled by 0.5 for clarity) using this Type 2 controller. It can be seen that this controller set-up produces better transient response of yaw rate and hence reaches steady state quickly. Furthermore, the vehicle response is much more in phase with the driver steering input, which clearly is an objective improvement. Moreover, neutral steer cost is slightly improved despite the reduced yaw rate; this is due to the reduced phase difference between the driver steering input and the subsequent yaw rate.

In order to produce this sharp transient response, the controller invokes a higher roll velocity than the conventional 2WS vehicle as shown in Figure 3.8. This plot also shows that the roll angle is more in phase with the driver steering input, and the maximum roll angle is found to be approximately of the same magnitude to that of a conventional vehicle.

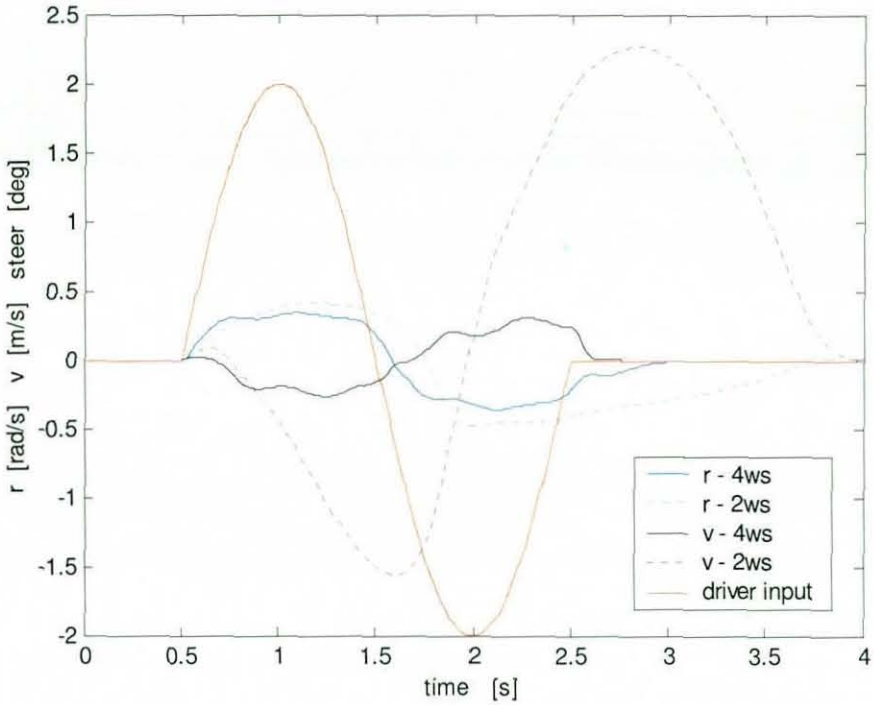

Figure 3.7 State Responses

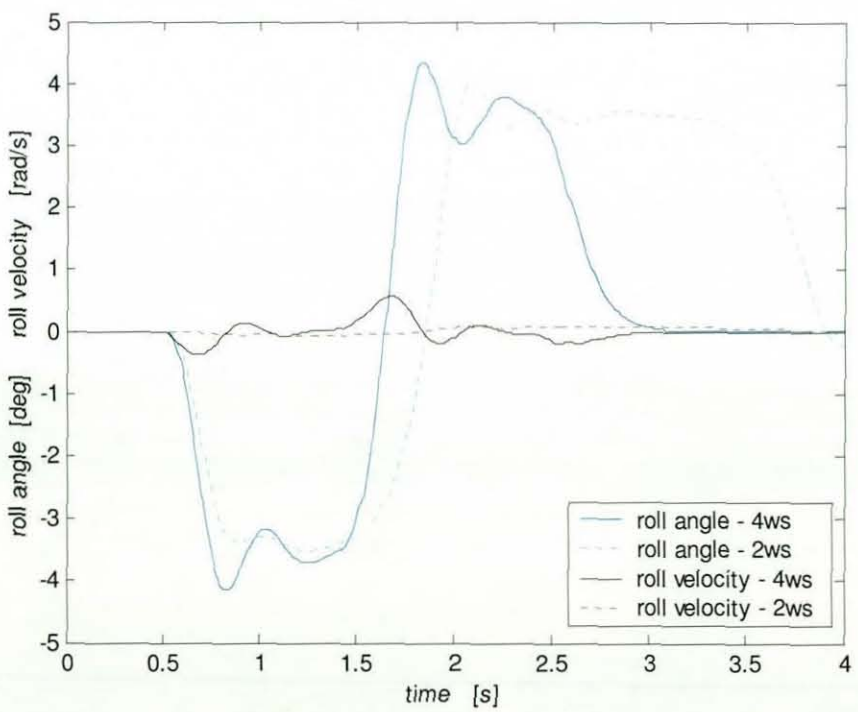

Figure 3.8 Vehicle Roll Motion

Type 3

All three weighting factors are now optimised simultaneously to seek a further reduction in the cost function. However, for this optimisation it was found that the Nelder-Mead optimisation was prone to finding local minima. An attentive 'Tabu Search' optimisation [Sait and Youssef, 1999] was therefore used in combination with Nelder-Mead. Tabu Search utilises solutions of the local neighbourhood and the best solution is stored. One of the unique features of the method is that the search continues even when no improved solution is found in the neighbourhood. This allows the search to 'escape' from local minima. In order to prevent cycling, recently visited solutions are stored in memory for a specified period of simulations. These form a *tabu list* and movement to these solutions is prohibited unless an aspiration criterion is met. This usage of memory makes Tabu Search distinctive from other algorithms.

From Table 3.1, it is noticeable that the Type 3 controller places much higher weighting on the roll angle, with roll velocity cost being kept relatively low. Furthermore, the weighting on the yaw rate error is reduced by a significant amount. Thus it is clear that there is a significant difference between controller types 2 and 3.

Controller	λ_1	λ_2	λ_3
Type 1	0.160	0	0
Type 2	0.160	0.011	0.4346
Type 3	0.0633097	27.539	0.39884

Table 3.1 Optimised Weighting Values

Table 3.2 shows the effect of different controller set-ups on the resultant cost. By including a roll damping with fixed λ_1, the overall cost is reduced by approximately half, compared to Type1. Moreover, the cost is reduced further by a noticeable amount under the Type 3 controller; an overall cost reduction of 60% is achieved when Type 3 controller performance is compared against Type 1. This

illustrates the importance of multi-parameter optimisation when designing a controller.

Controller	J_1	J_2	J
Type 1	300.868	12.9123	313.7803
Type 2	149.9495	12.2385	162.1880
Type 3	115.3567	11.5401	126.8976

Table 3.2 Resultant Cost using Different set-ups

3.3.2 Performance Evaluation

Having optimised both primary and secondary controllers, the incremental benefit of adding Secondary Control can be examined. Tests are carried out using four degrees of sinusoidal steer input (single lane change) at a forward velocity of 25 m/s. Case 1 refers to reference model control using a primary controller only. Case 2 refers to a reference model control approach using both primary and secondary controllers.

Table 3.3 shows that total cost is reduced considerably when the secondary controller is added using the reference model approach, justifying its use. The case 2 system controls the nonlinear dynamics reasonably well; it can be seen that linearity cost is improved by 45% over the case 1 controller. By contrast, around 4 % increase in the neutral steer cost is observed. Since linearity cost is the dominant factor, the dramatic reduction in this cost leads to a 42.5% reduction in total cost.

Controller	J_1	J_2	J
Case 1	209.2330	11.0674	220.3004
Case 2	115.3567	11.5401	126.8976

Table 3.3 Comparison of Direct & Reference Model Control

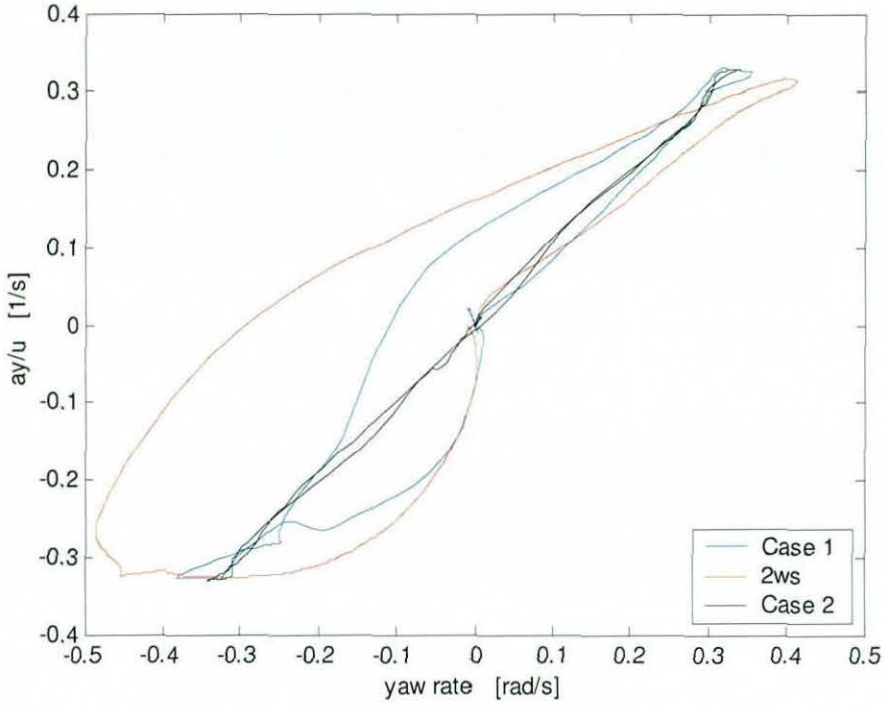

Figure 3.9 Linearity Cost

The linearity cost characteristic is shown in Figure 3.9, where the difference between the two controller applications is especially significant within the low yaw rate region. Moreover, although the Case 1 cost is better than the conventional 2ws vehicle cost, the relationship between yaw rate and lateral acceleration becomes highly nonlinear for the Case 1 controller when the yaw rate magnitude exceeds 0.25. This is clearly an undesirable effect.

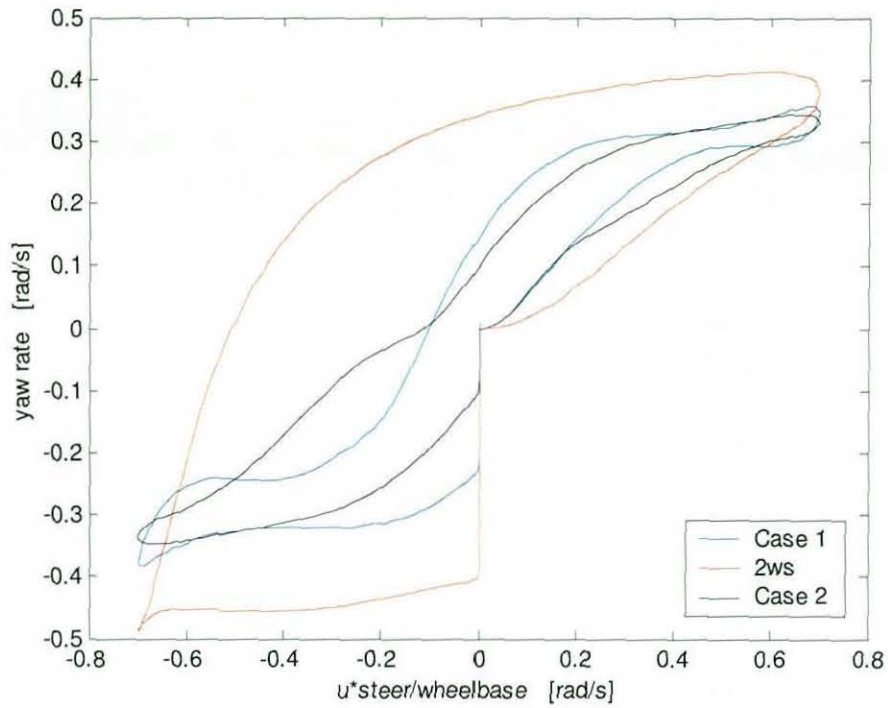

Figure 3.10 Neutral Steer Cost

Figure 3.10 shows the neutral steer cost characteristics, where the difference between Cases 1 and 2 is much smaller. Major improvement over the conventional vehicle is seen for both cases. It is noticeable that the conventional vehicle exhibits stronger understeer characteristics at the initial turn compared to the 4ws vehicle. When the steering angle is then reduced, the yaw rate shows noticeable hysteresis, in other words, the vehicle is oversteering for this phase of the manoeuvre. This hysteresis effect is much reduced for the 4WS vehicles. It is interesting to note also that when this controller is applied to a linear system, it is possible to achieve this plot with almost no hysteresis characteristics.

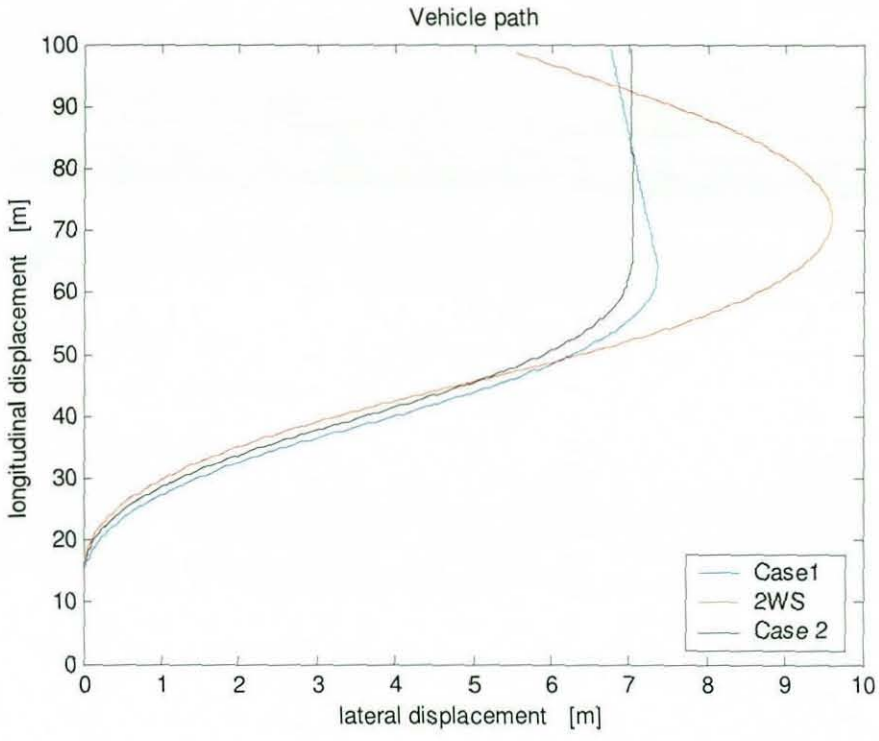

Figure 3.11 Vehicle Path

Resultant vehicle paths for the three cases are shown in Figure 3.11. The initial understeering characteristic of the conventional 2WS vehicle is noticeable compared to cases 1 and 2. Moreover, the terminal oversteer in the later part of the manoeuvre is significant on the vehicle paths. Although it is reduced considerably, same loss of control is also evident in the paths of the vehicle with the Case 1 controller.

Until now the control algorithms have been optimised and tested on a single lane change manoeuvre. To confirm that the resulting controllers are not uniquely tuned to this input, a simple design/test matrix of results was generated for two very different input conditions. One is a sinusoidal steer test and the other a random steer test. Due to the physical ability of a human driver, the steering input on the random steer test has a frequency limit of 5Hz.

The parameter optimisation process is first carried out for λ_1, λ_2 and λ_3 on each case. The controllers are then tested on both inputs. The resultant costs are shown in Table 3.4, with test types placed in columns and the controller types in rows. It is clear that the controller designed using a single lane change manoeuvre achieves better performance.

Table 3.5 shows the optimised parameter settings for both of the controllers and it can be agreed that they are noticeably different. The 'Random steer' controller has significantly less roll angle cost and much larger roll velocity cost, through the yaw rate error cost is kept small for both controllers.

Controller \ Test	Sinusoidal	Random
Sinusoidal	126.8976	9685.8
	(Ref. 1)	(14 % increase w.r.t. Ref. 2)
Random	216.2716	8482.2
	(70 % increase w.r.t. Ref. 1)	(Ref .2)

Table 3.4 Resultant Cost of Controller \ Test Swap

	λ_1	λ_2	λ_3
Sinusoidal	0.063310	27.539	0.39884
Random	0.018993	2.9259	1.9979

Table 3.5 Optimised Controller Parameters

3.4 Robustness Evaluation

In order to investigate the robustness of the controller, two further tests are carried out. One is a parametric sensitivity analysis, where various vehicle parameter values are altered within a small range and the subsequent changes in the cost are noted. The second is the analysis of additional rear passenger weight; this attempts to simulate the reasonably severe change in a vehicle parameter which the controller is expected to overcome in real life.

3.4.1 Sensitivity Analysis

5% changes are made to various vehicle parameters in order to assess the sensitivity of vehicle performance. The changes made to the parameters are as listed in Table 3.6 below.

No.	Parameter	Units	original	modified
1	Front axle load	kg	800	840
2	C.G. height	m	0.6	0.63
3	Rear roll centre	m	0.5	0.525
4	Rear damper	Ns/m	1200	1140
5	Front track	m	1.5	1.425
6	Front spring	N/m	20000	21000
7	Yaw inertia	kgm^2	2500	2625
8	Roll inertia	kgm^2	200	210
9	Tyre peak F_y	N	6054.9	5736

Table 3.6 *List of* Parameter Changes

The result of this analysis using the sinusoidal steer test is shown in Table 3.7.

	J1	J2	J_{tot}	% increase
Original	115.36	11.54	126.90	---
Front axle load	91.169	11.90	103.07	-18.78
C.G. height	118.19	12.05	130.24	2.63
Rear roll centre	147.15	11.37	158.52	24.92
Rear damper	117.55	11.55	129.11	1.74
Front track	95.021	11.73	106.75	-15.88
Front spring	111.64	11.52	123.16	-2.94
Yaw inertia	119.72	11.63	131.35	3.51
Roll inertia	118.35	11.56	129.91	2.38
Tyre peak F_y	108.60	12.50	121.10	-4.57

Table 3.7 Result of Sensitivity Analysis

Generally, the controller can be said to be robust to these variations since the changes in the resultant cost are fairly small. The most significant change in the cost is observed when the rear roll centre height is raised, and the increased front axle load and reduced front track are also significant. The cost is actually reduced for the latter two cases, however. It is interesting that improvement in the aggregate cost is observed when the parameter change induces understeer in the vehicle - represented by tests 1, 5 and 6. Also, changing the vehicle yaw inertia makes very little difference in terms of the state matrix (in the order of 10^{-4}), but its effect is still noticeable in the resultant cost.

3.4.2 Effect of Additional Rear Passenger Weight

In order to examine the robustness of the controller for a reasonably severe change, an additional rear passenger weight of 100 kg is considered. The passenger is positioned above the rear axle in the middle of the right hand side seat. As a consequence, several other parameters are altered as well as the vehicle mass and these are shown in Table 3.8 below.

Change in	Unit	Value
Vehicle Weight	kg	+ 100
Vehicle C.G. height	m	+ 0.0133
Yaw inertia	kg m^2	+ 191.8
Roll inertia	kg m^2	+ 14.06

Table 3.8 Altered Parameters and Their Values

When the 4ws active controller is applied to this additional rear passenger case, the overall cost rises from 126.90 to 367.7780 - a 290% increase. However, although this seems severe, the resultant path of the vehicle in Figure 3.12 shows otherwise. The paths of the active 4WS vehicle for both original and additional rear weight cases are very similar. This compares to the relatively disastrous effect seen for the conventional 2WS vehicle.

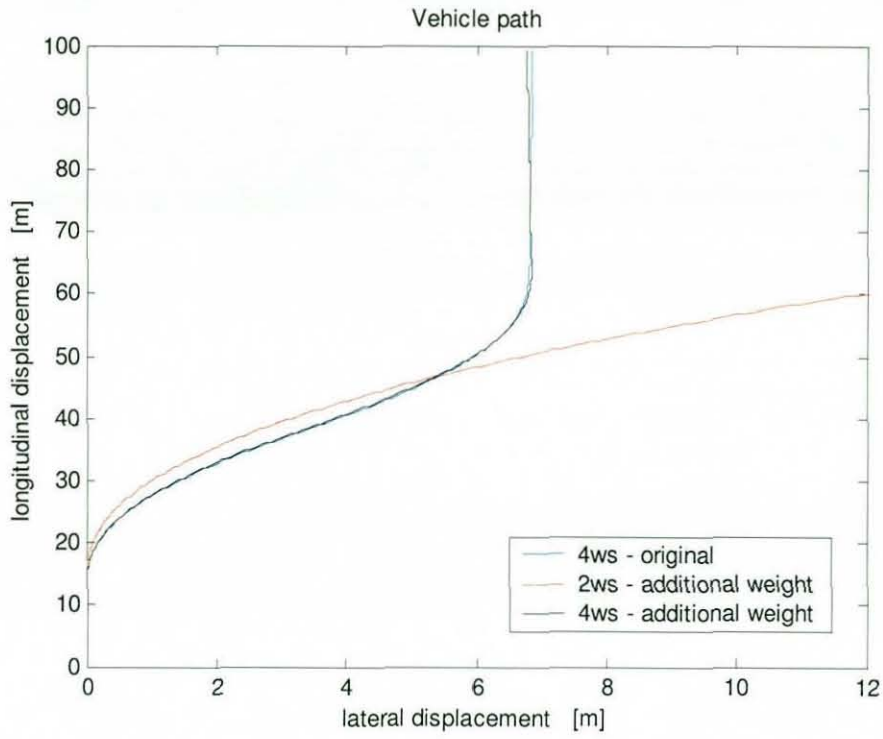

Figure 3.12 Vehicle Path

Table 3.9 shows that the percentage increase in the overall cost is due to poor performance in the linearity cost.

Costs			Root Mean Square Values			
J_1	J_2	J_{tot}	r_e	v_e	ϕ	p
			rad/s	m/s	rad	rad/s
208.2	5.67	189.8	6.28	55.8	8.44	6.42

Table 3.9 Percentage increase in Cost

Figure 3.13 shows the comparison of linearity cost for both tests together with the reference model performance and the command steering input. It is noticeable that the cost is particularly high in transient states at end of the manoeuvre and also when the steering crosses zero. Increased phase delay effect can also be seen for the additional rear passenger weight case.

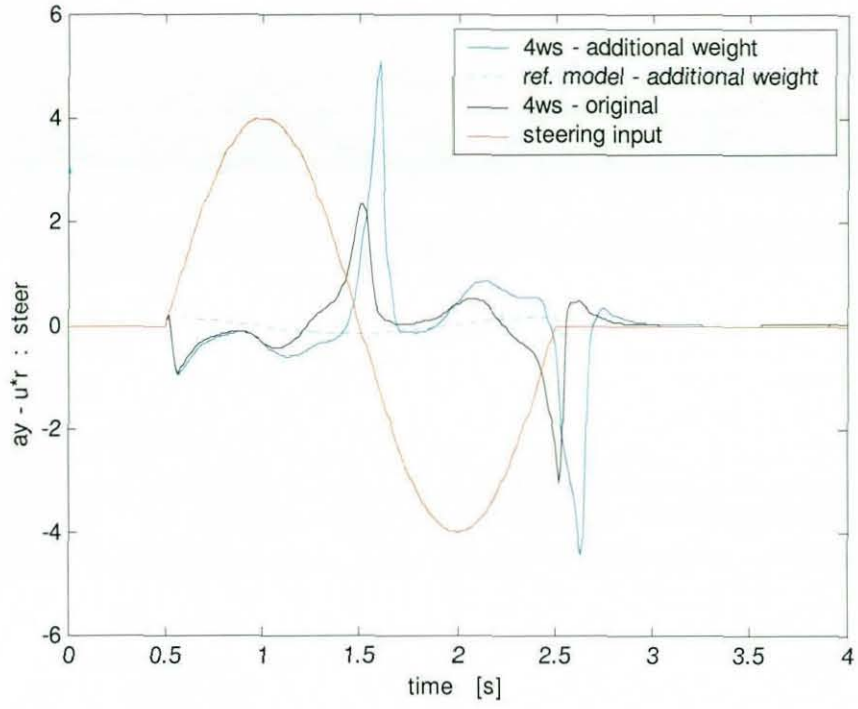

Figure 3.13 Linearity Cost Time History

Tabu Search, as explained in the section 3.3.1, can be used to investigate the effect of redesigning the controller, given the new vehicle parameters. The search result is as shown in the first row of Table 3.10 and a 32% reduction in the aggregate cost is achieved. Using this solution from Tabu Search as the initial condition, Nelder-Mead is used to determine the minimum condition and its result is shown in the second raw of Table 3.10. Results indicate the effectiveness of combining these two techniques. The higher values of λ_2 and λ_3 compared to Table 3.5 (sinusoidal) imply the need for improved control of roll displacement and velocity. Hence, although the added load tends to degrade dynamic performance, there is scope to reduce this effect by controller adaptation. More significantly, the vehicle path is robust to these changes, in that the same steer input produces roughly the same cornering behaviour. This "dynamic neutral steer" property is very desirable, as it reduces the need for the driver to compensate for vehicle parameter changes.

	λ_1	λ_2	λ_3	J_1	J_2	J_{tot}
Tabu search	0.063	37.98	1.994	229.236	14.0536	243.29
Nelder-Mead	0	85.45	2.847	195.749	14.8870	210.63

Table 3.10 Effect of Re-Optimisation

3.5 Conclusions

Linear optimal control theory has been applied to 4WS control in order to enhance vehicle handling dynamics. Both linearity and neutral steer cost functions are defined and assessed as being reasonably satisfactory. A linear reference model is used as a primary feedback and a secondary controller is applied in order to control the nonlinearity and extra degree of freedom. It is found that the secondary controller reduces the overall cost function by a considerable amount. Moreover, the secondary controller performs at its best when all available cost parameters are optimised simultaneously.

Robustness of the controller was investigated and it was found that the controller designed on the sinusoidal steer test inherits reasonably good robustness. Moreover, the sensitivity analysis revealed that the controller is robust to small changes in the various vehicle parameter values. These results indicate potential advantages in biasing the uncontrolled vehicle towards understeer. Also, there is scope in the future work to make the secondary controller adaptive or nonlinear to improve performance and robustness.

Chapter 4

Vehicle Path Optimisation using a Time–Variant Linear Optimal Reference Control: Part 1

In Chapter 3, a linear time-invariant reference model control structure was designed as a 4WS controller. The controller was developed with a 3DOF handling model, as described in Section 2.2 of Chapter 2. It showed that the system is able to control vehicle behaviour according to a certain prescribed dynamic characteristics.

This Chapter discusses the application of time-varying linear optimal control theory, which is an extension of the controller used in Chapter 3. The controller is applied to the vehicle path optimisation problem using a reference model control structure, which was used in Chapter 3.

One of the most obvious examples of vehicle path optimisation in real life is that of racing line determination and simulating obstacle avoidance manoeuvres. In this study, the racing line determination problem is solved using a time-variant linear optimal controller as described in Chapter 2. The controller is applied to a 3DOF handling model, which was also used for the 4WS study in Chapter 3.

The optimisation method is tested for extreme cases where a vehicle is at the limit of adhesion as well as for sub-limit cornering manoeuvres. The validity and robustness of the controller is then carefully examined. Finally, the effects of changing vehicle dynamic characteristics on the resultant optimum vehicle path are investigated. The part of this study was presented at the 6th International Symposium on Advanced Vehicle Control (AVEC 2002) in September 2002, Hiroshima, Japan.

4.1 Introduction

The nonlinear vehicle model is represented by time-varying linear models and controller gains are determined with respect to the linearised sequence. The solution is obtained through iterations where the previous result acts as a reference trajectory. An initial vehicle trajectory is set so that it roughly traces the road centre line. Alternatively, the initial trajectory can also be derived using an automated driver, such as that based on a convergent vector field approach [Gordon, 2002].

As a vehicle approaches the limit of its performance envelope, the nonlinearity of the system becomes very significant. In order to express this change in vehicle characteristics with respect to the operating conditions, the system is represented by continuous time-varying linear models. The advantages of linearising a system is that the solution guarantees local optimality, and the system itself can be investigated analytically at various operating points.

4.2 Control of 3 DOF Model

4.2.1 Controller Design

The time-varying linear optimal controller, described in Section 2.4 of Chapter 2, is used for this study, the motivation being that it is capable of representing varying vehicle characteristics with respect to various operating conditions. Moreover, since it is a linear method, optimality is guaranteed provided that the deviation from the linearised dynamics is controlled sufficiently small. Recall that the cost function is defined as follows.

$$J(u) = \frac{1}{2} x^T(t_f) M x(t_f) + \frac{1}{2} \int_0^{t_f} \left[x^T Q x + u^T R(t) u \right] d(t)$$

The optimal gain matrix $K(t)$;

$$K(t) = -R^{-1}(t) B^T(t) P(t)$$

is determined by solving the *matrix Riccati equation*, (2.54), in reverse time.

$$\dot{P} = -PA + PBR^{-1}B^T P - Q - A^T P \tag{2.54}$$

with the boundary condition,

$$P(t_f) = M \tag{2.55}$$

[Barnett, 1985]

The problem is formulated as the maximisation of a travelled distance within a given period of time. The LQR cost function is defined using two different objectives, which are to achieve:

i) the maximum distance for a given time period, and

ii) the minimum deviation from the previous trajectory

These cost functions work against each other; the second objective is only required in order to limit the change in dynamics from the previous iteration within the linear region. Provided this condition is met, the control actions only depend on the distance part of the cost function.

The first objective is implemented through the Riccati matrix at final time, in other words by setting an initial condition shown in Equation 4.1. A pseudo displacement state, Y_p, is introduced as a target value. The final state cost, M, shown in Equation 4.1 is formulated in terms of an error between the target and actual distance. M_c is a constant that is used to control the magnitude of this cost.

$$M = M_C * (Y_p - Y)^2 \tag{4.1}$$

Reference model structure is defined as shown in Figure 4.1.

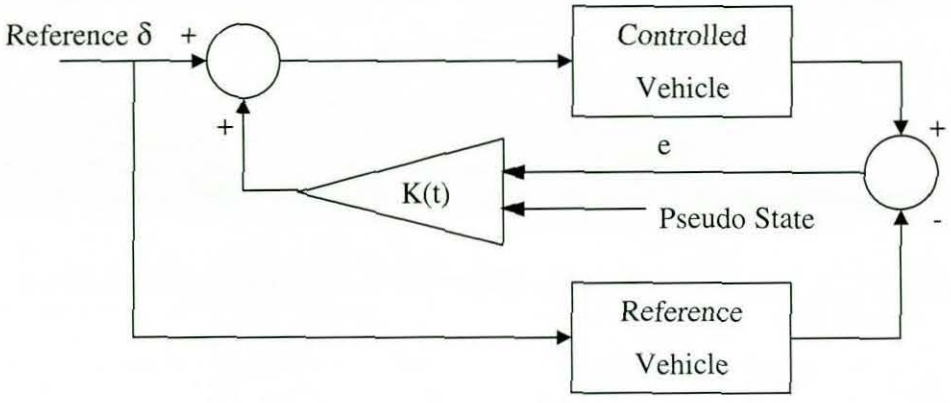

Figure 4.1 Reference Model Structure

From Figure 4.1, it can be seen that the controller works on the deviation of the states from the reference model rather than their absolute values, except for the pseudo state. The problem is solved iteratively, in other words, the reference system is defined by the solution at the previous iteration, and the new trajectory will then become a reference for the next iteration. Since the whole control strategy is based on the time-varying linear system, the deviation from the reference trajectory has to be kept adequately small so that the linearised models remain valid. This is achieved through an appropriate scaling of the control cost matrix *R*, which limits the magnitude of the control inputs and hence the subsequent change in the dynamics. Provided this condition is met, the control actions only depend on the distance part of the cost function – i.e. maximum performance becomes the sole objective.

For, the second objective, a quadratic road geometry constraint is applied through the Q matrix. Its magnitude is defined so that the nearest boundary has a cost of fixed magnitude. This means that the local gradient of this cost becomes steeper as the vehicle moves towards the edge of the road. This is required in order to ensure that the vehicle stays within the road boundary. This cost function is shown in Equation 4.2; it is time varying and also updated at every iteration. Therefore the reference trajectory always has a zero cost. This limits the change in control magnitude.

$$J_d = q(\delta x * m_1 + \delta y * m_2)^2 \tag{4.2}$$

where m_1 and m_2 are unit direction vectors, G_d is a weighting factor and q is used to control the cost magnitude as,

$$q = \frac{G_d}{\left(|\delta x||m_1| + |\delta y||m_2|\right)^2} \tag{4.3}$$

An example of the road geometry cost for a corner is shown in Figure 4.2. In this figure, the reference vehicle position is taken along the middle of the road (hence, having zero cost along the middle). The width of the road shown in this figure is much wider and the magnitude of the cost is much higher than the ones actually used. This is purely for graphical clarity purpose.

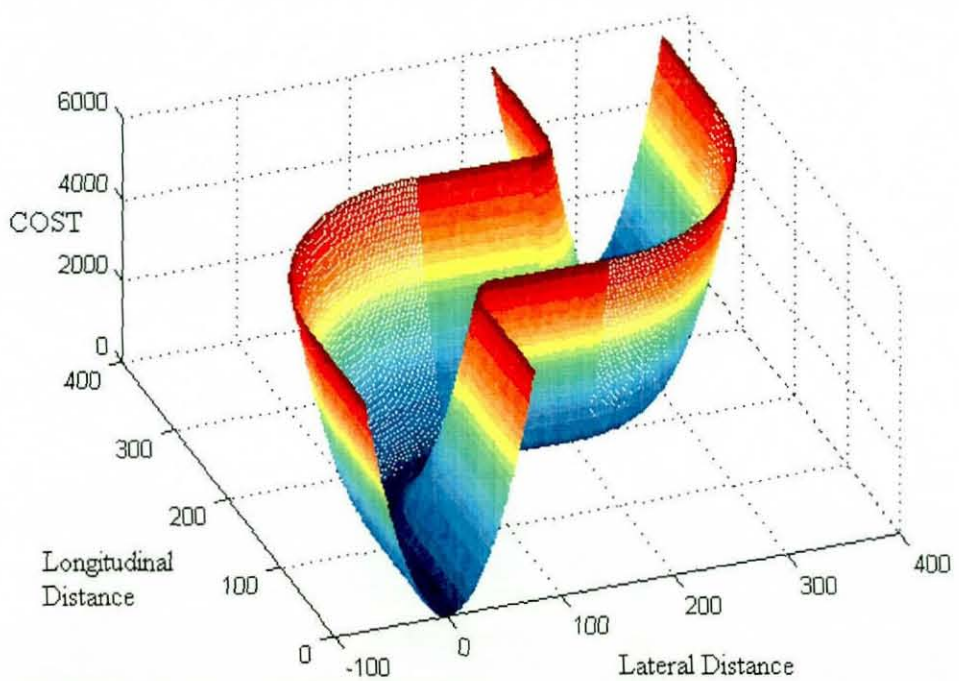

Figure 4.2 Road Geometry Constraints

Since the optimisation problem is solvered iteratively, the road geometry constraints are adjusted such that the reference trajectory always has the zero associated cost. As mentioned earlier, such formation of road geometry cost keeps the deviation from the previous trajectory (solution) to minimum. This is required in order to ensure that the linearised models remain valid within the optimisation

process. Figure 4.3 shows an example of the way in which the road geometry constraints are updated over the optimisation process. The figure shows road width on the x-axis with 0 as the centre line and associated cost on the y-axis. The road is 20 meters wide and the initial trajectory is set at the centre line (hence it has zero cost at the centre line). The red line shows the updated road geometry constraint when the vehicle is displaced 5m closer to the right hand side boundary. As the magnitude of the cost remains at a fixed value at the nearest boundary, the cost gradient is now steeper. The black line shows the cost profile when the vehicle is driven even closer to the boundary (similar to a corner apex condition). The associated cost gradient is very steep, which makes it very expensive to move away from this trajectory.

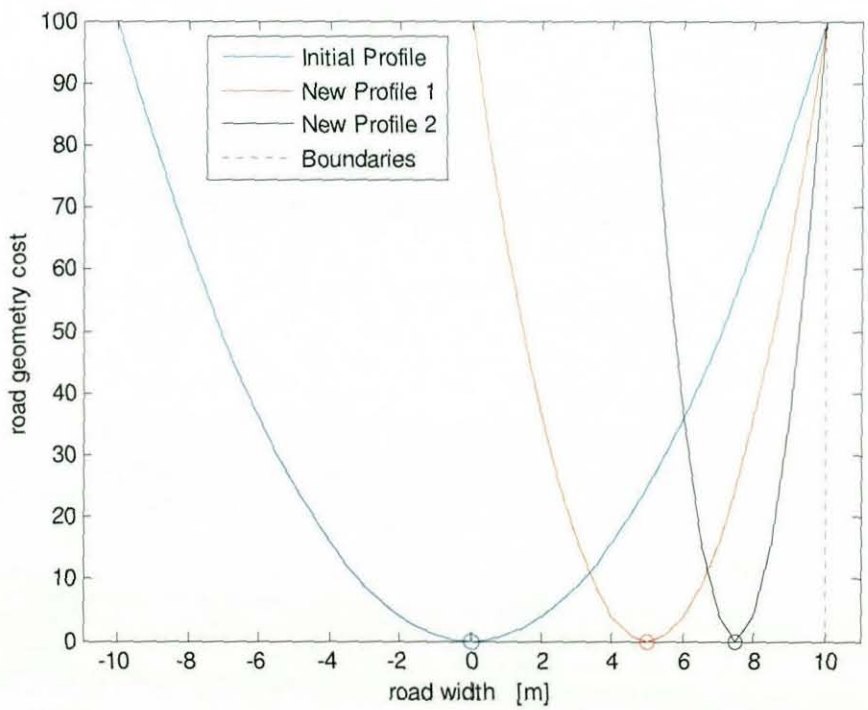

Figure 4.3 Updating Road Geometry Constraints

Figure 4.4 shows the flow chart of the optimisation algorithm. First of all, linearised models are obtained along a reference vehicle trajectory. The *matrix Riccati equation*, (2.54), is then solved in reverse time along the linearised

sequence. The optimal gain matrix, $K(t) = -R^{-1}(t)B^{T}(t)P(t)$, is determined and applied in forward time. The new trajectory then becomes a reference trajectory for a next iteration with zero associated road geometry cost, as explained earlier.

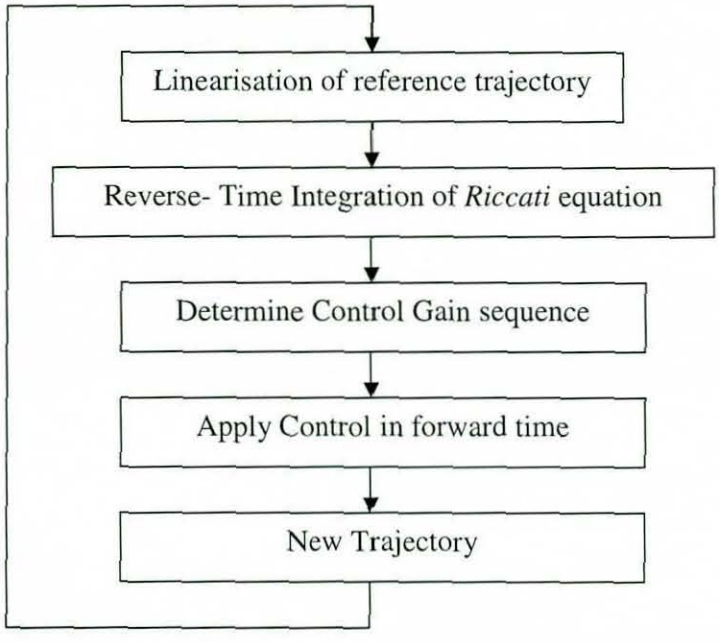

Figure 4.4 Optimisation Algorithm Flow-Chart

As mentioned previously, the optimisation method is formulated using a 3 Degree-of-Freedom (3DOF) vehicle handling model, where the forward vehicle velocity remains constant. Hence the single control input is the rate of change of steering angle.

4.2.2 Cornering Optimisation Initial Result

Figure 4.5 below shows the initial result of a double-corner optimisation. It can be seen that the controller is able to determine the apex for the first corner. However, the path is clearly not optimised for the second corner. Although the optimisation failed to find the second apex, it can be seen that it is driving the vehicle towards it. It is noticeable that the vehicle path becomes very close to the edge of the track at the end of the manoeuvre as well as at the first apex. This could prevent any further deviation from this "new reference" path, because the cost associated with

the road geometry is very high at these two points, hence it may lock the vehicle position.

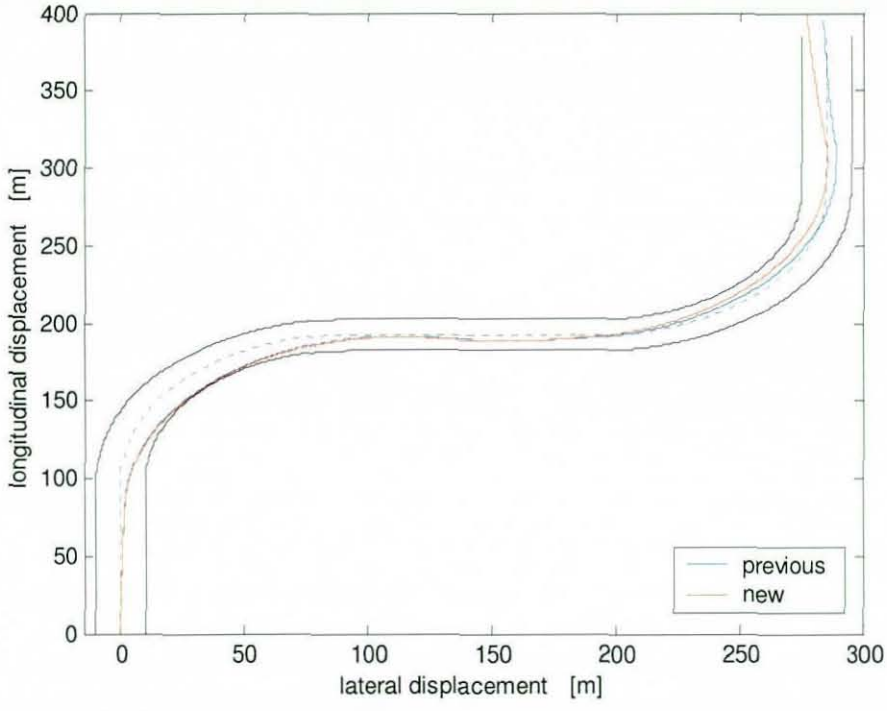

Figure 4.5 *Double Corner Optimisation Result*

4.2.3 Validation using Steady-State Simulation

Following the above result, it is clear that the validity of the optimisation method needs to be investigated. Steady-state simulation at limit handling condition is used for this purpose.

A steady-state steering pad test is emulated using a ramp steer simulation at the fixed vehicle forward velocity of 35 m/s. Steering angle is increased at a moderate rate of 1/3 degrees per second to ensure the steady-state. The result is processed using an understeer gradient calculation [Dixon, 1997], as used in Section 3.1 of Chapter 2. Figure 4.6 shows the resultant characteristics. From this figure, it can be discovered that the maximum lateral acceleration of 0.8G is achieved at 4.72 degrees of steering input.

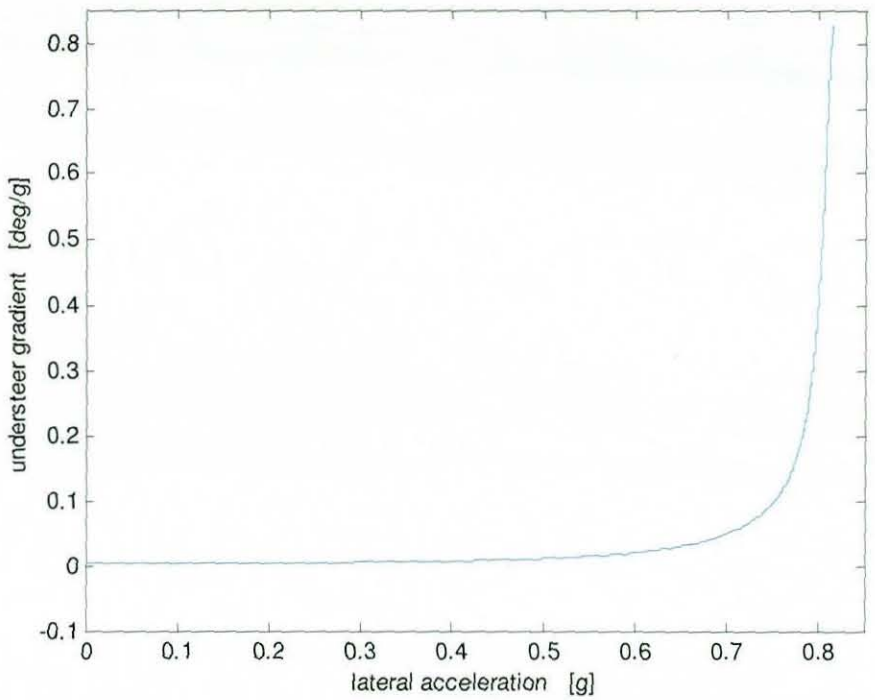

Figure 4.6 Understeer Gradient Characteristics

This steering angle, corresponding to the maximum lateral acceleration, is applied to an uncontrolled system together with the corresponding initial state conditions. Figure 4.7 shows the resultant vehicle trajectory with this constant steering angle input. The vehicle is driven at the minimum steady-state turning radius for a given vehicle forward velocity.

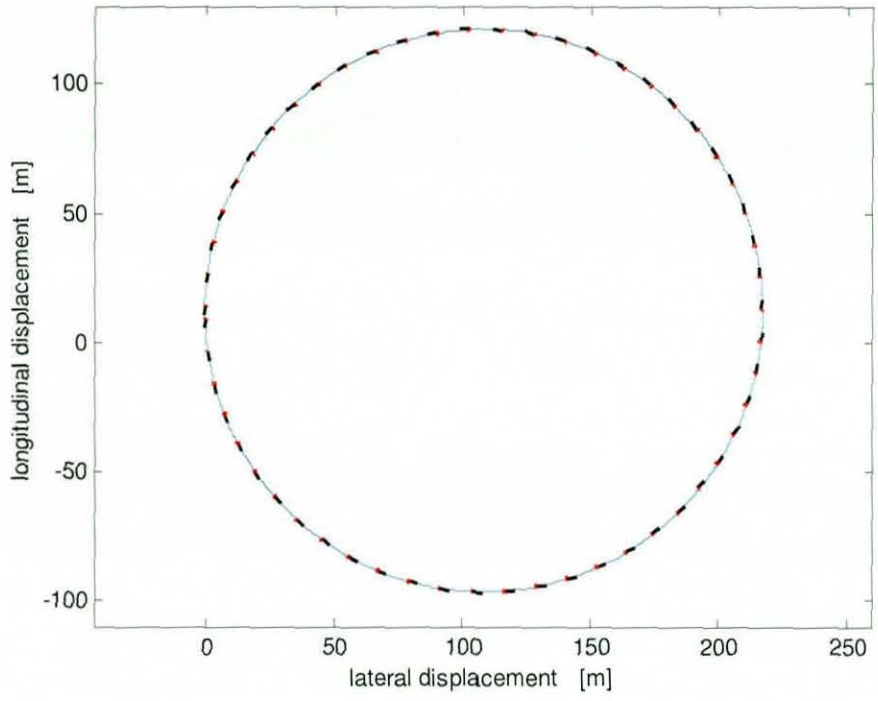

Figure 4.7 Vehicle Path with Constant Steer Input for Maximum Lateral Acceleration

The validation problem is formulated such that the final time is fixed at the point where this steady-state simulation reaches the quadrant of the circle shown in Figure 4.7. In other words, if the simulation is started from the co-ordinate [0, 0], the steady-state simulation takes the vehicle to the top of the circle ([110, 110]) within this given time period. Therefore, the pseudo displacement state is defined in terms of the final lateral distance covered by the steady-state simulation, hence it needs to be longer than 110 meters.

The assumption made in this validation exercise is that the optimisation can determine the steering input in order to displace a controlled vehicle to the target lateral displacement within a given amount of time. For the very first iteration, the reference steering angle is set zero for all time, however the states and lateral force initial conditions are set according to the peak lateral acceleration case. The resultant vehicle paths at the various stages of iterations are shown in Figure 4.8,

together with the target steady-state path (black dotted line). It can be seen that the vehicle trajectory is continuously updated in order to achieve the increased final lateral displacement value. The final displacement error at the final iteration is 0.4 % when compared to the steady-state reference.

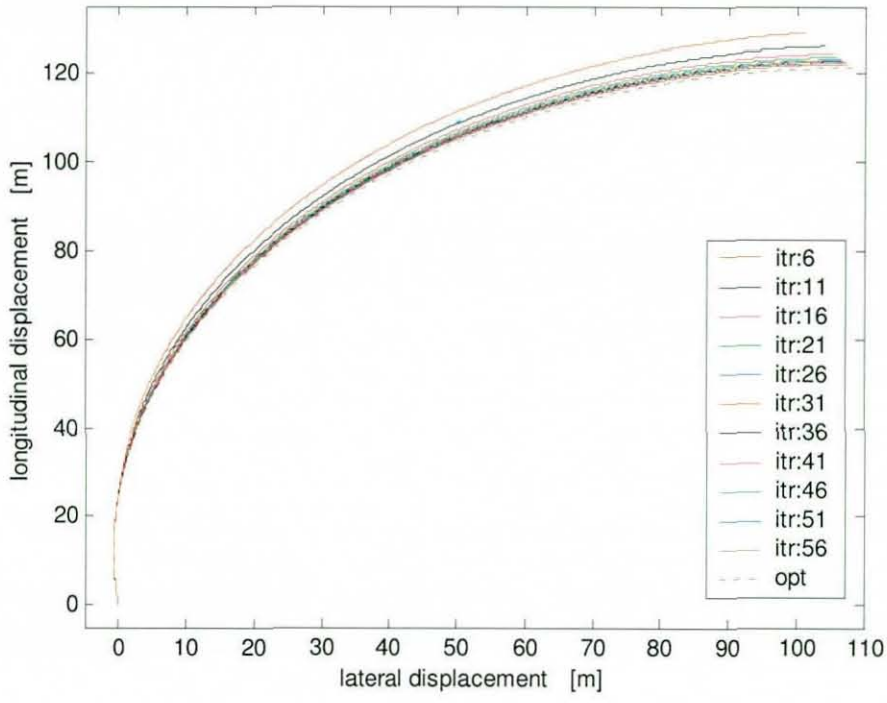

Figure 4.8 Vehicle Path Validation Result

The controlled steering angle characteristic is shown in Figure 4.9. It is clear that the resultant steering angle, represented by the blue line, is significantly different from the black dotted line, which is the steady-state optimum. However, the final displacements achieved are very similar in both cases. This is an interesting point from a controllability point of view. It can be argued that resultant steering angle may achieve very similar performance with more controllability retained in the dynamics throughout the manoeuvre. The optimised steering angle actually exceeds the target value after 4 seconds, hence one may think that the associated trajectory is less controllable. However, it can be observed that the optimised trajectory only crosses the point of limit adhesion momentarily, whereas the target trajectory stays on it all the time. Therefore the time-varying linear model for the

optimised trajectory retains non-zero gradient for majority of the time period. This will be investigated via determination of the Controllability Gramian, which will be discussed in the next chapter.

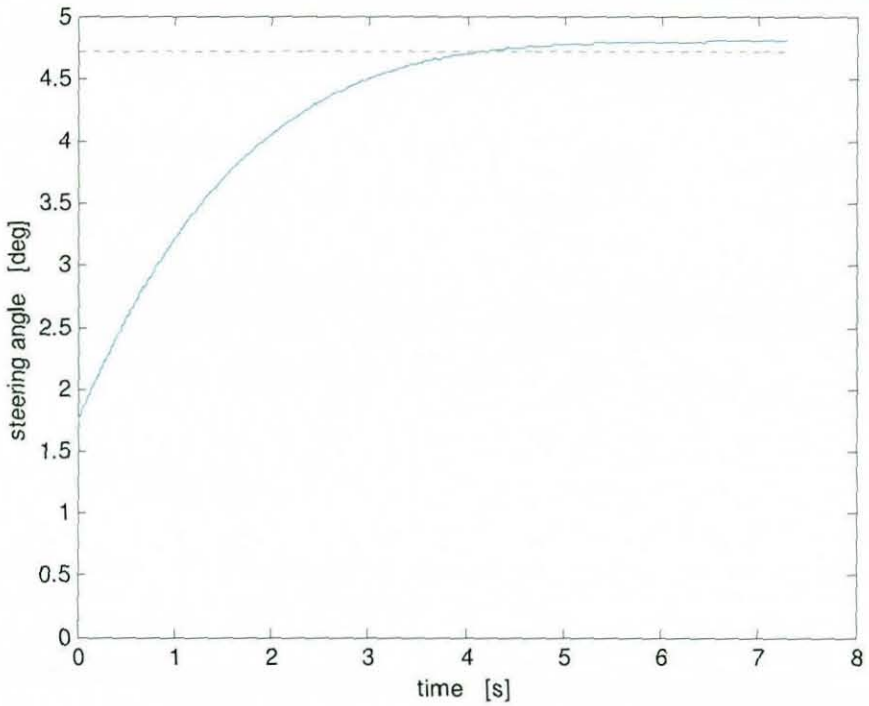

Figure 4.9 Resultant Steering Angle Profile

Figure 4.10 shows that the roll angle and velocity states are converging towards the optimal steady-state values. Noticeable oscillations are present at the earlier time period is present due to the "incompatible" combination of the initial states, which are taken from the peak performance, and relatively small steering angle magnitude. This oscillation reduces through the iterations as the steering angle profile becomes more suitable to the state initial conditions.

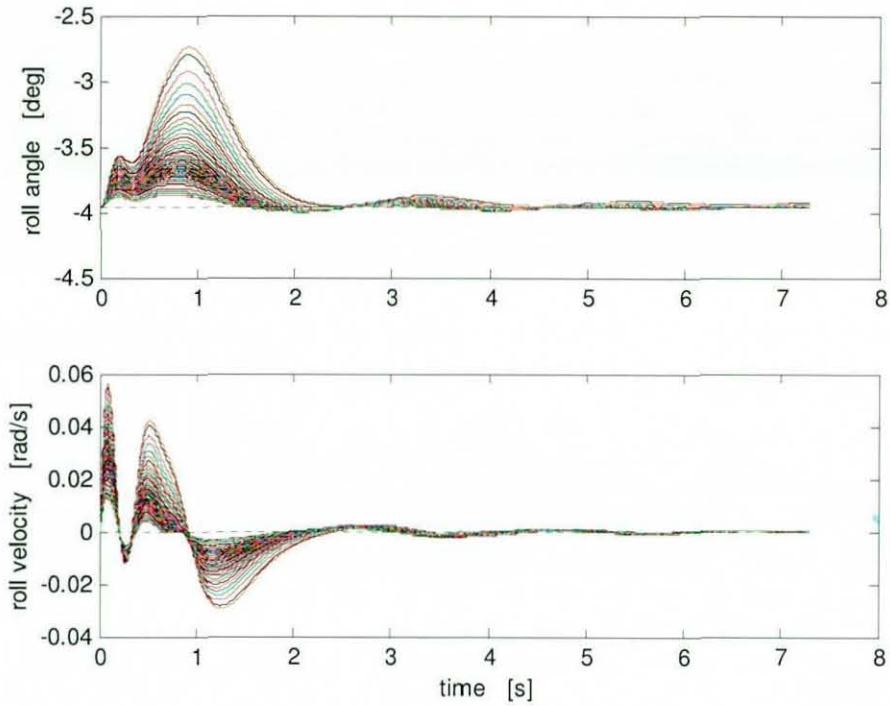

Figure 4.10 Roll Degree-of-Freedom characteristics

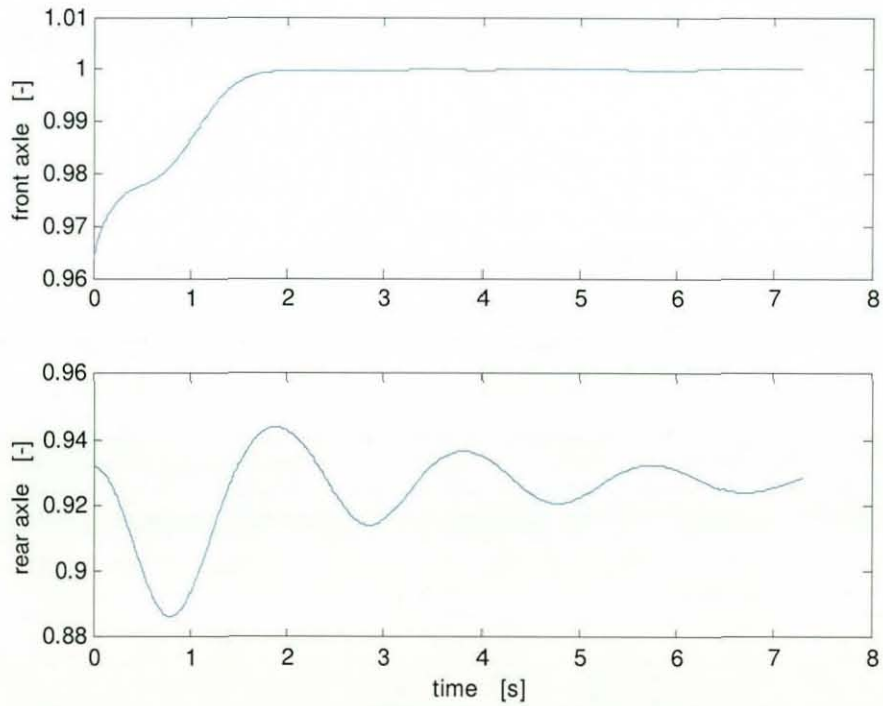

Figure 4.11 Normalised Tyre Forces

Normalised tyre forces are shown in Figure 4.11. A tyre is at the limit of adhesion when the normalised force is equal to 1.0 [Milliken, 1995]. It can be seen that the front tyres stay at the limit after the transient period of approximately 2 seconds. Moreover, rear tyres are also utilised at an average 93% of their capability with some oscillations. Therefore, together with the final lateral displacement and vehicle path result discussed earlier, it can be concluded that the optimisation method is capable of solving a problem at the vicinity of the friction limit.

4.2.4 Optimisation Issue

Although the accuracy of the result is acceptable in terms of the achieved final displacement and trajectory, it was found that the optimisation method itself is still not very stable. This is apparent as the cost sometimes increases when the optimisation becomes very close to the limit handling condition. An example of the optimisation result in terms of the final displacement over the iterations is shown in Figure 4.12. It is clear that beyond 56th iteration the cost fluctuates due to the reduction in final displacement achieved.

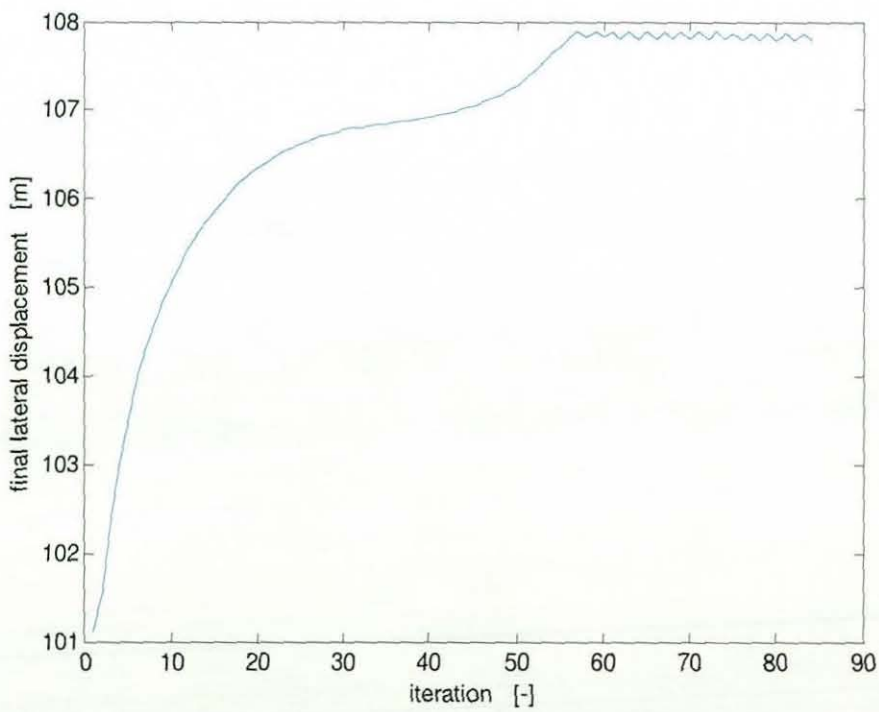

Figure 4.12 Optimisation Result over Iterations

From the definition of optimal control [Barnett, 1985], the result at the new iteration should always be an improvement on the previous iteration. However, this is clearly not the case in Figure 4.12. One possible cause of this error is on the regulation of control signal magnitude. If the control magnitude is large enough so that the dynamics can no longer be represented accurately by the time-varying linearised model, the optimisation fails. However, this can be and is carefully regulated via the magnitude of road geometry cost, Equations 4.2 and 4.3, and the control cost, R, in Equation 2.95.

In order to further investigate this issue, the concept of Controllability needs to be investigated, which will be discussed in the following chapters.

4.3 Summary

An iterative method for optimum path finding problem is established using linear time-varying controller, and is applied to a 3DOF vehicle handling model.

Path optimisation was performed for simple double-corner geometry (two 90 degrees bends connected by short straights). It is found that the optimisation was able to find the first apex, however, not the second (whilst it is still driving towards it). Since quadratic cost function is used for road geometry constraints, the cost gradient becomes significantly high when the vehicle path is very close to the edge of the road boundary. This then prevents further deviation at next iteration, hence the optimisation is not able to progress further from such point. Therefore, the optimisation needs to be formulated in order to avoid this at the early stages of the iteration process.

Because of the issue mentioned above, the validity of optimisation method needs to be investigated in another environment. Steady-state "steering pad" simulation was used for this purpose and was performed at limit handling condition. It was found that the method itself works satisfactory, using the front tyres at the limit

capacity whilst retaining some margin at the rear. The optimisation displaced vehicle within 0.4% of the theoretical maximum.

However, the optimisation encounters a problem when the system condition becomes poor near the limit handling situation. This is characterised by fluctuation of the resultant cost at later iterations. It is thought that the matrix becomes poorly conditioned due to lack of controllability and hence resulting in inappropriate control inputs. This is investigated in following chapters.

Chapter 5

The Controllability of a Nonlinear System with Linear Time–Varying Modelling Approach

In Chapter 3, the reference model 4WS control structure was designed in order to achieve particular dynamic characteristics. The hypothesis is that this particular dynamics are thought to be predictable and hence relatively easy to control. The system was represented using a linear time-invariant model.

In Chapter 4, a linear time-varying method is used in order to better represent the vehicle operating conditions through the various dynamic range, including at the limit of adhesion. This was applied to vehicle path optimisation problem and it achieved satisfactory result in terms of the final target. However, there was an issue with the optimisation where the cost fluctuates towards the end of the iterative method. In order to better understand the mechanism which this failure mode occurs, controllability theory must be studied.

In addition, near the limit of adhesion, a driver experiences that a vehicle becomes more "difficult" to control. The prescribed dynamics used in Chapter 3 may or may not make this task easier for a driver. Further research is required in order to investigate desirable dynamics for certain operating conditions. It is thought that the study of controllability could provide some insight into this topic.

In this chapter, in-depth discussion of controllability is presented. The brief overview of the controllability for a Linear Time-Invariant (LTI) system is followed by the theory for determining the controllability Gramian for a Linear Time-Varying (LTV) system, -applicable for the following chapters-, with two different methods. The first method uses the state transition matrix, and its

procedure and limitation are discussed. The alternative procedure (the ξ Method) is then presented and compared. Having defined the method to calculate controllability Gramian, its property is analysed. This is then used to determine the open loop control action both as a regulator and tracking controller to further understand the system dynamics. The method is firstly tested on the quarter car vehicle model due to its simplicity in its dynamics. It is then applied to a 3 Degree-of-Freedom (3DOF) handling model for steady-state and cornering simulation. The purpose of the steady-state simulation is the validation of the method, where the maximum achievable value (in terms of the set cost function) is known for a given test condition. Thus the relationship between a vehicle reaching the limit performance and controllability can be studied.

5.1 Introduction

Prior to designing a controller to target certain performance objectives, it is essential to determine whether the objectives can actually be met through the specified set of control inputs or not. When a vehicle is driven within a non-demanding environment, states are expected to be transferable from one value to the other within a "reasonable" range. By contrast, if a vehicle is at the limit of its performance envelope, the states can only be transferable in one direction. In other words, regardless of whether the control effort is increased or decreased, the states are transferred to the direction such that it degrades the resultant vehicle performance. This means that the objective function itself may have to be altered depending on the vehicle operating conditions or some other means of control needs to be applied. For example, the 4WS controlled vehicle described in the Chapter 3 may lose its controllability due to lateral force saturation. Then, it is no longer able to achieve the given objective function. Other means of control, such as direct yaw moment control or active suspension, could then be used to "regain" some controllability.

Most of the work undertaken within this research project involves a vehicle operating at or close to the limit of adhesion. Therefore it is important to understand this controllability information in order to assess the controller

performance. The actual integration of controllability into a controller, however, is outside the scope of this thesis.

As mentioned earlier, a 4WS controller was designed in Chapter 3 so that the vehicle has certain dynamic characteristics. If the controller was able to achieve the same level of performance with various vehicle set-ups (for example), it might be possible to argue that the one that retains the highest controllability is the desired set-up.

In order to analyse the dynamics of a nonlinear system, the system can be represented by a time-varying linear model [Silverman, 1967]. This enables one to investigate the controllability of the system analytically. When a nonlinear system is linearised at the peak of its performance range, the gradient of the linearised system approaches zero. Hence the system is insensitive to any input value variation. This fools the controller and it leads to a demand signal being unnecessarily large. Controllability information can be used to regulate the control effort accordingly in order to avoid such a situation in a formal manner.

In this chapter, the derivation and property of controllability is discussed in detail, especially in the case of linear time varying system. The theoretical approach is then compared against the more practical approach, and their relative merits and demerits are discussed.

5.2 Controllability of Time-Invariant System

The controllability of a time-invariant system is well documented in various literatures. Although time-invariant controllability is not directly applied in this thesis, it is studied here since its understanding is fundamental to further work described in this chapter.

Consider the constant system

$$\dot{x} = Ax + Bu \tag{5.1}$$

The above system is said to be controllable at $t = t_0$ if it is possible to define an unconstrained control signal that will transfer an initial state to any final state in a finite time interval $t_0 \le t \le t_1$ [Barnett, 1985]. The stronger condition of complete controllability requires every state to be controllable.

The solution to (5.1) can be written as [Barnett, 1985]

$$x(t) = e^{At}x(0) + \int_0^t e^{A(t-\tau)}Bu(\tau)d\tau \tag{5.2}$$

Assume that the final state is the origin of the state space, we have

$$x(t_1) = 0 = e^{At_1}x(0) + \int_0^{t_1} e^{A(t_1-\tau)}Bu(\tau)d\tau$$

or

$$x(0) = -\int_0^{t_1} e^{-A\tau}Bu(\tau)d\tau \tag{5.3}$$

$e^{-A\tau}$ can be written [Rugh, 1996]

$$e^{-A\tau} = \sum_{k=0}^{n-1} \alpha_k(\tau)A^k \tag{5.4}$$

Substituting (5.4) into (5.3) gives

$$x(0) = -\sum_{k=0}^{n-1} A^k B \int_0^{t_1} \alpha_k(\tau)u(\tau)d\tau \tag{5.5}$$

Define

$$\beta_k = \int_0^{t_1} \alpha_k(\tau)u(\tau)d\tau$$

Then (5.5) becomes

$$x(0) = -\sum_{k=0}^{n-1} A^k B\beta_k$$

$$= \begin{bmatrix} B & AB & A^2B & \cdots & A^{n-1}B \end{bmatrix} \begin{bmatrix} \beta_0 \\ \beta_1 \\ \beta_2 \\ \vdots \\ \beta_0 \end{bmatrix} \tag{5.6}$$

For a system to be completely controllable for given any initial state $x(0)$, (5.6) has to be satisfied. Therefore the system is completely controllable if and only if the controllability matrix

$$U = \begin{bmatrix} B & AB & A^2B & \dots & A^{n-1}B \end{bmatrix}$$

has rank n, or the vectors are linearly independent. [Barnett, 1985]

5.3 Controllability of Time-Varying System

The controllability theory for time-invariant system is then extended to a time-varying system. This information is used in the following chapters where the research is based on a time-varying linear model representation.

5.3.1 State Transition Matrix Method

Consider the uncontrolled linear time varying system

$$\dot{x}(t) = A(t)x(t), \qquad x(0) = x_0 \qquad (5.7)$$

If $A(t)$ is continuous for $t \geq 0$ then (5.7) has a unique solution for $t \geq 0$ given by $x(t) = X(t)x_0$, where $X(t)$ is the unique $n \times n$ matrix satisfying

$$\frac{dX}{dt} = \tilde{A}(t)X(t), \qquad X(0) = \mathrm{I}. \qquad (5.8)$$

[Barnett, 1985]

In order to solve (5.8) with the given initial condition for the state being the identity matrix, the *Scaling Matrix*, S, has to be defined.

The system equation with non-scaled states is : $\dot{x}(t) = A(t)x(t)$

Scaling is applied as follows

$$\dot{z} = \tilde{A}z$$
$$x = Sz$$

$$S\dot{z} = ASz$$
$$\dot{z} = S^{-1}ASz$$
$$\therefore \tilde{A}(t) = S^{-1}A(t)S$$

Scaling matrix is a diagonal matrix whose elements consist of the "typical large values" of the states. Having solved (5.8), *State Transition Matrix* is then defined as follows and it exists for all $t, t_0 \geq 0$, [Barnett, 1985].

$$\Phi(t,t_0) = X(t)X^{-1}(t_0) \tag{5.9}$$

By direct differentiation, it can be verified that

$$x(t) = \Phi(t,t_0)x_0 \tag{5.10}$$

is the solution of (5.7) with the initial condition of $x(t_0) = x_0$, [Barnett, 1985]. In other words, the transition matrix, $\Phi(t,t_0)$, transfers the states from x_0 to $x(t)$. From (5.10) and the definition of a system matrix, *A*, it is clear that the transition matrix can be expressed in exponential form as follows.

$$\Phi(t,t_0) = e^{A(t-t_0)} \tag{5.11}$$

Hence, the solution of the controlled system

$$\dot{x}(t) = A(t)x(t) + B(t)u(t) \tag{5.12}$$

subject to the initial condition $x(t_0) = x_0$ can be given using the state transition matrix as

$$x(t) = \Phi(t,t_0)\left[x_0 + \int_{t_0}^{t} \Phi(t_0,\tau)B(\tau)u(\tau)d\tau\right] \tag{5.13}$$

[Barnett, 1985]

The controlled system, (5.12), is said to be *completely controllable* (c.c.) if for any t_0, any initial state $x(t_0) = x_0$ and any given final state x_f there exists a finite time $t_1 > t_0$ and a control $u(t)$, $t_0 \leq t \leq t_1$, such that $x(t_1) = x_f$. The term "*completely*" implies that the definition holds for all x_0 and x_f. The control $u(t)$ is assumed piecewise continuous in the interval t_0 to t_1, in other words, continuous except at a finite number of points in the interval, [Barnett, 1985].

From the expression (5.13), the final state vector is expressed as

$$x_f = \Phi(t_1, t_0)\left[x_0 + \int_{t_0}^{t_1} \Phi(t_0, \tau) B(\tau) u(\tau) d\tau \right] \qquad (5.14)$$

Alternatively, using the property of the transition matrix $\Phi(t,t) = \mathrm{I}$, and rearranging the above expression, the following equation can be written.

$$0 = \Phi(t_1, t_0)\left[\left\{ x_0 - \Phi(t_0, t_1) x_f \right\} + \int_{t_0}^{t_1} \Phi(t_0, \tau) B(\tau) u(\tau) d\tau \right] \qquad (5.15)$$

Since $\Phi(t_1, t_0)$ is nonsingular, it follows that if $u(t)$ transfers x_0 to x_f, it also transfers $x_0 - \Phi(t_0, t_1) x_f$ to the origin in the same time interval, [Barnett, 1985].

The controlled system (5.12) is *c.c.* if and only if the $n \times n$ symmetric *controllability Gramian matrix*

$$W(t_0, t_1) = \int_{t_0}^{t_1} \Phi(t_0, \tau) B(\tau) B^T(\tau) \Phi^T(t_0, \tau) d\tau \qquad (5.16)$$

is invertible, where the state transition matrix, Φ, is non-singular, [Barnett, 1985]. $W(t_0, t_1)$ satisfies the following linear matrix differential equation.

$$\frac{d}{dt} W(t, t_1) = A(t) W(t, t_1) + W(t, t_1) A^T(t) - B(t) B^T(t) \qquad (5.17)$$

with the initial condition $W(t_1, t_1) = 0$, [Rugh, 1996]. This equation is solved reverse in time to determine the *Controllability Gramian.*

The following control input, $u(t)$, that transfers $x(t_0) = x_0$ to $x(t_1) = x_f$ is then defined on $t_0 \le t \le t_1$

$$u(t) = -B(t)^T \Phi^T(t_0, t) W^{-1}(t_0, t_1)\left[x_0 - \Phi(t_0, t_1) x_f \right] \qquad (5.18)$$

[Brockett, 1970]

For a simple regulator case (5.18) becomes

$$u(t) = -B(t)^T \Phi^T(t_0, t) W^{-1}(t_0, t_1) x_0 \qquad (5.19)$$

However, in practice, determining the controllability Gramian using the reverse-time state transition matrix, $\Phi(t_0, \tau)$, encounter its limitation when used for a well-damped system especially when τ values are large. In such a system, state values decay quickly to zero, hence the transition matrix would be very large. Moreover, as $X(t)$ is close to *singular* for such a system, the inverse of $X(t)$, Equation 5.9, is not well defined.

Although this result is still valid mathematically, it is not totally applicable in a practical sense. From experience, it is not difficult to understand that in order to transfer the states to the desired values, the control should be applied near the final time. This is because the effects from any control applied at the earlier time decay very quickly for a well-damped system. Thus such control has a little effect on the final state values.

In order to investigate the validity of the calculated state transition matrices, a free motion simulation is considered. A nonlinear vehicle is given an initial (set of states) condition equivalent to 1 degree of steering input and its uncontrolled motion is represented by the black dotted lines in Figure 5.1. State transition matrices are calculated based on this nominal trajectory. Using the property of the state transition matrix shown in (5.10), the states are reconstructed with the initial state deviation that corresponds to 10% of the initial value used in the nominal trajectory (blue lines). Red lines represent the nonlinear model trajectory with the initial condition of nominal value plus deviation. It shows that the state transition matrix is defined accurately only up to a certain time period. Beyond 0.35 seconds, the sensitivity to the shifted state value becomes significant and the solution diverges. The numerical problem involves the inversion of $X(t)$ is highlighted again in this example.

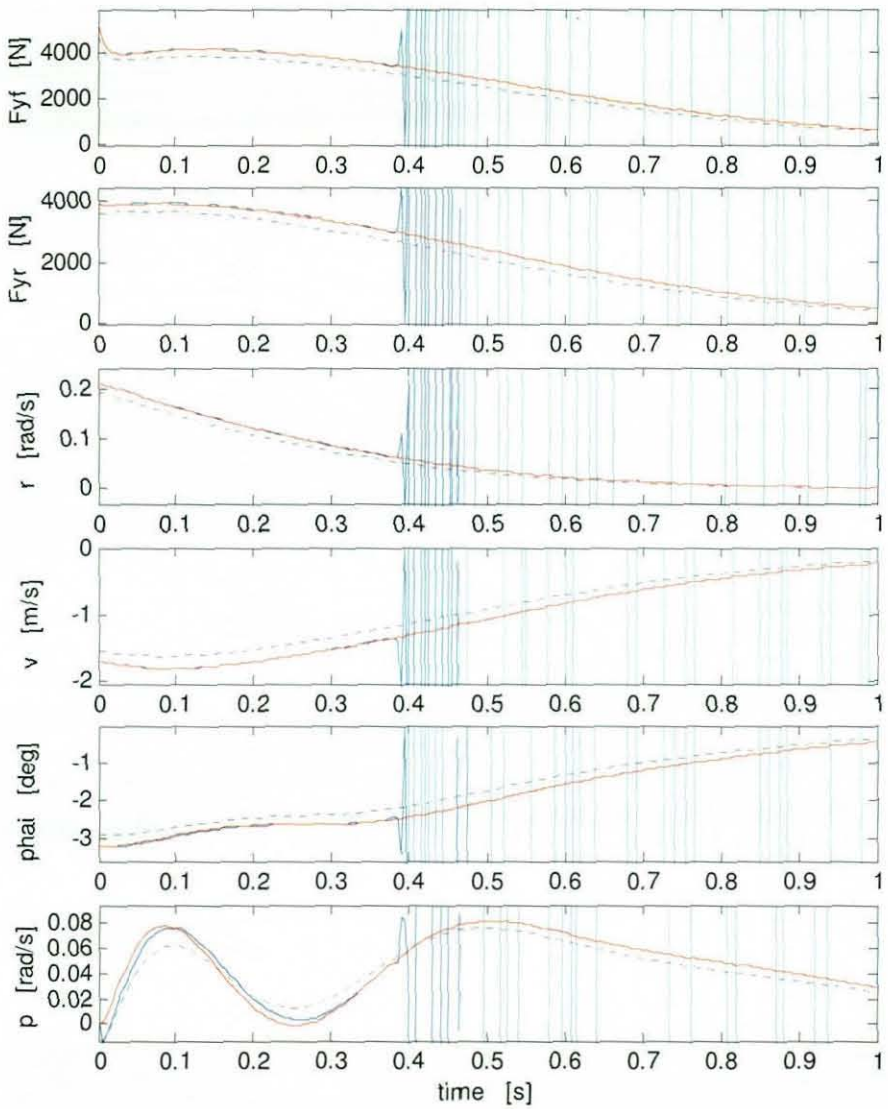

Figure 5.1 State Re-construction with State Transition Matrices

In order to rectify this numerical problem, the singular values of $X(t)$ are constantly monitored and the values that causes numerical instability are re-set according to the tolerance as defined below.

$$n\|X(t)\|\varepsilon \tag{5.20}$$

Where ε is the floating-point relative accuracy and n is the number of the states.

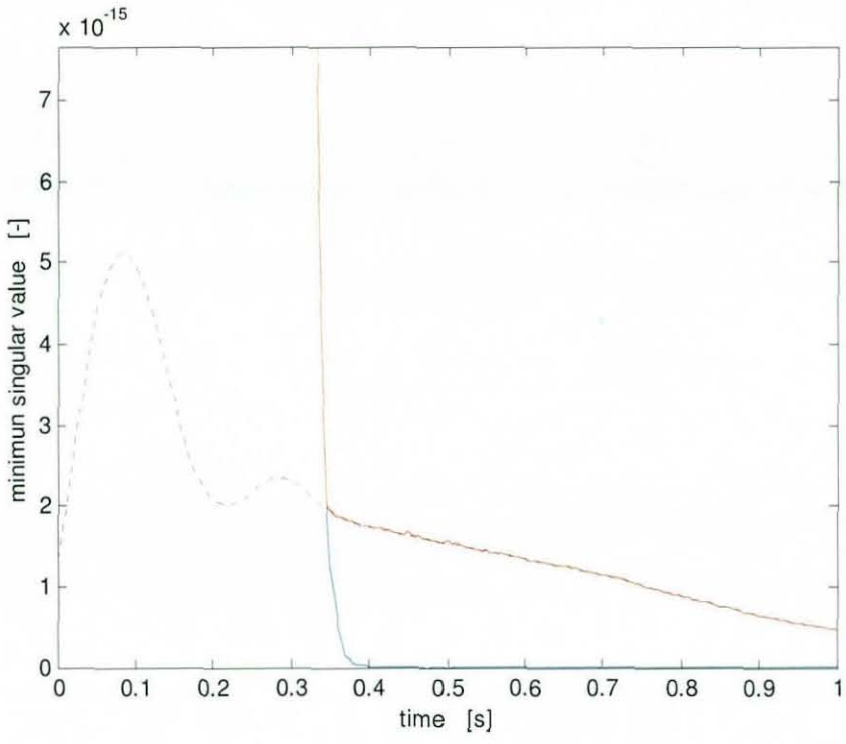

Figure 5.2 Minimum Singular Value of $X(t)$

It is clear from Figure 5.2 that certain minimum singular values are causing the numerical instability shown in Figure 5.1. The black dotted line shows the tolerance set by (5.20). The blue line is the "unconstrained" singular value where it becomes smaller than the minimum tolerance after 0.35 seconds. The new singular value is then set as shown by the red line.

The modified $X(t)$ value with the new singular values are then determined using the property of Singular Value Decomposition method [Press et al, 2007], i.e.

$$X(t)_{new} = U(t)S(t)_{new}V^{T}(t) \tag{5.21}$$

Figure 5.3 shows the resultant state reconstruction using the identical simulation environment as used for Figure 5.1. It is clear that the numerical instability problem has been solved and the accuracy of state transition matrices has been maintained.

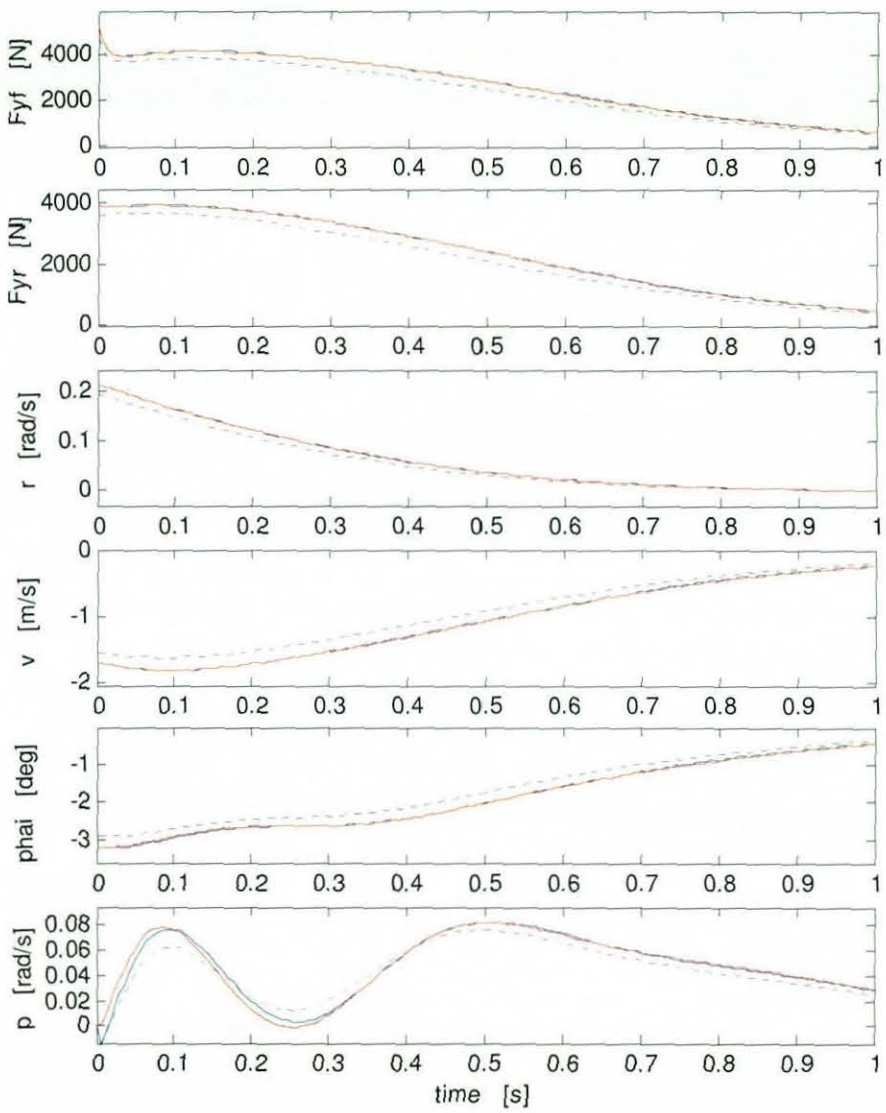

Figure 5.3 State Re-construction with modified Transition Matrices

5.3.2 ξ Method

In this section, the alternative method for calculating the controllability Gramian is presented. This method is investigated in order to circumvent the problem experienced in state transition matrix calculation for a well-damped system.

Consider an uncontrolled system defined in (5.7) with the scaled system matrix replacing the original matrix.

$$\dot{x}(t) = \tilde{A}(t)x(t)$$

The above differential equation can be solved reverse in time with the initial condition $x(\tau) = B(\tau)$, and the final state vector is defined as $\xi(\tau) = x(0)$. It must be noted that the system in reverse time has to be defined as $\dot{x}(t) = -\tilde{A}(t)x(t)$. It is then clear to see the relationship between $B(\tau)$ and $\xi(\tau)$ with the state transition matrix as shown below.

$$\xi(\tau) = \Phi(t_0, \tau)B(\tau) \tag{5.22}$$

Recall the definition of controllability Gramian in (5.16), the alternative expression using $\xi(\tau)$ is defined as

$$W(t_0, t_1) = \int_{t_0}^{t_1} \left(\xi(\tau)\xi^T(\tau)\right) d\tau \tag{5.23}$$

Unfortunately, it is found that ξ method has a setback similar to the state transition matrix method. Consider a following scalar system

$$\dot{x} = ax + bu \text{ with } a = -0.01 \text{ and } b = 1$$

Recall that $\xi(\tau)$ is determined reverse in time, using (5.22) we have

$$\xi(\tau) = e^{-a\tau}b \tag{5.24}$$

With (5.23), Controllability Gramian for the scalar system is then written as

$$W(t_0, t_1) = \int_{t_0}^{t_1} \left(\xi(\tau)\xi^T(\tau)\right) d\tau = \int_{t_0}^{t_1} \xi^2(\tau) d\tau \tag{5.25}$$

Substituting (5.24) into (5.25), and solving for the finite time integral case of $t_0 = 0, t_1 = 2$ gives a following result.

$$\begin{aligned} W(t_0, t_1) &= \int_{t_0}^{t_1} \xi^2(\tau) d\tau \\ &= \int_0^2 e^{-2a\tau} d\tau \\ &= -\frac{1}{2a}\left[e^{-2a\tau}\right]_0^2 \\ &= 0.204 \end{aligned}$$

The above result agrees with the solution obtained by solving the following continuous-time Lyapunov equation, clearly only applicable to *LTI* systems.

$$AW + WA^T + BB^T = 0 \tag{5.26}$$

The solution to the Lyapunov equation is obtained by infinite time integration forwards in time [Rugh, 1996].

$$W = \int_0^\infty \left(e^{A\tau} BB^T e^{A^T\tau} \right) d\tau \tag{5.27}$$

The limitation of the ξ method is noticed when (5.25) is solved with an infinite time limit. This is readily demonstrated as follows

$$\begin{aligned} W(t_0, t_1) &= -\frac{1}{2a}\left[e^{-2a\tau} \right]_0^\infty \\ &= -\frac{1}{2a}(\infty - 1) = \infty \end{aligned}$$

This is purely due to the fact that the differential equation is solved reverse in time. In other words, if $\xi(\tau)$ is defined forwards in time, the solutions of (5.25) and (5.27) agree. Comparison of (5.17) and (5.26), time-varying and time-invariant cases respectively, reveals that this sign discrepancy in reverse and forward time integration is included. This implies that the Controllability Gramian should be determined via (5.17), rather than via $\xi(\tau)$. However, this information is still required if one requires to determine an open-loop control. Open–loop control is used later on in this thesis for the purpose of validation and further investigation into the controllability – dynamics relationship.

There also is a limitation in solving a Lyapunov equation as the integration is defined with an infinite upper limit. This means that the *A* matrix has to have all the eigenvalues with negative real parts (i.e. negative definite), otherwise a finite solution cannot be obtained. Practically this is then incorrect in the case of a conditionally stable system (i.e. some of the states have eigenvalues with zero real part) when it is actually controllable.

The ξ method is applied to the LTI Quarter Car Model, as described in Chapter 2, in order to investigate its validity. Please refer to Table 2.1 of Chapter 2 for the system parameters used for the model. Quarter Car model is chosen for this validation due to the simplicity of its dynamics. The following figures highlight the accuracy of ξ method and its limitation.

From (5.19), it is clear that if the states initial condition is set as $\xi(\tau)$, then it should converge to final states of $B(\tau)$ when simulated forwards in time. Figure 5.4 shows the error between the actual calculated value and the free motion simulation result for a lightly damped system. The error increases as τ increases, however within the negligible magnitude. τ is the time available for control.

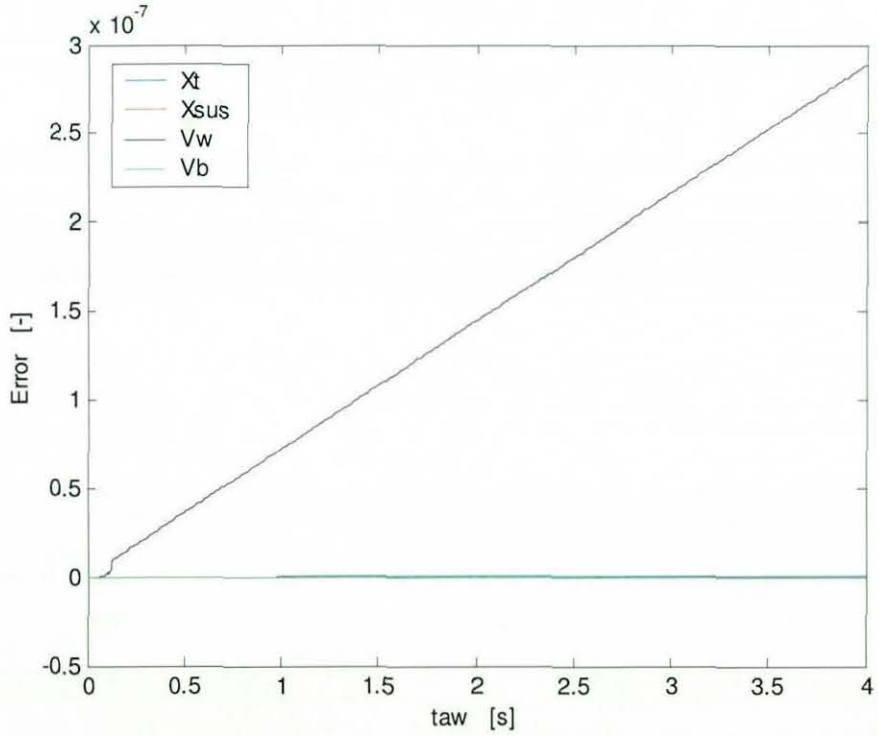

Figure 5.4 ξ Calculation Error

By contrast, Figure 5.5 shows the significant amount of error when the method is applied to a well-damped system.

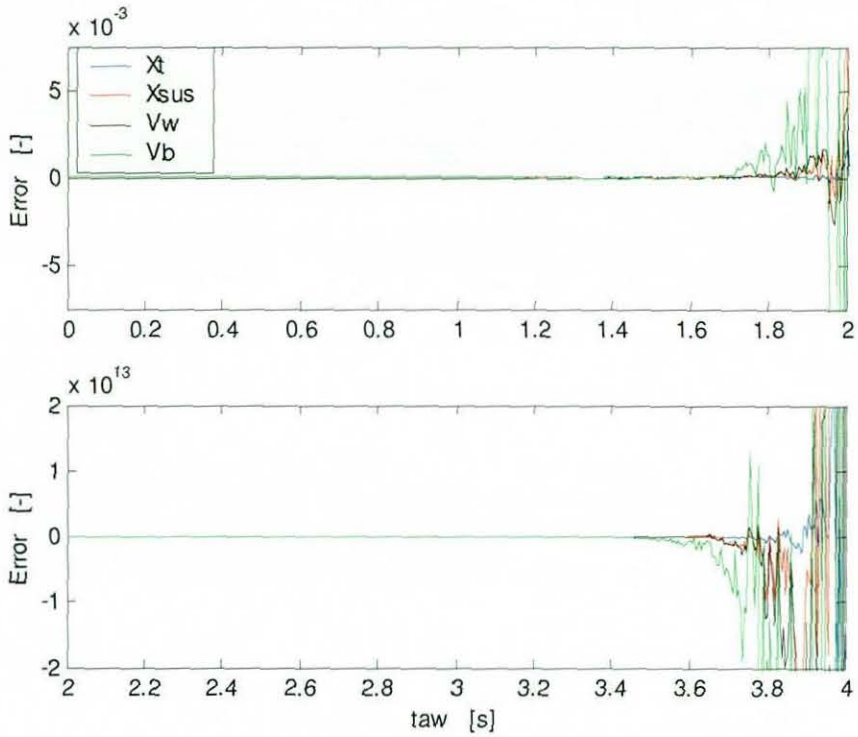

Figure 5.5 ξ Calculation Error for a well-damped system

For τ values less than 2 seconds, the calculation error is relatively small. However, the error grows to a considerable magnitude as the control time window is increased further. Thus the subsequent Gramian calculation would not be correct. The above figure indicates that "if you have plenty of time to apply control, the controller fails". Again, this is not correct practically for the same reason as discussed earlier.

5.3.3 Analysis of Controllability Gramian Matrix

In the previous two sections of this thesis, the different ways of calculating the controllability gramian matrix are discussed. It is noted that neither of the methods are perfect and have similar shortcomings. This section investigates the properties of the gramian matrix. Through this study, the influence of the two different calculation methods is examined further.

As stated in (5.16), the controlled system is *c.c.* provided the Gramian matrix is invertible. In order to investigate the invertibility, *Singular Value Decomposition*

(SVD) is performed rather than calculating its determinant. SVD is thought to be a better measure as it can always be performed and it is "almost" unique no matter how singular the matrix is. The condition number, which is the ratio between the largest and the smallest singular values, can then be used as a measure of invertibility. It has to be noted that the state values have to be well balanced in magnitude to gain a meaningful measure from a condition number. Figure 5.6 shows the condition number of the Gramian for the lightly damped system. Quarter car ride model is used with very small suspension stiffness and damping coefficients. The stiffness and damping values were reduced by factor of 100 compared to the baseline parameter values shown in Table 2.1 of Chapter 2.

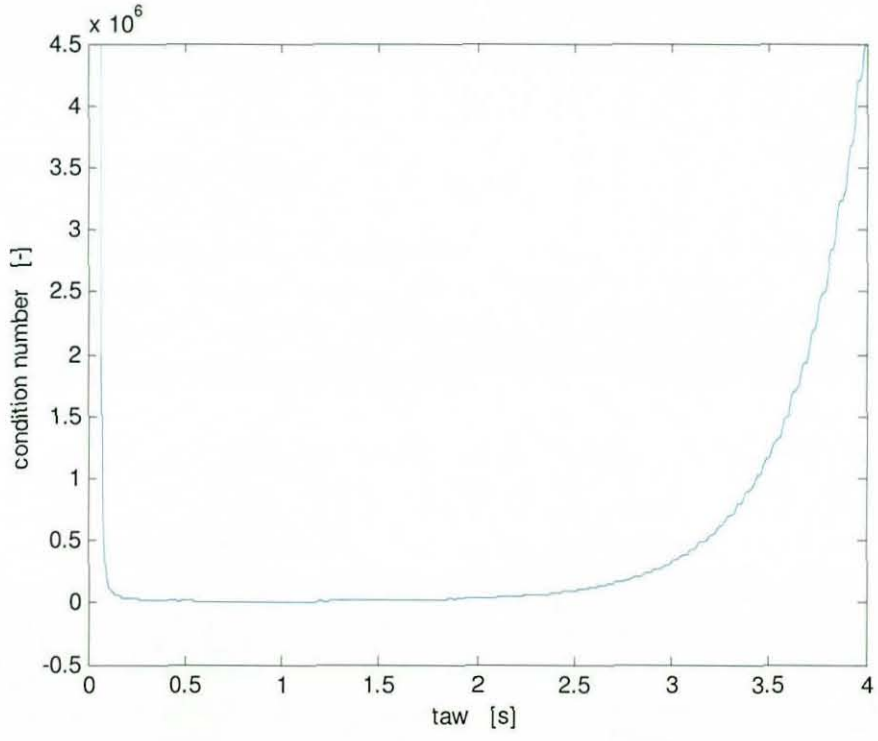

Figure 5.6 Condition Number of Gramian Matrix

It is clear from the above figure that the system is not controllable when the time allowed for control, τ, is very small. Moreover, the figure also indicates that the controllability degrades as τ becomes larger than the certain value. This is due to the dynamic characteristics of the uncontrolled system. Some of the states decay

to zero after approximately 2 seconds, this makes the relevant element of Gramian matrix very large, hence the characteristics shown in Figure 5.6.

Alternatively, the inverse of the minimum singular value can be used as a measure of controllability. This avoids the unbalanced state magnitude problem as discussed earlier, and the result is shown in Figure 5.7. It shows that the controllability improves as τ increases.

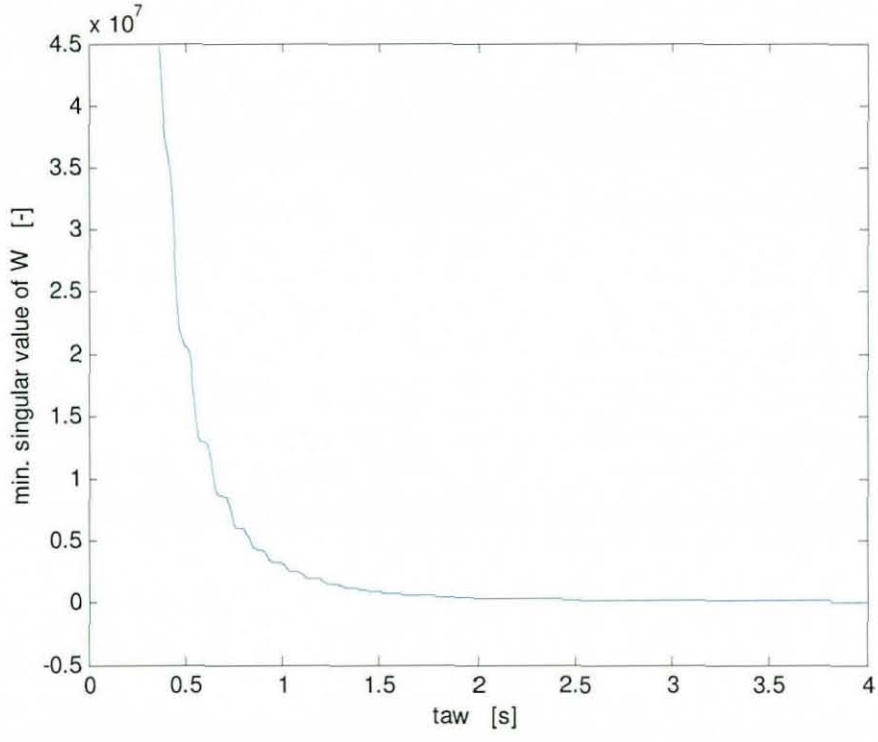

Figure 5.7 Inverse of Minimum Singular Value of Gramian Matrix

In order to assess the implications of Gramian matrix properties with respect to various operating conditions, a 3DOF vehicle handling model, as described in Chapter 2, is used. For Figures 5.6 and 5.7, Gramian matrices are determined using ξ matrix calculation. However, due to the problem of the ξ method mentioned earlier, Figure 5.8 is generated via solving (5.17) for the reference trajectories with various step steer angles (and hence various operating conditions).

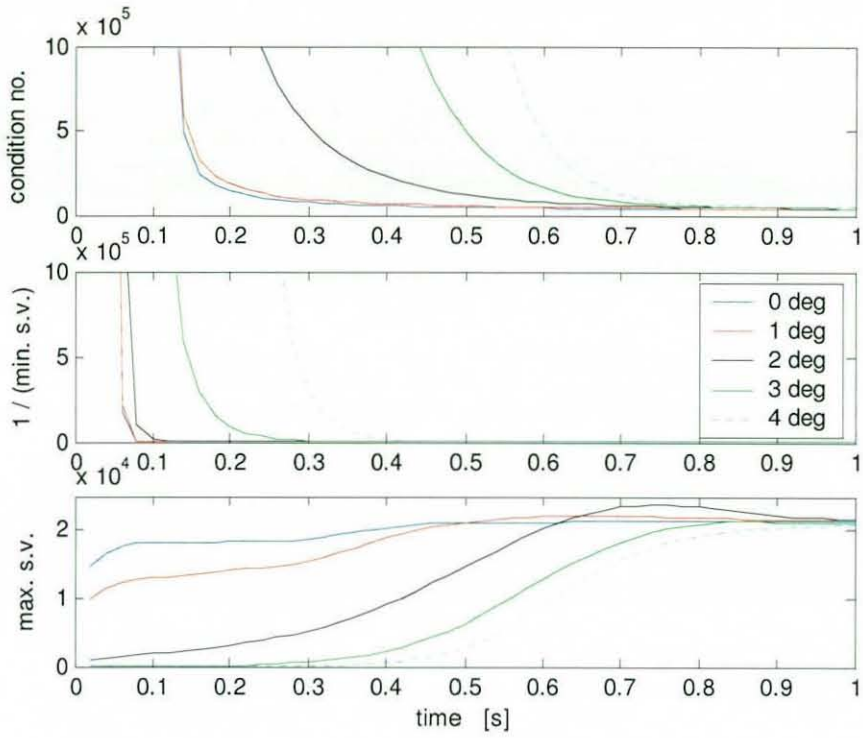

Figure 5.8 Gramian Information for Step Steer Simulation

It is clear from the condition number and the inverse of the minimum singular value that the system becomes less controllable as the magnitude of step steer is increased. This is because a controller requires more time to transfer the states as the input becomes larger. Moreover, it has to be noted that the interpretation of controllability varies depending on the particular parameter used for investigation. In other words, if the condition number is used, it can be concluded that all the vehicles have a similar controllability if more than 0.9 seconds is allowed for control. However, this time period, at which all the vehicles have similar controllability, is reduced to 0.5 seconds if the inverse of minimum singular value is used as a measurement parameter. Therefore, the decision needs to be taken carefully as to which parameter should be used as a measure of controllability.

Figure 5.9 shows the Gramian characteristics for a longer period of time. The condition number part of Figure 5.9 can be compared with Figure 5.6 where the Gramian was determined through the ξ method. Figure 5.6 saw a significant

increase in condition number when τ is large and its lack of correlation to real life was discussed. By comparison, the condition number is reasonably well controlled in Figure 5.9. However, for a measure of actual controllability, the inverse of minimum singular value information should be used as it relates most to reality.

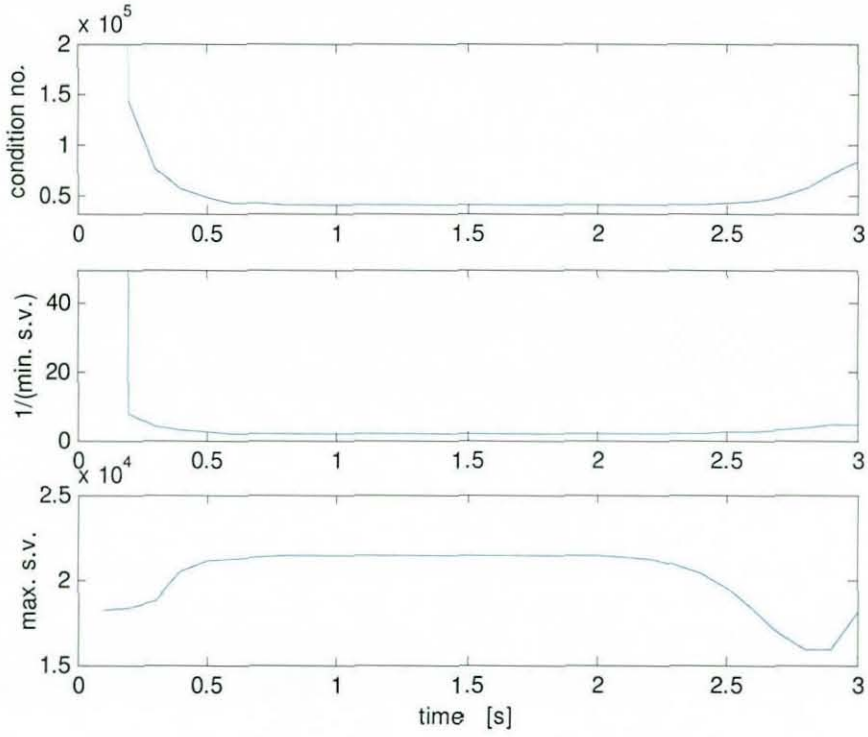

Figure 5.9 Gramian for longer final time

It has to be noted that this approach can only give an indication of controllability, it does not give the subsequent open loop control as it requires ξ matrix information. This open loop control input calculation is discussed in the next section.

5.3.4 Open-Loop Control using Gramian Matrix, Quarter Car Ride Model

The results of *Gramian* calculation shown in Figures 5.6, 5.7, 5.8 and 5.9 can then be used to define an application period for control input (suspension force). The upper τ value can be determined according to the tolerance set with respect to the magnitude of its calculation error. The lower limit can also be set with regard to

either the threshold in condition number or the magnitude of minimum singular value.

Open loop time-varying regulator control is defined in (5.18), this can be expressed in terms of $\xi(\tau)$ using the definition stated in (5.19). Figure 5.10 shows the control input (suspension force) profile with various τ, defined for a lightly damped system.

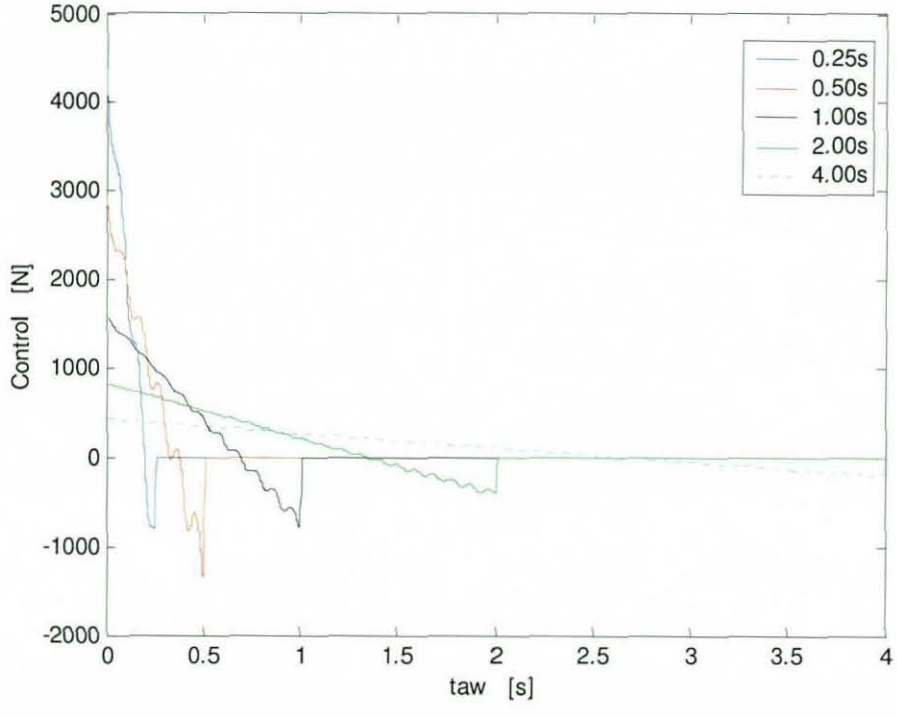

Figure 5.10 Control Input Profile

It is clear that the control magnitude increases as control time window, τ, reduces. It is inevitable that the large amount of effort is required to control states in a short amount of time. It is found that the system cannot be regulated when τ is decreased further than the smallest value shown in Figure 5.10, i.e. 0.25 sec. This is as expected since Figures 5.9 shows that the controllability becomes extremely poor when τ is reduced to approximately less than 0.25.

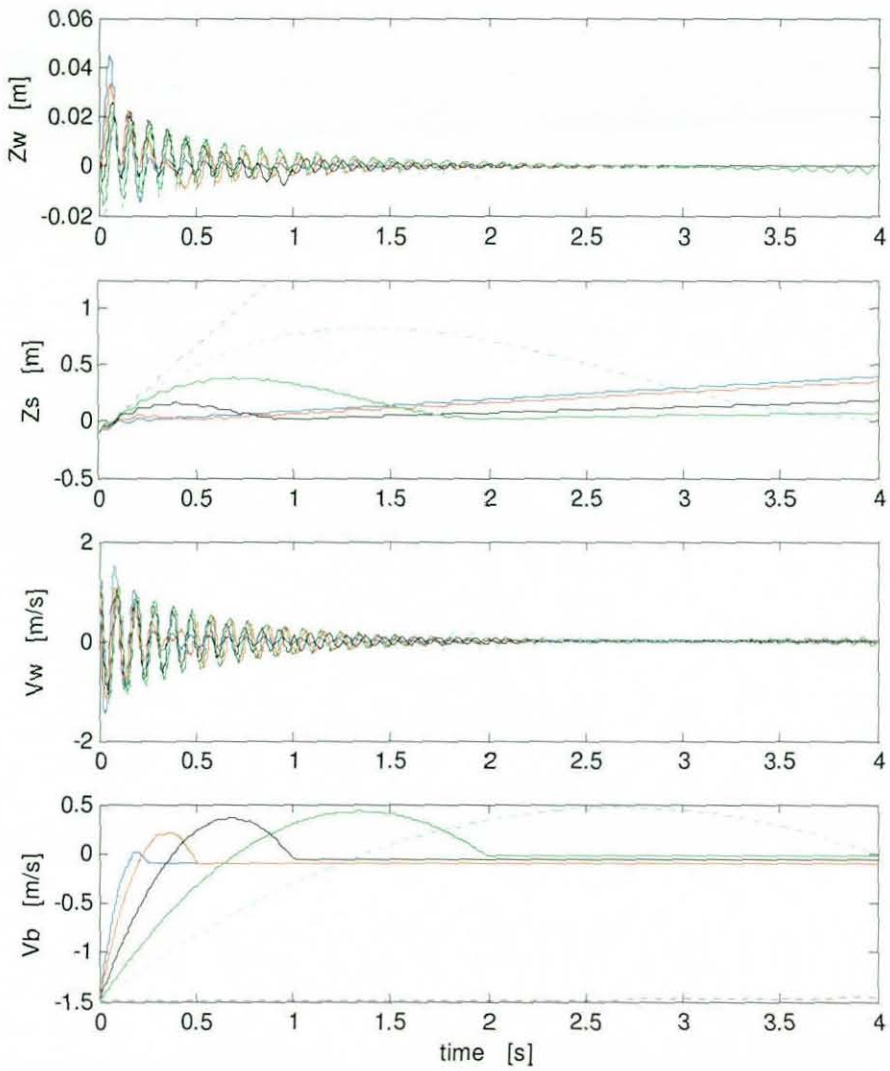

Figure 5.11 Open – Loop Control of Lightly-Damped System

Figure 5.11 shows the result of applying the control profile shown in Figure 5.10 to a Quarter Car vehicle ride model. It can be seen that the applied control successfully regulates the states within a specified time period. Steady-state error occurs since it is an open loop control policy, thus any error occurred during the process is not policed. Moreover, the sprung mass displacement is not controlled very well if τ is less than 0.5 seconds. The dotted black line indicates the corresponding response when there is no control present.

The equivalent result for a well-damped system, using "typical" values (as stated in Table 2.1 of Chapter 2) for suspension stiffness and damping, is shown in Figure 5.12 below. As discussed earlier, the controllability can only be determined within specified τ values due to the errors in ξ calculation. For the result shown in Figure 5.12, the *Gramian matrix* is calculated for $\tau \leq 0.5$ seconds, and the final time of control is set at 0.5 seconds.

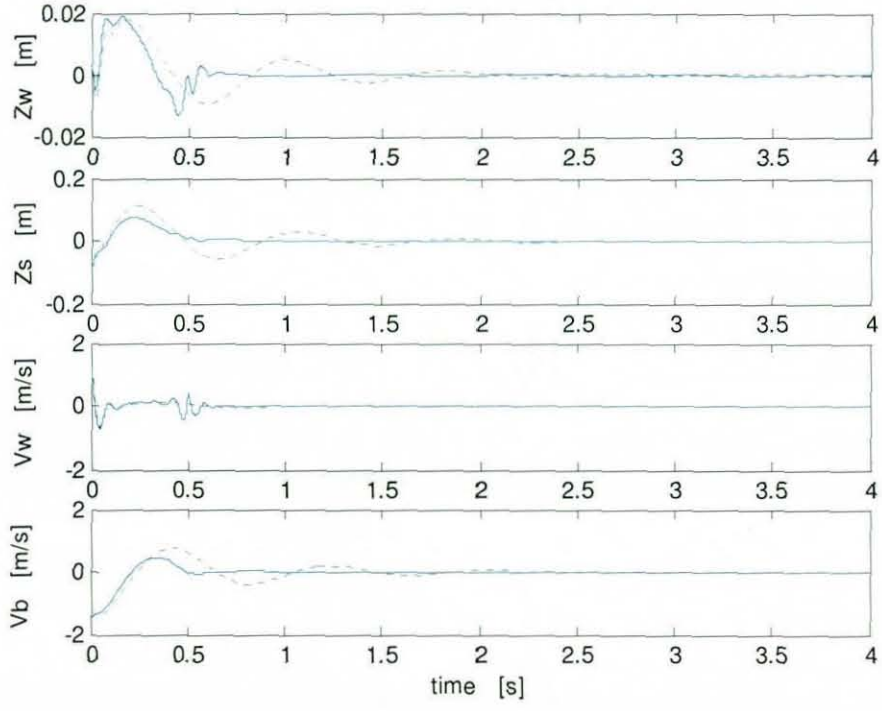

Figure 5.12 Open Loop Control of Well-Damped System

States are controlled reasonably well by the specified final time, however it is found that the range of "τ window" - at which the control can be applied successfully - is small. The maximum value of τ is approximately 0.9 seconds, the control magnitude determined beyond this τ value becomes small enough such that the change in the result is not recognisable. Minimum τ value is found to be approximately at 0.1 seconds.

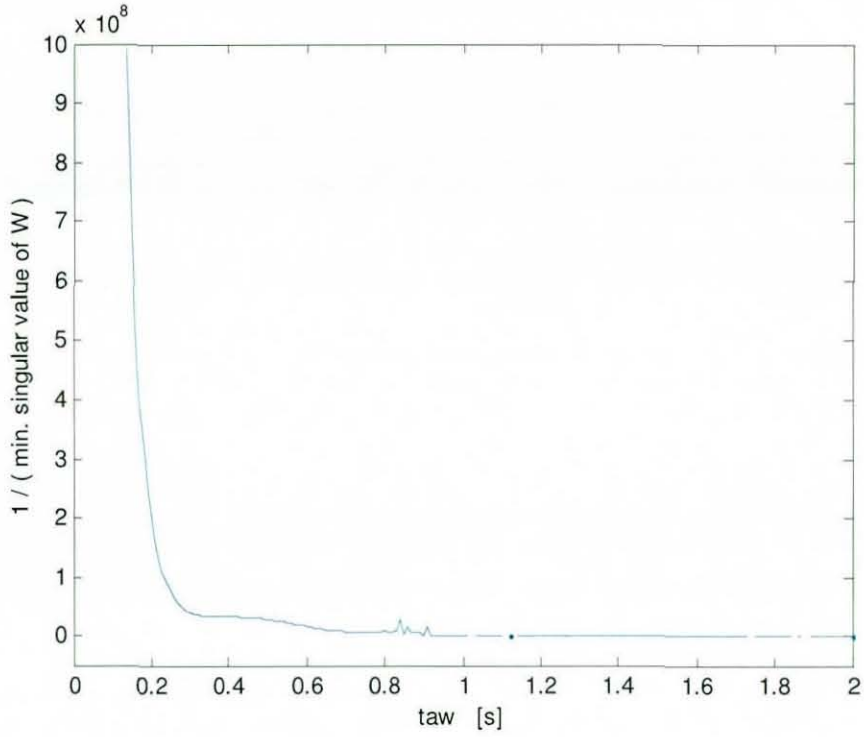

Figure 5.13 Inverse Minimum Singular Value of Controllability Gramian

Figure 5.13 shows the property of the controllability matrix used to determine an open-loop control shown in Figure 5.12. This is used in conjunction with the calculation error values shown in Figure 5.5.

5.3.5 Open-Loop Control using Gramian Matrix, 3DOF Handling Model

Having proved the validity of Open Loop control strategy using a Quarter Car Ride model, the controller is then defined using a 3DOF handling model. In order to investigate the validity of the method, the reference trajectory for 3DOF handling model is set so that it is effectively a time-invariant system. In other words, it has constant zero steering input with zero initial condition. Moreover, in order to avoid the numerical problem, the system is "flipped" in time.

$$\bar{t} = t_1 + t_2 - t$$

In this time co-ordinate, the original definition of open-loop control being a "regulator that transfers some non-zero initial states" has been transformed to a "controller that transfers initial zero states to some non-zero final states".

When determining Controllability Gramian, (5.17) is multiplied by –1 to retain the time-stability relationship. Steady-state value of the calculated Gramian matrix is compared against the time-invariant case, i.e. solution to the Lyapunov Equation, and is confirmed to be correct. Equation 5.8 is then applied to the system defined in the original time co-ordinates. Transition matrices are then determined in the stable direction as shown in (5.9). Subsequent open-loop control, equivalent to (5.19) is defined as follows.

$$u(\bar{t}) = -B(\bar{t})^T \Phi(t, t_0)^T W^{-1}(t_0, t_1) x_f \tag{5.28}$$

Finally, the resultant open-loop control is "flipped back" for the forward-time application. Figure 5.14 shows the resultant state transition. The blue line indicates the time-invariant reference trajectory. The black dotted line indicates the target final state value that is taken from the steady-state value of 0.05 degree step steer simulation. The red line clearly shows that the state transfer is achieved satisfactory within a given control period of 3 seconds.

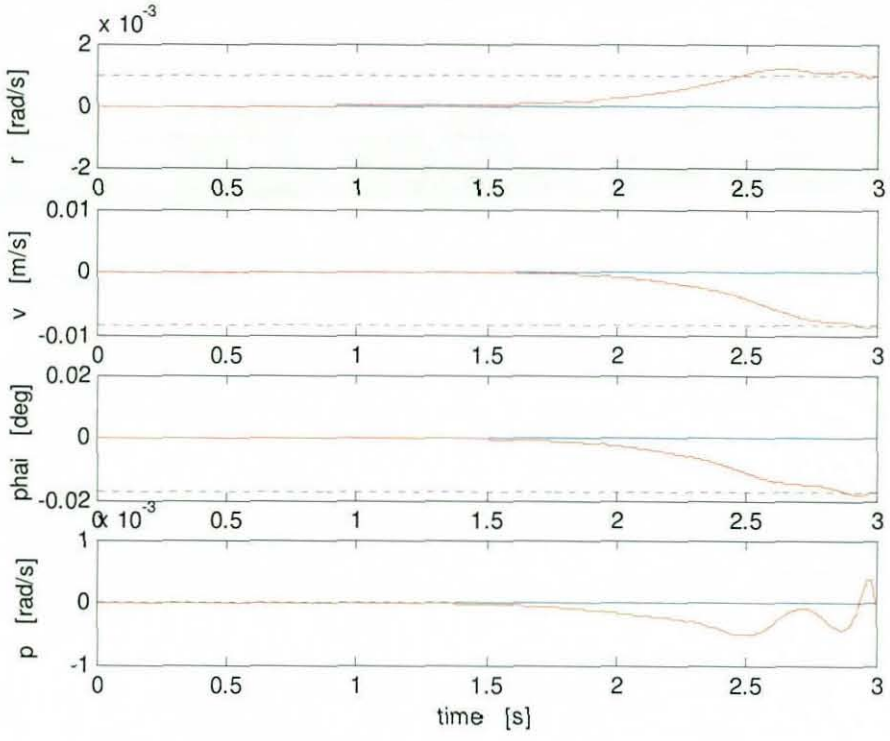

Figure 5.14 Open - Loop State Transfer Result

It is clear from Figures 5.14 and 5.15 that the state is only controlled within the "last minute". Although 3 seconds of control time is given, the controller produces very little steering angle at the early part of the period. As discussed previously, this is due to the dynamics of the system being well-damped. Any control applied at the earlier part of the manoeuvre will be damped out, hence will not be able to influence the final state values.

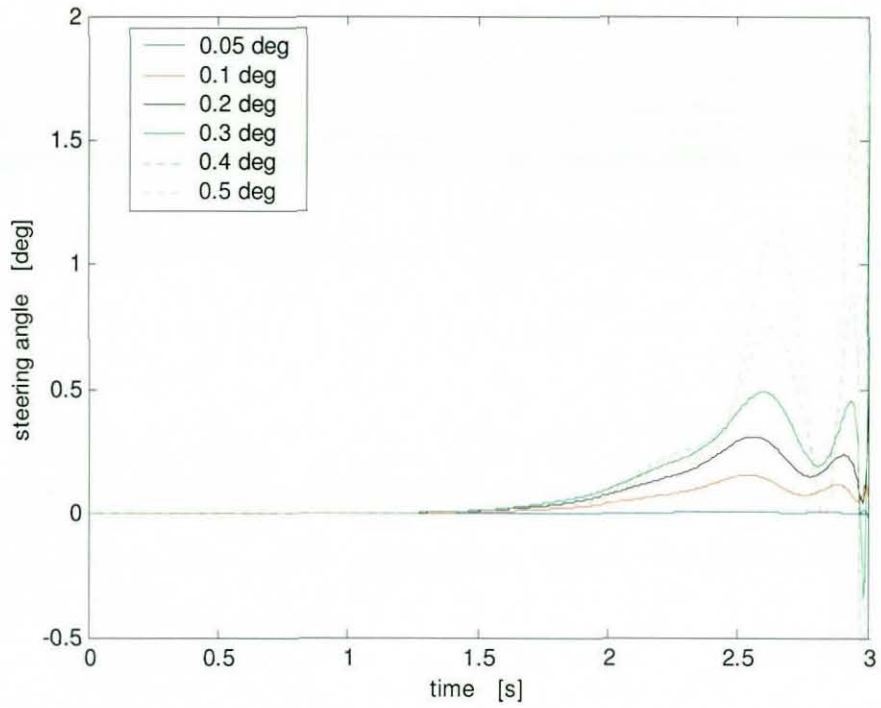

Figure 5.15 Control Steer Profile with various final state severity

Figure 5.15 also shows the variation in control steer magnitude and profile with respect to the various severities of the target final state. It is clear that as the target value becomes harder to achieve, the control magnitude becomes larger and more oscillatory. However, the time period during which some control is applied remains the same (approximately 1.5 seconds) for all cases.

Figure 5.16 shows the effect of varying control final time on the control input. The control magnitude becomes larger and more oscillatory as less time is allowed to transfer the states.

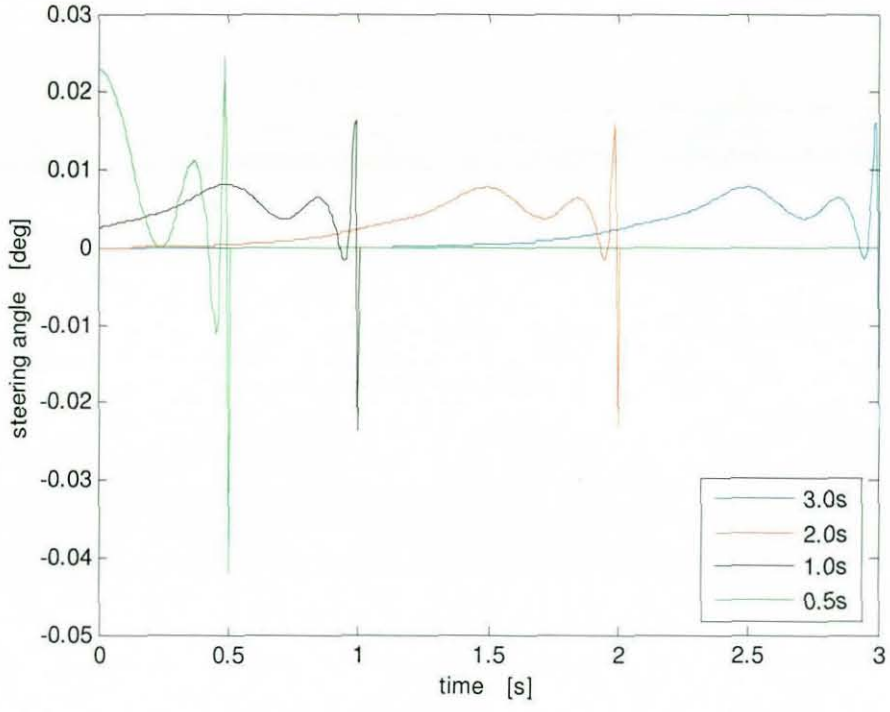

Figure 5.16 Control Steer Profile with various control final time

The resultant state transfers on the front and rear tyre lateral forces are shown in Figure 5.17. It is clear that both states are transferable within the time period as small as 0.5 seconds. In addition, the effect of the rapid change in steering angle at the very last moment of the time period is reflected in the front lateral force plot.

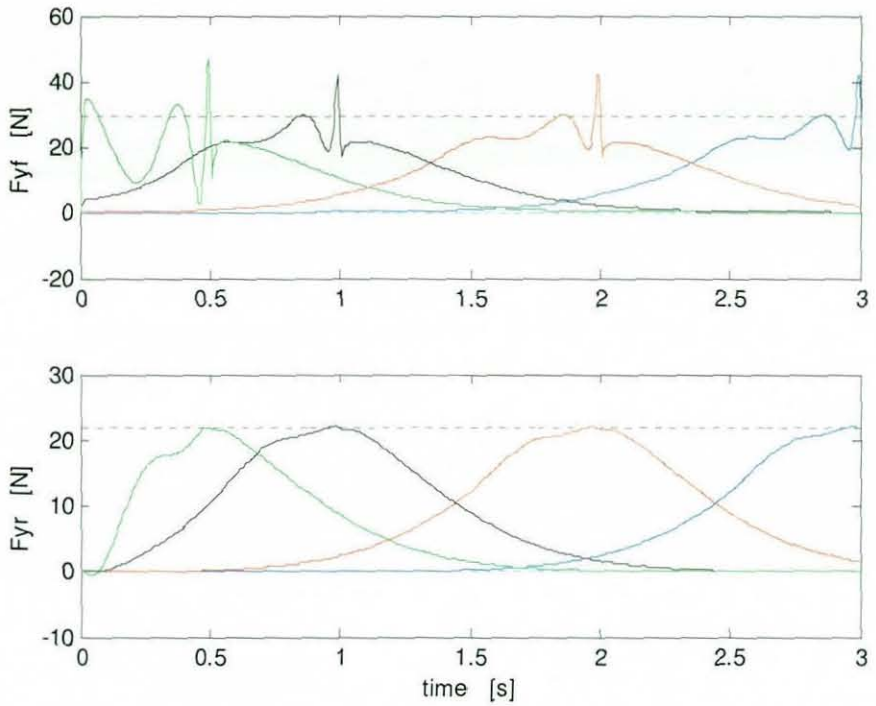

Figure 5.17 Transfer of tyre lateral force states

As shown in Figure 5.16, the control input magnitude varies with respect to τ. This variation comes from the property of Gramian matrix as shown in Figure 5.18. The minimum singular value has reached the steady-state value approximately beyond 1 second, hence the control steer would not change if the control final time were greater than 1 second. However, if the final time is smaller, then the inverse of minimum singular value increases. Since the Gramian matrix is inverted for the open-loop control, this results in larger control magnitude. The information from Figure 5.18 is consistent with the steering angle traces shown in Figure 5.16. It is also significant that the controllability degrades rapidly when the control period is less than 0.5 second.

Figure 5.18 also shows the effect of various reference trajectory severities on the inverse minimum singular value of Gramian matrix. It is shown that as the severity of the reference trajectory increases, the inverse of minimum singular value increases, hence indicating a reduction of controllability. Oscillation shown

in the case of 2 degrees of constant reference steer is due to the oscillation in the reference trajectory itself. One might think the reason why having a control period of 1.5 second is more controllable than 2.5 second, as shown in the figure. This is due to the fact that around 2.5 seconds, states are closer to the limit of its performance compared to the values at 1.5 seconds. Therefore the states are less transferable at 2.5 seconds. From the results acquired, it is confirmed that the minimum singular value gives a good measure of actual controllability rather than condition number or norm.

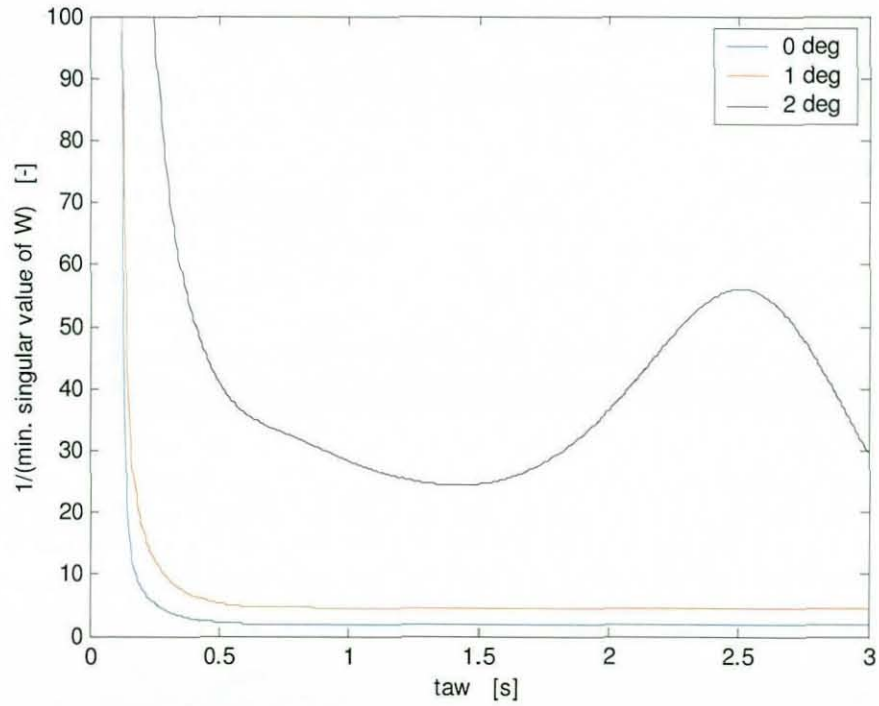

Figure 5.18 Inverse Minimum Singular Value of Gramian Matrix

As well as limiting the control application period, the control magnitude itself can also be regulated by utilising (5.18) as

$$\|u(t)\| \le \|B^T(t)\| \|\Phi^T(t_0,t)\| \|W^{-1}(t_0,t_1)\| \|x_0\| \qquad (5.29)$$

This information can be integrated within a time-varying optimal control of a nonlinear system.

Finally, the accuracy of the achieved final state values depends on the sampling frequency of linear models. Within the handling model, a numerical tyre force generation delay of 0.01 second is included. The controller produces a steering angle which influences front tyre force. The effect of front tyre force is then propagated through the dynamics of the system to alter the rest of the state values. Thus in order to achieve an accurate result, the sampling frequency has to be higher than 100 Hz. The percentage errors are as summarised in Table 5.1. Depending on the application (hence the error requirements), the sampling frequency has to be kept minimum as it increases the computational time heavily.

Sampling Frequency [Hz]	Front Lateral Force Error [%]
100	29
200	8
1000	0.33

Table 5.1 Effect of Sampling Frequency on the Computational accuracy

5.3.6 Analysis using a Moving "τ window"

So far, the controllability is investigated with regard to

i.) The various length of "τ window"

ii.) The operating conditions.

Instead of varying the above two factors, the fixed time "τ window" is used and is moved along a state trajectory in order to assess the controllability at different point in time. From the earlier studies, it is discovered that controller requires approximately more than 0.5 seconds to successfully transfer the states, as shown in Figure 5.18 (of course, depending on the demand severity). Figure 5.19 below shows the lateral force generated at the front tyre when the vehicle is subjected to 1.5 degrees of step steer. The trajectory has a slight oscillation before it reaches the steady-state value.

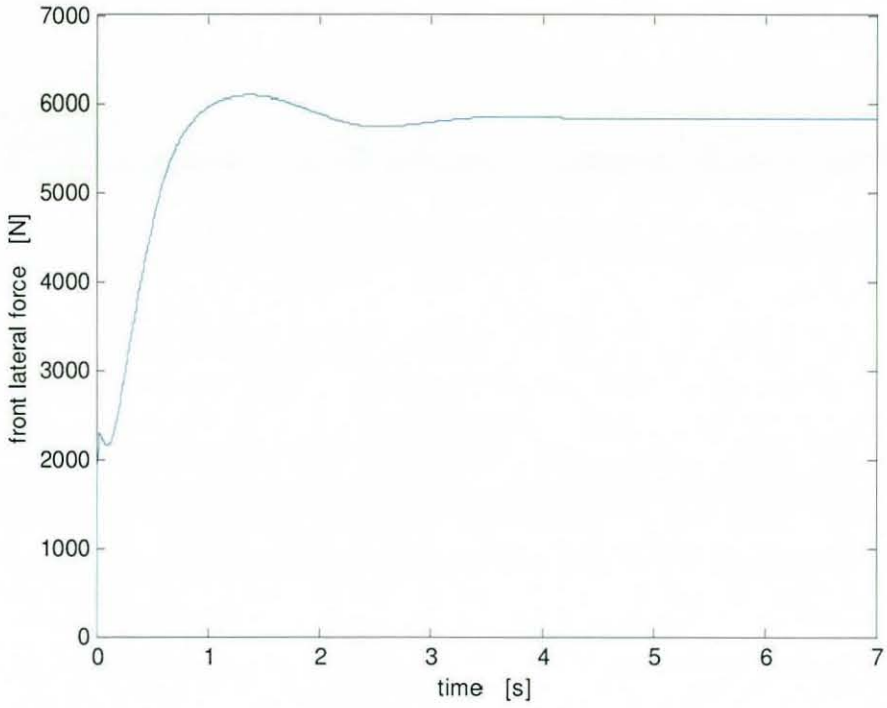

Figure 5.19 Front Lateral Force Trajectory

Figure 5.20 shows the inverse of minimum singular value of Gramian matrix. It is calculated based on the fixed length "τ window" of 0.5 second and is moved along the above trajectory with 0.25 seconds of overlap at each time. It can be seen that the graph shows some similarity to Figure 5.19. The vehicle is most controllable at the start of manoeuvre and the controllability decreases as the tyre force builds up. The point of minimum controllability corresponds to the time at which the front tyre force reaches its maximum value. The value oscillates as the tyre force oscillates. Most significantly, Figure 5.20 shows the nonlinear relationship between controllability and tyre force. Although the steady-state tyre force value is not hugely different from the overshoot peak at 1.5 second, the minimum singular value shows the significant difference. Moreover, although the tyre force at 0.5 seconds is less than 4 kN, significantly smaller than the steady-state value, the difference in controllability is not as large. Therefore it can be said that the controllability information shown in Figure 5.20 gives very good indication to

whether the vehicle is close to its limit of adhesion or not. Large changes at the moderate operating condition do not result in poor controllability.

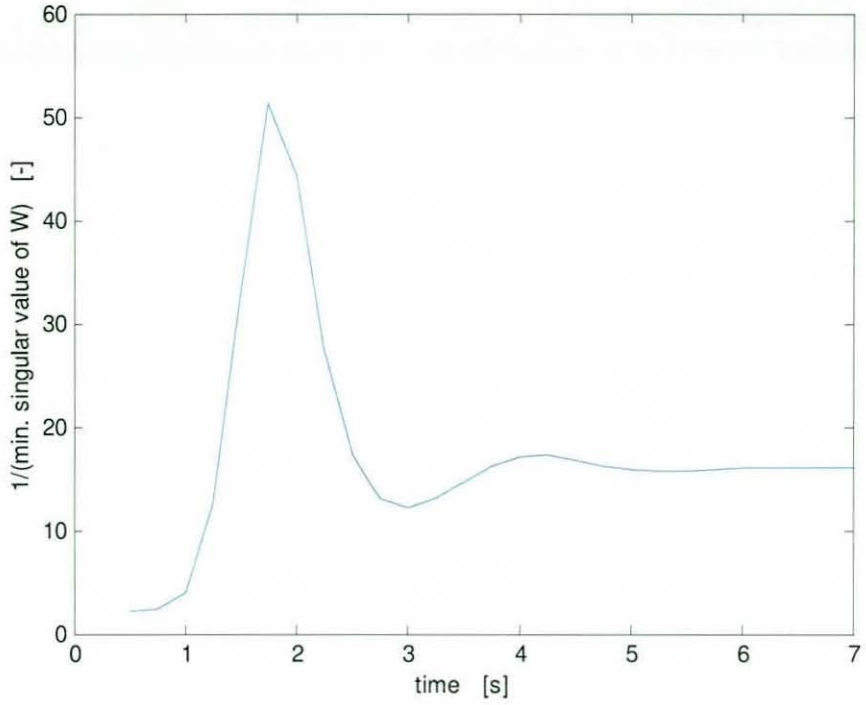

Figure 5.20 Controllability with moving 0.5 second "τ window"

Correlation between Figures 5.19 and 5.20 clearly show the varying controllability through the manoeuvre. Therefore, it can be concluded that this method of assessing the controllability using a "moving τ window" provides the most useful information.

5.3.7 Controllability Analysis on Vehicle Path Optimisation result

Recall the time-varying controllability discussed in Section 2.4 of Chapter 4, where the iterative optimisation encountered a problem when the vehicle was operating close to the limit of adhesion. This was despite of the fact that the control magnitude was regulated carefully so that the deviation from linearised models is kept small.

In order to investigate this issue, Controllability *Gramian* is determined for the result at iteration 56, where the best final displacement cost was achieved. The *Gramian* matrix was also calculated for the result at much earlier iteration where the vehicle is operating at more moderate condition.

Figure 5.21 shows the inverse of the minimum singular value of the *Gramian* matrix. It is calculated using a moving "τ window" of a fixed time period since this represented the actual controllability the best (as discussed in the previous section). The time window was set at 0.5 seconds and this window is moved along the trajectory with 0.25 seconds of overlap at each time, i.e. 27 controllability windows are determined in total for this particular simulation.

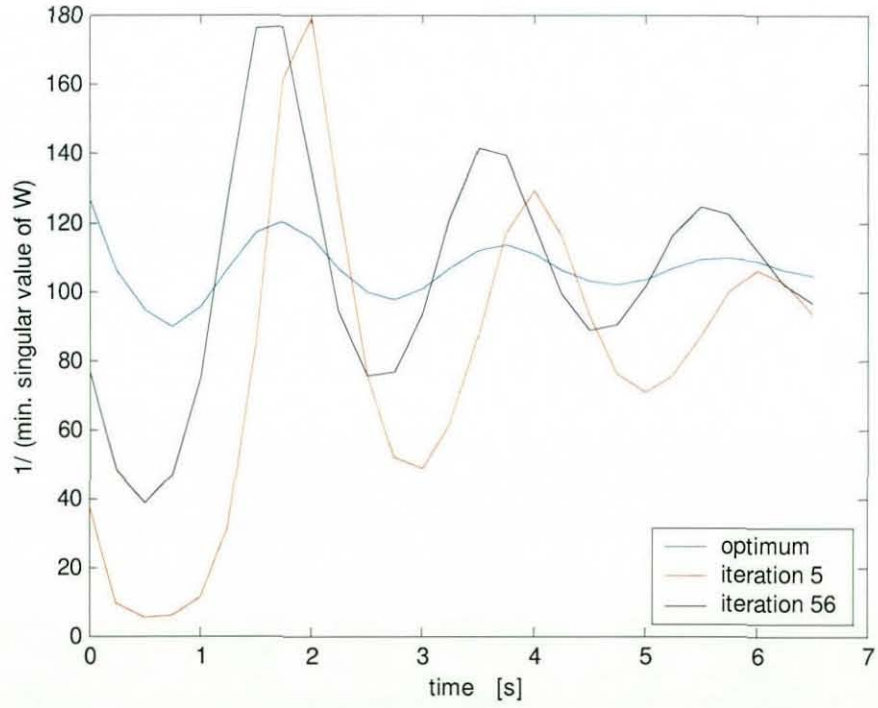

Figure 5.21 Controllability Gramian Information

Figure 5.21 shows that the controllability oscillates as the states oscillate. From the mean value, it can be seen that the vehicle is less controllable at the 56th iteration compared to the 5th iteration. In addition, the 56th iteration result has a

very similar mean value to the optimum constant steer / steady-state result. However, due to the oscillating dynamics in the trajectory at iteration 56, it is often less controllable than the steady-state reference. This trend can also be seen at iteration 5. Therefore, it is safe to conclude that although the mean values of the controllability are similar, the optimisation result is less consistent and has worse controllability in places due to the oscillatory dynamics.

Figure 5.22 shows the total tyre utilisation at both iterations. It is clearly shown that the tyres are used much closer to their limit at 56th iteration. The most notable difference is within the first 2 seconds, where the utilisation drops as low as 75% for the 5th iteration. This is reflected in Figure 5.21 where the vehicle has more controllability at iteration 5 during the corresponding time period. Moreover, there are points where the tyres are actually used more at the 5th iteration, compared to the later iterations. This is due to state oscillation caused by the under-damped dynamics, which is reflected on the controllability information in Figure 5.21.

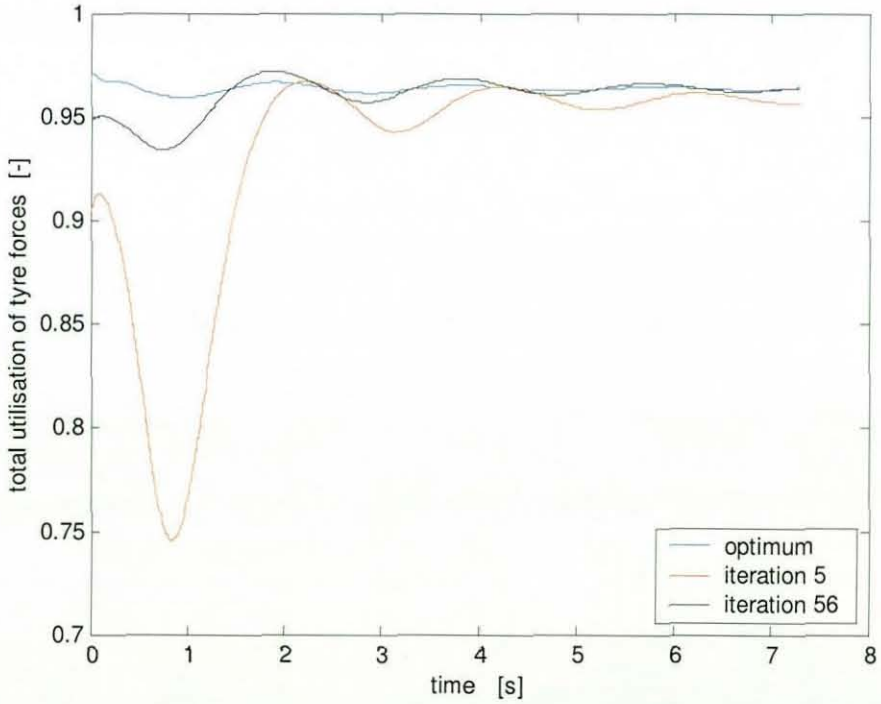

Figure 5.22 Total Tyre Force Utilisation

From these validation exercises, it can be concluded that the optimisation can drive the vehicle to the vicinity of its steady-state performance limit. This is supported by the controllability and tyre utilisation information, together with the final displacement and vehicle trajectory (which were discussed in Chapter 4). Therefore, the failure of the optimisation beyond 56^{th} iteration can said to be due to the lack of controllability.

5.4 Summary

In this Chapter, the controllability of a linear time-varying system is analysed and its properties are discussed in detail. The open loop control is then determined based on controllability information.

Two methods are examined in order to calculate the controllability *Gramian* matrix. It was found that both methods have their own shortcomings (i.e. matrix becomes close to singular or invalid solution on infinite time integral). By studying the properties of the *Gramian* matrix itself, it was concluded that the state transition matrix method provides more relevant result to real life. Moreover, the inverse of minimum singular value of the *Gramian* matrix was found to represent the actual controllability the best.

Open-loop controller was then designed using the *Gramian* matrix. This requires the calculation of transition matrix, which could not be well defined for well-damped system. By "flipping" the integration time step, it was possible to avoid the numerical problems. As a result, the controller was successfully derived and was used to study the relationship between the dynamics and controllability further.

The open-loop controller performance provided the data on the minimum time period required in order for the states to be successfully transferred. Moreover, "moving controllability window of fixed time period" is found to provide the most relevant information of the changing dynamics through the time.

The *Gramian* matrix information was used to investigate the optimisation issue described in the previous chapter, where the final displacement cost fluctuated over several iterations when the vehicle was operating close to the friction limit. The *Gramian* information showed that the optimised trajectory was often less controllable than the steady-state maxima due to its oscillating dynamics. This was further supported by tyre utilisation data. Hence, it can be concluded that the optimisation failure was a result of poorly conditioned matrix due to lack of controllability. In order to avoid this issue, controllability information needs to be integrated with within the optimisation in order to suitably regulate the controller input(s).

Finally, although it is not within the scope of this thesis, it remains as an interesting future project to investigate the formation of a cost function with the controllability information integrated within (i.e. "on-line" use of controllability). For example, the 4WS cost function described in Chapter 3, Equations 3.2 & 3.4, could include the influence of decreasing controllability as the vehicle reaches towards the friction limit. Hence, it enables to retain / guarantee a certain level of controllability throughout its trajectory.

Chapter 6

Vehicle Path Optimisation using a Time–Variant Linear Optimal Reference Control: Part 2

In Chapter 4, an iterative vehicle path optimisation strategy was established and validated using a 3DOF handling model, with the steering rate as the sole control input. It is found that the optimisation converges to a path that is in the vicinity of the steady-state limit (within 0.4% final displacement error). However, there was an issue with the optimisation, where the cost fluctuates over several iterations when the vehicle was operating close to the limit of adhesion. In order to investigate this issue, controllability theory was studied extensively in the previous chapter. From this study, it was concluded that the cost fluctuation was due to poorly conditioned matrix near the friction limit, which caused lack of controllability.

Having established that the fundamental optimisation method itself was functioning as intended, in this Chapter, the optimisation problem is extended to include longitudinal dynamics. This enables the simulation of more general manoeuvres and hence the results are more relevant to the real life problem. In addition, the robustness of the optimisation method itself is further investigated.

6.1 Controller Description

The optimisation method is developed using a 10 Degree-of-Freedom (10 DOF) vehicle handling model as described in Section 2.3 of Chapter 2. The controller now outputs driving torque demand as well as the steering rate demand.

The optimisation includes following cost functions:

1) Final state deviation, described by pseudo distance state M matrix

2) Quadratic road geometry constraints	Q matrix
3) Magnitude & relative balance between two control inputs	R matrix
4) Pseudo forward velocity deviation cost	Q_u matrix

Cost 4 is defined as shown in Equation 6.1 below, where $\tilde{U}$ indicates the forward velocity deviation between the previous and current iterations. Thus this cost encourages the forward velocity to be increased for the new trajectory.

$$Q_U = c*\left(U_p - \tilde{U}\right)^2 \tag{6.1}$$

Without this fourth cost function, the controller tends to concentrate on optimising the later part of the simulation. This is due to the fact that it is more effective to optimise the later part of the trajectory since it has a stronger influence on the final state values (due to the damping in the system). This was studied in detail in Chapter 5, where the open-loop controller was designed based on the controllability *Gramian* matrix. If the optimisation focuses its effort in the later part of the simulation, it drives the vehicle to first reach its limit only at the corresponding part of a trajectory. This then "locks" the result as the local gradient of road geometry cost becomes steep. Any control applied prior to this point in time will still have effects on the trajectory. However, as the later part of the trajectory has already reached the limit of adhesion and hence has a very poor controllability, the optimisation tends to fail. Therefore, Cost 4 is required to distribute the control effort more evenly throughout the time period.

As this optimisation is computationally very expensive, every effort was made to run the optimisation efficiently. It was found that the operations using Simulink slows down the computation considerably. Therefore all the state derivatives are determined within Matlab, and are integrated using fifth-order Runge-Kutta method with Cash-Karp constants [Numerical Recipes, 2007]. In addition, the linearisation code is also re-written within Matlab using the small perturbation theory. This speeded up the computation by a factor of four.

It is found that the sluggishness of the optimisation partly comes from its inability to optimise two control inputs, steering rate and longitudinal torque, simultaneously. The weightings in four different cost functions are determined so that the main objective, final displacement, remains as the dominant cost. In addition, the forward velocity deviation cost weighting is kept relatively low to ensure that it acts only as a supporting cost.

Moreover, when the optimisation reaches very close to the limit handling, the control magnitude has to be regulated to such that the deviation is very small. This is necessary since the linearised models become very insensitive when the actual nonlinear vehicle can be highly sensitive, as discussed in Chapter 4. This meant that the optimisation could only improve the result marginally towards the end of the process (diminishing return). The optimisation is said to be converged when the improvement in final displacement is consistently less than 0.4 %. This tolerance is set based on the steady-state validation results presented in Chapter 4.

6.2 Single Corner Optimisation

A simple 90-degree right-hand corner is used for testing the optimisation method. Initial vehicle forward velocity is set at 25 m/s together with the corresponding unsprung mass rotational dynamics, however, the rest of the states are initially all set to zero. The pseudo distance state is set to the lateral distance target. In addition, the forward velocity deviation pseudo-state is set to 5 m/s.

The intermediate results over the iterations are shown in Figures 6.1, 6.2 and 6.3. Figure 6.1 shows the change in the steering action over the iterations. The steering trace becomes more aggressive at earlier time periods in order to produce an appropriate initial opposite steer angle. After this counter-steer, steering angle raises much faster to the peak angle. This means that the steering angle is held near the region that produces the maximum lateral acceleration for much longer period of time.

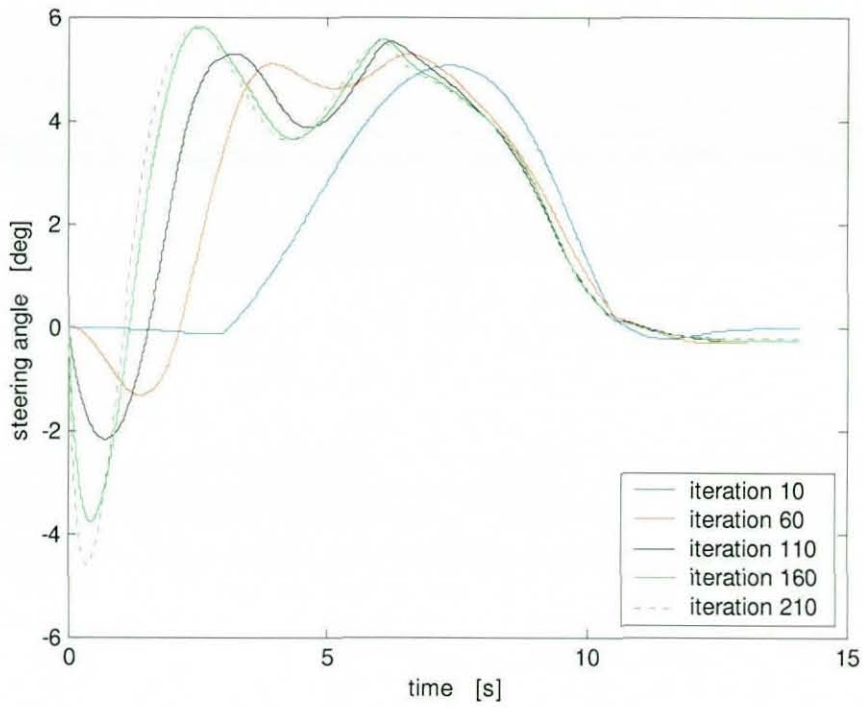

Figure 6.1 Steering Angle Profile

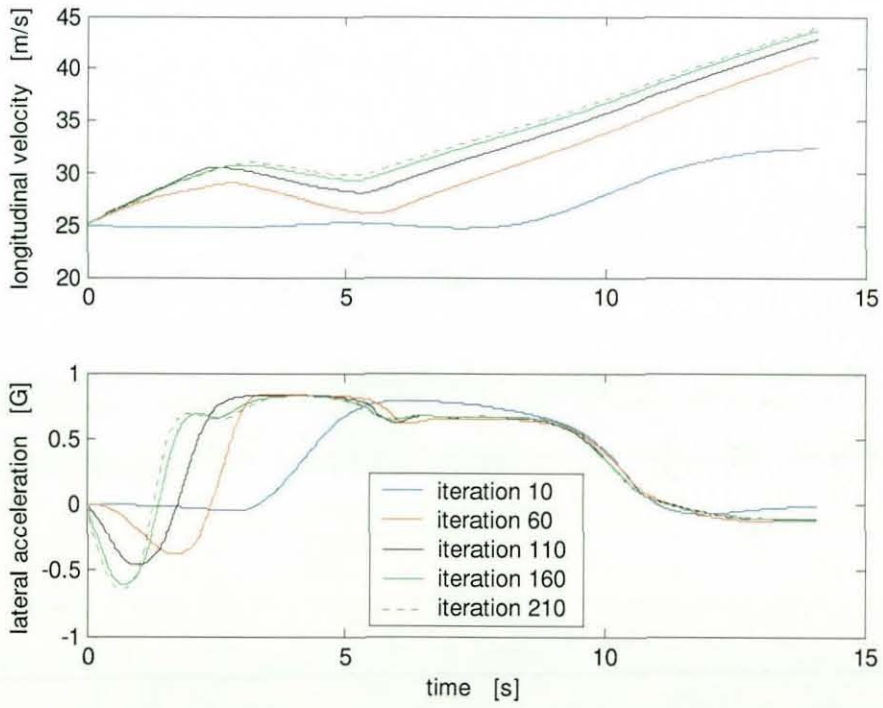

Figure 6.2 Forward Velocity and Lateral Acceleration Profile

From Figure 6.2, it can be noticed that the vehicle starts accelerating straight away as soon as the simulation starts. This initial acceleration keeps increasing until iteration 110. Beyond this iteration, the optimisation focuses more on increasing the minimum cornering speed. In addition, the corresponding braking point shifts earlier as well as the acceleration point after the apex. The effect of these changes over the iterations is clearly shown in the lateral acceleration plot in Figure 6.2. The steady-state is reached much earlier and is held near-constant for a longer period of time. Peak lateral acceleration was experienced during braking because the vehicle has steady-state understeer with no longitudinal acceleration.

Figure 6.3 shows the vehicle path variation over the iterations. The tendency for the convergence is clearly shown. The initial trajectory drives around the outside of road centre line for the majority part of the manoeuvre. Through the iterations, the path tends towards the apex at the middle of the curve and taking wide entry and exit in order to maximise the turning radius.

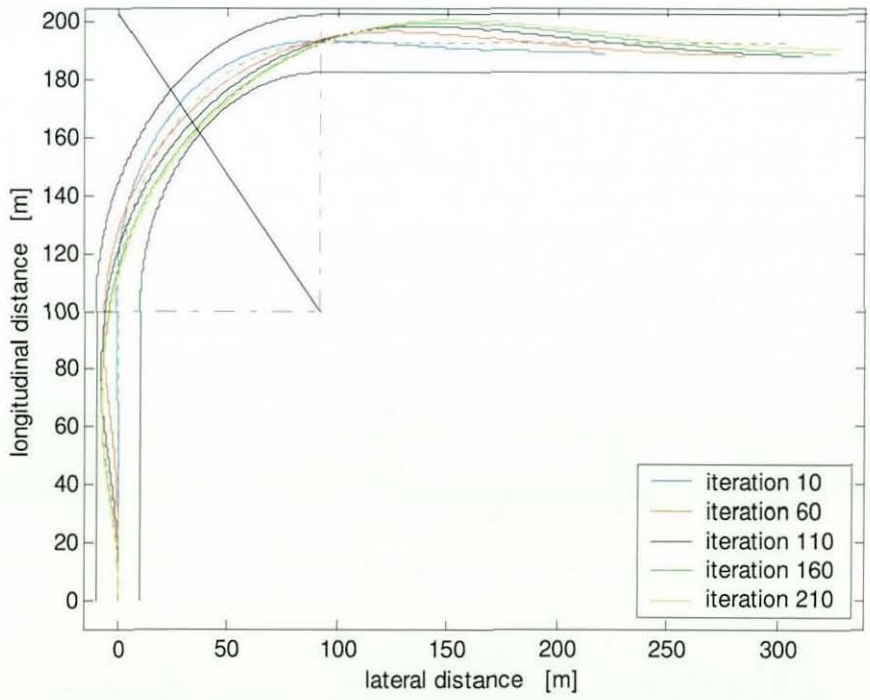

Figure 6.3 Vehicle Path Profile

Figures 6.4, 6.5 and 6.6 show the converged result of optimisation. It can be seen that the optimised vehicle path follows the classical out-in-out strategy. This is not surprising as this problem deals with an isolated 90 degree corner.

Figure 6.4 shows the steering angle and lateral acceleration profiles. An initial 5.2 degrees of opposite steer is clearly shown and it produces the corresponding lateral acceleration of 0.66 G with 0.32 seconds delay. This is followed by a quick turn-in, producing approximately 0.68 G lateral acceleration now in the opposite direction. It is then held between 0.65 G and 0.82 G for over 7 seconds whilst the vehicle negotiates the corner. The maximum lateral acceleration is produced just before the apex, and the second peak in the steering angle corresponds to the point at which the vehicle hits the apex at 5.9 seconds. Beyond this point, the steering angle is gradually decreased while the lateral acceleration remains almost unchanged for further 3 seconds. This is a combined effect of increasing forward velocity as shown in Figure 6.5 and tyre nonlinearity in the lateral direction. At around 9 seconds where the vehicle is closest to the outside road boundary, the steering angle continues to decrease and small amount of negative steer is applied towards the end as it tries to keep a vehicle straight without producing a significant drag.

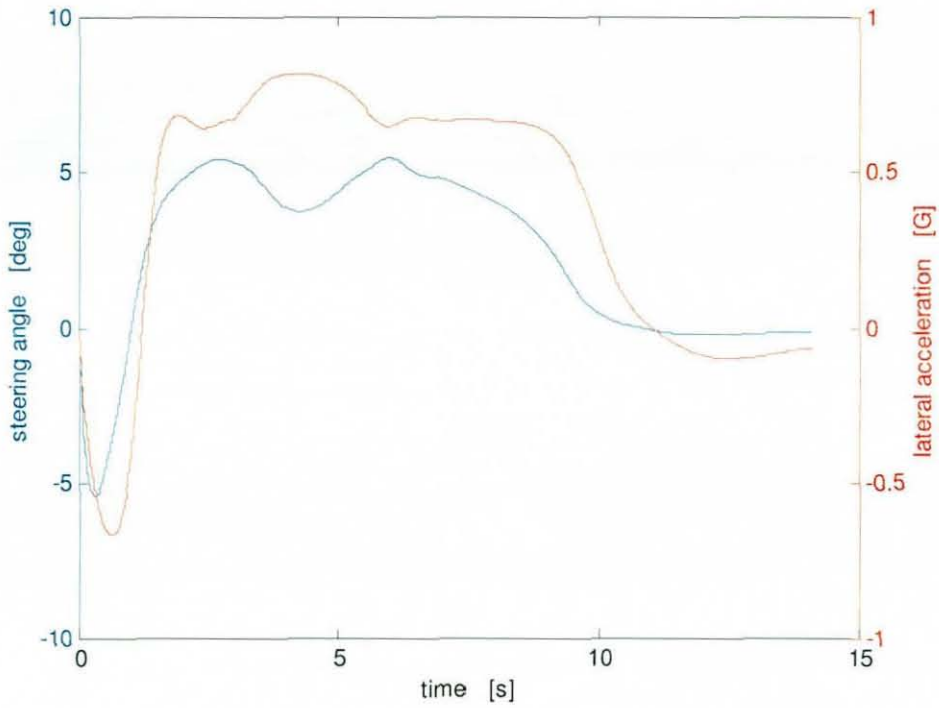

Figure 6.4 Steering Angle and Lateral Acceleration Profiles

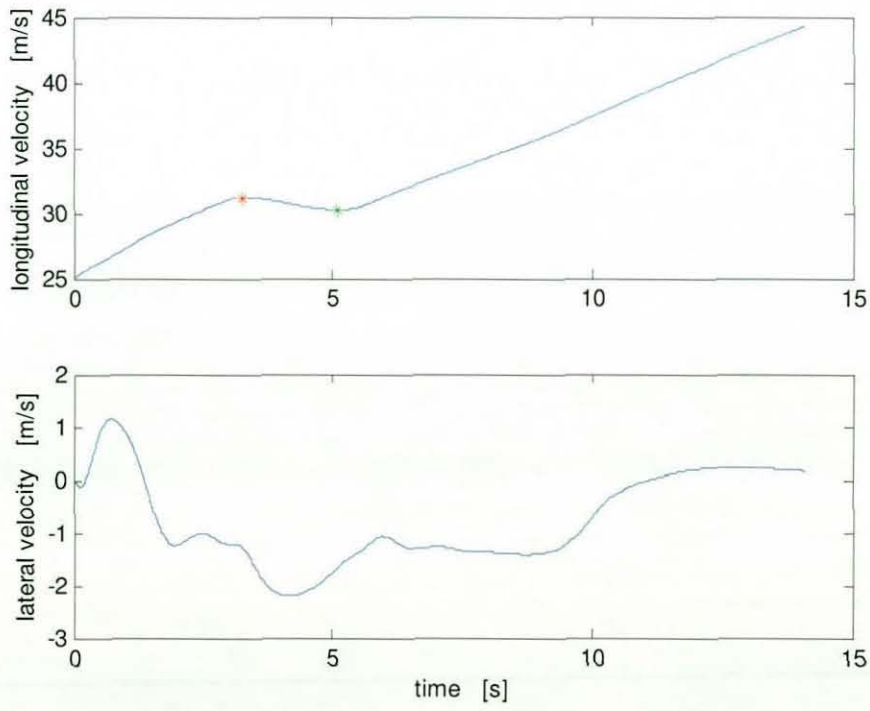

Figure 6.5 Longitudinal and Lateral Velocity Profiles

Figure 6.5 shows the longitudinal and lateral velocity profiles. It shows that the vehicle initially accelerates to just over 31 m/s, indicated by a red dot. The corresponding vehicle displacement on the track is marked also by a red dot in Figure 6.6. From this point onwards, the vehicle forward velocity is gradually decreasing as the vehicle heads towards the apex. It starts accelerating again from the point marked by a magenta dot until it reaches the maximum of 44 m/s at the end of the manoeuvre. The black dot on Figure 6.6 indicates the point where the peak lateral acceleration is experienced in the negative direction.

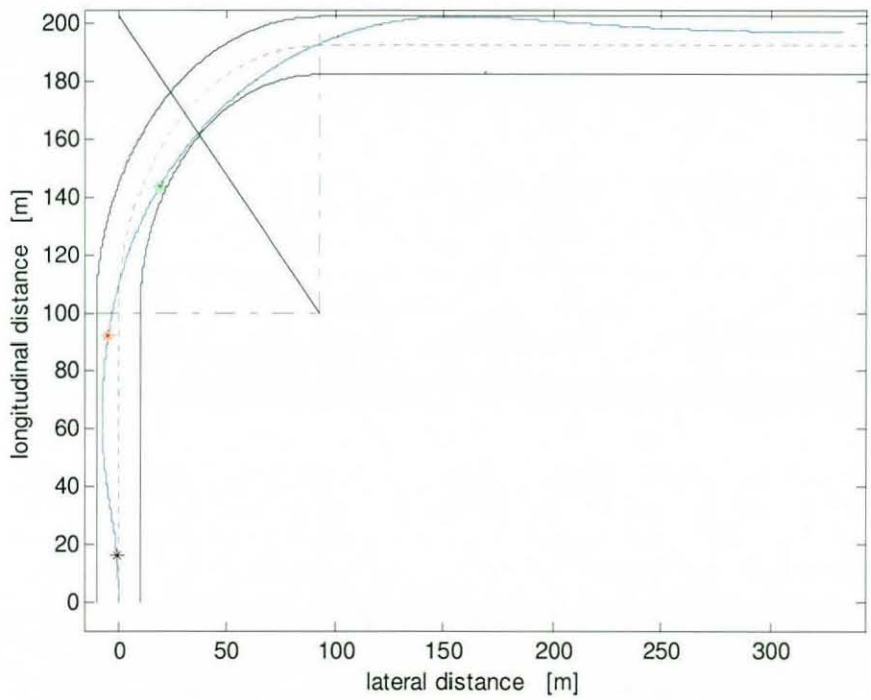

Figure 6.6 Optimised Vehicle Paths

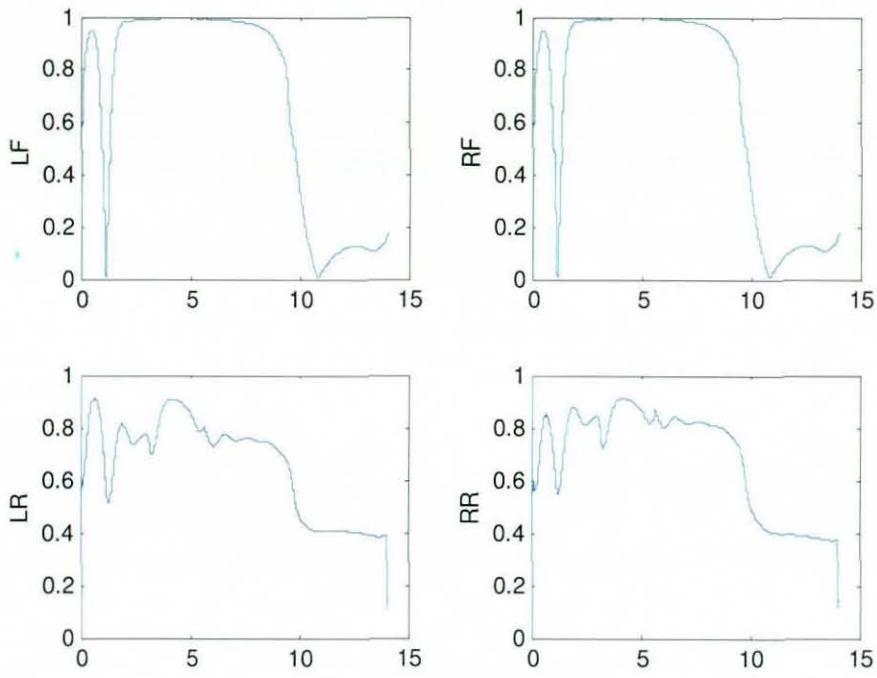

Figure 6.7 Normalised Tyre Forces

Figure 6.7 shows the normalised tyre forces, $F(\sigma)$, at all four corners of the vehicle. It can be seen that the front tyres are very close the limit of adhesion between 2 and 8 seconds, indicating the optimum steering input. Moreover, the effectiveness of the initial opposite steer can also be seen. The tyre lateral force is used within 5% of its maximum value despite very limited amount of time is available to control. By contrast, the rear tyres do not reach their peak at any stage of the manoeuvre. This is because the vehicle is not grip limited under traction, but is limited according to the engine power of the vehicle which is set at 100 kW, i.e. approximately 130 bhp. From Figure 6.4, it can be seen that the steering angle is small after 10 seconds. During this period, the vehicle is accelerating at the constant rate as shown in Figure 6.5. Under this pure-acceleration condition, only 40% of the tyre friction envelope is utilised. Even whilst cornering with significant lateral acceleration, the tyre utilisation rarely reaches 90%. Therefore, if the balance of a vehicle is shifted towards the front (i.e. larger friction circle at

the front tyres), then the optimisation result is expected to improve. This is investigated later in this Chapter where the vehicle set-ups are altered.

This optimisation took 350 iterations to converge to this solution, taking just under 12 hours. (Note that this result was obtained in 2002 with the PC equipped with 2GHz CPU and 785MB RAM) As shown in Figure 6.8, the optimisation performance improves only by a very small amount beyond 200th iteration due to the reasons discussed earlier.

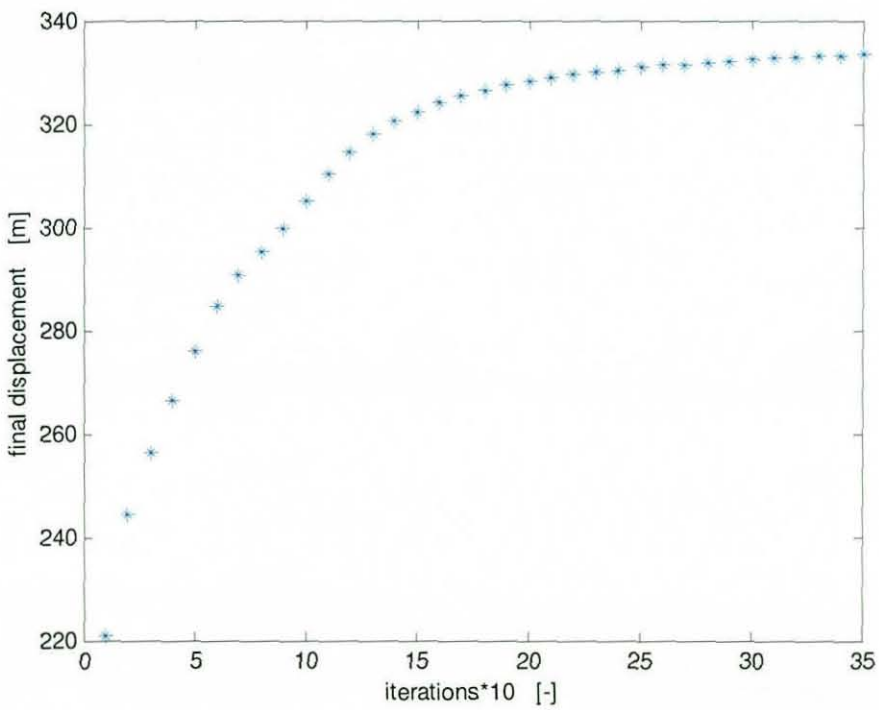

Figure 6.8 Optimisation Performance over iterations

6.3 Optimisation Validation

The previous section described the optimisation result achieved for a single cornering manoeuvre. Tyre utilisation figures show that the vehicle is driven in the vicinity of its performance limit. Following this result, three separate studies are made in order to further investigate the robustness and the validity of this optimisation.

6.3.1 Sensitivity to Controller Parameters

In this section, the robustness of the optimisation method with respect to changes in certain controller parameter settings is investigated. The results of the optimisation should remain unchanged, provided the optimisation method is working correctly. Otherwise, it means that the result is highly coupled to the controller parameter setting itself, this obviously makes the result much less meaningful.

In order to investigate this controller parameter sensitivity on the optimisation results, the pseudo-forward velocity deviation value, U_p, is altered. Since this parameter acts as a "supporting" function to distribute the control effort, it is thought to be a suitable parameter for such robustness investigation. On the standard setting, this is set to 5 m/s. It is then changed to 3m/s and 7m/s, and the results are shown in Table 6.1 below.

U_p [m/s]	Final Distance achieved	% error	Iterations
3	328.48	0.04	546
5	328.63	0 (ref)	352
7	329.14	0.2	314

Table 6.1 Effect of U_p Change on Optimisation

It is clear that the optimisation results (final distance) remain largely unchanged regardless of the variation in U_p value. Moreover, the quicker convergence is observed with the increased U_p value, as expected. Since the optimisation remains valid for all three cases, one should set U_p = 7m/s for the quicker convergence.

These results demonstrate that this pseudo state is serving its function as intended. In other words, it is controlling a vehicle forward velocity increase throughout the time period, hence spreading a control effort without affecting the main optimisation objective (maximise lateral displacement) itself.

Table 6.2 shows the resultant cost of the three optimisation results discussed above. As the forward velocity deviation pseudo-state acts only as a supporting cost in order to run optimisation properly (as explained earlier), its magnitude should be insignificant compared to the main cost (final displacement). Table 6.2 shows that the final displacement cost is in the order of 1000 times larger than that of U_p.

U_p [m/s]	Final Displacement Cost [1000]	U_p Cost
3	24.54	6.22
5	24.50	17.27
7	23.43	34.05
7*	40.00	338.90

Table 6.2 Resultant Cost Magnitudes

Figure 6.9 shows the lateral acceleration profile over time. The similarity among these profiles confirms the earlier discussion, where the results are said to be robust with respect to the tried controller set-up variations.

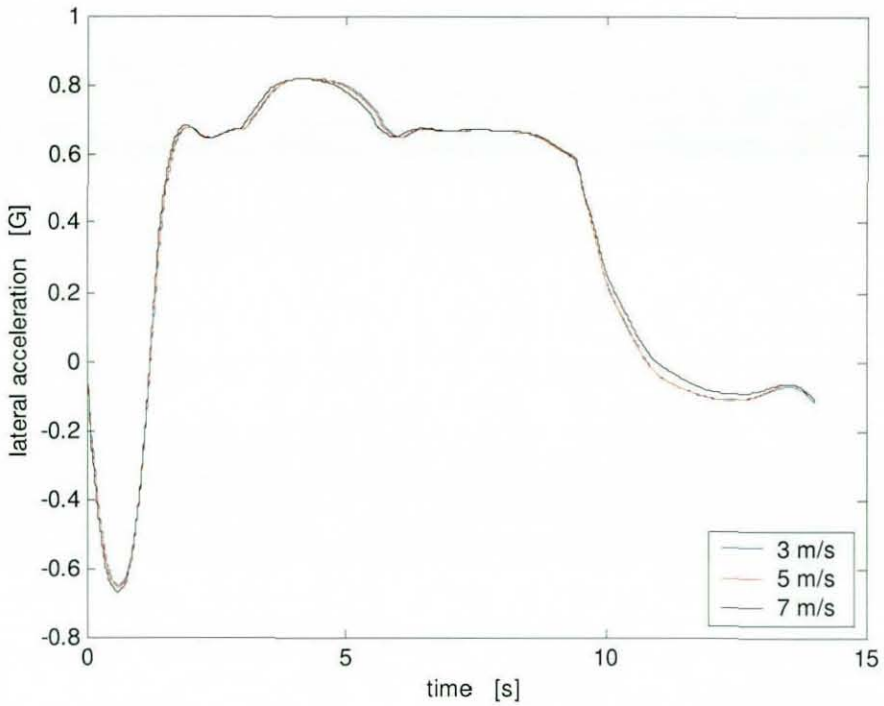

Figure 6.9 Lateral Acceleration Profile with Various U_p

The numbers on the last row of Table 6.2, highlighted in blue, show the result of experimental optimisation where the weighting constant, c, in Equation 6.1 is increased by a factor of 10. Although the forward velocity cost remains relatively small compared to the maximum distance cost, Figure 6.10 clearly shows the effect of this high weighting. The vehicle maximises its forward velocity by tracing an outside edge of the corner with the expense of poor maximum distance achievement. Judging from the magnitude of relative cost, it is clear that the main objective of this optimisation remains as maximising the final distance. However, it focuses on increasing the vehicle speed since this becomes much more effective to reduce the final distance cost during the relatively early part of the iterations. Consequently, the path becomes very close to the road geometry boundary, which in turn prevents further deviations, as discussed previously.

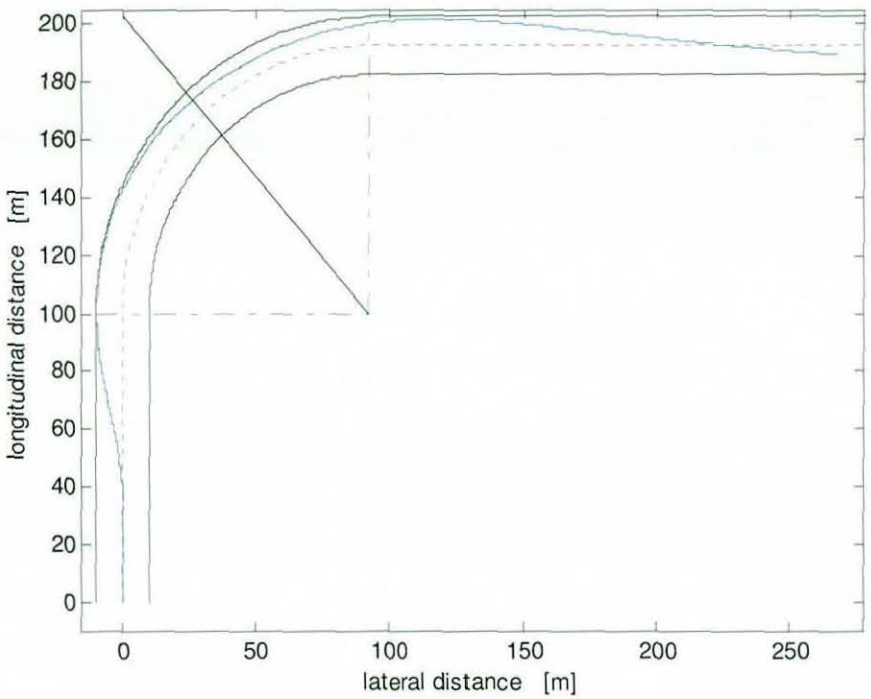

Figure 6.10 Resultant Vehicle Path with High U_p weighting

Figure 6.11 shows the controller performance over the iterations. The optimisation is continued until 660th iteration, and the final lateral displacement achieved is less than 270m (as oppose to the achieved displacement shown in Figure 6.8, which exceeds 330m). Between the 100th and 500th iterations, the displacement only improved by 10 metres. Moreover, the final displacement value starts fluctuating beyond this point. In other words, the optimisation result over the iterations no longer forms the 1st order curve shown in Figure 6.8. It is clear from Figures 6.10 and 6.11 that the optimisation 'stalls' when the vehicle forward velocity cannot be increased much further due to the road geometry constraints. Therefore it can be concluded that this cost weighting ratio between vehicle forward velocity deviation and final displacement is not sufficiently low.

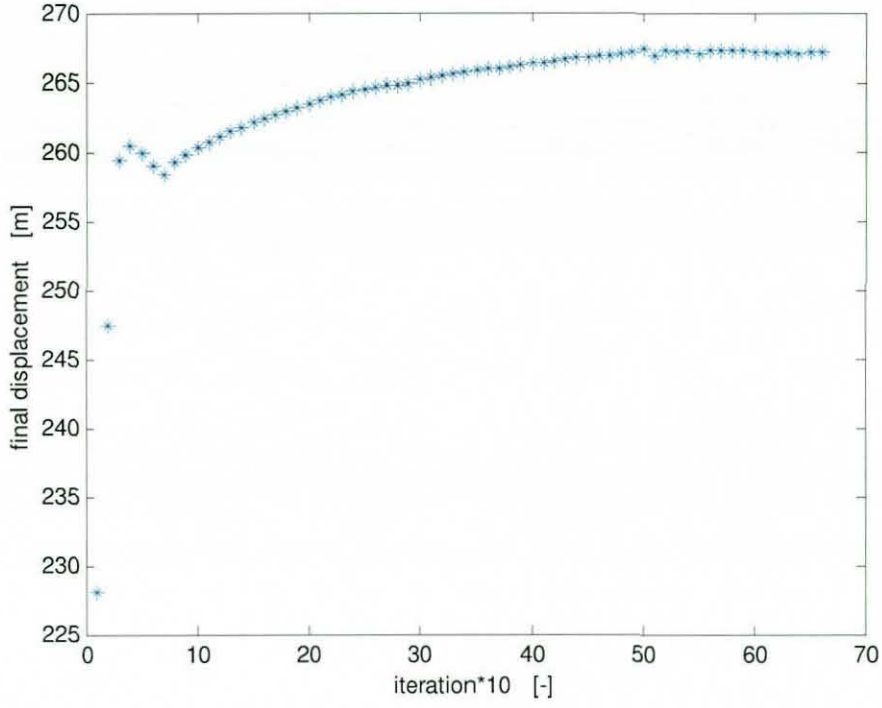

Figure 6.11 Resultant Cost with High *Up* weighting

In summary, it is proved that the optimisation method itself is robust with respect to reasonable changes in the controller parameter. However, it has to be noted that if the controller setting is modified significantly, in this case bay a factor of 10, the optimisation failed due to imbalance between two cost functions. The optimisation is no longer valid in such cases.

6.3.2 Effect of Engine Power Increase

Recall Figure 6.7, showing the tyre force utilisations when the optimisation converges. It was discussed that the rear tyres were not used up to their capacities, possibly due to the engine power limitation. In order to further investigate this hypothesis, the optimisation is performed with twice the original engine power.

Figure 6.12 shows the tyre utilisation using the intermediate result. Tyres are now used more fully both at the front and rear axles, compared to the optimum result achieved with the standard setting. This is more significant whilst cornering and at

the exit. It is noted that the tyre force utilisation is actually lower going into the corner. This is due to the optimisation failure beyond certain iterations, hence this part of the manoeuvre has not been optimised. The mechanism of this failure is discussed later on.

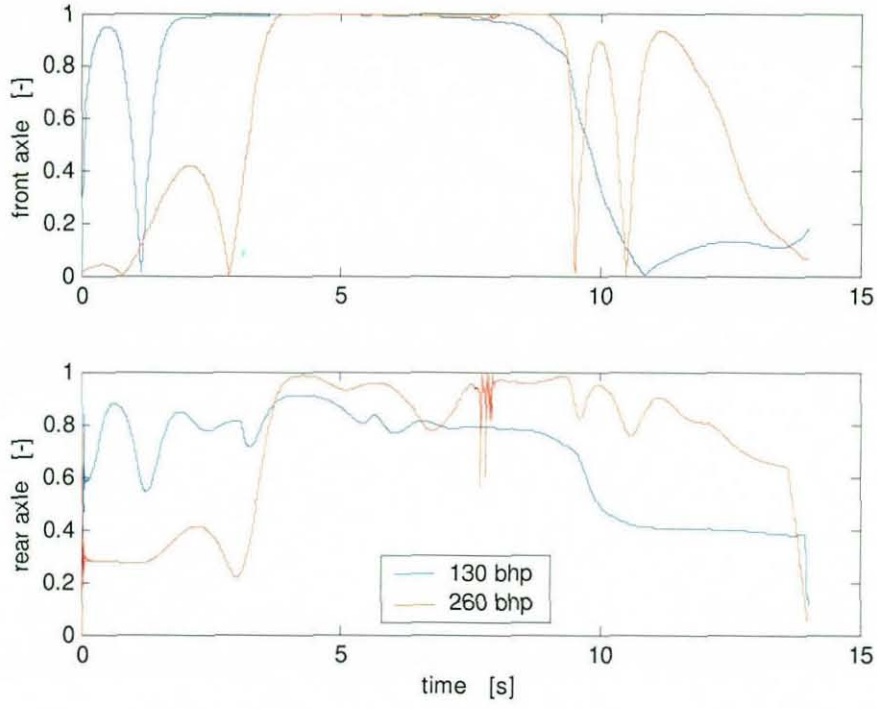

Figure 6.12 Tyre Force Utilisation with increased engine power

High frequency oscillation can also been on the rear tyre utilisation. In order to investigate the cause of this oscillation, individual wheel velocities are plotted in Figure 6.13. It shows that the significant wheel spin occurs when accelerating out of the corner. Right tyres are lightly loaded due to the lateral weight transfer as this is a right-hand corner simulation. Since the vehicle model only has an open-differential, this results in more severe wheel spin at right rear tyre, as shown in Figure 6.13. The slower front wheel velocity seen elsewhere is due to the part of the lateral velocity component created by a steering action acting as a drag.

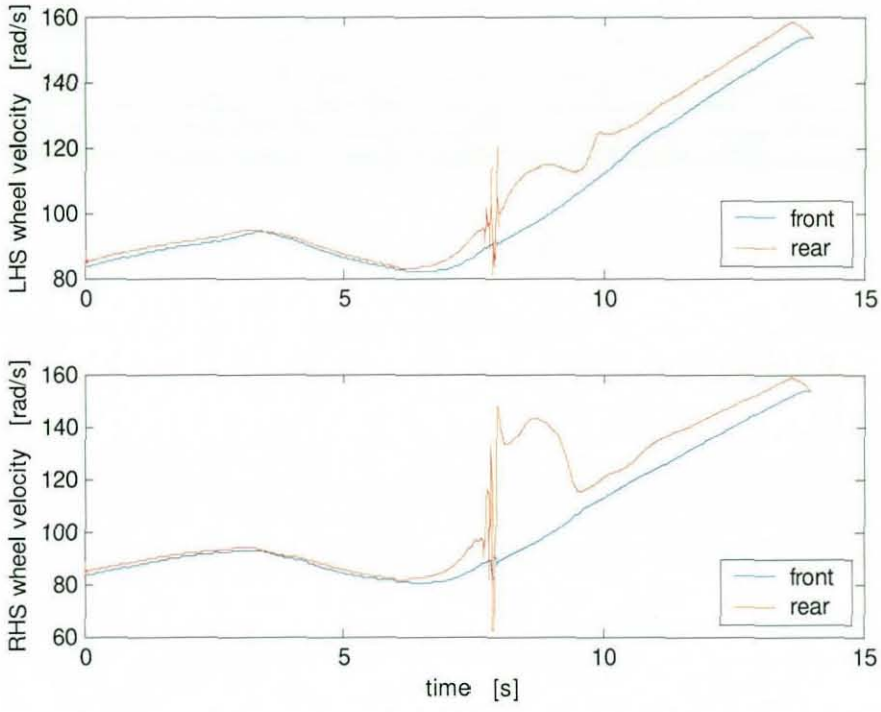

Figure 6.13 Wheel Angular Velocities

The effect of this wheel spin in terms of handling balance can be seen from the yaw angle time history shown in Figure 6.14. At the point where the wheel spin occurs, knee point can be observed, indicated by a red star mark. The yaw angle increases at higher rate during this wheel spin, showing a classic "power – sliding / oversteer" situation.

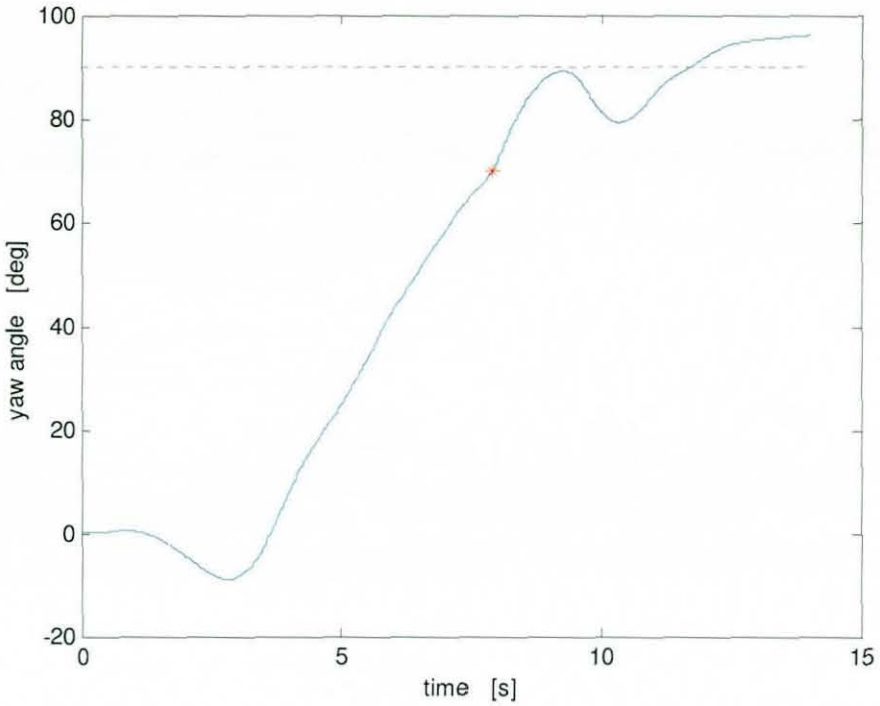

Figure 6.14 Yaw Angle time history

As briefly mentioned earlier, the optimisation actually failed at the later iterations. There are a few potential reasons resulting in this error. As shown in Figures 6.12 and 6.13, there are high frequency oscillations in wheel velocity states. Hence, the integration tolerance might not have been set adequately small. However, this is discovered not to be the case, as tighter tolerance did not alter the result. Another possible cause is within the dynamics of the vehicle itself.

Since the driveline is modelled with minimum complication, it does not include the engine inertia. This means that even the very sudden changes in the torque demand can be met quickly, causing the high frequency oscillation. This means that the resultant dynamics is outside the linearised representation at that particular moment in time, hence the controlled system is no longer optimum. In order to examine its effect, the additional 2.5 kgm^2 driveline inertia is included in the unsprung mass dynamics. Figure 6.15 shows the tyre utilisation, it no longer has the high oscillations seen in Figure 6.12. Moreover, the optimisation did not

fail afterwards, thus it can be concluded the failure experienced earlier was indeed due to the uncontrollable and un-modelled high frequency dynamics.

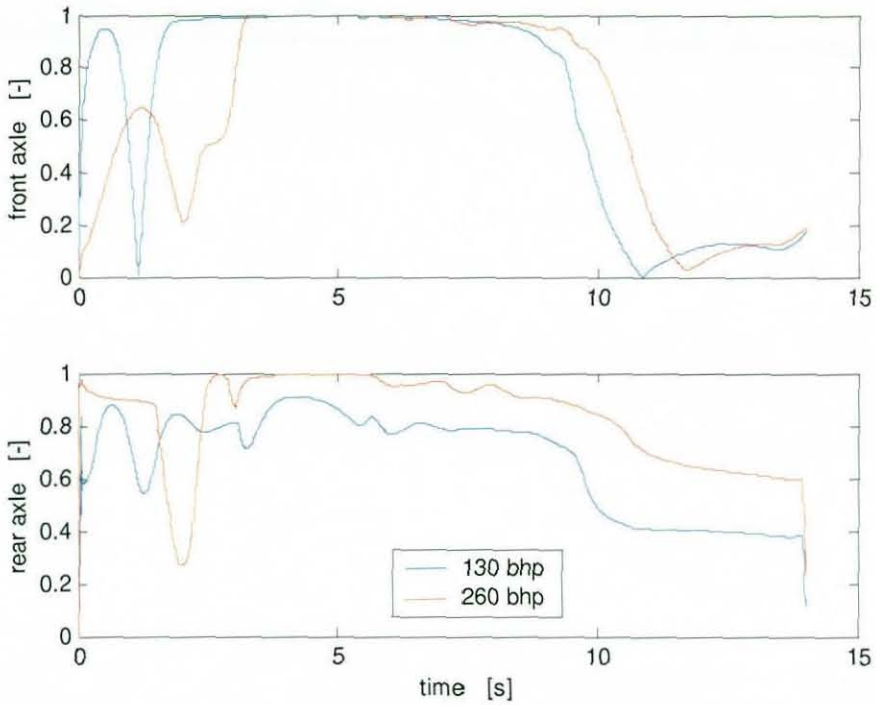

Figure 6.15 Tyre Force Utilisation with Increased Unsprung Mass Inertia

Having addressed the high frequency oscillation issue mentioned earlier, the optimisation was re-processed. However, the resultant path shown in Figure 6.16 is clearly not optimum. The path is similar to the one shown in Figure 6.10 where the forward velocity deviation cost was set very high. Significant increase in the engine power makes the torque control more effective than the steering rate control. By utilising this extra freedom allocated in one of the two control inputs, the vehicle is driven very close to the outside boundary of the road geometry at earlier iterations. As discussed earlier, this "locks" the result due to the quadratic road geometry cost having very steep gradient when a vehicle is near the boundary. More significantly, both front and rear tyres are both used completely during certain period in time (around 5 seconds mark). This means that the controllability of the system is very poor.

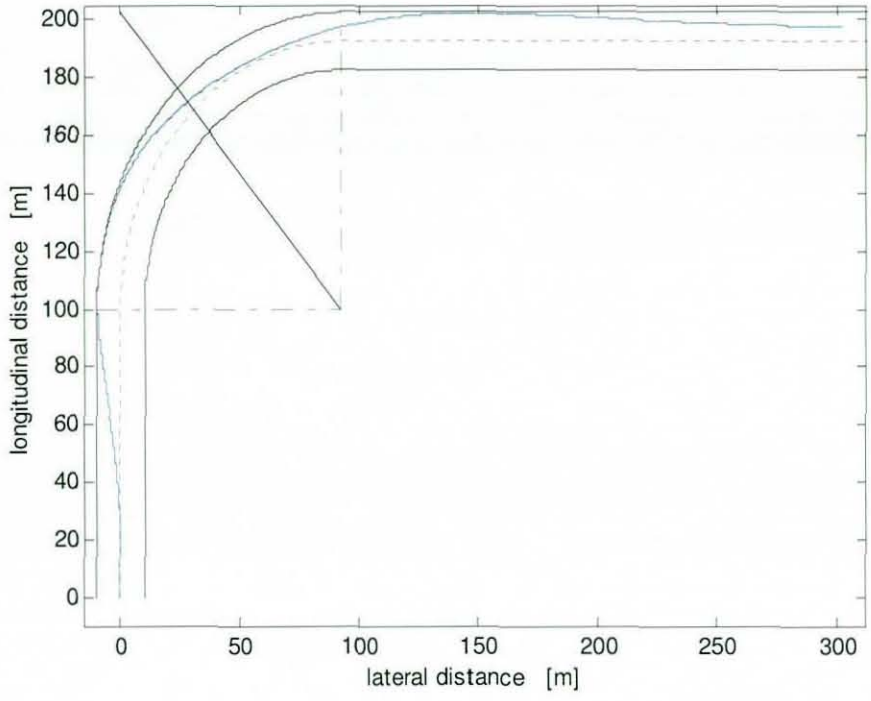

Figure 6.16 Resultant Vehicle Paths

The control input cost weighting, R, between steering rate and torque is altered to give relatively more freedom in steering control. This has a normalising effect on the increased engine torque available. This also enables to avoid both front and rear tyres reaching their limit simultaneously. It is found that this alternation has a significant effect on the optimisation result. Figure 6.17 shows the resultant vehicle path, it is clear that the optimisation now finds the apex of the corner successfully. Moreover, it can be seen that the optimum path is very similar to the one with half the engine power until vehicles hit the apex. After the apex, the vehicle with more engine power exits the corner with smaller turning radius. The vehicle forward velocity plot shows an interesting comparison where the higher powered vehicle takes apex later, hence maximising the benefit of engine power for the exit.

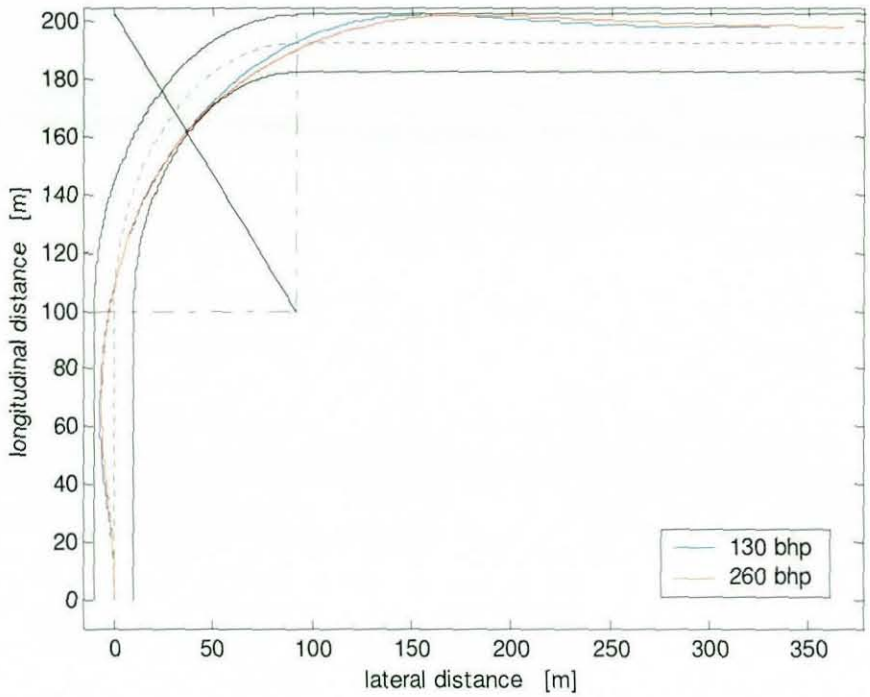

Figure 6.17 Vehicle Path Comparison with different Engine Power

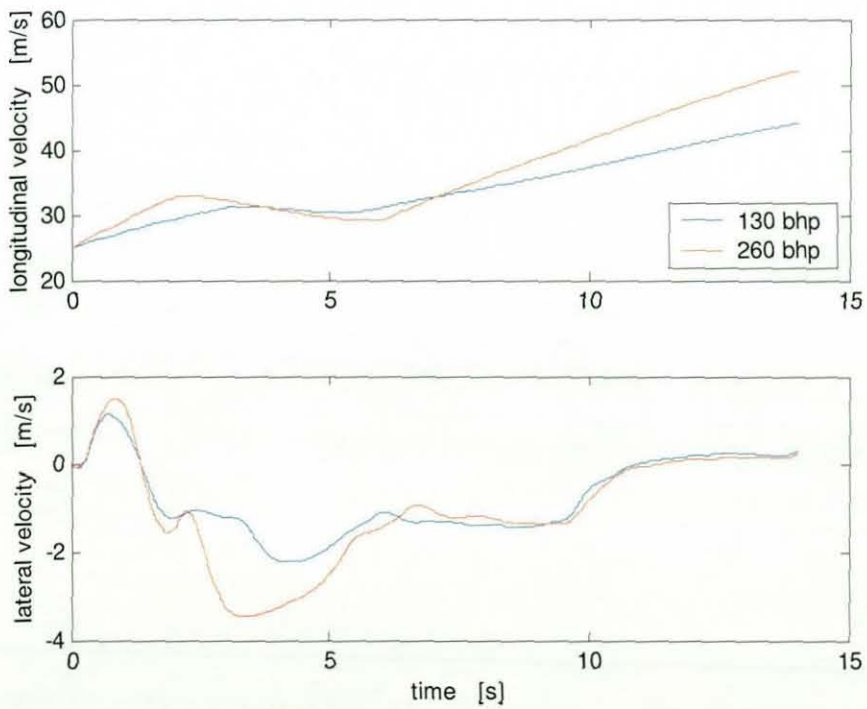

Figure 6.18 Vehicle Forward & Lateral Velocities Comparison

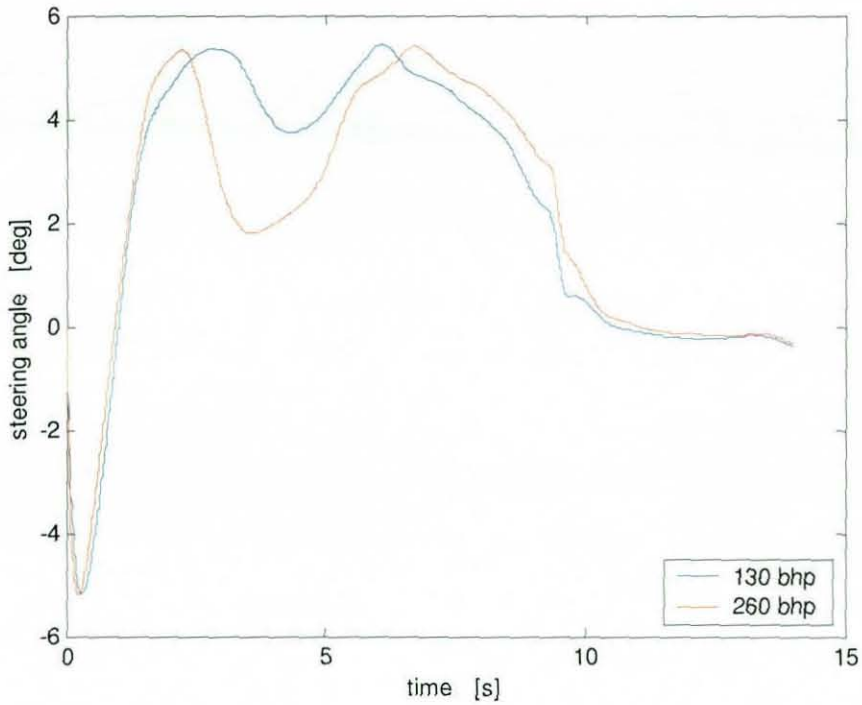

Figure 6.19 Steering Angle Comparison with different engine power

From Figure 6.19, it can be seen that the steering time history has a similar overall shape regardless to the engine power available. However, the steering angle is reduced further due to the heavier deceleration experienced with 260 b.h.p. vehicle. In addition, the steering angle is increased at the exit of the corner to cope with increased understeer.

Figure 6.20 shows the resultant tyre utilisation, it is clear that the rear tyres are used more fully with the increased engine power. Rear tyre forces reach very close to the friction limit, however with still some margin left. In order to carry out the optimisation successfully, this is an important factor. If both front and rear tyres reach their respective limits during the early stage of the optimisation, as shown in Figure 6.15, the controller suffers from what seems to be a lack of controllability. Consequently, the optimisation results in failure as seen in Figures 6.10 and 6.16. By altering the control input cost matrix, R, the controller is set so that it finds the

front tyre limit first whilst maintaining the relatively low usage of rear tyres. Once the front tyres are near the limit, the rear tyre utilisation starts increasing.

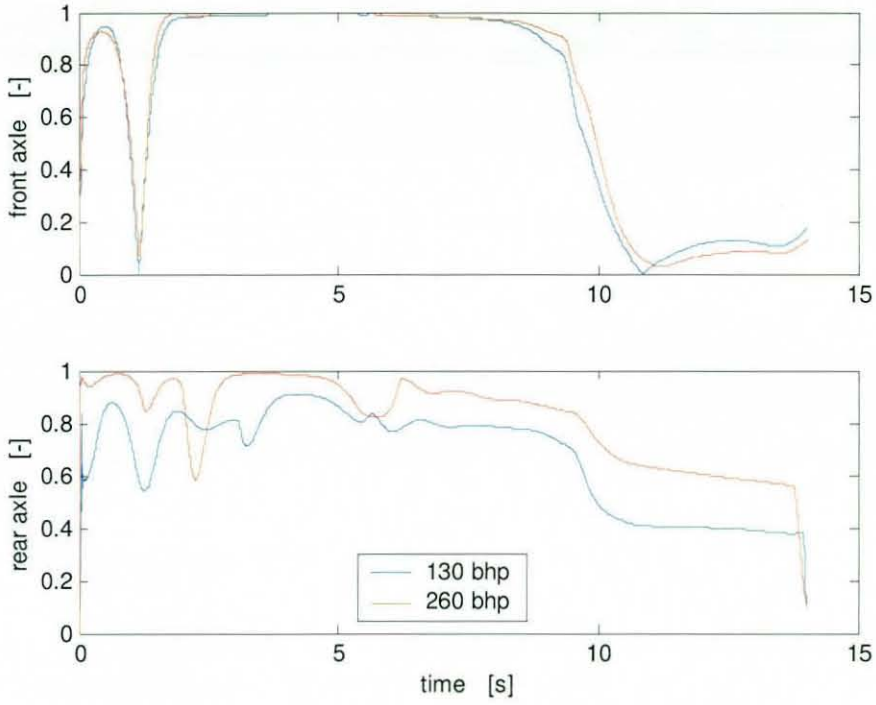

Figure 6.20 Tyre Force Utilisation Comparison with different engine power

In summary, the increased engine power made the rear tyre utilisation higher. Hence, it confirms the earlier hypothesis on the low utilisation of rear tyres. This study also highlighted a couple of interesting issues. First, lack of driveline inertia caused an optimisation failure as the linearised representation become invalid. Secondary, the increased engine power caused an imbalance between the steering rate and the engine torque controllers. This also resulted in controllability issue when both front and rear tyre forces saturated simultaneously. These issues are solved by increasing the inertia and modifying the R matrix respectively.

6.3.3 With Higher Initial Vehicle Forward Velocity

The results acquired so far show that the vehicle does not experience heavy braking at all. This is due to the low initial vehicle forward velocity setting. In order to experiment in the braking action more, the initial forward velocity is

increased to 32 m/s. It is found that when the initial velocity is set much higher than this value, it is difficult to generate an initial trajectory which does retain some controllability. Clearly, having higher initial velocity means that the more severe braking is required to keep the vehicle within the road boundary. If this causes both front and rear tyres to be very close to their friction limits, the controllability becomes poor, thus the optimisation cannot be successfully performed.

Figure 6.21 below shows the comparison of the steering angle profile between the 25 m/s and 32 m/s initial forward velocity.

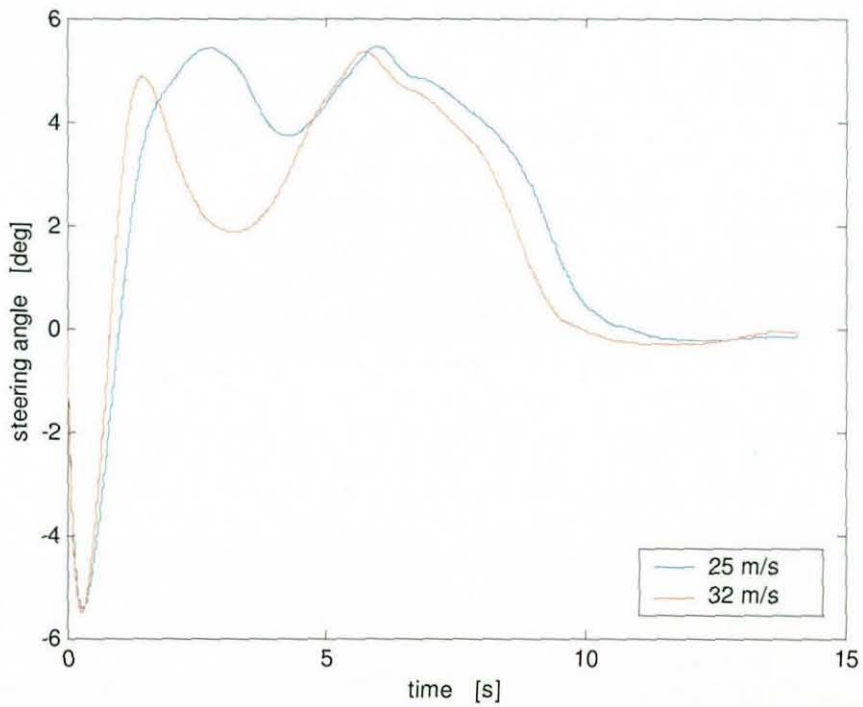

Figure 6.21 Steering Angle Comparison with different Initial Velocities

Although the overall profile is similar, the difference is clearly shown both in magnitude and phase. From the very similar initial opposite steer input, the vehicle with higher initial velocity uses higher steering rate to reach its peak steering angle. The initial peak steering angle itself is less. The entire steering angle profile is shifted due to the velocity difference. Figure 6.22 shows the

difference in the forward velocity time history. The minimum cornering velocity occurs at a similar point (as expected), and hence more severe braking is applied with the increased initial forward velocity. Corresponding lateral acceleration is also higher and the steady-state phase occurs at earlier time.

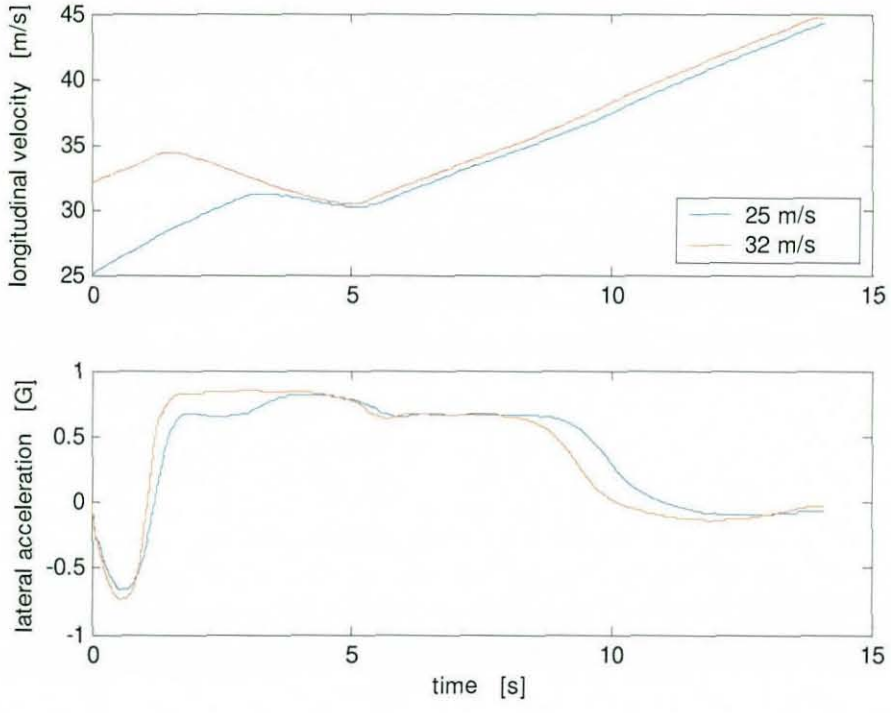

Figure 6.22 Forward Velocity and Lateral Acceleration Comparison

From Figure 6.23, it can be seen that the resultant vehicle path is generally similar. The difference is noticed at the entry of the corner where the vehicle with higher velocity does not move to the outside as much. This is due to the saturated tyre capability and the resultant lateral acceleration as shown in Figures 6.24 and 6.22 respectively. From the tyre utilisation profile in Figure 6.24, it can be seen that both front and rear tyres reach their friction limit simultaneously between 2 to 4 seconds. During this period, the vehicle is experiencing a constant deceleration. Combined effects of this deceleration and generated lateral force saturate the rear tyre.

With the higher initial velocity setting, it is confirmed that the optimisation is able to drive a vehicle at its maximum deceleration capability. Having already covered the pure cornering event in Chapter 4 and the traction event in the previous section (6.3.2), this completes the investigation into this optimisation method. It is shown that the optimisation is capable of finding a limit of adhesion in all these manoeuvres.

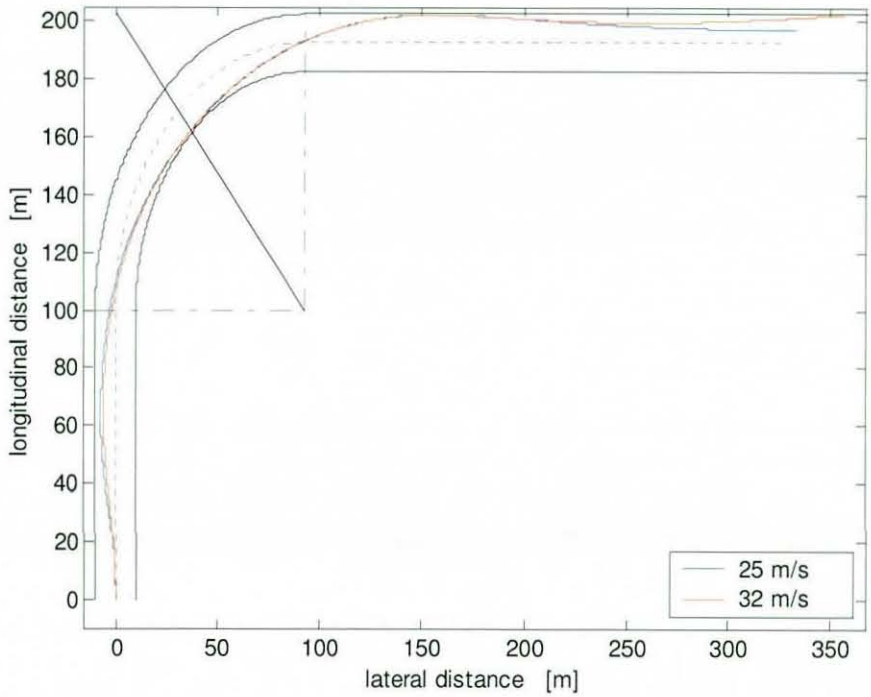

Figure 6.23 Vehicle Path Comparison with different Initial Velocities

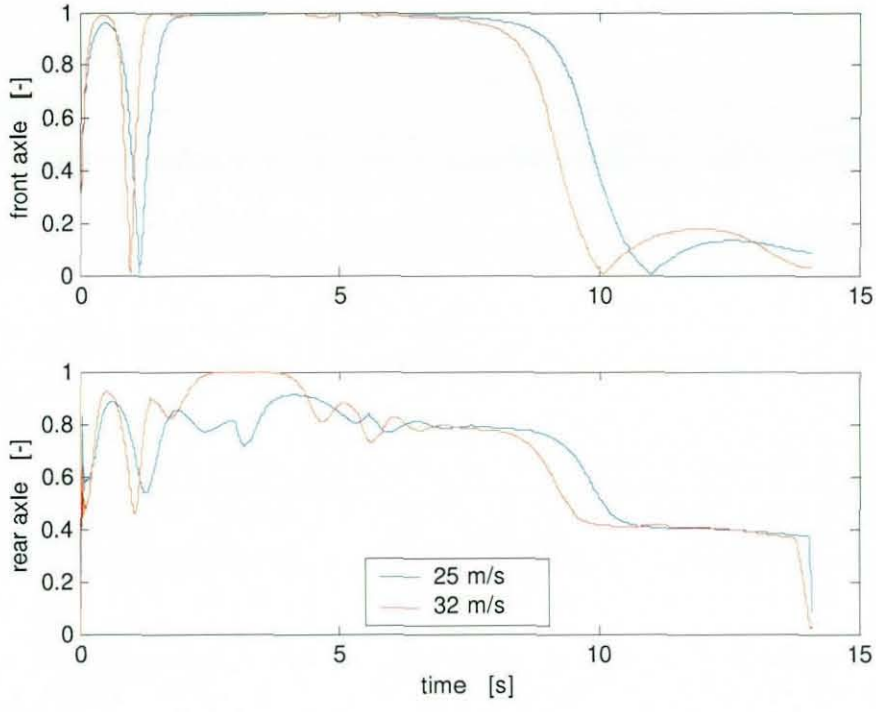

Figure 6.24 Tyre Force Utilisation Comparison with different Initial Velocities

6.4 Combined Corner Optimisation

The optimisation method is so far successfully applied to determine the optimum driving line through an isolated single corner. In this section, the method is applied to a more complex problem using combined corner geometry. The aim is to investigate whether the optimisation is capable of prioritising the control manoeuvre with respect to certain road geometry.

Road geometry consists of 90 degrees right hand corner (exactly the same as the one used so far) followed by a short 50 meters straight section and 90 degrees left hander which is then followed by a long straight (more than 300 meters). Figure 6.25 shows the road geometry.

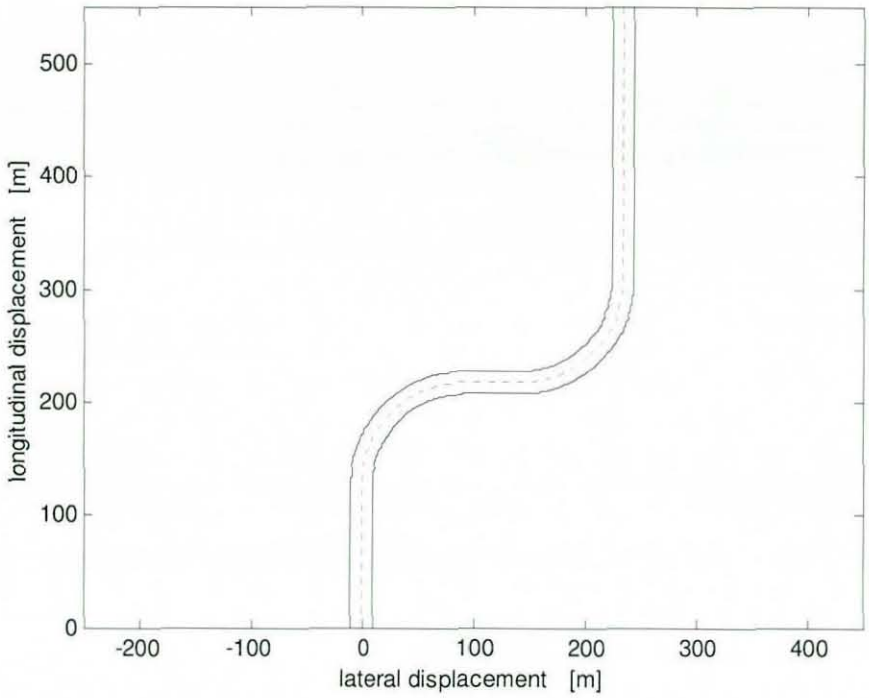

Figure 6.25 Combined Corners Geometry

In a real environment, a driver makes a decision in choosing a racing line based on the knowledge of the circuit geometry, the vehicle characteristics and their sensitivities. For example, a track layout could have a chicane, followed by a sweeping right-hander and then by a long straight. Provided there is only one vehicle on the track, the decision is made to either maximise the straight-line speed or minimise the time through the chicane, depending on their sensitivity to overall lap time gain.

In order to investigate such a "prioritisation" problem, the road geometry is set so that the intermediate straight is too short to treat the two corners independently. Therefore the controller is required to treat it as one corner, and make a decision in prioritising the certain part of the track with the expense of the other parts. In addition, the second corner is followed by much longer straight than the other two straights. This is to put a higher sensitivity on getting the second corner exit correct, in order to maximise the final displacement.

A part of the optimised vehicle path is shown in Figure 6.26. It is shown that the controller does not treat the two corners with an equal importance. The line through the first corner is largely compromised in order to place the vehicle in a desirable position for the second corner. If the first corner is taken as an independent corner, a vehicle will take out-in-out approach as shown earlier (Figure 6.6). However, this does not necessarily allow the vehicle to enter the following corner with the same out-in-out approach. As the second corner is followed by a long straight, there might be an advantage by putting a higher importance to get the second corner exit correct.

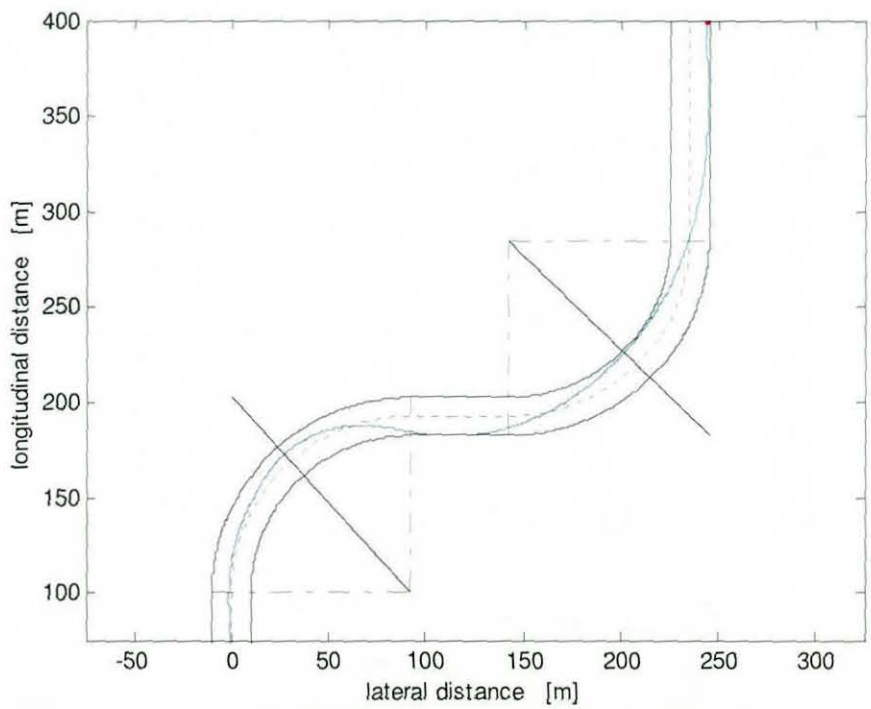

Figure 6.26 Line through a Combined Corner

From the vehicle forward velocity profile shown in Figure 6.27, it is clear that the two corners are treated as a one combined corner. The vehicle continues to decelerate very deep into the corner, marked by a red dot in Figure 6.26. From this point onwards, the vehicle accelerates all the way along, including the cornering phase.

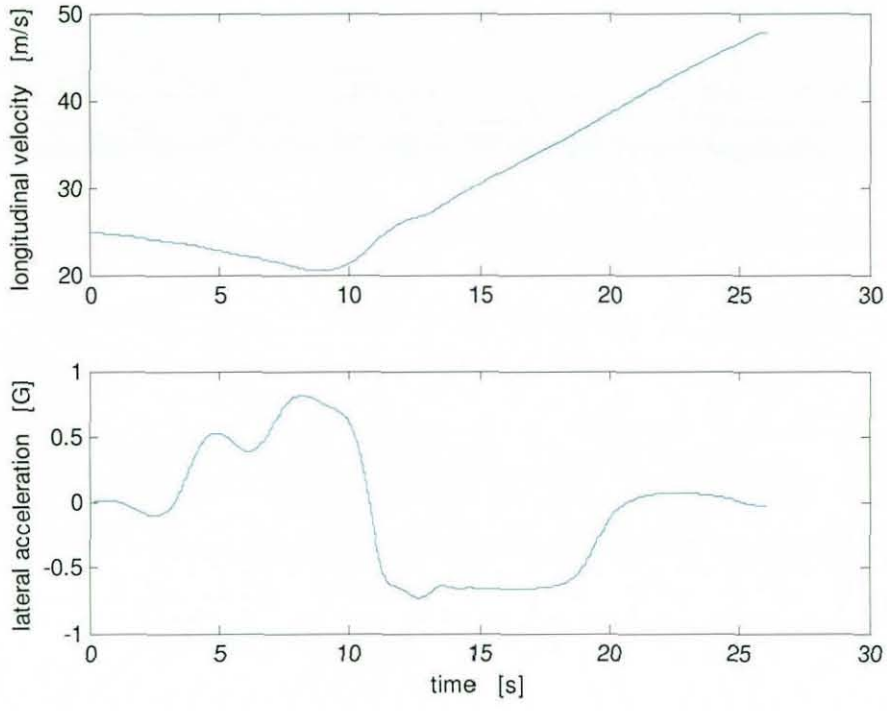

Figure 6.27 Forward Velocity & Lateral Acceleration Profiles

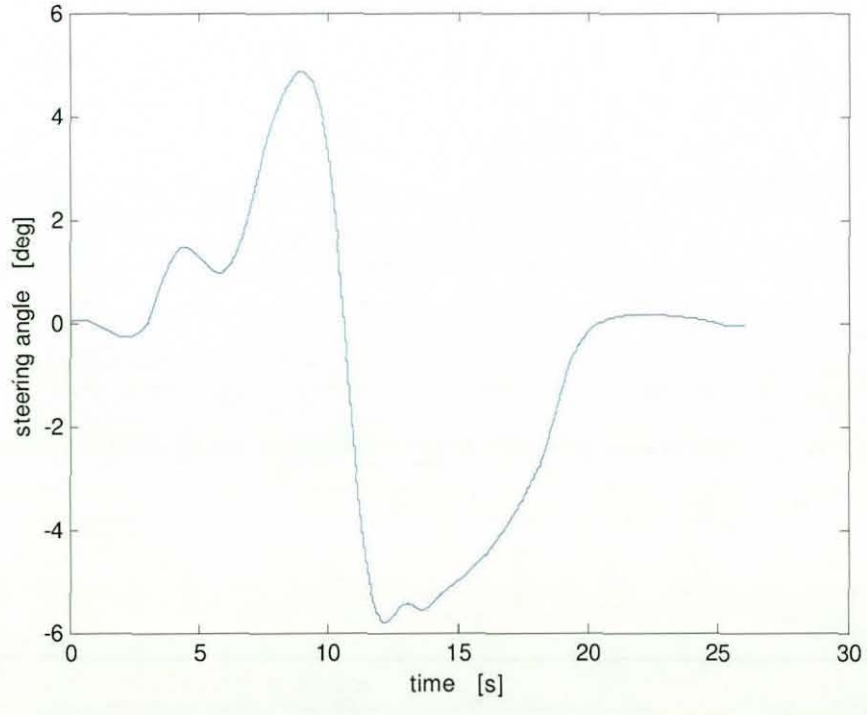

Figure 6.28 Steering Angle Profile

Steering angle time history is shown in Figure 6.28, where the significant difference between the first and second corners is noticed. It can be seen that the steering angle profile until 10 seconds is largely compromised. This sub-optimal manoeuvre through the first corner is confirmed by investigating tyre force utilisation, shown in Figure 6.29. It shows that the front tyres rarely reach their limit before 10 seconds. Moreover, the rear tyre usage is very low indicating non-severe braking. By contrast, front tyres are used fully through the second corner, and the corresponding rear tyre usage of around 80 %. These levels of utilisation are similar to the one experienced in Single Corner Optimisation result, shown in Figure 6.7.

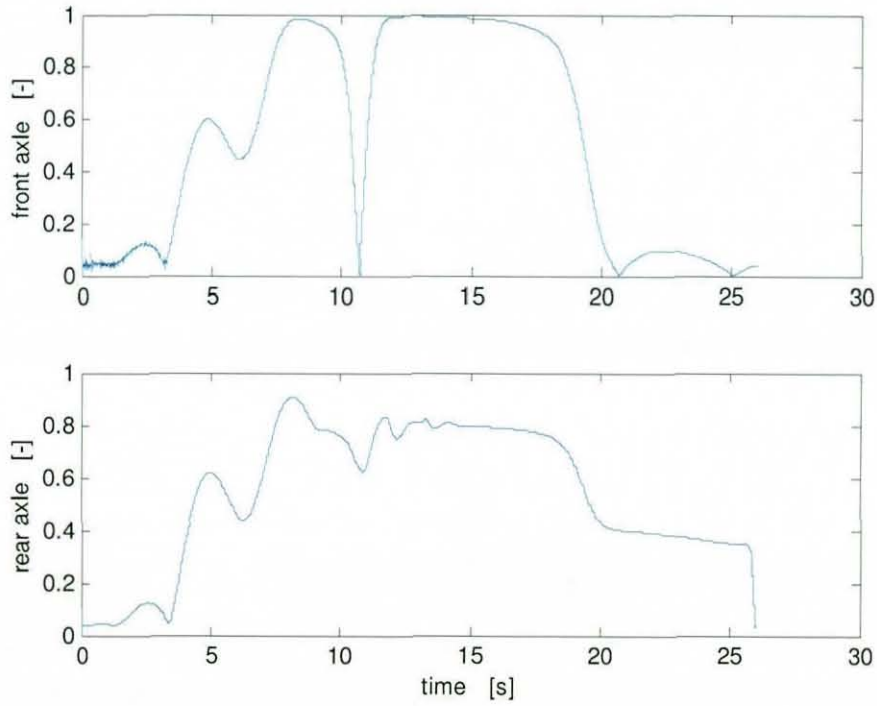

Figure 6.29 Tyre Force Utilisation

In order to further investigate whether the above result actually shows the prioritisation strategy in negotiating this combined corner or not, the road geometry is modified with a much longer intermediate straight of 300 meters. Thus the two corners are now effectively de-coupled. From the single corner

optimisation results, it can be seen that the intermediate straight has to be at least 200 meters long to ensure this de-coupling.

Figure 6.30 shows the vehicle path over the iterations. Unfortunately, this result suggests that the optimisation did not solve this prioritisation problem successfully. It is clearly shown that the optimisation concentrated its effort only on the second corner. As mentioned earlier, due to the elongated straight between the first and second corners, it is not necessary to compromise the line through the first corner. Hence, this indicates a problem in the optimisation itself.

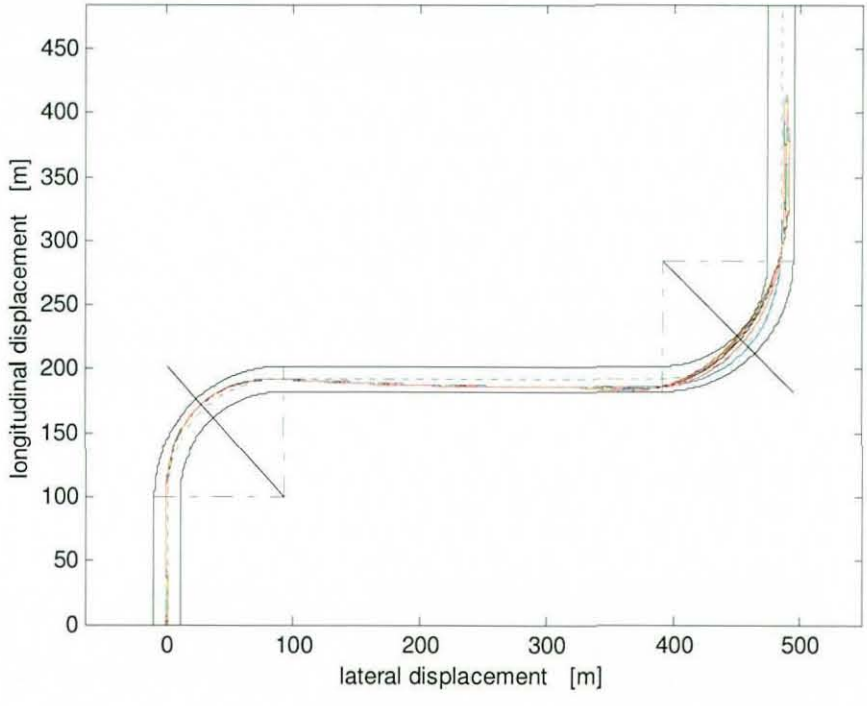

Figure 6.30 Vehicle Path Convergence

Figure 6.31 confirms the optimisation failure, where the tyre utilisation for the first part of the course is far away from their limits. Moreover, whilst negotiating the second corner, it can be seen that the tyres are not used as much compared to the result from the single corner optimisation shown in Figure 6.7.

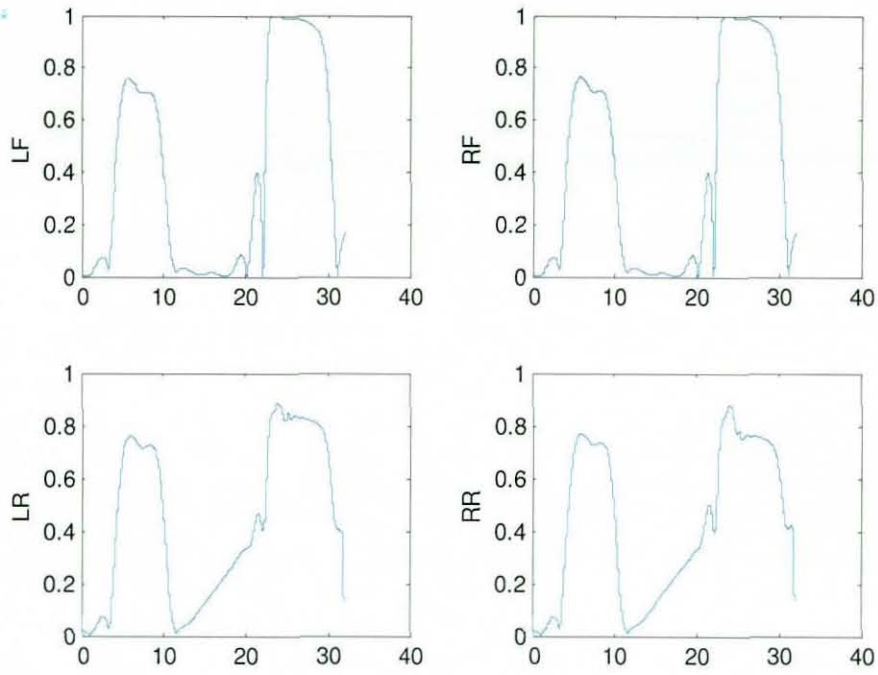

Figure 6.31 Tyre Force Utilisation

The possible causes of this failure are investigated. It is thought that the main aim of the cost function, to displace a vehicle to the furthest position, can be achieved more effectively by focusing on improving the latter part of the trajectory first. However, this meant that the optimisation converges to "out-in-out" line for the second corner whilst the line through the first corner still remaining largely unchanged. Any attempt to then optimise the path through the first corner poses a problem as the subsequent changes in the vehicle position through the second corner have a very high cost. This is because the vehicle is already placed very close to the boundary around the second corner. As a result, the optimisation converges to the result which is clearly not optimised for the entire track layout. For a single corner optimisation, pseudo-forward velocity cost was used successfully in order to spread the control effort through the whole manoeuvre, hence avoiding this local convergence issue. However, this "uneven convergence" remains to be a problem for more complex corner geometry.

In an attempt to counteract this problem, the input cost matrix, R, is made time varying. It is set so that the control effort at the early part of the manoeuvre has a significantly smaller cost than the one at the later part of the manoeuvre. However, this change was not successful as it only suppressed the control magnitude through the earlier part of the course. It did not change the strategy which the optimisation worked.

Although it was not possible to find the exact cause of this problem, an interesting difference is observed between this result and the one with the 3DOF model in Chapter 4. The 3DOF model result shown in Figure 4.3 finds the first apex successfully. By contrast, the 10DOF model result fails to find the first apex. Although the length of last straight is different between the two simulations, the difference in the results / optimisation strategies clearly seems to be linked to the forward velocity degree of freedom. Further research (outside the scope of this thesis) is required in order to understand exactly how this extra degree of freedom influenced the optimisation strategy.

6.5 Summary

This Chapter described the application of vehicle path optimisation using a 10DOF vehicle handling model. The optimisation method is based on the one developed for a 3DOF model, as described in Chapter 4, however, is extended with an additional control input (engine torque demand).

The Single corner optimisation result showed that the method is capable of finding a line within the vicinity of the friction limit. The converged path clearly shows "out-in-out" line through the corner to maximise the cornering speed whilst utilising the available tyre forces. Results over the iterations improved continuously in a first order manner, suggesting that the optimisation was run successfully.

Validation exercises are performed and the main findings are as follows.

1) The optimisation method is robust with respect to the controller setting changes within a "reasonable" magnitude.
2) Initially, the vehicle was under-powered so that rear tyres were not fully used to their limit (i.e. not an optimisation issue).
3) With higher engine power, it was found that the input cost matrix, R, had to be weighted differently in order to keep the similar authority to both steering and torque control.
4) If the front and rear tyres reach their limits simultaneously, it prevents from running the optimisation properly.
5) Initially, the vehicle was not put on its limit under braking. When the initial vehicle forward velocity was increased, the optimisation successfully solved the problem with limit braking.

Finally, the optimisation technique was applied to a slightly more complex corner. This is to investigate whether the controller was capable of prioritising a certain part of manoeuvre in order to achieve the best overall gain. The result showed that the controller concentrated on maximising the performance in the latter half of the manoeuvre as it has the higher sensitivity to final displacement. Time-varying R matrix was used to solve this issues, however, was not successful.

When comparing this result against the 3DOF model result shown in Chapter 4, it shows interesting contrast. In order to understand this mechanism, further research is required.

Chapter 7

Influence of Vehicle Characteristics on Path Optimisation and Controllability

In Chapters 4 and 6, an iterative method for optimising a vehicle path for a given road geometry has been developed. It was found that the method was able to drive a vehicle at the vicinity of friction limit for simple single corner geometry. Two methods were developed, one with a single control input (steering rate) and the other with two control inputs (steering rate + engine torque). Although the iterative optimisation itself was successful, it was discovered that the controller strategy had to be set up carefully in order to avoid controllability issues.

In Chapter 5, implications of controllability on the optimisation results were discussed in detail. In Chapter 6, one of the optimisation failure showed loss of controllability when both front and rear tyre forces saturated simultaneously. Hence, it can be argued that vehicles that retain more controllability near the limit may be able to achieve a better solution. So far, a "standard" vehicle set-up was used for all the simulation.

This chapter investigates if the optimisation process / result are heavily coupled with the underlying vehicle dynamics itself or not. In order to investigate this, the single corner optimisation problem (as used in Chapter 6) is applied to various vehicle set-ups. Steady-state and transient parameters are changed independently in order to map the vehicle dynamics to the optimisation result in a straightforward way.

In addition, the cost functions used in the 4WS controller work in Chapter 3 is also used in the analysis. This is to investigate the potential relationship between

4WS handling objectives and the optimisation results. Is vehicle that has linear handling characteristics through the most of operating condition really 'easy' to drive?

7.1 Steady-State Parameter Influence

In order to investigate the effects of steady-state vehicle characteristics, the optimisation method is applied for vehicles B, C, D and E. The specifications of these vehicles are outlined in Chapter 2. Vehicles B and C have more understeer characteristics compared to the reference, Vehicle A. Similarly, vehicles D and E have more oversteer characteristics. All the simulations are set so that they trace a similar vehicle path at the start of the optimisation. This gives the same final displacement cost to start the optimisation with. As a consequence, the corresponding steering angle time histories differ among the vehicles (and hence the subsequent dynamics condition). These small differences in steering angle at the first iteration should not affect the final result as they will be overwritten by the steering rate controller through the iteration process. It is worthwhile investigating whether this difference in steady-state characteristics has any effects on the optimisation strategy itself as well as the result.

The summary of results is shown in Table 7.1 below. In general, it can be seen that the final distance achieved and the mean velocity forward increase as the vehicle weight is shifted towards the rear axle, i.e. more steady-state oversteer. Table 7.1 also shows the total tyre utilisation along the manoeuvre. The utilisation actually reduces as the distance result improves. Hence, it can be said that more oversteering vehicles are able to achieve better result (increased final distance) with more margin left in tyre capability. This result is further investigated later on in this section.

	Unit	C	B	A	D	E
Weight Distribution	%	65	62.5	57	50	40
Final Distance	m	326.59	328.43	333.51	332.44	334.48
Tyre Utilisation	-	2.77	2.73	2.69	2.63	2.55
Mean Forward Velocity	m/s	33.72	33.88	34.17	34.32	34.50
Mean Abs. Lat. Acc.	g	0.468	0.468	0.478	0.484	0.474

Table 7.1 Steady-State Dynamics Effects

Figure 7.1 shows the comparison of the optimised vehicle paths. It shows that these results all follow similar path throughout the manoeuvre. Only notable difference is the vehicle position at the exit straight.

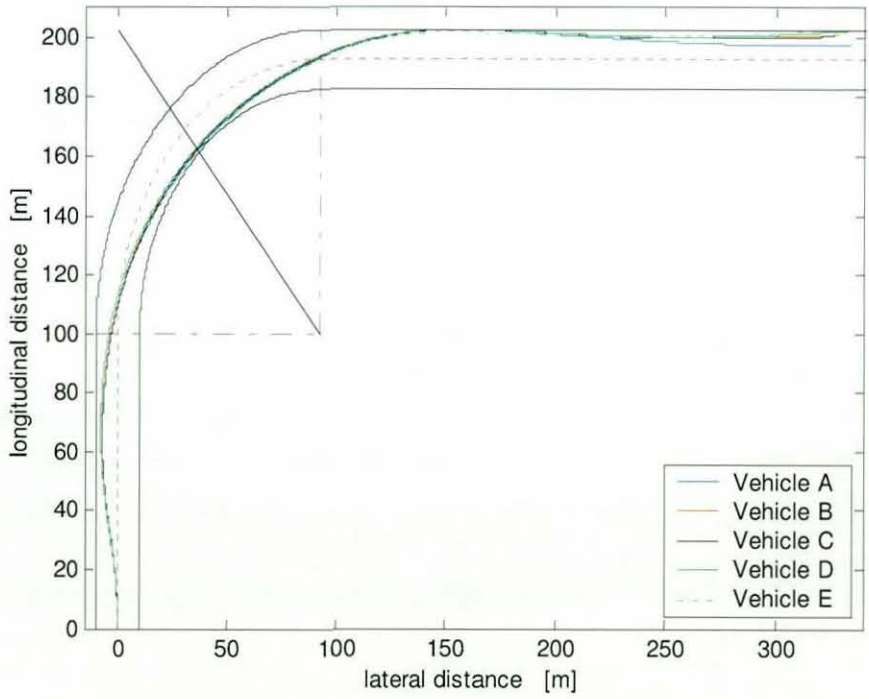

Figure 7.1 Vehicle Path Comparison

From Figure 7.1 and the steering angle characteristics shown in Figure 7.3, it can be seen that all vehicles tend to move wide during the approach to the corner, in order to maximise the turning radius. However, the understeer vehicles (B & C) are not displaced as wide. The oversteer vehicles (D & E) have less initial opposite steering angles. However, due to the vehicle characteristics, more lateral accelerations are produced at the equivalent steering angle and hence the increased lateral displacement. This general reduction in steering angle is clearly shown for Vehicle E in Figure 7.3. Moreover, after the second peak in the steering angle, the oversteer vehicles reduce steering angle earlier than the others.

This result indicates that there is really only one optimum line when negotiating this corner. The controller produces slightly different demands to best compensate for the differences in vehicle dynamics.

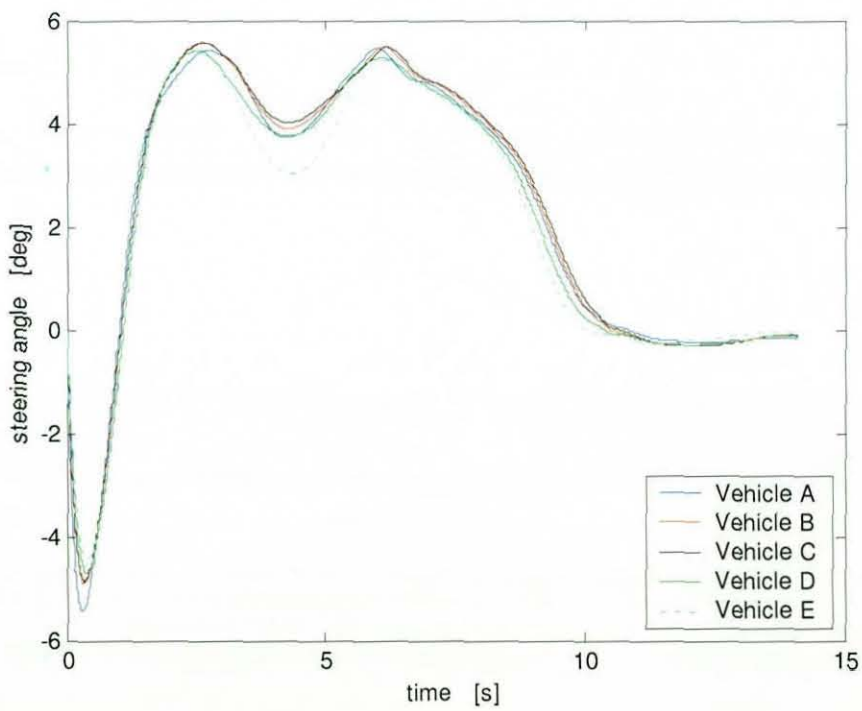

Figure 7.2 Steering Angle Comparison

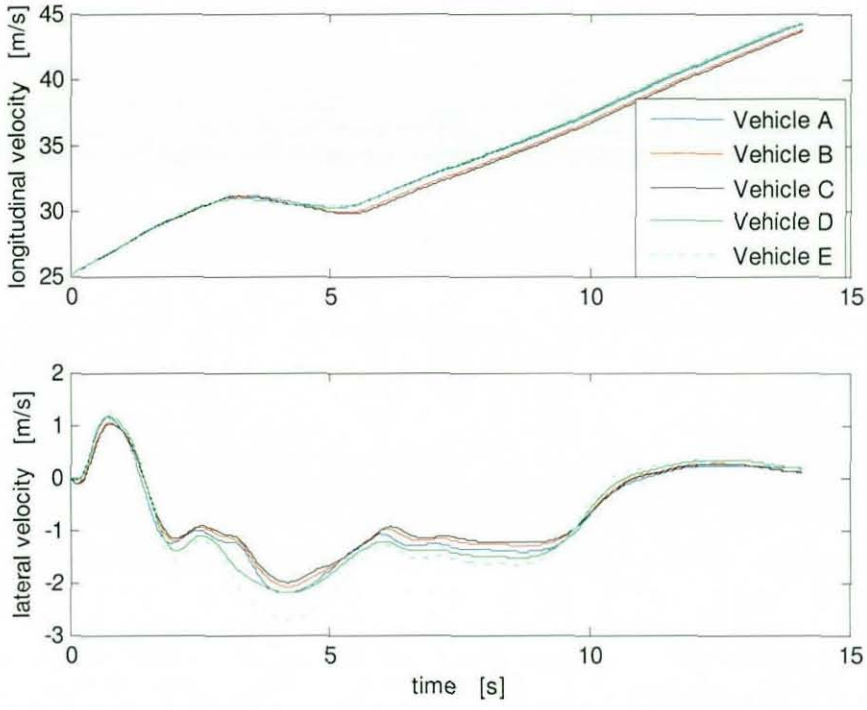

Figure 7.3 Longitudinal and Lateral Velocities Comparison

Figure 7.3 shows the vehicle longitudinal and lateral velocities. It can be seen that the acceleration at the start of the manoeuvre is very similar for all vehicles. However, the maximum velocities achieved before braking are lower for oversteer vehicles due to higher lateral sliding. In the mid-corner, the oversteer vehicles decelerates less, however with the higher lateral sliding. Cornering speed is kept more constant with earlier acceleration points at the exit. This means that these vehicles are able to reach higher velocities at the end of the straight since all the vehicles accelerate with the maximum engine power available (i.e. torque limited rather than grip limited). In addition, the lateral velocity profiles show that its magnitude and oscillation are reduced with the increased understeer setting.

The tyre force utilisations at both front and rear axles are investigated and are shown in Figures 7.4. The utilisation figures themselves do not have the actual size of the friction circles. Hence, when comparing the different vehicle set-ups, it should be investigated together with the magnitudes of tyre forces shown in

Figure 7.5. Figure 7.4 shows that all vehicles use front tyres to their limit whilst cornering, and there is not much difference among the vehicles. The differences are more apparent at the entry and exit of the corner. In terms of initial opposite steer effect, Vehicle A seems to use the friction circle most and also at the earliest point in time. Towards the end of the manoeuvre, the most oversteering vehicle E has considerably less steering angle as shown in Figure 7.2. Its effect on tyre utilisation is clearly shown in Figure 7.4.

As the vehicle is set to understeer more, the rear tyres utilisation increases compared to the front. The only exception is during braking (just before 5sec), where this trend is reversed. Considering the differences in achieved final distances, it is clear that the more oversteer vehicles (w.r.t. the reference vehicle A) are better suited to negotiate this corner.

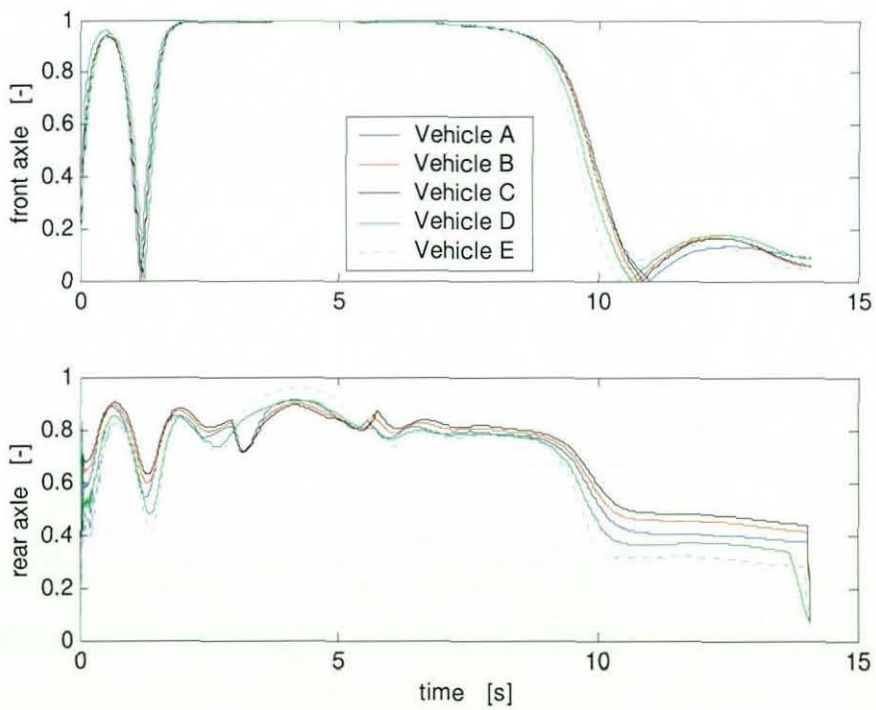

Figure 7.4 Front & Rear Axle Tyre Utilisation

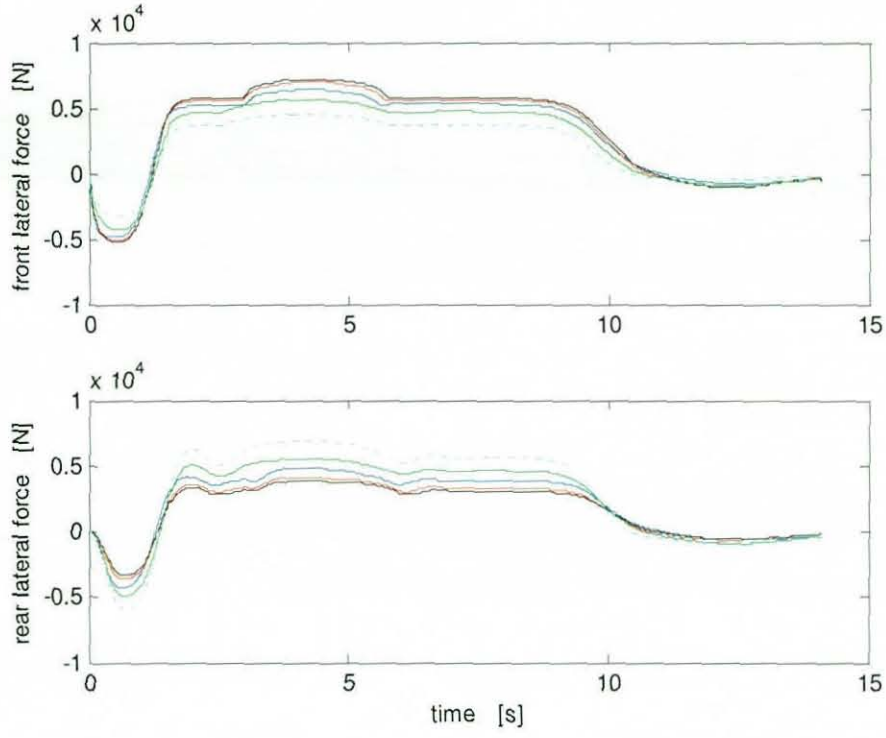

Figure 7.5 Front & Rear Axle Tyre Lateral Force

7.1.1 Investigation using 4WS Cost

In the previous section, the optimisation results are analysed in terms of handling balance and tyre utilisation. In this section, these results are discussed from a particular handling index view point. Recall Chapter 3 where a 4WS controller was developed with the aim to achieve certain dynamic characteristics by minimising two cost functions. One is to achieve a linear relationship between lateral acceleration and yaw rate with respect to the vehicle forward velocity. The other is to achieve a neutral steer yaw rate gain through the wide lateral acceleration range. In Chapter 3, these costs are defined as shown in Equations 3.2 and 3.4 below.

$$J_1 = \int \left(a_y - ur\right)^2 dt \tag{3.2}$$

$$J_2 = \int \left(r - \frac{u}{l}\delta_d\right)^2 dt \tag{3.4}$$

These cost functions were used as the handling objectives for 4WS controller, as it is thought that these would give predictable dynamics and hence relatively easy to control. Both linearity and neutral steer costs, as shown above, are calculated for the optimised trajectories with various vehicle set-ups. This is listed in Table 7.2, together with the maximum displacement achieved through the optimisation. Please note that the results are based on the passive vehicle as used for Chapters 4 and 6, not the active 4WS vehicle used in Chapter 3.

	Unit	C	B	A	D	E
Weight Distribution	%	65	62.5	57	50	40
Final Distance	m	326.59	328.43	333.51	332.44	334.48
Linearity Cost	-	10.12	10.77	12.55	11.80	15.66
Neutral Steer Cost	-	5.09	5.05	4.95	4.59	4.19

Table 7.2 Effects of Steady-State Dynamics on 4WS Costs

Figure 7.6 shows the general trend such that Linearity Cost increases and Neutral Steer Cost reduces as vehicle setting is changed towards more steady-state oversteer. As mentioned earlier, the optimisation result improves as the oversteer tendency is increased. This suggests that having nonlinear relationship between lateral acceleration and yaw rate does not become a severe disadvantage for path optimisation. However, the yaw rate gain with respect to the steering angle input seems to be important in controlling a vehicle. This might be due to the steering action being directly influenced by a controller.

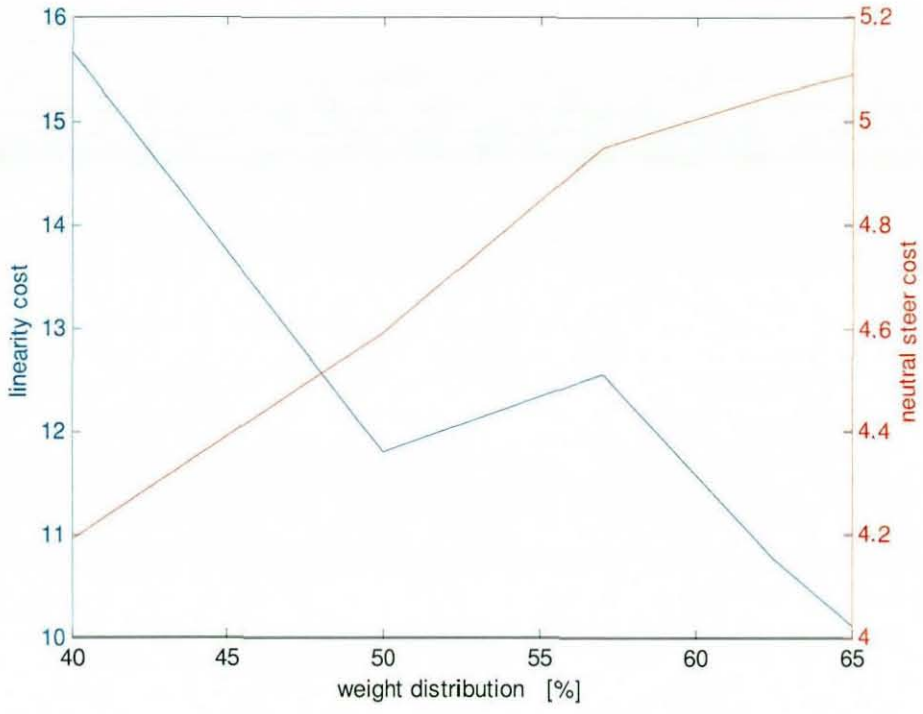

Figure 7.6 Four-Wheel-Steer Costs vs. Weight Distribution

7.2 Transient Parameter Influence

Hoffman et al [Hoffman, 1966] and Hogg et al [Hogg, 1992] suggested that the yaw damping has a significant influence on the driver's path following ability. This could be linked to the optimisation's ability to control a vehicle in order to trace a desired path. Hence, the yaw damping is altered in order to investigate its effect on the optimisation result. Definition of yaw damping based on the bicycle model is stated in Equation 2.33.

$$\zeta = \frac{mC_2 + I_{zz}C_0}{2umI_{zz}\omega_n} \tag{2.33}$$

It shows that this parameter is affected by mass, yaw moment of inertia, wheelbase, front and rear tyre cornering stiffness and fore/aft weight distribution of a vehicle. Total mass and wheelbase remain fixed for this study in order to retain a fundamental reference dimension/set-up of a vehicle. In addition, fore/aft weight distribution change has already been investigated in the steady-state parameter effect section, using vehicles B, C, D and E. Therefore the effect of

varying the yaw damping is investigated using vehicles F, G and H which simply have different yaw moment of inertia values. Summary of the results is shown in Table 7.3 below.

	Units	I	F	A	G	H
Yaw Moment of Inertia	kgm^2	3500	2863	2500	2142	1820
Maximum Distance	m	332.47	334.39	333.51	333.15	333.63
Tyre Utilisation	-	2.67	2.67	2.69	2.68	2.70
Mean Forward Velocity	m/s	34.12	34.21	34.17	34.15	34.18

Table 7.3 Transient Dynamics Effects

The results are very interesting, where the best performance is achieved with vehicle F that has 2863 kgm^2 yaw moment of inertia. Vehicle "F" has the set up such that the yaw radius of gyration equals to the distance between CoG to the rear axle. Increasing or reducing the inertia from this value resulted in the poorer performances. However, reducing the inertia further to 1820 kgm^2 with Vehicle H improved the result slightly. This yaw inertia effect on the final displacement is plotted in Figure 7.7. It must be noted that the yaw inertia value is not necessarily varied at a small enough increment to be able to conclude at which exact value the optimisation performs at the best or worst. However, the results suggest that there are multiple points at which the vehicle performs well. Casanova [Casanova et al, 2000] investigated the influence of yaw inertia variation on his minimum time manoeuvre optimisation result. He found increase in unbalanced yaw moment during the transient phase of the manoeuvre. However, as the length each of transient phases was very small, hence its effect on minimum manoeuvre time was negligible until the yaw inertia is increased to unrealistic values. He also compared the results using "g-g" diagram and found that the vehicle with the largest inertia operated more away from the edge of the diagram. This is due to longer transient phase, as expected.

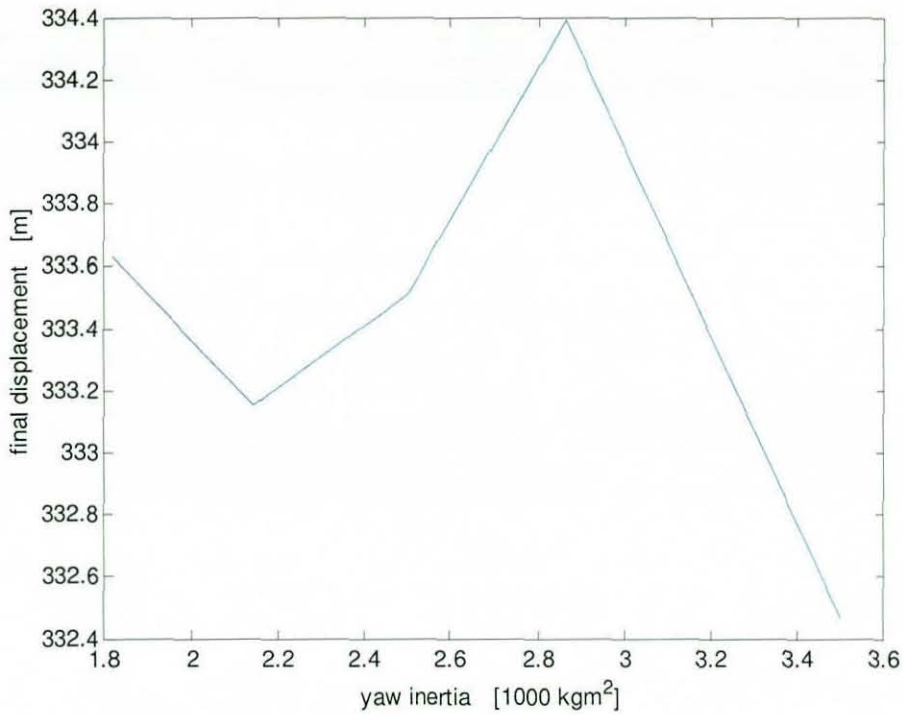

Figure 7.7 Final Displacement with various Yaw Moment of Inertia

Figure 7.8 again shows that the resultant vehicle paths do not vary considerably with the different values of yaw inertia. However, the initial vehicle displacement trend, where it moves towards the outside of the corner, shows the obvious result where the vehicle with the lowest yaw inertia is displaced outwards the most. This lateral displacement is reduced as the yaw inertia is increased. The corresponding steering angle time history is shown in Figure 7.9. It shows that vehicle I (highest inertia) produce the largest initial opposite steer angle and vehicle H (lowest inertia) produces the least. Towards the exit of the corner, vehicles with larger inertia tend to reduce the steering angle earlier. Again, this steering profile and the resultant vehicle path show that the controller is compensating for the difference in dynamics in order to effectively trace a single optimum line through this corner.

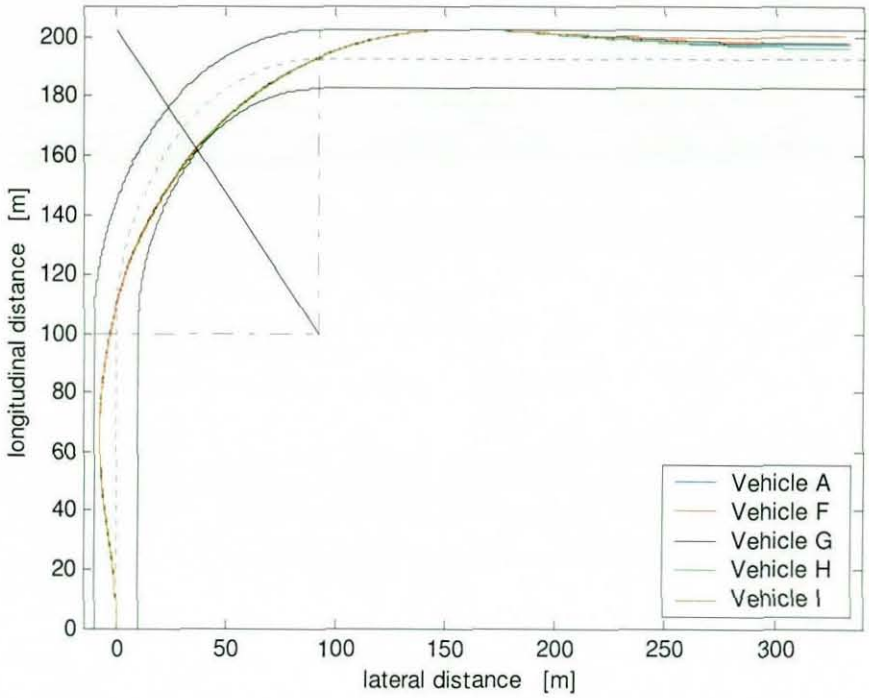

Figure 7.8 Vehicle Path Comparison

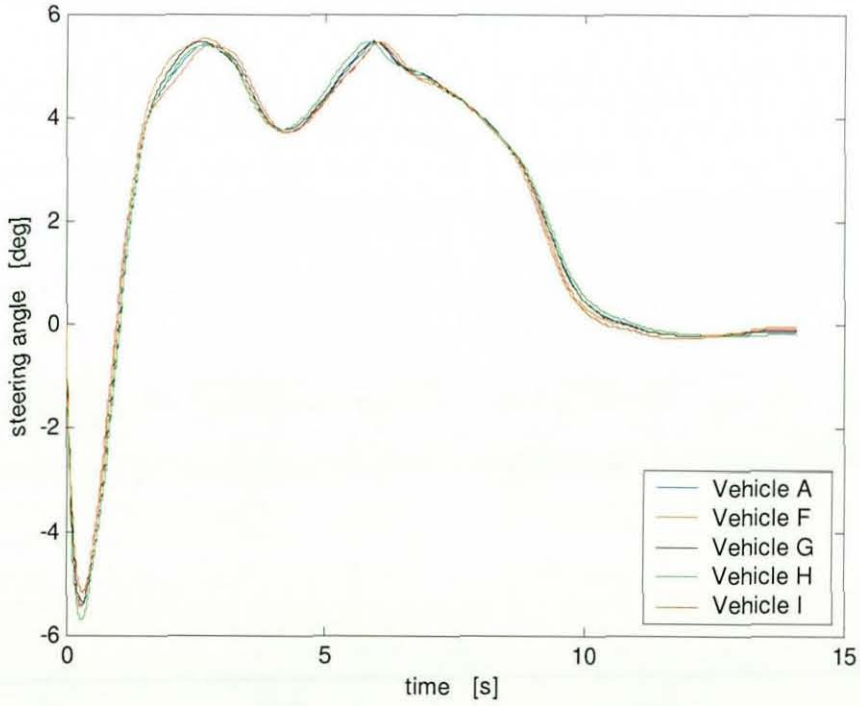

Figure 7.9 Steering Angle Comparison

7.2.1 Investigation using 4WS Cost

Linearity and neutral steer costs are used for further assessment as per steady-state analysis. From Table 7.4 and Figure 7.10, it can be seen that both costs have the same trend as the one shown in Table 7.2 and Figure 7.6. It is consistent in the way that the best result, the maximum final displacement, is achieved when the minimum neutral steer cost is achieved. Obviously, having higher yaw inertia value slows the transient yaw dynamics. This seems to help controller keeping the vehicle with relatively more desired yaw rate – steering angle relationship. When the inertia is reduced from the value at which the best result is achieved, 2863 kgm^2, the increase in neutral steer cost is steeper. By contrast, the cost increases at much more moderate rate when the inertia is increased further.

	Units	I	F	A	G	H
Yaw Moment of Inertia	kgm^2	3500	2863	2500	2142	1820
Maximum Distance	m	332.47	334.39	333.51	333.15	333.63
Linearity Cost	-	13.99	13.11	12.55	12.15	12.19
Neutral Steer Cost	-	4.94	4.92	4.95	4.99	5.03

Table 7.4 Effects of Transient Dynamics on 4WS Costs

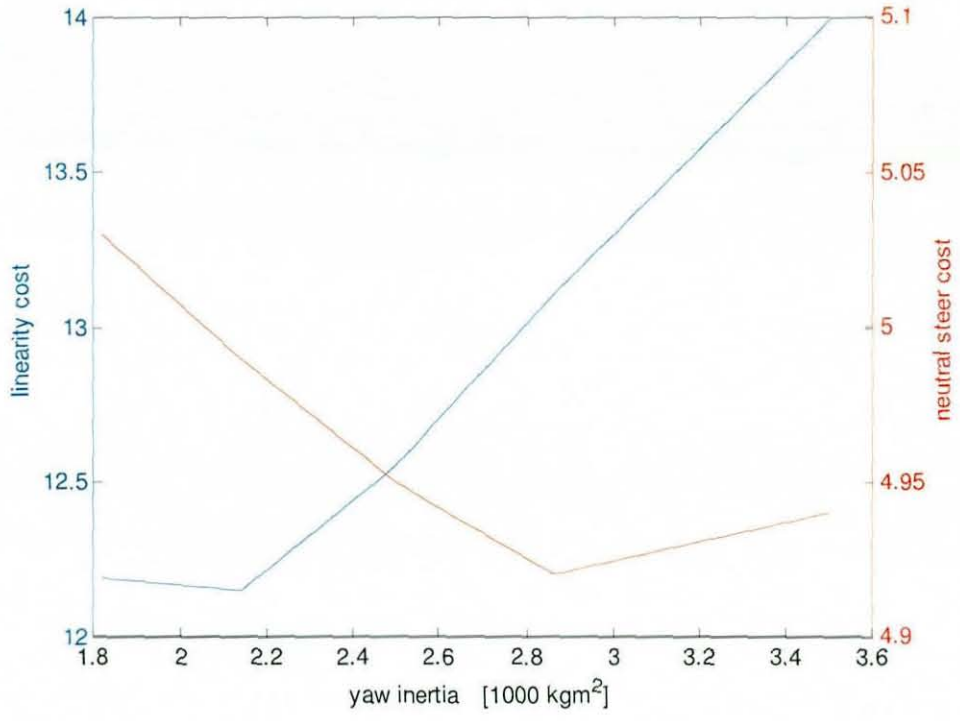

Figure 7.10 Four-Wheel-Steer Costs vs. Yaw Moment of Inertia

7.3 Controllability & Vehicle Dynamics – Brief Study

In the previous sections, vehicle path optimisation is performed with various different vehicle characteristics. Its performance was examined by using not only its resultant cost (achieved final displacement), but also by using 4WS objective functions defined in Chapter 3.

In Chapter 5, the property of controllability *Gramian* matrix was used successfully in understanding the vehicle path optimisation result. In this section, it is used to investigate the coupling of vehicle dynamics and controllability. Step steer input is used as its result contains both steady-state and transient data.

First, steady-state dynamics effects are investigated using vehicles C & D, with the standard vehicle A as a reference. As mentioned earlier, vehicles C and D respectively have more steady-state understeer and oversteer. In order to ensure

that all vehicles operate at the equivalent severity, the magnitude of steering inputs are altered among the vehicles. Step steer of 1.5 degrees is applied to the reference vehicle A and the resultant total lateral acceleration is recorded. Step steer magnitudes for vehicles C and D are set to 2.0 and 1.1 degrees respectively, so that the same amount of lateral acceleration is produced. Controllability Gramian is determined for the simulations and the inverse of its minimum singular value is shown in Figure 7.11.

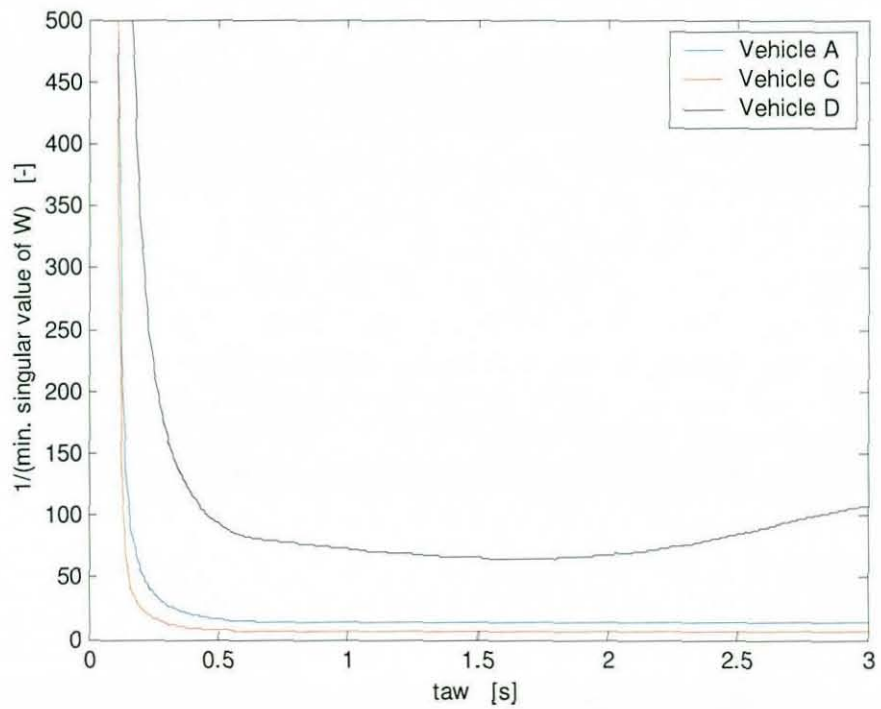

Figure 7.11 Gramian property for different vehicle set-ups

Regardless of the vehicle set-up differences, the lack of controllability when time allowed for control is less than 0.5 is apparent. Figure 7.11 shows that vehicle D – oversteer - has the least controllability for all different τ values. As the setting is moved more towards steady-state understeer, the controllability is improved. Moreover, although the percentage difference in weight distribution with respect to the reference vehicle A is similar (7 - 8 %) for both vehicles C & D, the controllability does not change significantly between vehicles A & C. By comparison, there is a considerable difference between A & D, hence the

relationship between the vehicle balance and controllability is nonlinear. For the limited variation in vehicle set-ups and operating conditions, it can be concluded that, for a conventional front-wheel-steer vehicle, vehicles with more steady-state understeer characteristics have better controllability.

Having investigated the steady-state dynamics effects on the controllability, vehicles F and H are used to investigate the transient dynamics effects. Figures 7.12 and 7.13 respectively show the front tyre lateral force and controllability profiles with respect to the various yaw inertia values. Constant "τ window" of 1 second is used and is moved along the trajectory. From Figure 7.12, it can be seen that the controllability trend is different depending on the point of time along the trajectory (consistent with the previous findings).

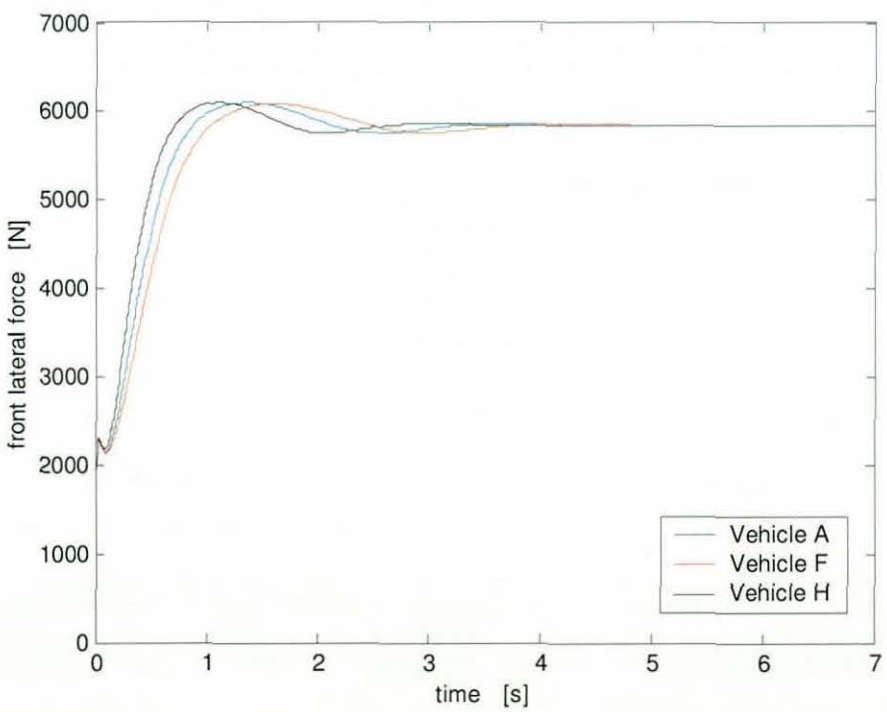

Figure 7.12 Front Lateral Force Profile with various Yaw Inertia

During the transient period of the manoeuvre, i.e. between 0 and 1 second, it shows that the vehicles with less yaw moment of inertia have less controllability. This is because a vehicle has achieved higher lateral forces more quickly with less

yaw inertia. Hence the vehicle is operating at more severe dynamics range at this particular point in time. However, beyond the point where the vehicle reaches its steady-state approximately at 2.5 seconds, vehicles with higher inertia has less controllability. As the variation in yaw inertia does not have an effect on the steady-state force values, all vehicles are operating at equally severe operating conditions. The difference in the controllability despite of this suggests that the vehicles with higher inertia require larger effort to transfer the state within a given time window of 1 second. In other words, they are less sensitive to the input variation which shows up as less controllable. This is in agreement with the finding of Sharp [Sharp, 2005], where he found that for good tracking performance with short preview distance, yaw inertia and mass should be small. In other words, for a given time window of 1 second, reducing vehicle inertia means reaching closer to a full preview distance (if the full preview distance is greater than 1 second).

Figure 7.13 shows another interesting characteristic for vehicle H, which has the least yaw moment of inertia. There is a relatively sharp peak when the front lateral force reaches its maximum value, whereas the corresponding peaks for the other vehicles are more moderate. Any quick changes in controllability are undesirable for a driver, since one has to adapt his/her control strategy quickly to compensate for such changes. The sharpness of this peak as well as its magnitude suggests that the small inertia actually makes it more difficult to control when a vehicle is closer to the limit of adhesion. By contrast, it is easier to control when a vehicle is operating at moderate steady-state condition.

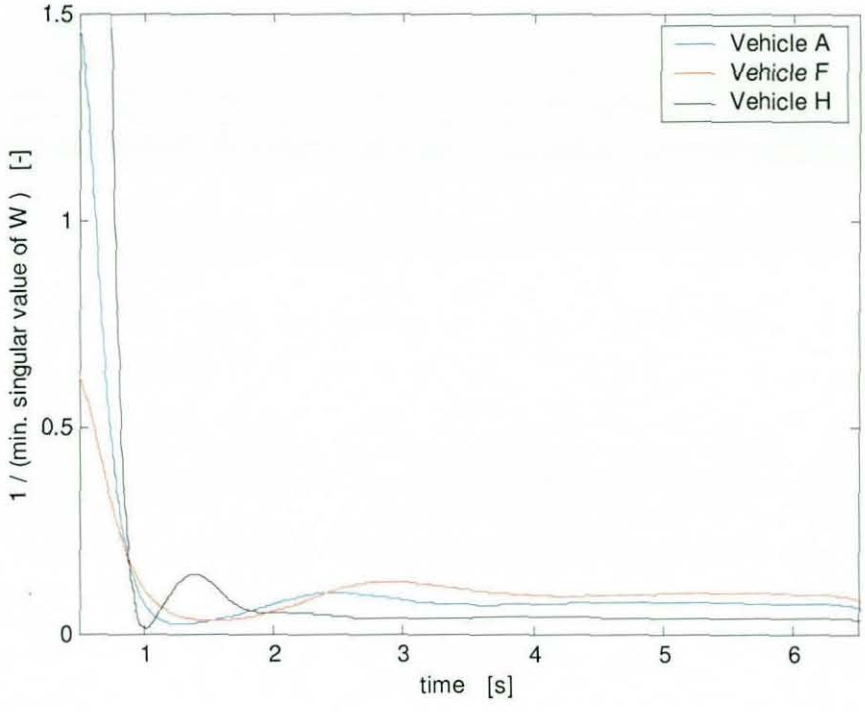

Figure 7.13 Transient Dynamics Effect on Vehicle Controllability

7.4 Summary

Using the single corner optimisation problem formulated in the previous chapter, simple vehicle parameter sweeps are performed in order to investigate the relationship between the vehicle dynamics and the optimisation result.

Despite the significant magnitudes of the changes experimented either on the weight distribution or the yaw moment of inertia, all the results converge to a very similar path. This suggests that there is only one optimum line through this simple corner geometry as one might expect. The performance difference in terms of achieved final displacements are noticed, although, not very significant. Thus it is difficult to draw clear conclusion sorely from this relatively simple comparison study alone. Only clear finding is that more oversteering vehicle was able to achieve better result with more margin left in rear tyre force capacity. Even though the controller is able to take advantage of this extra margin on rear tyres, it

may or may not be the case for a human driver (for various reasons: i.e. less accurate internal model, delay in control action, noisier feedback signal etc). Casanova et al [2002] also found that the simulated optimum weight distribution was significantly more rearward than the experiment results in real life.

The handling objectives used for 4WS control in Chapter 3 is re-introduced here in order to investigate the implication of such dynamics characteristics on the path optimisation result. It is found that the neutral steer cost function has a strong correlation with the vehicle path optimisation performance. Whereas the linearity cost did not show noticeable correlation. This could be because the neutral steer cost function is influenced directly by the control input, whereas the linearity cost is controlled indirectly.

The effects of varying vehicle characteristics are studied also from controllability point of view. Step steer simulation was used for this study, as the result contains both transient and steady-state data. Although only the limited numbers of changes are made, it highlighted a few interesting points. For the range of dynamics covered in this study, it is found that

i.) Vehicle with more steady-state understeer retains higher controllability

ii.) Having less yaw inertia makes it more controllable at moderate operating condition

iii.) However, it makes a vehicle less controllable around the limit of adhesion

In this Chapter, results are analysed in a very straightforward manner. In order to further understand the interaction among vehicle dynamic characteristics, optimisation performance and controllability, more detailed mathematical analysis is required. However, this is outside the scope of this thesis and hence remains as a future research project.

Chapter 8

Discussion and Conclusions

8.1 Discussion & Conclusions

The existing literatures show that many control systems have been applied in order to enhance vehicle dynamics. Control systems such as Four-Wheel-Steer (4WS), Direct Yaw Moment Control (DYC) and Roll Moment Distribution Control have been investigated by many researchers and some has been implemented on mass production vehicles. Similarly, many different control theories, both linear and nonlinear, are used to achieve the "desired" vehicle characteristics. In this thesis, the research was conducted using a linear optimal control strategy as it guarantees the optimum solution, although not necessarily globally, and the results can be investigated more analytically.

Chapter 3 described a 4WS controller using a linear time-invariant optimal control with a reference model structure. This structure allowed the controller to be designed based on the very simple 2DOF bicycle model as a reference model. The nonlinearity of the actual vehicle, represented by the 3DOF handling model with nonlinear tyres, is controlled well using the secondary feedback controller. In addition, Tabu Search method is applied in order to perform multi-parameter optimisation required within the design stage. The handling objectives of the controller are set so that the vehicle exhibits a consistent (hence predictable) dynamics until the tyre capacity saturates. These targets are successfully achieved, showing that only the very basic vehicle information is required for the primary controller. Robustness of the controller was investigated and it was found that the controller designed on the sinusoidal steer test inherits reasonably good robustness. Moreover, the sensitivity analysis revealed that the controller is robust to small changes in the various vehicle parameter values.

As shown by many literatures, even with a vehicle equipped with an active steering control suffers from tyre saturation. Hence, change in vehicle characteristics cannot be avoided under such situation [Mokhiamar, 2003, 2005]. Moreover, if the control strategy was not formed properly, it is possible for the controller to have an adverse influence on the resultant dynamics. The controller designed in this thesis simply regulated the amount of control authority in order to avoid such situation. Canale et al [Canale, 2008] proposed a control structure using Internal Model Control (IMC), which was able to guarantee robust stability in the presence of saturation function. Sharp et al [Sharp 2000] applied time-invariant linear optimal control technique, but used saturation functions within the controller.

Time-varying modelling approach is used as a next step in order to better represent the vehicle operating conditions throughout the various dynamic range, including at the limit of adhesion. In Chapter 4, iterative vehicle path optimisation problem is formulated using a linear time-varying optimal control, with a reference model structure. The controller is applied to the 3DOF handling model, which was also used for the 4WS study. The validation study was carried out using the steady-state simulation on the limit handling condition. It showed that the optimisation method works satisfactory, utilising the available tyre forces to find a manoeuvre close to the friction limit. The optimisation displaced vehicle within 0.4% of the theoretical maximum. However, there are a couple of issues with the optimisation. Due to the nature of the quadratic road geometry cost function, the solution could get locked if the vehicle runs very close to the edge of the road. Hence, the optimisation needs to be formulated in a way such that it avoids this at the early stages of the iteration process. It is also found that the optimisation encounters a problem when the system condition becomes poor near the limit handling condition. It is hypothesised that the matrix becomes poorly conditioned due to lack of controllability and hence resulting in inappropriate control inputs.

In order to understand this optimisation failure within the vicinity of friction limit, Chapter 5 analyses the controllability of a linear time-varying system and discusses its properties in detail. The study started with the determination of the calculation method for controllability Gramian matrix, which provides the fundamental information on system controllability. Two methods of calculation are examined and it is found that both methods have their own shortcomings. However, from studying the properties of the gramian matrix itself, it is concluded that the state transition matrix method provided more relevant information to real life problems. Moreover, the inverse of minimum singular value of the gramian matrix is found to best reflect the actual controllability of the vehicles. The resultant Open-Loop control is defined based on the gramian matrix and was applied to transfer the states to the prescribed values successfully within the various time constraints. It is found that the controllability generally becomes very poor when there is less than 0.5 second is available to transfer the states. Moreover, "moving controllability window of fixed time period" is found to provide the most relevant information of the changing dynamics through the time.

These findings / methods are then used to understand the optimisation issue found in Chapter 4, where the final displacement cost fluctuated over the several iterations when the vehicle was operating close to the friction limit. The *Gramian* information showed that the optimised trajectory was often less controllable than the steady-state maxima due to its oscillating dynamics. This is further supported by tyre utilisation data. Hence, it is concluded that the optimisation failure is a result of poorly conditioned matrix due to lack of controllability. In order to avoid this issue, controllability information needs to be integrated within the optimisation process in order to suitably regulate the controller input(s).

Having established that the vehicle path optimisation method itself is functioning correctly, the problem formulation is then extended to include longitudinal dynamics in order to perform simulation of more general manoeuvres and hence the results are more relevant to the real life situation. The single corner optimisation result showed that the method is capable of finding the driving line

within the vicinity of the friction limit. The converged path clearly showed "out-in-out" line through the corner to maximise the cornering speed whilst utilising the available tyre forces. The robustness of the controller is assessed by investigating the controller parameter sensitivity on the optimisation result. Initial result showed rear tyres were not fully used to their limit, whilst the front tyre utilisation was on the limit. The validation exercise with increased engine power and initial forward velocity showed that the optimisation can make full use of all available tyre forces, if required. Therefore, it proved that the control strategy formulation was capable of determining a solution which involves a coupling of longitudinal and lateral dynamics demands. The repeatability of optimisation result was very good with respect to small changes in initial conditions. It is interesting that Casanova et al [Casanova, 2000] found other local solutions as well as the optimum solution. It is reported that the optimiser trades reduce corner entry speed for increased corner exit speed on certain occasions. This was not seen from the work covered in this thesis.

The optimisation technique is then applied to slightly more complex corner geometry. Its aim is to investigate whether the controller was capable of prioritising a certain part of manoeuvre in order to achieve the best overall gain. Unfortunately, this optimisation problem could not be solved successfully. The optimisation concentrated on the latter part of the manoeuvre as it had higher sensitivity to the final cost. It was not possible to improve the optimisation strategy by regulating the control effort with respect to time. For the lap time optimisation problem, Casanova et al [Casanova, 2000] discretised the track into short, totally de-coupled segments in order to reduce the sensitivity of the cost in later part of road section compared to earlier controls. He reported the maximum length of 200m achieved the best balance between optimisation robustness and computational time, although this depends on the complexity of road geometry. Although this is clearly a possible option, this structure is not expected to provide insight into "prioritisation" problem. This is simply because the controller may not have a necessary "preview" of the road geometry ahead in order to make a prioritisation decision. More recently, Kelly [Kelly, 2008] studied influence of

preview distance on minimum time manoeuvre optimisation result. For a corner followed by a long straight, longer preview distance achieved better result by maximising the exit speed with the expense of entry speed. It was found that the optimisation performance stabilised beyond 250m preview distance. Such approach could be adapted for the optimisation issues encountered in this thesis.

Finally, the coupling of the optimisation result and the vehicle dynamics itself is investigated. In the earlier study, one of the optimisation failure showed the loss of controllability when both front and rear tyre forces saturate simultaneously. Hence, it can be argued that the vehicles that retain more controllability near the limit may be able to achieve a better solution. In order to investigate this, the vehicle paths optimisation is performed with various vehicle set-ups. It is found that all the vehicles converge to a very similar path, suggesting that there is only one optimum line through the simulated corner. Since a single 90 degrees bend is used for this study, such result is as expected. Future work with more complex corner geometry may provide further insight. Although the differences are not very significant, it showed that more oversteering vehicle was able to achieve better result with more margin left in rear tyre capacity. The handling objectives used for the 4WS controller work are also used in the analysis to investigate if such indices have any correlation to the path optimisation results. It is found that the neutral steer cost function has a strong correlation with the vehicle path optimisation performance. Whereas the linearity cost did not show noticeable correlation. However, this is only a "soft" numerical result. In order to further understand the interaction among vehicle dynamic characteristics, optimisation performance and controllability, more detailed mathematical analysis is required.

The effects of varying vehicle characteristics are also studied from controllability point of view. Although the study is relatively simple and limited, it showed that understeer tendency improves controllability. It also showed that the increase in yaw inertia makes a vehicle more controllable at the limit, however, it makes it less controllable at moderate operating conditions. These results accords well with our practical driving experience. In addition, these findings show interesting

relation to Sharp's findings, [Sharp, 2005], where he found that the yaw inertia should be small in order to achieve good tracking performance with short preview distance. Moreover, the results showed that the controllability variation with time as well as its absolute magnitude is a key factor. If a vehicle has dynamic characteristic such that the controllability changes suddenly when certain dynamics is exhibited, a driver has to adapt very quickly in order to compensate and produce a correct control action. This can be mentally and physically challenging and may not enhance the safety.

8.2 Recommendation for Future Work

- Inclusion of the controllability information within the cost functions of 4WS or any other active handling dynamics control strategy. The objective is to maintain certain controllability throughout the manoeuvre. For instance, if the vehicle starts losing control, the original handling performance cost function can be overwritten to retain higher controllability for safety
- Formal integration of the controllability information with the time-varying optimisation technique used for vehicle path optimisation. This thesis used controllability only as an "off-line" post processing tool.
- More detailed analysis of the relationship between vehicle dynamics, path optimisation result and controllability. This thesis focused more on establishing the optimisation methods, hence formal analysis of the result from vehicle dynamics point of view is still required to gain further insight.
- Modification of time-varying optimal controller to reflect certain human dynamics. Example of such dynamics includes but not limited to variable time lag, bandwidth, noise and offsets.
- Comparison of controllability information with other researchers' findings of handling quality such as Sharp's work on required preview distance.
- Validation work of above theoretical investigation, possibly using a driver-in-loop simulator.

References

Abe, M. [1992]
Vehicle Dynamics and Control
Sankai-do, Chapter 9, pp. 209-228

Abe, M. [1994]
Comparison of 4WS and DYC for improvement of Vehicle Handling Performance
Proc. of AVEC '94, Tsukuba, Japan

Abe, M. [1996]
On Advanced Chassis Control Technology for Vehicle Handling and Active Safety
Proc. of AVEC '96, Aachen, Germany

Abe, M. [1997]
Advanced Chassis Control Technology for Vehicle Handling and Active Safety
JSAE Automotive Engineering, vol. 51, iss.11, pp. 11-19

Abe, M., Kato, A., Suzuki, K. and Kano, Y. [1998]
Estimation of Vehicle Side-Slip Angle for DYC by Using On-Board-Tyre-Model
Proc. of AVEC'98, Nagoya, Japan

Abe, M and Kano, Y. [1999]
Improvement of Vehicle Handling Safety with Vehicle Side-Slip Control by DYC
Vehicle System Dynamics, vol. 33, pp. 665-679

Abe, M., Ohkubo, N. and Kano, Y. [1994]
Comparison of 4WS and Direct Yaw Moment Control (DYC) for Improvement of Vehicle Handling Performance
Proc. of AVEC'94, Tsukuba, Japan

Ackerman, J. [1994]
Yaw Rate and Lateral Acceleration Feedback for Four-Wheel-Steering
Proc. of AVEC '94, Tsukuba, Japan

Alfi, A. and Farrokhi, M. [2009]
Hybrid state-feedback sliding-mode controller using fuzzy logic for four-wheel-steering vehicles
Vehicle System Dynamics, vol. 47, no. 3, pp. 265-284

Anderson, B.D.O. [1982]
Internal and External Stability of Linear Time-Varying Systems
SIAM Journal of Control and Optimisation, vol. 20, iss. 03, pp. 408-413

Anderson, B.D.O. and Moore, J.B. [1990]
Optimal Control – Linear Quadratic Methods
Prentice Hall

Aoki, Y., Li, Z. and Hori, Y. [2006]
Robust Design of Body Slip Angle Observer with Cornering Power Identification at Each Tire for Vehicle Motion Stabilisation
Proc. of AMC'06, International Workshop on Advanced Motion Control, Istanbul

Barnett, S. and Cameron, R.G. [1985]
Introduction to Mathematical Control Theory
Clarendon Press, Chapter 6, pp. 279

Best, M.C. and Gordon, T.J. [1998]
Real-Time State Estimation of Vehicle Handling Dynamics using an Adaptive Kalman Filter
Proc. of AVEC '98, Nagoya, Japan

Best, M.C., Gordon, T.J. and Dixon, P.J. [2000]
An Extended Adaptive Kalman Filter for Real-time State Estimation of Vehicle Handling Dynamics
Vehicle System Dynamics, vol. 34, pp. 57-75

Best, M.C. and Gordon, T.J. [2000]
Combined State and Parameter Estimation of Vehicle Handling Dynamics
Proc. of AVEC '00, Ann Arbor, USA

Best, M.C. and Gordon, T.J. [2002]
Simultaneous Optimisation of Vehicle Parameter and Control Action to Examine Validity of Handling Control Assumptions
Proc. of AVEC '02, Hiroshima, Japan

Brockett, R.W. [1970]
Finite Dimensional Linear Systems
John Wiley and Sons, NY

Bryson, A.E. [1999]
Dynamic Optimization
Addison-Wesley, MA

Canale, M. and Fagiano, L. [2008]
Stability control of 4WS vehicles using robust IMC techniques
Vehicle System Dynamics, vol. 46, no. 11, pp.991-1011

Casanova, D., Sharp, R.S. and Symonds, P. [2000]
Minimum Time Manoeuvring: The Significance of Yaw Inertia
Vehicle System Dynamics, vol. 34, pp.77-115

Casanova, D., Sharp, R.S. and Symonds, P. [2000]
Sensitivity to mass variations of the fastest possible lap of a formula one car
Vehicle System Dynamics, vol..35, pp. 119-134

Casanova, D., Sharp, R.S. and Symonds, P. [2001]
Construction of race circuit geometry from on-car measurements
Proc Instn Mech Engrs, vol. 215, Part D, pp. 1033-1042

Casanova, D., Sharp, R.S. and Symonds, P. [2002]
On the optimisation of the longitudinal location of the mass centre of a formula one car for two cicuits
Proc. of AVEC '02, Hiroshima, Japan

Chen, D.C., Crolla, D.A., Alsted, C.J. and Whitehead, J.P. [1996]
A Comprehensive Study of Subjective and Objective Vehicle Handling Behaviour
Vehicle System Dynamics, vol.25, pp. 66-86

Chen, D.C. and Crolla, D.A. [1997]
Subjective and Objective Measures of Vehicle Handling: Drivers & Experiments
Vehicle System Dynamics, vol. 29

Chen, D.C., Crolla, D.A., Alsted, C.J. and Whitehead, J.P. [1998]
Vehicle Handling Assessment Using a Combined Subjective-Objective Approach
Vehicle Dynamics and Simulation, SP-1361, SAE980226

Cipelli, M., Schiehlen, W. and Cheli, F. [2008]
Driver-in-the-loop simulations with parametric car models
Vehicle System Dynamics, vol. 46, Supplement, 2008, pp. 33-48

Cole, D.J., Pick, A.J. and Odhams, M.C. [2006]

Predictive and linear quadratic methods for potential application to modelling driver steering control

Vehicle System Dynamics, vol. 44, pp. 259-284

Cole, D.J. and Pick, A.J. [2008]

A Mathematical Model of Driver Steering Control Including Neuromuscular Dynamics

Journal of Dynamic Systems, Measurement and Control, vol. 130

DeCuyper, J., Furmann, M., Kading, D. and Gubitosa, M. [2007]

Vehicle dynamics with LMS Virtual. Lab Motion

Vehicle System Dynamics, vol. 45, Supplement, 2007, pp.199-206

Dixon, J.C. [1997]

Tires, Suspension and Handling

Society of Automotive Engineers, Warrendale

Chapter 2, pp. 77; Chapter 6, pp.351, Chapter 7, pp. 452

Dixon, P.J. [2004]

The Influence of the Sideslip Target on the Performance of Vehicles with Actively Controller Handling

Doctoral Thesis, Loughborough University

Friedland, B. [1986]

Control System Design: An Introduction to State-Space Methods

McGraw Hill Inc, NY

Furukawa, Y. and Abe, M. [1996]

On-Board-Tyre-Model Reference Control for Cooperation of 4WS and Direct Yaw Moment Control for Improving Active Safety of Vehicle Handling

Proc. of AVEC '96, Aachen, Germany

Furukawa, Y. and Abe, M. [1998]
Direct Yaw Moment Control with Estimating Side-Slip by Using On-Board-Tyre-Model
Proc. of AVEC '98, Nagoya, Japan

Gillespie, T.D. [1992]
Fundamentals of Vehicle Dynamics
Society of Automotive Engineers, Warrendale

Gordon, T.J. and Best, M.C. [1999]
Lyapunov Control of Vehicle Handling Dynamics
JSAE Review, vol. 20, pp. 253-258

Gordon, T.J., Best, M.C. and Dixon, P.J. [2002]
An Automated Driver based on Convergent Vector Fields
Automotive Engineering, vol. 216, pp. 329-347

Hancock, M.J., Williams, R.A., Fina, E. and Best, M.C. [2007]
Yaw motion control via active differentials
Transactions of the Institute of Measurement and Control 29, 2 (2007), pp. 137-157

Hancock, M.J., Williams, R.A., Gordon, T.J. and Best, M.C. [2005]
A comparison of braking and differential control of road vehicle yaw-sideslip dynamics
Proc. IMechE, vol. 219, part D: J. Automobile Engineering

Harada, H., Araki, Y. and Oya, M. [1996]
Control Effects of Active Rear Wheel Steering on Driver-Vehicle System
Proc. of AVEC '96, Aachen, Germany

Higuchi, M. [1996]
Handling Analysis and Prediction during Cornering
Proc. of AVEC '96, Aachen, Germany

Higuchi, A. and Saito, Y. [1992]
Optimal Control of Four Wheel Steering Vehicle
Proc. of AVEC '92, Yokohama, Japan

Hirano, Y. and Fukatani, K. [1996]
Development of Robust Active Rear Steering Control
Proc. of AVEC '96, Aachen, Germany

Hirano, Y. and Ono, E. [1994]
Non-linear Robust Control for an Integrated System of 4WS and 4WD
Proc. of AVEC '94, Tsukuba, Japan

Hoffman, E.R. and Joubert, P.N. [1966]
The Effect of Changes in Some Vehicle Handling Variables on Driver Steering Performance
Human Factors, 1966, vol.8, no.3, pp. 245-263

Hogg, A.S., Dickison, J.G., Maddison, S.J. and Yardley, A.J. [1992]
Design and Prediction of Vehicle Handling and Stability
I.MechE. Proc. 925050, pp. 35-40

Holzmann, F., Bellino, M., Spiegelberg, G. and Sulzmann, A. [2006]
Improvement of the driving safety using a predictive vehicle dynamical model
Proc. of IEEE 2006, Kunming, China

Inagaki, H., Akuzawa, K. and Sato, M. [1992]
Yaw Rate Feedback Braking Force Distribution Control with Control-by-Wire Brake System
Proc. of AVEC '92, Yokohama, Japan

Inoue, H. and Sugasawa, F. [1992]
Comparison of Feedforward and Feedback Control for 4WS
Proc. of AVEC '92, Yokohama, Japan

Ishio, J., Ichikawa, H., Kano, Y. and Abe, M. [2008]
Vehicle-handling quality evaluation through model-based driver steering behaviour
Vehicle System Dynamics, vol. 46, pp. 549-560

Kageyama, I. and Jo, H. [1996]
An Advanced Vehicle Control Method using Independent Four-Wheel-Steering System
Proc. of AVEC '96, Aachen, Germany

Kelly, D.P. [2008]
Lap Time Simulation with Transient Vehicle and Tyre Dynamics
Doctoral Thesis, Cranfield University

Kiencke, U., Majjad, R. and Kramer, S. [1999]
Modelling and performance analysis of a hybrid driver model
Control Engineering Practice, vol. 7, pp. 985-991

Kleine, S. and van Niekerk, J.L. [1998]
Modelling and Control of a Steer-by-Wire Vehicle
Vehicle System Dynamics, vol. 28, pp114-142

Koike, Y. and Doya, K. [2003]
Driver Model Based on Reinforced Learning with Multiple-Step State Estimation
Electronics and Communications in Japan, Part 3, vol. 86, no. 10

Komatsu, A., Gordon, T.J. and Best, M.C. [2000]
4WS Control of Handling Dynamics using a Linear Optimal Reference Model
Proc. of AVEC '00, Ann Arbor, USA

Komatsu, A., Gordon, T.J. and Best, M.C., 2002
Vehicle Path Optimisation using a Time-Variant Linear Optimal Reference Control
Proc. of AVEC '02, Hiroshima, Japan

Lee, A.Y. [1995]
Performance of 4WS Vehicles in Lane Changing Manoeuvres
SAE 950316

Li, D., Du, S., and Yu, F. [2008]
Integrated vehicle chassis control based on direct yaw moment, active steering and active stabiliser
Vehicle System Dynamics, vol. 46, Supplement, pp. 341-351

Lin, Y. [1992]
Improving Vehicle Handling Performance by a Closed-Loop 4WS Driving Controller
SAE 921604

Liu, Z. [2004]
Stability and Oscillations in a Time-Delayed Vehicle System with Driver Control
Nonlinear Dynamics 35, pp. 159-173

Lugner, P. and Mittermayr, P. [1992]
Controlled Additional 4-Wheel Steering at Critical Driving Conditions
Proc. of AVEC '92, Yokohama, Japan

Lugner, P., Pacejka, H. and Plöchl, M. [2005]
Recent advances in tyre models and testing procedures
Vehicle System Dynamics, vol. 43, no. 6-7, pp413-436

Lugner, P. and Plöchl, M. [1994]
Theoretical Investigations of the Interaction Driver-Feedback-Controlled Automobile
Proc. of AVEC '94, Tsukuba, Japan

Lugner, P. and Plöchl, M. [1999]
A 3-Level Driver Model and its Application to Driving Simulations
Vehicle System Dynamics, Supplement. 33, pp. 71-82

MacAdam, C. [2003]
Understanding and Modelling the Human Driver
Vehicle System Dynamics, vol.40, no.1-3, pp. 101-134

MacAdam, C., Ervin, R., Bareket, Z. and Fancher, P. [1998]
Using Neural Networks to Identify Driving Style and Headway Control Behaviour of Drivers
Vehicle System Dynamics, vol. 29, 1998

Matsumoto, S. and Yamaguchi, H. [1992]
Braking Force Distribution Control for Improved Vehicle Dynamics
Proc. of AVEC '92, Yokohama, Japan

McLean, J.R. and Hoffmann, E.R. [1973]
The effects of restricted preview on driver steering control and performance
Human Factors, 1973, vol.15, no.4, pp. 421-430

Meng, X., Lee, K.K., and Xu, Y. [2006]
Human Driving Behaviour recognition based on Hidden Markov Models
Proc. of IEEE 2006, Kunming, China

Milliken, W.F. and Milliken, D.L. [1995]
Race Car Vehicle Dynamics
Society of Automotive Engineers, Warrendale

Mitschke, M. [1994]
Control Loop for Driver-Vehicle with 4WS
Proc. of AVEC '94, Tsukuba, Japan

Miura, Y., Tokutake, H. and Fukui, K. [2007]
Handling qualities evaluation method based on actual driver characteristics
Vehicle System Dynamics, vol. 45, no. 9, pp807-817

Mokhiamar, O. and Abe, M. [2002]
Active wheel steering and yaw moment control combination to maximise stability as well as vehicle responsiveness during quick lane change for active vehicle handling safety
Proc. IMechE., vol. 216, Part D: J. Automobile Engineering

Mokhiamar, O. and Abe, M. [2003]
Examination of different models following types of yaw moment control strategy for improving handling safety of a car – caravan combination
Proc. IMechE., vol. 217, Part D: J. Automobile Engineering

Mokhiamar, O. and Abe, M. [2005]
Experimental verification using a driving simulator of the effect of simultaneous optimal distribution of tyre forces for active vehicle handling control
Proc. IMechE., vol. 219, Part D: J. Automobile Engineering

Motoyama, S., Uki, H., Isoda, K. and Yuasa, H. [1992]
Effect of Traction Force Distribution Control on Vehicle Dynamics
Proc. of AVEC '92, Yokohama, Japan

Nagai, M. [2007]
The perspectives of research for enhancing active safety based on advanced control technology
Vehicle System Dynamics, vol. 45, no. 5, pp413-431

Nagai, M. and Ohki, M. [1989]
Theoretical Study on Active 4WS by Virtual Vehicle Model Following Control
Int. J. of Vehicle Design, vol.10, no.1, pp.16-33

Nagai, M., Ueda, E. and Moran, A. [1994]
Integration of Linear Systems and Neural Networks for the Design of Nonlinear Four-Wheel-Steering System
Proc. of AVEC '94, Tsukuba, Japan

Nagai, M., Yamanaka, S. and Hirano, Y. [1996]
Integrated Control Law of Active Rear Wheel Steering and Direct Yaw Moment Control
Proc. of AVEC '96, Aachen, Germany

Naito, G., Yaguchi, E. and Ozaki, K., 1992
Improving Vehicle Dynamics by Torque Split Control System
Proc. of AVEC '92, Yokohama, Japan

Pacejka, H., Bakker, E. and Nyborg, L. [1987]
Tyre Model for use in Vehicle Dynamics Studies
SAE 870421

Pacejka, H.B., Bakker, E. and Lindner, L. [1989]
A New Tyre Model with an Application in Vehicle Dynamics Studies
SAE 890087

Pick, A.J. and Cole, D.J. [2007]
Dynamic properties of a driver's arms holding a steering wheel
Proc. IMechE, vol. 221, Part D: J. Automobile Engineering

Pick, A.J. and Cole, D.J. [2008]
A Mathematical Model of Drive Steering Control Including Neuromuscular Dynamics
Journal of Dynamic Systems, Measurement, and Control, May 2008, vol. 130

Plöchl, M. and Edelmann, J. [2007]
Driver models in automobile dynamics application
Vehicle System Dynamics, vol. 45, no. 7-8, pp. 699-741

Press, W.H., Teukolsky, S.A., Vetterling, W.T. and Flannery, B.P. [2007]
Numerical Recipes 3rd Edition: The Art of Scientific Computing
Cambridge University Press, Cambridge

Prokop, G. [2001]
Modelling Human Vehicle Driving by Model Predictive Online Optimisation
Vehicle System Dynamics, vol. 35, no. 1, pp.19-53

Raksincharoensak, P., Mizushima, T. and Nagai, M. [2006]
Direct Yaw-Moment Control Adapted to Driver Behaviour Recognition
Proc. SICE-ICASE International Joint Conference, pp. 534-539

Raksincharoensak, P., Mizushima, T. and Nagai, M. [2008]
Direct Yaw Moment control system based on driver behaviour recognition
Vehicle System Dynamics, vol. 46, Supplement, pp.911-921

Rugh, W.J. [1996]
Linear Systems Theory
Prentice Hall, Chapter 9 (Controllability and Observability)

Sait, S.M. and Youssef, H. [1999]
Iterative Computer Algorithms with Applications in Engineering
IEEE Computer Society, Chapter 4, pp. 183-248

Sakai, S., Sado, H. and Hori, Y. [2002]
Dynamic Driving / Braking Force Distribution in Electric Vehicles with Independently Driven Four Wheels
Electrical Engineering in Japan, vol. 138, no.1, pp. 79-89

Sharp, R.S. [2005]
Driver steering control and a new perspective on car handling qualities
Proc. IMechE, vol. 219, Part C: J. Mechanical Engineering Science

Sharp, R.S. [2007]
Optimal stabilization and path-following controls for a bicycle
Proc. IMechE, vol. 221, Part C: J. Mechanical Engineering Science

Sharp, R.S. [2007]
Motorcycle Steering Control by Road Preview
Journal of Dynamic Systems, Measurement and Control, 2007, vol. 129

Sharp, R.S., Casanova, D. and Symonds, P. [2000]
A Mathematical Model for Driver Steering Control, with Design, Tuning and Performance Results
Vehicle System Dynamics, vol. 33, pp.289-326

Shibahata, Y., Simada, K. and Tomari, T. [1992]
The Improvement of Vehicle Manoeuvrability by Direct Yaw Moment Control
Proc. of AVEC '92, Yokohama, Japan

Silverman, L.M. and Meadows, H.E. [1967]
Controllability and Observability in Time-Variable Linear Systems
SIAM Journal of Control, vol. 5, iss01, pp. 64-73

Song, J.G. and Yoon, Y.S. [1998]
Feedback Control of 4WS using Time Delay Control
Int. J. of Vehicle Design, vol.19, no.3, pp. 282-298

Tran, V.T. [1992]
Handling Control with Additional Rear Wheel Steering
I.MechE. Proc. 925050

Wakamatsu, K., Akuta, Y., Ikegaya, M. and Asanuma, N. [1996]
Adaptive Yaw Rate Feedback 4WS with Friction Coefficient Estimator between Tyre and Road Surfaces
Proc. of AVEC '96, Aachen, Germany

Wang, B., Abe, M. and Kano, Y. [2002]
Influence of driver's reaction time and gain on driver-vehicle system performance with rear wheel steering control systems: part of a study on vehicle control suitable for the aged driver.
JSAE Review 23 (2002), pp 75-82

Waterhouse, B. [2002]
Investigate the Effects of the Mass Moment of Inertia Relationship on the Transient Response of a Motorcar Using a 2 Degree of Freedom Model
Final Year Project report, Loughborough University

Yamakado, M. and Abe, M. [2008]

An experimentally confirmed driver longitudinal acceleration control model combined with vehicle lateral acceleration

Vehicle System Dynamics, vol. 46, Supplement 2008, pp 129-149

Yoshioka, T., Adachi, T., Butsuen, T. and Okazaki, H. [1999]

Application of sliding-mode theory to direct yaw-moment control

JSAE Review, vol. 20, pp. 523-529